Universidade Federal de Juiz de Fora

Engenharia Elétrica

Programa de Pós-Graduação em Engenharia Elétrica

Rafael Alberto Garcia Tinoco

New Methodologies for Constructing Steady-State Security Regions of Electric Power Systems

Juiz de Fora

2019

Rafael Alberto Garcia Tinoco

New Methodologies for Constructing Steady-State Security Regions of Electric Power Systems

Dissertação apresentada ao Programa de Pós-Graduação em Engenharia Elétrica da Universidade Federal de Juiz de Fora, na área de concentração em Sistemas de Energia , como requisito parcial para obtenção do título de Mestre em Engenharia Elétrica.

Orientador: João Alberto Passos Filho

Juiz de Fora

2019

Rafael Alberto Garcia Tinoco

New Methodologies for Constructing Steady-State Security Regions of Electric Power Systems
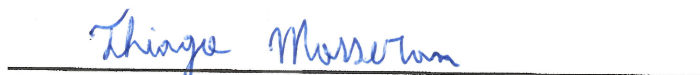
Dissertação apresentada ao Programa de Pós-Graduação em Engenharia Elétrica da Universidade Federal de Juiz de Fora, na área de concentração em Sistemas de Energia , como requisito parcial para obtenção do título de Mestre em Engenharia Elétrica.

Aprovada em:

BANCA EXAMINADORA

Prof. João Alberto Passos Filho , D.Sc. - Orientador
Universidade Federal de Juiz de Fora

Prof. Jose Luiz Rezende Pereira, Ph.D.
Universidade Federal de Juiz de Fora

Eng. Thiago Jose Masseran Antunes Parreiras, D.Sc.
CEPEL - Centro de Pesquisas de Energia Elétrica

ACKNOWLEDGEMENTS

RESUMO

Este trabalho apresenta duas metodologias alternativas do processo de construção das Regiões de Segurança Estática (RSE). Esta ferramenta é amplamente utilizada para a avaliação da segurança de sistemas elétricos de potência, principalmente no ambiente de tempo real. Neste contexto, o principal objetivo deste trabalho é aprimorar a metodologia de obtenção das RSE, que são utilizadas em diversos programas comerciais como, por exemplo, o programa de análise de redes ANAREDE, desenvolvido pelo Centro de Pesquisas de Energia Elétrica (CEPEL), no Brasil.

A primeira metodologia apresentada neste trabalho consiste em adicionar um indicador de estabilidade de tensão as RSE convencionais, com base nos cálculos das impedâncias de Thévenin e de carga. As RSE avaliam simultaneamente uma quantidade significativa de limites físicos e operacionais da rede, como: nível de tensão, limites térmicos nas linhas de transmissão e transformadores, entre outros. Contudo, atualmente as metodologias de obtenção das RSE não utilizem especificamente um indicador da condição de estabilidade de tensão do sistema analisado. Por outro lado, atualmente os sistemas elétricos operam perto de seus limites operacionais. Isto ocorre devido ao aumento continuo da carga e às restrições (econômicas, ambientais etc.) que limitam expansões adequadas, aproximando os sistemas das condições de instabilidade de tensão. Portanto, adicionar um indicador de instabilidade de tensão nas RSE torna-se um recurso útil e necessário para a ferramenta.

A segunda técnica proposta neste trabalho visa reduzir significativamente o esforço computacional da metodologia convencional, criando um novo procedimento baseado no algoritmo "Particle Swarm Optimization" (PSO). Uma série de modificações e ajustes dos parâmetros usados no algoritmo PSO é necessária para adaptá-lo à construção das RSE. Os resultados mostram que a metodologia proposta é confiável, uma vez que o impacto da aleatoriedade usada no algoritmo PSO não tem um impacto significativo na qualidade das RSE, e também demonstra que a metodologia proposta apresenta um ganho computacional significativo quando comparado com a metodologia convencional de obtenção das RSE.

Palavras-chave: Estabilidade de Tensão, Região de Segurança Estática, Impedância de Thévenin, Análise em Regime Permanente, Segurança de Sistemas de Potência, *Particle Swarm Optimization.*

ABSTRACT

This paper presents two alternative methodologies of the Steady-State Security Region (SSSR) construction process. This tool is widely used for security assessment of electric power systems, especially in the *real-time* environment. In this context, the main objective of this work is to improve the methodology for obtaining SSSRs, which is used in several commercial programs, such as the network analysis software ANAREDE, developed by the Electric Energy Research Center (CEPEL), in Brazil.

The first methodology presented in this paper consists on adding a voltage stability indicator to the conventional SSSR, based on the Thévenin and load impedance computations. The SSSR simultaneously evaluate a significant amount of physical and operational limits of the network, such as voltage level, thermal limits on transmission lines and transformers, among others. However, the current methodologies for obtaining the SSSR do not specifically possess an indicator of the voltage stability condition of the analyzed system. On the other hand, electric power systems currently operate near their operating limits. This is due to the continuous increase in load and the restrictions (economic, environmental etc.) that limit proper expansions, bringing systems closer to voltage instability conditions. Therefore, adding a voltage instability indicator in the SSSR becomes a useful and necessary feature for the tool.

The second technique proposed in this work aims to significantly reduce the computational effort of the conventional methodology, creating a new procedure based on the Particle Swarm Optimization (PSO) algorithm. A series of modifications and adjustments to the parameters used in the PSO algorithm are required to adapt it to the construction of SSSRs. The results show that the proposed methodology is reliable, since the impact of the randomness used in the PSO algorithm does not have a significant impact on the quality of SSSRs, and also demonstrate that the proposed methodology presents a significant computational gain when compared to the conventional methodology used for obtaining the SSSRs.

Key-words: Voltage Stability, Steady-State Security Region, Thévenin Impedance, Steady-State Analysis, Power System Security, Particle Swarm Optimization.

LIST OF FIGURES

LIST OF TABLES

ACRONYMS

SSSR	Steady-State Security Region
DSA	Dynamic Security Assessment
MLP	Maximum Loading Point
VSI	Voltage Stability Index
PSO	Particle Swarm Optimization
PF	Participation Factor
GPF	Group Participation Factor
IPF	Individual Participation Factor
IMPR	Importing Region
EXPR	Exporting Region
SSD	Steady-State Security Distance
PSVSR	Power System Voltage Stability Region
CVSR	Complex Voltage Stability Region
SNB	Saddle Node Bifurcation
PoC	Point of Collapse Method
CPF	Continuation Power Flow
PMLFS	Pair of Multiple Load Flow Solutions Method
VVC	Reactive Power and Voltage Control
MINLP	Mixed-Integer Non-Linear Problem
GEP	Generation Expansion Problem
DG	Distributed Generation
IWA	Inertia Weights Approach

CONTENTS

1 INTRODUCTION

This introductory chapter aims to provide a general view of the current situation of the power systems, the main challenges of modern electric networks are discussed and how they have been evolving over the years; Besides that some aspects of the security assessment of power systems are reviewed, detailing the main components of the DSA methods. Finally, the motivations and objectives of this work are described.

1.1 INITIAL CONSIDERATIONS

Electrical energy has become an essential element in modern society, over the last decades dependence on electricity has only grown and this tendency will be even greater in the future. Electrical energy is present in many aspects of daily life such as entertainment, transport, education, etc. Also in vital applications as medicine (hospitals), agriculture, food industry and many more.

Everything that was mentioned before created the necessity to design and construct electric power systems, which are one of the largest and most complex creations of humankind. They are composed of generators, transmission lines, transformers, loads, etc. Joining all these components together brings dynamic and steady-state characteristics that turn the analysis of power systems a crucial task for operating them.

The most bulk power systems are formed of thousands of nodes and at any time generation most supply the load and electrical losses. Generators vastly far from each other and from the consumption points connected by highly loaded transmission lines must function with synchronism, and it must be performed on a daily cycle [1], these are just a few of the complications that power systems bring to engineers.

The main goal of electric power systems is to transform available energy from different sources to electrical energy and to deliver it to the cities, industries or any consumption point. Energy is rarely consumed in its electrical form, instead, it is re-transformed into other types such as heat, light or mechanical energy. One of the benefits of dealing with electricity is that transporting and controlling it can be achieved with relative ease and with satisfactory efficiency [2].

Acting as consequence of the increasing electrical load, many countries have acquired as policy and norms to develop, in a sustainable way, new forms of generating electrical energy from renewable resources (solar, wind, etc) to apply strategies of energetic efficiency to satisfy the necessity of society, and to preserve the environment. As a matter of fact, this rising need for permanent electricity supply around the world brings an urgent request for formulating and implanting strategies from the governments that help to develop a balanced expansion of the generation sector [3].

In order to increase the capacity of the transmission subsystem, it must suffer adequate expansions in its infrastructure, this is crucial to attend the new loads in a reliable manner. In fact because of the new normative requirements in the energetic market which is very competitive, decentralized and with a policy of free access to the transmission system, many countries are operating with their transmission lines close to their limits prioritizing economic gains and compromising the power system reliability thus, turning a policy of expansion vital to ensure electricity supply for society. Although in several countries necessary expansions in both generation and transmission are not possible due to economic or normative (environmental issues) restrictions. Therefore, many transmission lines carry quantities of energy for which they were not designed, directly impacting the power system security bringing it closer to the maximum loading point (MLP).

Taking into consideration all the difficulties that expansions in electric power systems carry, interconnections between isolated subsystems in a country or even between neighboring countries, became a feasible and efficient solution to attend the increasing demand for electrical energy in modern society. In general, terms interconnected systems are advantageous in many aspects, such as incrementing the energetic resources allowing the optimization of the mentioned, increasing the systems' reliability since the loads can be attended from different transmission paths thus, the system can bear a larger amount of contingencies. On the other hand, interconnections need a bulk transmission system, since a larger amount of energy might be flowing through the transmission lines, besides that the operation becomes more complex since a higher attention to coordination is needed, also constant changes in the voltages might occur due to infinite load changes and the coordination between controls and protection becomes essential [2].

Power systems that operate with highly loaded circuits are strong candidates to present voltage stability problems, which is associated with the system's capability of maintaining adequate voltage levels in all its nodes under both, normal and contingency conditions. If the system is not strong enough to survive after any disturbance, a voltage stability problem may occur. It is characterized by voltage drops in some of its nodes, and if immediate corrective actions are not taken adjacent regions might be affected, resulting in a partial or total blackout of the system. Voltage stability problems occur in power systems that are highly loaded, as it was explained before, and also in electric networks that present weak reactive power supply. Voltage collapse is considered an instability since it affects various electrical equipment and often it involves the whole system, although generally, it starts in a specific portion of the electric network [4].

Voltage stability is a very important topic within power systems analysis and it has brought the necessity of developing criteria and security margins to operate the systems. The oldest approach to warrant voltage security is based on ensuring that certain voltage levels are acceptable under normal and contingency conditions for the studied network.

However, this technique does not warrant satisfactory security margins to safely operate a system, since the voltage collapse point might be reached even with acceptable voltage levels [4].

According to [5]:

> (...) "Most major grid blackouts are initiated by a single event (or multiple related events such as a fault and a relay misoperation) that gradually leads to cascading outages and eventual collapse of the entire system. With hindsight, one can often identify means of mitigating the initial event or minimizing its impact to reduce the risk of the ensuing cascading trips of lines and generation. Given the complexity and immensity of modern power systems, it is not possible to totally eliminate the risk of blackouts. However, there are certainly means of minimizing the risk based on lessons learned from the general root causes and nature of these events."

All that was mentioned before has contributed to many major blackouts around the world to occur due to voltage instability, some of them are mentioned below [2], [5]:

- New York Power Pool disturbances of September 22, 1970;

- Florida system disturbance of December 28, 1982;

- French system disturbance of December 19, 1978;

- French system disturbance of January 12, 1987;

- Northern Belgium system disturbance of August 4, 1982;

- Swedish system disturbance of December 27, 1983;

- Japanese system disturbance of July 23, 1987;

- U.S. - Canadian system disturbance of August 14, 2003;

Growth in complexity, load, and dependence of electrical energy in society, made that designing, planning and operating power systems require special attention, aiming that high standards are achieved in efficiency, security, quality and reliability in the given service.

1.2 POWER SYSTEMS SECURITY

The main goal of power system operators is to manage their systems and maintaining a high standard of reliability, which refers to the possibility of a power grid to keep acceptable operation over a long period of time. It also indicates the capability of

providing satisfactory electricity service on a continuous basis, with the least number of interruptions possible for a prolonged amount of time [6].

Different from reliability which qualifies the performance over time, the security of a power system concerns the grade of danger in its capability to keep operation even under imminent contingencies without interruption of electricity supply. It is associated with the bulkiness of the system and, thus it relays on the network's operating condition as well as the possibility of contingencies that may occur due to disturbances [7].

Since power systems were created warrant a safe operation has been an essential task, when the security margins are not adequate the network becomes vulnerable to severe, and on some occasions, fatal faults that turn into enormous economic losses in the form of fines or ruined equipment.

In previous times, when systems were designed, built, regulated and operated by a unique entity, normally owned by the government, electrical grids tended to be more secure, since unified planning guaranteed that the generation sector and the transmission network kept the same increment rate of the load, therefore minimizing the probabilities of equipment's overloading that might lead to catastrophic contingencies. Maintenance was, in general, more rigorous, and from an operational point of view, predicting contingencies and operating, in general, was simpler since there were fewer generator and transmission owners hence, coordinating the operation and taking corrective actions in case of disturbances was made in a cooperative manner [8].

Although several countries still work under the previously mentioned scenario the tendency in the electrical sector is to open its markets, this has brought several new possible sources of disturbances and factors that reduce the robustness of the system thus decreasing the predictability of operation. To guarantee that a power system operates with satisfactory security margins and reliability it must be correctly planed with security as the main objective it also has to be monitored constantly during operation to warrant that acceptable security margins are achieved permanently under normal and emergency conditions. This new scenario in the electric power industry has increased the necessity of developing new technologies in the field of security assessment and also changed the requirements for the capabilities of power system analysis tools.

Historically, the security and reliability assessment in power systems has been approached in an off-line environment generally performed for planning and expansion studies using both, steady-state and dynamic methodologies. The off-line analysis aims to determine the degree of risk of instability and explore the characteristics of the phenomenon which might be a consequence of disturbances that may occur on an electrical grid. It basically consists of using computational tools to assess all types of stability (voltage, angular and frequency) and determine if the current operating condition and possible scenarios with contingencies are stable. Although when this is attempted in an on-line

environment becomes a much harder task.

Real-time security assessment is more reliable if compared with *off-line* analysis, since in order to maintain permanent control of the power system security there is the necessity of advanced tools for dynamic and steady-state analysis, with the ability of computing, in acceptable periods of times, the security margins, these have to be obtained quickly enough so that the operators may take preventive actions in case of disturbances or imminent load increments.

Lately, the use of security assessment software tools has been very common around the world, these tools achieve considerable high effectiveness in terms of costs and their implementation is relatively simple, they increase significantly the performance of grids, making continuous security analysis guiding the operators to maintain acceptable security margins. The task of establishing power systems security in a real-time manner is generally named as *on-line dynamic security assessment* or *on-line* DSA, which evaluates both, dynamic and steady-state security.

Utilizing *on-line* DSA the current operating point is analyzed constantly and the system stability is determined cyclically in a short period of time that has to be fast enough to allow protections to act or to permit operators to take corrective or preventive actions. Since these methods are used in *real-time* operation, the grade of uncertainty that is associated with the analysis made in an *off-line* environment is nearly eliminated. With this approach the system is enhanced with a feature that is similar to a radar that continually sweeps the electric network for possible contingencies that may occur due to a disturbance, generally a *N-1* or any *N-x* analysis is added in the security assessment [8].

On-line DSA measures the current system condition and gives the information to operators or automatically triggers control or protection systems. The measurements are obtained from different sources such as SCADA systems or PMUs. Nowadays every power system possesses a SCADA system thus is the main source of data around the world, although PMUs have a great advantage in terms of speed, accurate and continuous data besides being synchronized by GPS. This clearly increases the accuracy of the models. Another essential element of *on-line* DSA is modeling the system since all the security information relies on the accuracy of the model it might be the most important part of the DSA tool. Conventional state estimators are the principal supply of power flow models (for steady-state analysis). The main components of an *on-line* DSA system are shown in Figure 1.

In terms of hardware and software, there are several aspects that must be addressed, firstly reliability, which is very important for any on-line system. Besides using the correct code for computing the correct security margins, reliability has to be extended to hardware (task management workstation, computational servers, data server, and the communication circuits). One way to approach reliability is through the use of redundancy [6].

Figure 1 – *On-line* DSA system components
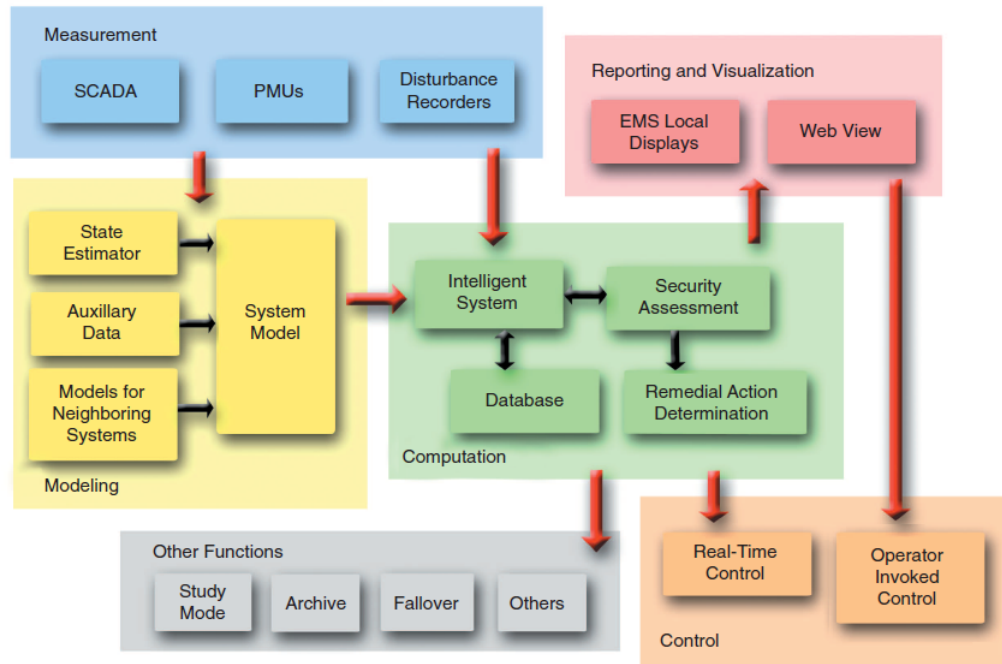
Source: [8].

Scalability is another important component in an on-line DSA system because it is well known that power grids evolve over time, increasing its size and complexity, therefore increasing the computational power requirements. For example, more disturbances analysis might be needed or a significant increased in the number of nodes hence, an expansion in the DSA system must be planned to be performed without the necessity of large changes in terms of software and hardware architecture. Typically the most common approach is to use multi-server architecture, by doing so the computing power can be increased easily by adding new servers [6].

Several works have been presented showing the use of these technologies around the world as it can be seen in [9], [10], [11] or [12], they all show that a vast amount of data is available and the scope is to display it in the simplest manner to be able to guide the operators to take actions as fast as possible, so it can be said that accessibility is another main task of the *on-line* DSA systems, a schematic of a commonly used hardware architecture for DSA systems is shown in Figure 2.

Some other aspects that are important, referring to software and hardware, should also be taking into consideration, those might be portability, which is important when maintenance is needed; security in terms of software has become crucial in the latest days, so that only qualified persons can access sensitive information and take actions if needed.

Figure 2 – *On-line* DSA hardware architecture
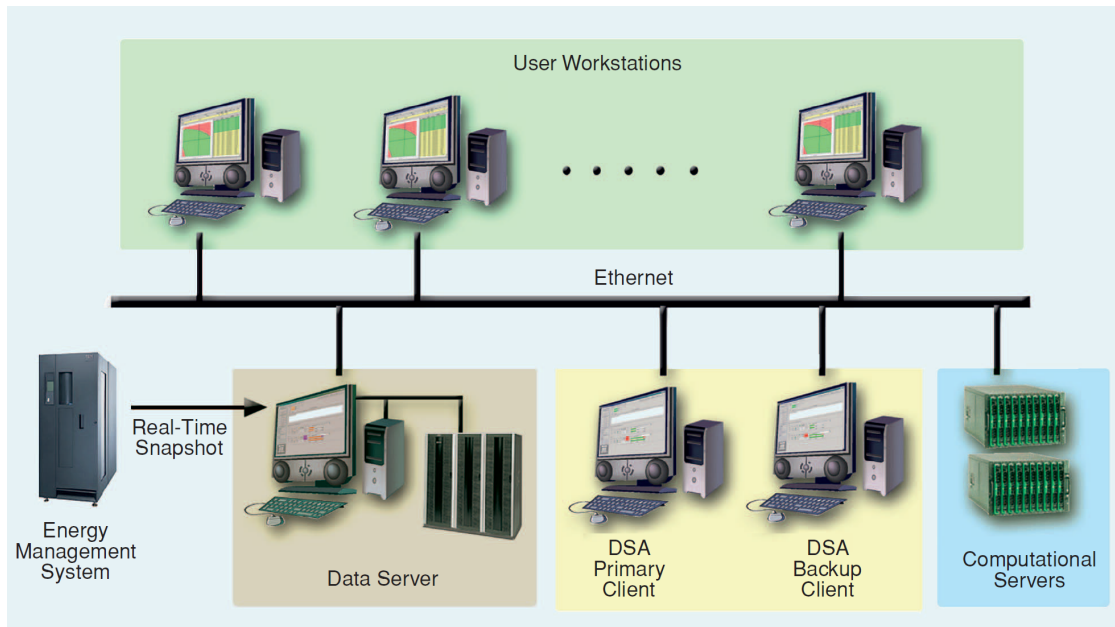
Source: [6].

1.3 OBJECTIVES AND MOTIVATIONS

As mentioned before power systems have largely changed in the last decades and with this, new challenges involving security assessment were born. Many tools capable of monitoring power systems security are being used around the world thru DSA systems, one of these tools was detailed in [13], which is the steady-state security region (SSSR), it is a very effective method to monitor electric networks security in both *on-line* and *off-line* environments. Although the mentioned tool covers a lot of the operational and physical limits associated with steady-state security assessment it still lacks a voltage stability indicator which, as was disused in the previous subsections is one of the main problems of highly loaded systems.

A large number of methods have been proposed in the literature to analyze the voltage stability phenomenon under steady-state conditions. Some of the most known methods are the P-V curves which illustrate the change in the nodal voltage profile when the system presents load increments, the P-V curves illustrate the distance between the current operating point and the MLP, this distance is used to measure the risk of voltage collapse in a power system. The P-V curves are obtained by the continuation power flow (CPF) method which consists of a series of power flow solutions in a predictive and corrective stage until the MLP is reached. At the end of the CPF method, the most critical nodes of the system (in terms of voltage stability) might be obtained by analyzing the tangent vector [2].

Another technique that is largely used in voltage stability analysis is the Q-V curve,

which provides the needed reactive power injection to maintain a specified voltage level. As well as the P-V curves the Q-V plots also give a measurement of the proximity of the current operating point to the MLP, this distance is called the reactive power margin and by analyzing them it is possible to obtain the most critical nodes of an electric network.

Even though the P-V and V-Q curves are very common in voltage stability analysis they present important issues when it is tried to transfer them to an *on-line* environment for *real-time* operation of a power grid, since they need several power flow solutions to be obtained, this increases greatly the computational effort on tools that already need a significant amount of time to analyze the systems' security. Another disadvantage of using these tools for real-time operation is that they produce one curve for each node of the analyzed system, which requires a high amount of time to obtain an accurate analysis of the full system. This would be even more problematic for tools that evaluate a large number of scenarios (contingencies), turning these methods infeasible for voltage stability assessment in *on-line* environments.

An index that allows monitoring voltage stability is presented in [14], this indicator is based on the maximum power transfer criteria from the electrical circuits theorems, where at the MLP the Thévenin impedance's module is equal to the load impedance's module. This methodology overcomes the problems mentioned before since it requires very low computational effort and its results are easily analyzed.

One of the main objectives of this work is to enhance the tool presented in [13] by adding a fast voltage stability indicator presented in [14]. With the enhanced methodology is expected to be able to detect voltage instability for different dispatch profiles and in case of disturbances in a more practical way than the classical tools, besides this, the aim is to display the possible voltage stability problems in an understandable way, possible by a simple graphical inspection, this would become very helpful for decision making in control rooms of power systems.

On the other hand, although the SSSR is a very effective tool in power systems security assessment, it requires a significant computational effort and that translates into a considerable amount of time due to the need of many power flow solutions (this will be addressed in future chapters), making difficult to analyze large fully modelled power system in *real-time* operation with this methodology. Therefore, another objective of this work is to improve the computing time required by the construction process of the SSSR. To achieve a reduction in the computational effort to build the SSSR, a new methodology based on the well known Particle Swarm Optimization (PSO) algorithm will be developed, with the new methodology is expected to significantly reduce the computational effort, when compared with the methodology presented in [13], without compromising the accuracy of the SSSR.

The PSO algorithm uses various constants in its process, most of them are used

with the same value in any optimization problem but, since this is a special problem, another objective of the proposed methodology is to normalize values for all the constants needed in the PSO algorithm, in order to achieve that, a series of tests that justify the utilization of the proposed values of the constants are going to be performed.

1.4 STRUCTURE OF THE WORK

The second chapter presents a bibliographic review, it is divided into three subsections, the first one will address papers and books that describe SSSR and how they are used in control rooms of power systems around the world. The second subsection presents methods utilized to analyze voltage stability problems which include methodologies capable of determining the MLP, security margins or the most critical nodes of a system. Some of them use the equivalent Thévenin impedance to achieve this goal which is the base concept of one of the proposed methods. The last subsection presents a brief review of the evolution that the PSO algorithm has experimented since it was first introduced.

In chapter 3 the construction process of the SSSR is described, detailing the mathematical formulations and all the important aspects that have to be taken into consideration. The voltage stability index that is used to construct the enhanced SSSR is also explained, describing the concepts of fundamental electrical circuits that are being used and showing how to calculate the equivalent Thévenin impedance and the load impedance. Finally, it is presented the proposed methodology to join these two tools to create an enhance SSSR that allows detecting voltage instability.

The fourth chapter addresses the new proposed methodology to build SSSR using the PSO algorithm. The mathematical fundaments of the PSO algorithm are described, also its parameters. In order to adapt the PSO to the analyzed problem new approaches to determine the parameters are needed, these are deeply explained as well as the optimization model, the problem variables and the treatment of the initial population.

Chapter 5 presents the results of the simulations performed to validate both methodologies. Firstly the enhanced SSSR, including the voltage stability indicators, is constructed for a small scale system, it serves as a tutorial to show step by step the calculations needed. Then the proposed SSSR is built for two bigger systems and is compared with the current methodology. In further pages, the new methodology which uses the PSO algorithm as the base is tested for the same systems utilized in the previous method comparing it with the conventional methodology in terms of performance and quality.

Chapter 6 contains the conclusions obtained with the analysis made on the simulations, describing the strengths and weaknesses of the proposed methodologies and also provides some suggestions for future works.

2 BIBLIOGRAPHIC REVIEW

This chapter is divided into three subsections, the first subsection reviews a series of works related to the SSSR, with the objective of showing the different applications where this tool can be used and also the modifications that had been made in the mentioned tool. The second subsection presents some of the most cited articles regarding voltage stability assessment. Some of these papers propose new mathematical methodologies to analyze voltage stability and other works do not propose new methodologies, but they perform comparisons between existent tools that are being used in the power systems control rooms. Lastly, the third subsection introduces a brief view of the evolution that the PSO algorithm has experienced over the years and its common applications in power systems. The main purpose of this chapter is to provide a better understanding of the tools that are going to be used in the proposed methodologies.

2.1 STEADY-STATE SECURITY REGIONS

2.1.1 Dynamic and steady-state analysis of electric power systems by integrated computational application

This work can be found in [15], it performs a series of analysis under both steady-state and dynamic conditions with a commercial program named ORGANON, which is a tool that assesses power systems security thru the generation of SSSR and several others tools and it is used by the Brazilian electric system operator (ONS). The author describes the main concepts and methods that the ORGANON tool uses.

Firstly the tools that the ORGANON software uses for the steady-state analysis are presented, beginning with the formulation of the conventional power flow and its solution by the Newton-Raphson method with contingency and sensitivity analysis, CPF method and synthetic dynamics power flow. It performs tests with a small size system and compares the results with the software ANAREDE.

It also presents the tools available for dynamic analysis in the mentioned software, those include (*i*) step tests in synchronous generators, (*ii*) time-domain simulation analysis and (*iii*) dynamic contingency analysis. The theoretical concepts of these analyses were presented and results of simulations made with a small size system.

Lastly, it illustrates the tools available for security assessment, which include both steady-state and dynamic analysis. There are two steady-state tools for security assessment in the software, the first one is the steady-state contingency analysis for an operating point, which provides a report, in the form of tables, for each contingency showing if there is any limit violation for a fixed dispatch configuration.

The second tool in this software for steady-state security assessment is the SSSR,

in this work the basics of the SSSR are discussed, it describes how the power system that is going to be analyzed has to be divided into three generation groups and one of these groups has to act as a "swing" group to be able to close the power balance since several dispatch scenarios are tested to obtain the SSSR, it also shows how to input the data into the software. The work also mentions how the obtained SSSR takes into consideration contingency analysis and discusses the limits that are used by ORGANON to construct the SSSR. The limits used in this software are: (*i*) voltage violation, (*ii*) Overload limit on transmission lines and (*iii*) security limit (convergence or active generation limit). Finally, it shows the nomograms obtained when a small-scale 9-bus system is analyzed in different scenarios, explaining how each graph would be used in a power system control room.

For the dynamic assessment, as for the steady-state analysis, there are two tools for security evaluation, the first one is dynamic contingency analysis for an operating point, which is similar to the tool used in steady-state security analysis, with the difference that the contingencies analyzed are short circuits in transmission lines and the limits evaluated under dynamic conditions. The work also presents a dynamic security region that follows the same philosophy of the SSSR. The difference is that the dynamic security region analyses the solution for the contingencies with a time-domain simulation different from the SSSR that uses a conventional power flow solution.

However, the work focuses on the use of the ORGANON software and does not describe the techniques needed to obtain these regions.

2.1.2 Assessment of Load Modeling in Power System Security Analysis Based on Static Security Regions

In the work presented in [13], the definition of the SSSR is made and the construction process of the mentioned tool is detailed, in this subsection, the steps of this process will be briefly discussed, the details and mathematical formulations will be reviewed in a further chapter. The steps of the construction process are defined as follows:

- Division of the system into three generation groups: The SSSR is a three-dimensional graph in which, each axis represents a generation group and the selection of these groups is an essential part of the building process for an SSSR. It depends on the type of study that is desired, for example, a generation group might be composed of only one generator, by a set of power plants of the same region, or a set of hydroelectric plants of the same watershed. Since the core of the construction process is to explore the maximum number of possible dispatch scenarios, one of the generation groups is designated as the "swing" group, which is responsible for maintaining the power balance, modifying its generation profile according to the variations of the other two groups.

- Limits and directions: To explore the different dispatch scenarios of the power system, a strategy consisting of analyzing directions around the original operating point (base case) is adopted. The operating point is treated as the origin of the Cartesian plane if the solution space is thought as a two-dimensional space. Search Directions are determined by choosing the angles formed between the fictitious horizontal axis and the desired direction. For each direction, a series of generation steps are made, representing different dispatch scenarios for which is obtained a power flow solution to discover if there are violations of any limit, normally the limits used to construct the SSSR are nodal voltage, thermic limits on transmission lines, convergence of the Newton-Raphson method, active and reactive generations limits.

- Definition of the exporting region (EXPR) and the importing region (IMPR): In the previous stage it was explained that for each direction, several power transfer steps are made to explore different dispatch scenarios. Based on the direction that is being analyzed, a generation group can be increasing or decreasing its generated power; in other words, it is exporting or importing power. Therefore, it is important to determine which groups are composing the EXPR and IMPR for the different examined angles. To determine these regions, an analysis for each quadrant of the Cartesian plane is performed, hence the angle or direction directly impacts on the determination of the EXPR and IMPR and it also influences the rate in which the groups increase or decrease their generation. The EXPR and IMPR can be composed of a maximum of two generation groups.

- Calculation of participation factors: After defining the EXPR and IMPR regions, it is necessary to determine how much power will be imported or exported by each group and by each generator (each group can be composed of several generators). It is possible by the calculation of the participation factors (PFs) in terms of percentage. There are two types of PFs:

  - Group participation factors (GPFs);
  - Individual participation factors (IPFs).

The GPFs are necessary when the EXPR or IMPR is formed by two generation groups, they determine what percentage of power each group contributes to its correspondent region. Their calculation is performed by a trigonometric analysis based on each explored angle. IPFs are essential when a group is constituted by more than one generator, they define the proportion that each generator will increase (EXPR) or decrease (IMPR) its original dispatch. The IPFs can be calculated taking into consideration two aspects depending on the study that is being performed: the original dispatch or the maximum power of each generator.

2.1.3 Construction of steady-state security regions of electric power systems utilizing branched generation transfer directions

The main purpose of [16] was to provide an alternative method to construct the SSSR based on a modification of the traditional methodology which uses directions around the operational point (base case) to explore the maximum amount of dispatches scenarios possibles by performing a series of power transfer steps between regions (this methodology will be detailed in further chapters).

The technique proposed in the mentioned reference consists of creating a triangular net that homogeneously covers the feasible solution space, which is composed of several dispatch scenarios of the three generation groups that have to be created. The methodology aims to reduce the number of analyzed dispatch profiles close to the operating point to increase the density of analysis performed far from the operating point. As a result is expected a uniform layer, which has the same distance between the dispatch scenarios that are going to be analyzed. This method is supposed to reduce the uncertainties that are between each direction of the conventional methodology, in other words, it tries to improve the accuracy of the SSSR and it also aims at reducing the computing time of the conventional technique.

In order to create the mentioned net the paper proposes the creation of different levels of dispatch scenarios, the distance between levels is determined by the generation transfer step, which is also the length of the triangles' sides, thus the generation transfer step parameter is crucial in this method, in terms of computing time and accuracy of the SSSR. An illustration of this methodology is shown in Figure 3.

Figure 3 – Triangular net for the construction process of SSSR
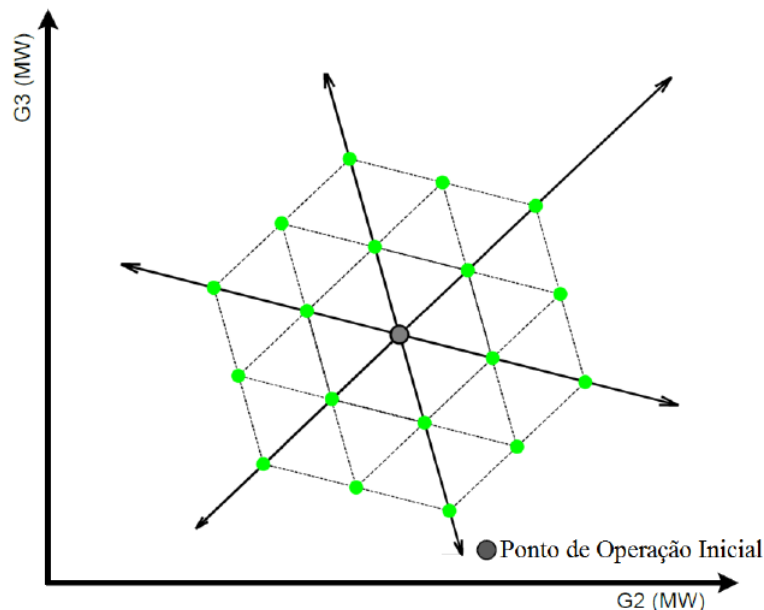
Source: [16].

Besides the creation of different levels, the methodology proposes that the feasible solution space be divided into six sectors, each of these sectors has a reference direction and there is a 60 degree offset between them as can be seen in Figure 3. The construction algorithm is divided into three stages as follows:

- Base case evaluation: In this step, only the operating point is evaluated by the solution of the conventional power flow. A contingency analysis is also performed to determined if the operating point satisfies the *(N-1)* criterion.

- Parallel direction to the reference direction of the analyzed sector: In this stage is determined the angle of the direction that the tool of maximum power transfer will follow. The author proposes an initial angle of 45 degrees, for the remaining sectors the reference direction has an offset of 60 degrees. Then the PFs are calculated (GPFs and IPFs) and is initiated the power transfer between the IMPR and EXPR, and a conventional power flow solution is obtained for each of the new dispatch scenarios.

- Reference direction of the sector with 60 degrees offset from the new direction: Starting from the direction created in the previous stage, a new generation transfer direction is adopted with an offset of 60 degrees in relation to the direction analyzed in stage 2. Then the PFs are calculated again and the same process of the previous stage is followed.

After these steps are completed for the six sectors is expected to obtain the SSSR of the analyzed system.

2.1.4 Damping Nomogram Method For Small-Signal Security Assessment Of Power Systems

This work can be found in [17], it discusses the main characteristics of the assessment of power systems security it also describes the voltage security assessment, the transient security assessment an the small-signal security assessment of electric power networks.

The authors propose a nomogram method based on the analysis of oscillation damping factors to be used for small-signal security assessment of power systems and describes its computational implementation.

The proposed method takes as staring point an operating point from the analyzed system and a list of contingencies, different scenarios are generated throughout variations on the generation profiles of the generators of the system, which previously separated into three groups, aiming to determine the security regions to small-signal for the electric power system that is being analyzed.

The results of the security assessment to small-signal can be visualized on a set of nomograms, which are capable of displaying important information about the damping factors of the oscillation modes of power systems. On the mentioned nomograms, the security regions are defined by the minimum damping factor of the oscillation modes obtained and monitored for all the feasible operating points that were analyzed.

The results of this method can be used for determining stability margins and security levels of the analyzed systems, also from this results corrective actions associated with the dispatch profile of the system or the control systems can be taken, aiming to increase the damping factors of the oscillation modes thus, improving the security levels of power systems.

2.1.5 Steady-state security regions of power systems

In 1982 [18] was one of the first works that discussed the SSSRs in power systems, according to the mentioned reference an SSSR is:

> (...) "a set of real and reactive power injections (load demands and power generations) for which the power flow equations and the security constraints imposed by equipment operating limits are satisfied."

In this paper, the method to find the SSSR of a power system is formulated as a search for satisfying conditions to find power flow solutions within the set of security constraints that were pre-established. To achieve that, accurate active and reactive power injections are obtained at each bus, so if each of these injections is situated within acceptable limits, the system is warranted to operate with satisfying security.

The work presents the conventional power flow equations and the decoupled power flow equations, which are the two tools that are used to construct the SSSR. The paper also shows the mathematical formulation of the physical and operational limits, that are presented in the form of constraints. The limits proposed in this article are voltage on nodes, current on transmission lines that it relates to the angular difference between the nodes where the transmission line is placed, reactive and reactive generation limits on PV buses and "swing" bus. The SSSR is defined for a fixed system configuration.

It was proposed to find a set of active and reactive power injections for which the power flow equations were satisfied as well as the security constraints (limits) to be able to construct the SSSR. The adopted methodology to determined the mentioned power injections had two steps: *(i)* divide the problem into two simpler problems; *(ii)* the results of those problems are used to solve the original problem (that are the conventional power flow equations).

Dividing the problem into simpler problems consisted of solving the decoupled power flow equations, the first subproblem consists of determining a set of reactive power injections for which there is a solution to the mentioned equations that satisfies the voltage constraints. The second subproblem consisted of determining, that for any voltage inside the constraint, a set of active power injections where there is a solution to the decoupled power flow equations and that satisfies the angle constraints (which are related to the current on transmission lines). The results of these two problems are used to solve the full power flow equations and construct the SSSR.

The obtained results were expressed in terms of limits of active and reactive power injections at each bus. In other words, the SSSR that were obtained in this work were hyper-boxes in $\mathbb{R}^n$.

Figure 4 – Steady-state security region of a 2-bus system
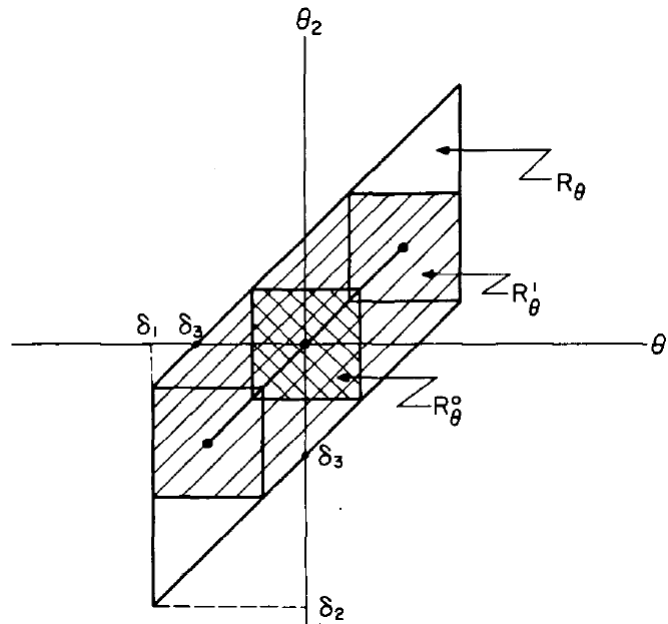
Source: [18].

As it is possible to observe in Figure 4 the SSSR obtained in this paper was complex to understand, and because it uses the decoupled power flow method as a tool to construct the graph it would not be feasible to use in the present day since the power systems are highly loaded hence, making the decoupled power flow inefficient.

2.1.6 Steady-state security assessment method based on distance to security region boundaries

The method presented in [19] introduced the concept of steady-state security distance (SSD) aiming to provide a quantitative measure of security margins for power systems operators. It formulated the mathematical approach of the SSSR as a non-linear optimization problem, using the constraints that were suggested in [18] which is a problem

that takes a large amount of time to be solved thus making it an infeasible approach to construct SSSR in practical applications. With this context, this paper proposed an alternative methodology to solve the optimization problem which consisted of dividing the original problem into two steps, (*i*) identify the active boundaries that delimit the SSSR and *(ii)* solving the original problem with partial constraints.

Firstly the paper presents the tools that are going to be used to solve the problem, those are the linear power flow method and the mentioned constraints that were originally presented in [18], then it provides the definition of SSD, which is the "distance" between an analyzed operating point and the different boundaries that delimit the SSSR. With this definition in mind the objective function is formulated in terms of active generation output, defining that when the distance to the nearest boundary is large, the system has better security margins. The complete optimization model is formulated which in this paper only utilizes power flow on transmission lines and active generation constraints. When there is no feasible solution to the presented optimization model, it means that the examined constraint is inactive. SSD to these constraints is defined as "infinity" because they could never be reached without violating other constraints. For the sake of clarity inactive constraints are illustrated in Figure 5 where curves 1, 3 and 4 are inactive.

Figure 5 – Inactive boundaries illustration
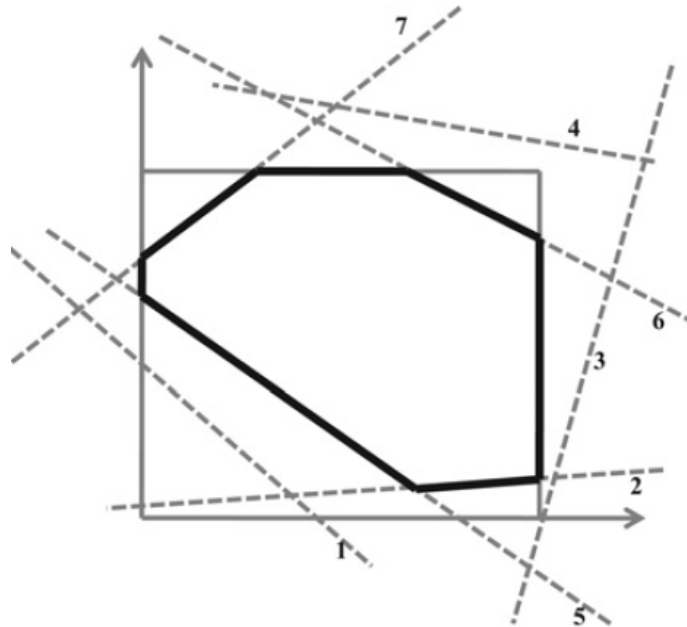
Source: [19].

The proposed methodology of the work consists in the two steps mentioned before, the first one aims to identify which are the active boundaries since in a real power system there are hundreds of transmission lines but only some of them reach their limits, therefore, the majority of these constraints are inactive.

With the purpose of identifying the active limits, the paper proposed the solution of a new optimization model that maximizes the power flow on each branch of the system and the constraints only consider active generation, demand, and power flow. Since the approach is defined with the linear power flow equations, the new optimization problem is a simplified linear programming model. When the solution of this model provides a flow greater than the maximum capacity of the transmission line, that branch becomes a potential active boundary, therefore it is included in the solution of the next step.

The second step consists of solving the original problem but in a reduced form, only taking into consideration the constraints that were identified in the previous step. When this is performed it is expected to reduce the number of constraints by approximately 90%. In the presented results there was a high computing time gain but, because this method uses the linear power flow formulation and takes into consideration only limits on active generation and flow on transmission lines, it becomes impractical for assessment of real power systems.

2.1.7 Development of Power System Voltage Stability Region (PSVSR) for Static Voltage Security Assessment

In work [20] a new tool to monitor steady-state voltage stability is proposed, it is named the power system voltage stability region (PSVSR). It also describes the development of software, implemented in C++ on windows environment, that obtains the PSVSR. The tool aims to provide the power system operator global and symmetric information about the steady-state voltage stability and thermal limits of transmission lines.

According to the mentioned reference in real power systems, the preponderance of small stability disturbances are associated with voltage stability and most of them are monotonous. Therefore, the work focusses on steady-state voltage stability. The PSVSR for a particular network arrangement is defined as a region in injection space that includes all operating points that are stable in terms of steady-state voltage stability. Operating points that are not voltage stable stay outside of the security region. The PSVSR is obtained by modal analysis, that is, depending on the eigenvalues of the Jacobian matrix (from the Newton-Raphson method). Aiming to obtain critical power injection points for a specific network configuration, the authors use the CPF method. The injection space of the PSVSR is defined as active generation power of different regions. Therefore the displayed PSVSR are three-dimensional graphs whose axes represent the active power generation of given areas of the system.

In order to make the PSVSR a feasible tool for *on-line* applications, the paper proposes a voltage stability region in cut-set complex power space, because according to the author operators usually monitor voltage stability limits by observing the power

transfer limits only on the critical transmission lines. Therefore if a voltage stability region in cut-set complex power space (CVSR), (that is, in essence, analyze only the known critical nodes) is expected to have a large reduction in the computing time. The author found that the CVSR possesses a linear property, which can approximate the boundary of the CVSR using hyper-plane(s). As it was explained before power system operators usually use thermic limits on branches to monitor voltage stability hence, it was proposed that the presented tool incorporates the mentioned limit, an example of a CVSR obtained in Central-China system is presented in Figure 6.

Figure 6 – CVSR of Central-China Power System
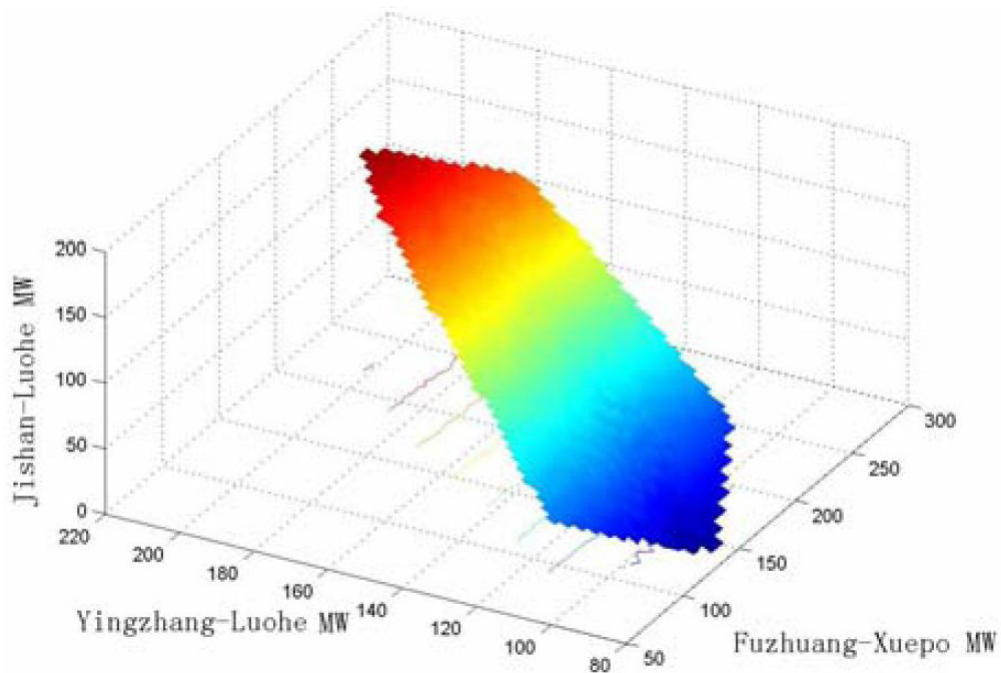
Source: [19].

The methodology proposed to construct the CVSR followed the following steps:

- Most critical nodes are selected by using participation factors or local voltage indicator;

- The cut-set space is created to divide the system into two parts;

- Using the CPF method, a set of critical points in terms of voltage stability is obtained to form the boundary of the CVSR. The load increasing direction is based on the load forecast. Generation dispatching modes is determined according to the schedule;

- Least Square Approximation method is used to determine the coefficients of the hyper-plane with computed voltage stability critical points.

2.2   VOLTAGE STABILITY ASSESSMENT

2.2.1   **A real-time voltage instability identification algorithm based on local phasor measurements**

This paper can be found in [21], it proposes an index of voltage instability risk which is based on local phasor measurements, utilizing a high sampling rate. The index consists of computing the Thévenin equivalent circuit in real-time. The mentioned reference details a novel algorithm used in *real-time* to obtain the Thévenin voltage and impedance.

Obtaining local phasor measurements of voltage and current on a node, a voltage stability analysis can be performed through the Thévenin equivalent circuit since voltage instability is associated with the condition that the modules of the Thévenin impedance and the load impedance be equal, this equality is corresponding to MLP [21].

Assuming the Thévenin equivalent circuit in its simplest form, the article aims to calculate the Thévenin voltage and impedance utilizing the voltage and current values measured in the load. From a Thévenin equivalent circuit (2.1) can be deducted. Where $\vec{V_L}$ is the load voltage, $\vec{E_{Th}}$ is the Thévenin voltage, $\overline{Z}_{Th}$ is the Thévenin impedance and $\vec{I_L}$ is the load current.

$$\vec{V_L} = \vec{E_{Th}} - \overline{Z}_{Th} \times \vec{I_L} \tag{2.1}$$

Assuming that the load impedance $(\overline{Z}_L)$ is given by the addition of the resistance R_L and the reactance X_L, and that the mentioned impedance possesses an angle θ as shown in (2.2), the author illustrates the following definitions in (2.3) and (2.4).

$$\overline{Z}_L = |Z_L| \angle \theta \tag{2.2}$$

$$\vec{V_\Delta} = \overline{Z}_{Th} \times \vec{I_L} = R_{Th}\vec{I_L} + jX_{Th}\vec{I_L} \tag{2.3}$$

$$\vec{E_{Th}} = \vec{V_L} + \vec{V_\Delta} \ \ with \ \ \vec{E_{Th}} = E_{Th}\angle\beta \ \ , \ \ \vec{V_L} = V_L\angle\theta \ \ and \ \ \vec{I_L} = I_L\angle 0° \tag{2.4}$$

Separating equation (2.4) into the real and imaginary parts equations (2.5) and (2.6) are obtained:

$$E_{Th}\cos\beta = R_{Th}I_L + V_L\cos\theta \tag{2.5}$$

$$E_{Th}\sin\beta = X_{Th}I_L + V_L\sin\theta \tag{2.6}$$

Since in transmission systems the resistance is much smaller than the reactance the article assumes that $R_L = 0$ to find an initial approximation of β as shown in (2.7), it also makes an initial estimative of the Thévenin voltage (E_{Th}^0) as demonstrated in (2.8). The deduction of the equations for the maximum and minimum Thévenin voltage (E_{Th}^{max} and E_{Th}^{min}) can be found in [21] and they are given as a function of the angle β.

$$\beta = \cos^{-1}\left(\frac{V_L \cos\theta}{E_{Th}}\right) \tag{2.7}$$

$$E_{Th}^0 = \frac{E_{Th}^{max} - E_{Th}^{min}}{2} \tag{2.8}$$

As can be seen in equation (2.8) the initial value of the Thévenin voltage is an approximation within its bounds although it has to be updated to its correct value, this is done utilizing an analogy that depends on the increment or decrement of the load. The updated Thévenin voltage is given by (2.9), where ϵ defines how much E_{Th} will change, k is a constant explained by the author and i corresponds to the instant in time that is being analyzed.

$$E_{Th}^{i+1} = E_{Th}^i + \epsilon \;\; where \;\; \epsilon = min(\epsilon_{min}, \epsilon_{sup}, \epsilon_{lim}) \tag{2.9}$$

$$\epsilon_{min} = |E_{Th}^{i-1} - V_L^i| \tag{2.10}$$

$$\epsilon_{sup} = |E_{Th}^{i-1} - E_{Th}^{max(i)}| \tag{2.11}$$

$$\epsilon_{lim} = |E_{Th}^{i-1} \times k| \tag{2.12}$$

Summarizing the proposed algorithm it consists of estimating an initial Thévenin voltage with (2.8) with angle calculated by (2.7). After these estimations, the Thévenin reactance is calculated with (2.6), after a small period of time update the Thévenin voltage following (2.9) and calculate the Thévenin reactance with the new values.

2.2.2 A new efficient unified strategy to compute voltage collapse point and voltage stability enhancement by generation shift

The work presented in [22] proposes a method to calculate the saddle-node bifurcation (SNB), based on the combined use of the CPF method, the point of collapse method (PoC) and the method of a pair of multiple load flow solutions (PMLFS) with Lagrange interpolation utilizing only their advantages.

The article cites the main characteristics of the existent methodologies that compute directly or indirectly the MLP. According to the author even with the CPF being a very robust method, it requires a large computational effort, hence it becomes slow. The PMLFS together with the Lagrange interpolation may also compute the collapse point and it is faster than the CPF, although it has issues when the system is operating under light loading conditions. The PMLFS is an exact method that has a quadratic convergence but it also presents problems when the initial conditions are not good. Taking into consideration the characteristics mentioned before the authors propose a method that combines the three discussed techniques, but only utilizing the advantages of each one of them to compute the collapse point.

Figure 7 – Lagrange interpolation with the use of multiple load flow solutions

Source: [22].

Figure 7 shows a P-V curve for a specified node of a power system with four operating points (A, B, C, D). From those operating points, a third-order polynomial that represents the mentioned curve can be obtained, as presented in (2.13), the MLP can be approximated by computing the derivative of (2.13) and equalizing to 0. In the following equation a,b,c, and d are the polynomial coefficients.

$$k(V) = aV^3 + bV^2 + cV + d \tag{2.13}$$

Although the method described before is already efficient when the system is operating under light loading conditions the solutions of the power flow in the lower region of the P-V curve might not exist. Therefore, it is necessary an index that indicates when the system is operating under high loading conditions where the solutions in the lower side of the P-V curve are granted. The relation dv/dk from the CPF is a good indicator

of high loading in a power system. The methodology of this paper proposes to find the collapse point by solving the CPF up to a point that is close to the maximum loading condition, if a load level analyzed by the relation dv/dk is determined to be high (point A in Figure 7), then the PMLFS is executed to find the correspondent solution in the lower section of the P-V curve (point B in Figure 7). After finding the unstable point the CPF is executed again to find a new stable point and its correspondent unstable solution with the PMLFS (represented by C and D if Figure 7, respectively), with these 4 points a third-order Lagrange polynomial can be obtained hence, an approximate of the collapse point can be computed by equalizing to zero the derivative of the mentioned polynomial. The final step consists of executing the PoC aiming to find the real collapse point from the previous approximation.

2.2.3 **Estimating the voltage stability of a power system**

This paper can be found in [23], it proposes an index to estimate voltage stability in a power system, it is named the L indicator. It is calculated for each bar of the system, providing a quantifiable margin between the critical point and each node of the system. The L indicator can take values between zero (system without load) and one (MLP).

In the mentioned reference the mathematical formulation is given by an analysis of a simple two bus system after this it provides the formulation generalizing for n nodes, equation (2.14) represents a power system. Where the subscript L and G indicate the load and generation nodes respectively, the I vector corresponds to the currents and V to the voltages, Y_{xx} are the sub-matrices of the admittance matrix.

$$\begin{bmatrix} I_L \\ I_G \end{bmatrix} = \begin{bmatrix} Y_{LL} & Y_{LG} \\ Y_{GL} & Y_{GG} \end{bmatrix} \cdot \begin{bmatrix} V_L \\ V_G \end{bmatrix} \tag{2.14}$$

Expanding the previous equation gives (2.15), that presents the voltages in the load buses. Where Z_{11} and F_{12} are given by (2.16) and (2.17) respectively.

$$V_L = Z_{LL} \cdot I_L - Z_{LL} \cdot Y_{LG} \cdot V_G = Z_{LL} \cdot I_L + F_{LG} \cdot V_G \tag{2.15}$$

$$Z_{LL} = (Y_{LL})^{-1} \tag{2.16}$$

$$F_{LG} = -Z_{LL} \cdot Y_{LG} \tag{2.17}$$

For a specific load bus j the voltage is given by (2.18), where α_L and α_G denote the load and generation buses respectively.

$$V_j = \sum_{i \in \alpha_L} Z_{ji} \cdot I_i + \sum_{i \in \alpha_G} F_{ji} \cdot V_i \tag{2.18}$$

Defining the substitution: $V_{0j} = - \sum_{i \in \alpha_G} F_{ji} \cdot V_i$ (2.19) can be obtained:

$$V_j + V_{0j} = \sum_{i \in \alpha_L} Z_{ji} \cdot I_i \tag{2.19}$$

Multiplying both sides of equation (2.19) by the voltage conjugate (V_j^*), (2.20) can be obtained.

$$|V_j|^2 + V_{0j} \cdot V_j^* = V_j^* \left(\sum_{i \in \alpha_L} Z_{ji} \cdot I_i \right) \tag{2.20}$$

Substituting the definition presented in (eq:sj) the equation (2.20) can be transform into (2.22), where θ is the angle between V_{0j} and V_j.

$$S_j = V_j^* \left(\sum_{i \in \alpha_L} Z_{ji} \cdot I_i \right) = a_j + jb_j \tag{2.21}$$

$$|V_j|^2 + |V_{0j}| \cdot |V_j| \cdot (\cos\theta + j\sin\theta) = a_j + jb_j \tag{2.22}$$

Separating the real and imaginary part of (2.22):

$$|V_{0j}| \cdot |V_j| \cdot \cos\theta = a_j - |V_j|^2 \tag{2.23}$$

$$|V_0 j| \cdot |V_j| \cdot \sin\theta = b_j \tag{2.24}$$

Eliminating θ from the previous equations:

$$|V_j|^4 - \left(2a_j + |V_{0j}|^2\right) |V_j|^2 + a_j^2 + b_j^2 = 0 \tag{2.25}$$

Solving for V_j (2.26) can be deducted:

$$|V_j|^2 = \frac{(2a_j + |V_{0j}|^2) \pm \sqrt{\Delta}}{2} \quad where \quad \Delta = \left(2a_j + |V_{0j}|^2\right)^2 - 4(a_j^2 + b_j^2) \tag{2.26}$$

Since in the MLP there is only one possible voltage, then $\Delta = 0$. The voltage on the collapse point (V_jc) must satisfy (2.27) and (2.28).

$$2|V_jc|^2 = 2a_j + |V_0j|^2 \tag{2.27}$$

$$|V_jc|^2 = \sqrt{a_j^2 + b_j^2} = |S_j| \tag{2.28}$$

From equations (2.19) and (2.28):

$$\left| \frac{V_j + V_{0j}}{V_j} \right| = \left| \frac{V_j^* \sum\limits_{i \in \alpha_L} Z_{ji} \cdot I_i}{V_j \cdot V_j^*} \right| = \frac{|S_j|}{|V_j|^2} \tag{2.29}$$

Sin in the voltage collapse point equation (2.29) is equal to 1, the author defines the indicator L to be:

$$L = \left| 1 + \frac{V_{0j}}{V_j} \right| \tag{2.30}$$

According to [23], the main objective in power systems in order to guarantee voltage stability is to maintain $L < 1$.

2.2.4 A posturing strategy against voltage instabilities in electric power system

In this paper [24] the author proposes as a voltage stability indicator of power systems, the minimum singular value of the Jacobian matrix, from the conventional Newton-Raphson method.

The methodology proposed in the mentioned reference is based on the power flow equations, as shown in equation (2.31), where f are the power flow equations, x are the state variables and p are the active and reactive loads of the system.

$$\overline{f}(\overline{x}, \overline{p}) = 0 \tag{2.31}$$

When (2.31) is derived and equalized to 0, equation (2.32) can be obtained.

$$d\overline{f}(\overline{x}, \overline{p}) = 0 \tag{2.32}$$

If $\overline{x}$ and $\overline{p}$ are regarded as parametrized by a scalar t, then (2.33) may be written explicitly as:

$$\left(\frac{\partial \overline{f}}{\partial \overline{x}}\right) \cdot \left(\frac{d\overline{x}}{dt}\right) = -\left(\frac{\partial \overline{f}}{\partial \overline{p}}\right) \cdot \left(\frac{d\overline{p}}{dt}\right) \tag{2.33}$$

If equation (2.33) is solved, a solution pair (x^*, p^*) such that $\overline{f}(\overline{x^*}, \overline{p^*}) = 0$ is needed and a prescription for the motion of parameter vector $\overline{p}$ as t varies. When (2.31) is derived with respect to the active and reactive loads equation (2.34) can be computed, where $(\overline{I})$ is the identity matrix and $\overline{f_p} = \partial \overline{f}/\partial \overline{p}$.

$$\overline{f_p}(\overline{x}, \overline{p}) = \overline{I} \tag{2.34}$$

Then equation (2.35) can be obtained, where $\overline{f_x} = \partial \overline{f}/\partial \overline{x}$. This equation provides the basis for characterizing static voltage collapse as well as steady-state stability limits [24].

$$\overline{f_x} \cdot \left(\frac{d\overline{x}}{dt}\right) = -\left(\frac{d\overline{p}}{dt}\right) \tag{2.35}$$

Assuming that the load on a generic node i is changing, it is desired to find when the relation $d\overline{p_i}/d\overline{v_i} = 0$, for it is corresponding to the voltage collapse point, in that case equation (2.35) can be written as:

$$\overline{f_x} \cdot \overline{y} = -\left(\frac{d\overline{p}}{dV_i}\right), \quad where \quad \overline{y} = \frac{d\overline{x}}{dV_i} \tag{2.36}$$

Since at the voltage collapse point the relation $d\overline{p_i}/d\overline{v_i} = 0$ and $\overline{y} \neq 0$, it can be seen that the Jacobian matrix is singular at that point. Starting from this, the author proposes to create an index, based on the Jacobian matrix, which will indicate how close is the analyzed system from the MLP. This index is given by the minimum singular value of the Jacobian matrix $(\sigma_{min}(\overline{f_x}))$. The mentioned indicator can be computed with (2.37), this index tends to zero when the system is near the maximum power transfer point.

$$\sigma_{min}(\overline{f_x}) = ||\overline{f_x}^{-1}||^{-1} \tag{2.37}$$

According to the author, a disadvantage of using the minimum singular value index is a large amount of CPU time required in performing a singular value decomposition for a large matrix. The computation speed can be significantly improved using parallel processing.

2.2.5 A fast method for determining the voltage stability limit of a power system

This work can be found in [25], it proposes a fast method to find the maximum load, especially the reactive power demand, at a particular PQ node before reaching the collapse point. The mentioned reference uses the base operating point to find an equivalent system of two nodes to analyze the voltage stability problem.

The article demonstrates the concept of voltage stability problem using a simple two bus system because the same concept is later applied to determine the maximum loading capacity of a particular load bus in a large power system. Considering the simple two bus system of Figure 8.

Figure 8 – Two bus system
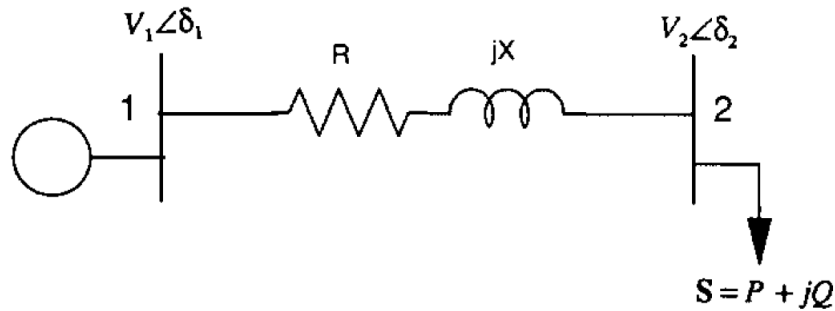
Source: [25].

The generator located at bus 1 transfer power thru a transmission line that has impedance $Z = R + jX$ to the load bus 2. Node 1 is considered the swing bus thus maintaining fixed its voltage magnitude V_1 and its angle δ_1. Hence, for a given value of V_1 the relationship between the voltage magnitude at node 2 V_2 and the the apparent load $S = P + jQ$ can be expressed as:

$$V_1^2 = V_2^2 + 2(RP + XQ) + (R^2 + X^2) \cdot \frac{P^2 + Q^2}{V_2^2} \tag{2.38}$$

If it is assumed that $x = V_2^2$, equation (2.38) can be written in polynomial form as follows:

$$a_1 x^2 + b_1 x + c_1 = 0 \tag{2.39}$$

Where:

$$a_1 = 1$$

$$b_1 = 2(RP + XQ) - V_1^2$$

$$c_1 = (R^2 + X^2)(P^2 + Q^2)$$

The positive values of V_2 can be obtained from equation (2.39) as follows:

$$V_2^H = \left(\frac{-b_1 + d^{1/2}}{2a_1}\right)^{1/2} \tag{2.40}$$

$$V_2^L = \left(\frac{-b_1 - d^{1/2}}{2a_1}\right)^{1/2} \tag{2.41}$$

Where d is given by:

$$d = b_1^2 - 4a_1c_1 = V_1^4 + 4[2PQRX - V_1^2(RP + XQ) - R^2Q^2 - X^2P^2] \tag{2.42}$$

In equations (2.40) and (2.41) denote the high voltage or stable voltage and the low voltage or unstable solution respectively. When the load is null ($P = Q = 0$), V_2^H and V_2^L become V_1 and 0 respectively, and as the load increases, V_2^H decreases while V_2^L increases. This will continue until $V_2^H = V_2^L$, the load power at which this happens is called the critical power and the corresponding voltage is the critical voltage, at this point the value of d in equation (2.42) becomes zero. Therefore, the condition of the maximum load apparent power (S_m) can be obtained by setting the value of d in (2.42) to zero. This gives the following equation:

$$a_2S_m^2 + b_2S_m + c_2 = 0 \tag{2.43}$$

where:

$$a_2 = 4[RX\sin(2\theta) - R^2\sin^2\theta - X^2\cos^2\theta]$$

$$b_2 = -4V_1^2(R\cos\theta - X\sin\theta)$$

$$c_2 = V_1^4$$

The apparent load power S_m can be obtained from the solution of (2.43):

$$S_m = \frac{V_1^2}{2}\frac{|Z| - (R\cos\theta + X\sin\theta)}{(R\sin\theta + X\cos\theta)^2} \tag{2.44}$$

It can be noted that the other solution of equation (2.43) is not feasible due to its negative value. The corresponding value of the critical voltage (V_{cr}) can be found from (2.40) or (2.41) when the value of S_m is known, this by setting $d = 0$ and evaluating b_1 at the maximum load apparent power S_m. Therefore, the critical voltage for a given load PF angle θ is computed as follows:

$$V_{cr} = \left[\frac{V_1^2 - 2S_m(R\cos\theta + X\sin\theta)}{2}\right]^{1/2} \tag{2.45}$$

After formulating the problem the author proposes a method for determining the two bus equivalent system or Thévenin equivalent for each bus. The methodology consists of finding the Thévenin impedance and Thévenin voltage. The two expressions for these parameters are equations (2.46) and (2.47) respectively, where Z_{Th} is the Thévenin impedance, Z_{kk} is the kth diagonal element of the Z matrix, Z_k^L is the load impedance on node k, V_k is the voltage on node k and V_{Th} is the Thévenin voltage.

$$Z_{Th} = \left(\frac{1}{Z_{kk}} - \frac{1}{Z_k^L} \right)^{-1} \tag{2.46}$$

$$V_{Th} = \left(1 + \frac{Z_{Th}}{Z_k^L} \right) V_k \tag{2.47}$$

When the Thévenin equivalent circuit of a general power network "seen" from a particular load bus is determined, all the equations derived from the analysis made with the two bus system can be used to assess the voltage stability problem associated with that bus.

2.2.6 Fast method for computing power system security margins to voltage collapse

A method for determining the MLP of a power system as well as determining the loading margin is presented in [26]. Sensitivity analysis is used to drive the system from the base case operating point to the vicinity of the critical point along a predefined load increase direction. In case the sensitivity analysis drives the system to the infeasible operating region, a special load flow method with step size optimization is used so that relevant information can be obtained to restore the feasibility. Finally, the critical point is estimated from a certain number of conventional load flow calculations for different operating points in the vicinity of the critical point, by increasing the load along the predefined direction.

After determining the operating point of a power system by solving a conventional power flow, given a predefined load increase direction a sensitivity analysis can be performed, where it can be shown that changes in the reactive power at generating units ΔQ_G can be expressed as a function of changes in the control variables and parameters by:

$$\Delta Q_G = S_{wu}\Delta u + S_{wp}\Delta p \tag{2.48}$$

Where S_{wu} and S_{wp} are sensitivity matrices. Suppose that the load bus i is to be increased up to the point where a generator reaches its reactive generation limit. For a

system that has NG generation nodes, the load increase is defined as follows:

$$\Delta S_i = \min_{j} \left[\frac{(Q_{Gj}^{lim} - Q_{Qj})}{\sigma} \right], \ j = 1, ..., NG \tag{2.49}$$

Where ΔS_i may represent an increase in real power, reactive power or both, Q_{Gj} and Q_{Gj}^{lim} are the actual generated reactive power and the reactive power limit at bus j respectively. σ is a sensitivity factor obtained from S_{wp}.

The basic idea is to compute load increases iteratively until the MLP is reached. Although when several load increases are made, a value higher than the MLP might be reached, driving the system to an infeasible operating region, in other words, the load is higher than the maximum allowable power of the system. In order to overcome this issue, the author proposes an especial power flow with optimized step size, that provides important information to perform adjustments in the loads thus, allowing the system to operate within the feasible operating region and close to the collapse point.

When an operating point close to the MLP is found, successive power flow solutions are obtained towards the specified load increments direction until the collapse point is reached, by doing this, it is possible to compute the loading margin. The previously mentioned process is illustrated in Figure 9.

Figure 9 – Illustration of methodology
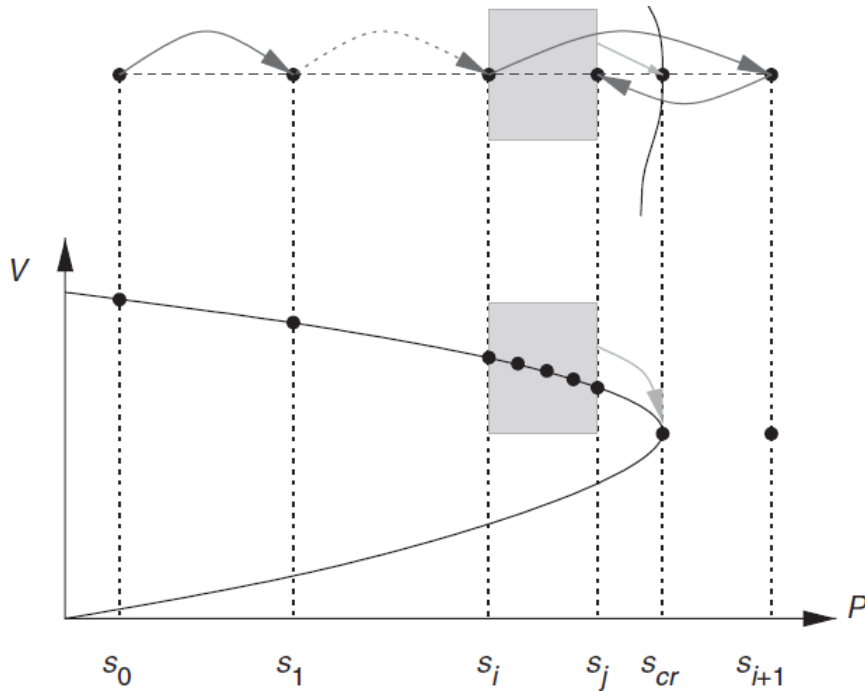
Source: [26].

2.2.7 Development of indicators based on Thévenin equivalent circuits for security voltage assessment in power systems

In this work, that can be found in [14], presents several indexes that help to determine the distance between a system's operating point and the MLP. All the indicators proposed in the mentioned reference are based on the maximum allowable power transfer of electric linear system, where at the voltage collapse point the Thévenin impedance module matches the load impedance module. These indexes are computed for each node of the analyzed system, showing which of them operate close to the MLP, providing a classification of the most critical nodes of the system.

The main contribution of this work is that, to compute these indexes the sensitivity analysis of the Jacobian matrix of the power flow solution is used, hence the process is extremely fast. The mathematical formulation of one of these indicators is going to be detailed in the next chapter because it is one of the tools utilized to construct SSSR with voltage stability security limits.

2.3 PARTICLE SWARM OPTIMIZATION ALGORITHM

2.3.1 Particle Swarm Optimization

In 1995 the particle swarm optimization was presented in [27], it introduced the concept of optimization of non-linear continuous functions.

According to the author:

> (...) "particle swarm optimization has roots in two main component methodologies. Perhaps more obvious are its ties to artificial life in general, and to bird flocking, fish schooling, and swarming theory in particular. It is also related, however, to evolutionary computation, and has ties to both genetic algorithms and evolutionary programming."

The author describes the evolution of particle swarm intelligence simulations that were made at that moment. The first satisfying simulation consisted of initiate a random "bird" population with a position on a pixel grid with X and Y velocities. At each iteration the algorithm determined, for each "bird" or particle, which other particle was its closest neighbor, then it assigned the velocities X and Y of the particle that was being analyzed, that simple rule created a synchronous movement. Although, the problem was that quickly the group of particles stayed in the same position without changing directions. Therefore, a stochastic variable named "*craziness*" was inserted into the algorithm. At each iteration, a random change in X and Y velocities was added.

A second simulation was later performed, where a two-dimensional vector with XY coordinates was added. Each particle was meant to evaluate its current position with the following equation:

$$Eval = \sqrt{(presentX - 100)^2} + \sqrt{(presentY - 100)^2} \qquad (2.50)$$

The particles were programmed to find the position $(100, 100)$, at that position the value of (2.50) would become 0.

Then each particle "remembered" its best position (XY coordinates) which had resulted in that value. The mentioned value was named "$pbest$". Then the velocities were adjusted in a simple fashion, depending on the updated position a random amount weighted by a parameter of the system was added or subtracted from the current velocity.

Each particle also "knew" the globally best position that one member of the flock had found and its value. This was accomplished by simply assigning the array index of the agent with the best value to a variable called "$gbest$".

Later the authors found that the algorithm works just as well, and looks just as realistic, without craziness, so it was removed. Next, it was shown that optimization actually occurs slightly faster when the nearest neighbor velocity matching is removed. The variables "$pbest$" and "$gbest$" and their increments are both necessary. Conceptually "$pbest$" resembles autobiographical memory, as each individual remembers its own experience. On the other hand, "$gbest$" is conceptually similar to publicized knowledge, or a group norm or standard, which individuals seek to attain.

Although the algorithm already worked well, velocity adjustments were based on a crude inequality or, as explained before, they were adjusted according to their current position and according to the authors that made it harder to understand. Therefore, rather than simply testing the particles' current position, velocities were adjusted according to their difference, per dimension, from best location, as follows:

$$v = v + rand \times p\_increment \times (pbest - present) \qquad (2.51)$$

The authors determined that there was no satisfying manner to guess whether the increment factor (local or global) should be larger. Therefore, these terms were also eliminated from the algorithm. The stochastic factor was then multiplied by 2 to give a "weight" of 1 so that particles would move over the target about half the time. Then the following equation was determined:

$$v = v + 2rand(pbest - present) + 2rand(gbest - present) \qquad (2.52)$$

2.3.2 **The particle swarm: social adaptation of knowledge**

This work can be found in [28], it discusses different approaches that can be used with the PSO algorithm, it also introduces a new parameter for improving the performance of the algorithm.

First of all it discusses the use of generic constants in equation (2.52), that depend on the type of problem, instead of using fixed values of 2 thus, the mentioned equation can be rewritten as:

$$v = v + c_1 rand(pbest - present) + c_2 rand(gbest - present) \qquad (2.53)$$

The author called the second term of (2.53) the "cognitive" element of the particles since that is the term that gives the particle an individual behavior. The third term of the previous equation was named the "social" part which represents the collaboration among the particles.

A new parameter was added to the algorithm which is associated with the particles' velocities, the mentioned parameter is v_{max} which limits the maximum value that the velocity can acquire during each iteration. According to the author, this parameter has three objectives:

- Keeping the computer from overflowing;

- Realistically simulate the incremental changes of human learning and attitude change;

- Determine the granularity of search of the problem space.

The mentioned limit is easy to implement by specifying that if:

$$v > v_{max} \quad then \quad v = v_{max} \qquad (2.54)$$

$$v < -v_{max} \quad then \quad v = -v_{max} \qquad (2.55)$$

The authors then discuss the use of different variations of the algorithm to optimize a function, first, it uses the full particle swarm model, in other words using equation (2.53), and using different parameters of c_1, c_2 and v_{max}. The authors conclude that Some parameter combinations were rather vulnerable to local optima, and others were not. In general, when v_{max} was low, particles had more difficulty escaping from locally optimal regions. v_{max} determines how large steps through the data space each particle is allowed to take; when these steps are constrained to be small, individuals may be unable to step out of poor regions.

Afterward, a different approach was used name the "*cognition-only*" model. The paper mentions that cognitive science has tended to treat individuals as if they were isolated, and as if cognition occurred inside the head, privately. As mentioned before the "cognitive" part of equation (2.53) which represents the private thinking. Thus it was possible to test the cognitive part of the particle swarm algorithm by reformulating the mentioned equation as follows:

$$v = v + c_1 rand(pbest - present) \tag{2.56}$$

In the different tests made by the author, this version of the PSO algorithm was only slightly more vulnerable to failure than was the full model, in terms of finding a global optimum. It appeared that most of the time this version failed to converge, the problem was more one of failure to find an optimal region than of being captured by local attractors. Individuals in this version tended to search the areas in which they had been initialized, and, at least when v_{max} and c_1 were both small, they failed to move into optimal regions. In median comparisons, the "*cognition-only*" model required more iterations than the full model to converge to the optimal solution.

The "*cognition-only*" model performed rather well. As an adaptive method, the individual approximation to the optimum seemed to function satisfactorily, though not nearly as well as the full model. This version was susceptible to failure only when both parameters (c_1 and v_{max}) were set very low, but required more iterations to satisfy the criterion of the global optimum. This model serves as base for one of the methodologies developed in this dissertation, this will be detailed in further chapters.

Another approach was also tested, it was called by the author the "*social-only*" model, it consisted on only using the third term of equation (2.53) as follows:

$$v = v + c_2 rand(gbest - present) \tag{2.57}$$

This model implies a social process with no special tendency for individuals to return to a previous position that had proven successful for themselves in the past. Rather, individuals compare the effectiveness of positions of neighborhood members and change toward those that are relatively successful. the "*social-only*" algorithm converged faster than the full model, and faster than the "*cognition-only*" version in the author's testes.

2.3.3 A modified particle swarm optimizer

This article can be found in [29], it introduces a new parameter to improve the PSO algorithm performance, this parameter is called the inertia weight w. This w plays the role of balancing the global search and local search of the algorithm.

As explained before, equation (2.53), that serves to update the particles' velocities at each iteration, consists of three parts, the first part is the previous velocity of the particle, the second and third terms provide the particles a "cognitive" and "social" behavior. Without these terms, each particle would continue updating its position with the same velocity and trajectory until reaching any boundary. In this case, the PSO algorithm would not find a satisfying solution unless the desired solution is on the same trajectory of the mentioned particle, but that would be a rare case.

On the other hand, as the author explains, without the first term of the equation, the particles' velocities would only be dependent on their current positions and their best positions in history, the velocity itself would be memoryless. For example, if it is assumed that a generic particle i has the best global position, then this particle would keep the same position until another particle takes over the best global position thus, it would not explore new spaces. Therefore, it can be said that the search process for PSO without the first part of (2.53) is a process where the search space becomes smaller along with the iterations hence, it resembles a local search algorithm.

By adding the first part of the equation, the particles tend to expand the search space, that is, they have the ability to explore new solution spaces. Although, according to the article, for different problems, there should be different balances between the local search ability and global search ability.

Considering what was mentioned before, the author added the inertia weight parameter w to the PSO, aiming to balance the local and global search aiming to generalize the algorithm for all types of problems. This parameter can be a positive constant or even a positive linear or non-linear function of time. The new PSO equation for updating the velocity can be written as follows:

$$v = wv + c_1 rand(pbest - present) + c_2 rand(gbest - present) \qquad (2.58)$$

To be able to see the difference that this new parameter brought to the PSO algorithm several tests were made by the author. In this article several conclusions were obtained, the first one was that for a small value of w ($w < 0.8$) if the PSO find a global optimum, it finds the solution with a small number of iterations, and that all the particles tend to move together quickly. That shows that when a small value of w is used, the PSO resembles a local optimum search algorithm. In other words, if the global optimum solution is near the initial search space, then the PSO will find the desired solution, otherwise, it will not be able to find a satisfying solution.

On the other hand, the paper explains that when a large value of w is adopted ($w > 1.2$), the PSO has a greater possibility to find a global optimum solution, even if the desired solution is not close to the initial search space, this is possible because the

particles tend to explore new areas. It was also proven that configuring the parameter in this manner would make the PSO use more iterations to find the optimal solution and that it has more chances of failing to find the global optimum.

When a medium value of w ($0.8 < w < 1.2$) was used in the article, the PSO had the best performance (when w was a fixed constant) but it also took a considerable amount of iterations to find the optimal solution. It was concluded that, for a fixed value of w, the bigger the inertia weight is, the less dependent on the initial population the solution is, and the more capable of exploiting new search areas.

According to the author for any optimization search algorithm, generally, it is desired to possess more exploitation ability at the beginning of the iterations to find a good "seed", then it is better to have a more exploration ability to fine search the local area around the "seed". Therefore, the paper proposed to defined the inertia weight w as a decreasing function of "time" (iterations) instead of a fixed positive value, this is defined as follows:

$$w^h = (w_{ini} - w_{end}) \times \frac{h_{max} - h}{h_{max}} + w_{end} \qquad (2.59)$$

Where, h is the current iteration number, h_{max} is the maximum number of iterations, w_{ini} is the initial inertia weight and w_{end} is the inertia weight when h_{max} is reached. This provides the PSO algorithm with a hybrid behavior between exploitation and exploration.

In this paper were made tests with a high initial value (1.4) and linearly decreased to 0 when the iteration number reached its maximum value. The results were much better than the ones obtained when the inertia weight parameter was set as a positive constant, in terms of failure and the number of iterations needed to find the global optimum.

2.3.4 Particle swarm optimization: basic concepts, variants and applications in power systems

This work can be found in [30], it presents a detailed overview of the concepts used in the PSO algorithm and its different variants. It also provides a very complete survey on the power systems applications that have taken advantage of the powerful nature of the PSO algorithm as an optimizer. For each application were detailed technical aspects that are required for solving the problem with the PSO technique, such as its variant, particle formulation and the most efficient objective functions are also explained.

The author lists the following as key advantages of the PSO algorithm over other similar optimization techniques such as the genetic algorithm:

- PSO is easier to implement and there are fewer parameters to adjust;

- In PSO, every particle remembers its own previous best value as well as the neighborhood best; therefore, it has a more effective memory capability than the genetic algorithm;

- PSO is more efficient in maintaining the diversity of the swarm (more similar to the ideal social interaction in a community), since all the particles use the information related to the most successful particle to improve themselves, whereas in the genetic algorithm, the worse solutions are discarded and only the good ones are saved; therefore, in the genetic technique the population evolves around a subset of the best individuals.

In the following subsections, the main applications of the PSO algorithm in power systems are discussed as they were mentioned in [30].

2.3.4.1 *Reactive power and voltage control*

Firstly the author explains the main problem of reactive power and voltage control on power systems, which are susceptible to unexpected contingencies or simply load variations that change the networks' configuration. Therefore, maintaining the voltage levels within acceptable ranges for costumers is one of the most important tasks of the system's operators. To accomplish this, power utilities can control the generating units, transformers taps, FACTS devices and shunt compensation in a way that they generate the necessary reactive power to keep voltage levels at satisfying levels. As mentioned in this article an *on-line* strategy to achieve this is named "reactive power and voltage control" or VVC.

VVC needs to warrant that voltage security is met, such that the system does not move towards uncontrolled voltage collapse. VVC is formulated in the mentioned reference as follows:

$$Minimize \sum Loss \tag{2.60}$$

Subject to the following constraints:

- Voltage at each node must lie within its permissible range.

- Power flow of each branch must be lower than the maximum allowable.

- Transformer tap positions must be within the available range of steps.

- Generator reactive powers must lie within their permissible range.

The author discussed that conventional analytical optimization techniques tend to be difficult to apply in this application due to the large dimension if the problem. On the other hand, PSO is an efficient optimizer that can handle mixed-integer non-linear optimization problems (MINLP) with ease and can be a better strategy to solve the mentioned problem.

2.3.4.2 *Power system reliability and security*

As discussed in this article, the reliability indices of a power system have been determined through contingency analysis over the years, which for a large grid, considering several faults, can be extremely complex and requires a high computing effort. The author cites applications were the PSO is used for identifying the set of network elements, which if disconnected, would possibly lead to a cascading series of events resulting in widespread damage to the network, for this specific application the PSO algorithm is used to solve a binary optimization problem.

Another application presented in this paper is the feeder reconfiguration, which is a technique used for improving the quality/price of service supplied to the customers while maintaining/increasing the system reliability. This problem is formulated as a non-linear optimization problem subject to the security constraints that are desired for the distribution network, these might be not exceeding the feeder capacities or node voltage level while keeping the radial structure of the network. As mentioned by the author, several researchers have successfully implemented the application of binary PSO in feeder reconfiguration in the distribution system. In all cases, the particles are defined as an array formed by binary numbers, each binary number is associated with a switch in the distribution system that can be open or closed.

One of the techniques, cited by the author, that helps to improve the power system reliability where the PSO is utilized is identifying points on the security border of the power system thus, finding vulnerability indicators for the operating point. In this case, the PSO is used to evaluate the security index of the electric grid in real-time. The aim is to determine as many points on the security edge as possible. It is achieved by defining a separate group (within the swarm) for each point to be placed on the edge, where each operating point is defined as a particle.

Lately, the PSO algorithm has also been used to solve the under voltage load shedding problem. The concept of dynamic security constraint optimal power flow is implemented to develop the optimization model. According to the author, benchmarks have been performed comparing the PSO and genetic algorithms for this specific problem, and the PSO generates better solutions than the genetic algorithm.

2.3.4.3 *Generation expansion problem (GEP)*

It is discussed in this article that, the deregulation of electrical markets has created a high competition in the generation sector. This has brought the generation expansion problem (GEP) to become an important topic for investors when they make economic decisions. The solution of this problem consists of determining what, when, where and how to install new power plants to satisfy the power system requirements while constraints such as demand, reliability, security, operating conditions, power quality are maintained within acceptable margins.

The GEP aims to maximize profits but also, to minimize investment risks over long-term planning. This problem can be mathematically formulated as a large dimensional, non-linear, non-convex, mix-integer and highly constrained optimization problem with the objective function set to minimize the investment cost. The complexity of the GEP highly increases if many practical constraints are taken into consideration. Therefore, efficient tools to solve the GEP have to be implemented.

According to the author, the traditional optimization techniques are also used to solve the GEP but they present weakness when handling qualitative constraints and they are slow in computational performance. Hence, in the later years the heuristic methods, like the PSO algorithm, have been largely used in this application, showing as the main advantage their flexibility to handle a vast amount of qualitative constraints that are common in the GEP in the deregulated power industry.

2.3.4.4 *State estimation*

This article describes state estimation as a critical element in distribution power utilities, especially with the insertion of distributed generation (DG) to the electric grid. Network operators need to estimate in real-time and in an accurate way the loads and DG outputs, while the available measurements through the grid are normally limited. State estimation is formulated as follows:

$$Minimize \ \ J(x) = \sum_i w_i \cdot (z_i - f_i(x_i))^2 \tag{2.61}$$

Where x_i, z_i and w_i are the state variables i, measurement values (generally voltages and currents) for measurement variable i and its related weighting factor respectively. f_i is the power flow equation that associates the state variable x_i to the measurement variable z_i.

As cited in this paper the above minimization problem can be solved with conventional techniques, using statistical or sensitivity analysis methods, although these techniques assume that the objective function is differentiable and continuous. However, this is not

true due to non-linear devices present in the electric grid, such as shunt compensation, DGs and transformers with on-load tap changers. These devices make the system equations and, hence, the objective function, non-linear, discontinuous and not differentiable. Therefore, the PSO algorithm becomes a strong alternative to solve the mentioned problem due to its strong non-linear optimization abilities.

2.3.4.5 *Other applications*

The paper lists several more applications in power systems where the PSO has been reportedly used in literature:

- Economic dispatch;

- Load flow and optimal power flow;

- Power system identification and control;

- Electric machinery;

- Capacitor and FACTS placement;

- Generator Maintenance and Unit-Commitment Scheduling;

- Short-Term Load Forecasting;

- Generator Contributions to Transmission System.

In Table 1 are specified the different variants of the PSO that are used in each power system application.

Table 1 – Application of PSO Variants in Power Systems

Aplication	PSO Variant
Reactive power and voltage control	Conventional PSO, Integer PSO, Adaptive PSO
Economic Dispatch	Conventional PSO, Evolutionary Programming PSO
Power System Reliability and Security	Conventional PSO, Binary PSO
Generation Expansion Problem	Conventional PSO, Stretching PSO, Composite PSO
State Estimation	Conventional PSO, Hybrid PSO (with Genetic algorithm)
Load Flow and Optimal Power Flow	Conventional PSO, Hybrid PSO, Vector Evaluated PSO, PSO with Passive Congregation, Dissipative PSO
Power System Identification and Control	Conventional PSO, Hybrid PSO
Electric Machinery	Conventional PSO
Capacitor Placement	Conventional PSO, Integer PSO
Generator Maintenance Scheduling	Conventional PSO, Evolutionary Programming PSO
Short-Term Load Forecasting	Conventional PSO
Generator Contributions to Transmission System	Vector Evaluated PSO

2.4 CHAPTER SUMMARY

This chapter provided a summarized view of some of the papers that have being published related to the topics that are studied in this work. A division of the three main tools that are used in the proposed methodologies was made. Firstly works related to the SSSR were discussed, where it could be seen that that the security regions can also be used for dynamic analysis of power systems, thus, this tool is not tieded to steady-state analysis. Later several papers that presented methodologies for the analysis of voltage stability were shown, some of these papers proposed methods based on the Thévenin impedance, which is going to be essential in the first methodology proposed in this work. The last section of this chapter reviewed the origins and evolution of the PSO algorithm throughout various papers, different approaches for this method were shown, finally a summary of the main power systems applications of this optimazation algorithm was discussed.

3 ENHANCED STEADY-STATE SECURITY REGION

This chapter will address the first methodology that is developed in this work, it combines the SSSR presented in [13] and the voltage stability index (VSI) presented in [14], in order to create an enhanced SSSR that allows monitoring the voltage instability condition in a power system. In section 2.1.2 was given a brief explanation of the construction process of the SSSR. Therefore, in the following section of this chapter, a detailed explanation of the SSSR definitions and details about the construction process will be provided. Section 3.2 will give a detailed explanation about the VSI, including its mathematical formulations, advantages and disadvantages. Finally the proposed methodology to construct the enhanced SSSR will be detailed.

3.1 STEADY-STATE SECURITY REGION REVIEW

3.1.1 **Characteristics**

The SSSR is a very effective tool to analyze the security of power systems, under steady-state conditions. It is a three-dimensional graph that shows the region where a power system can operate without violating any limit, from a list that is pre-established before. Each axis represents the active generated power of a generation group. Therefore, the power system has to be divided into three generation sets, an illustration of the SSSR is presented in Figure 10.

Figure 10 – Illustration of the SSSR
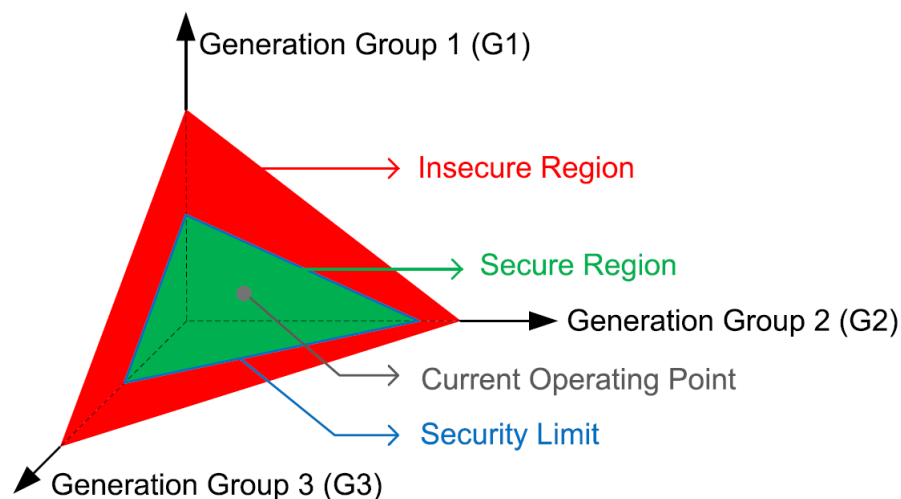
Source: [13].

The safe operating zone is created around the original operational point and it is bounded by the violation of a limit or several limits. Normally the limits that are used to construct the SSSR are voltage level on nodes, thermic limits on transmission lines, active and reactive power generation and convergence of the power flow problem.

This tool accomplishes one of the most important and difficult challenges of on-line assessment, that is, to display in an understandable and easy manner the safest dispatch profile of a power system. The SSSR allows, by simple visual inspection, to determine the security of an electric grid, in essence, it is only necessary to observe the "distance" between the operating point and the nearest limits.

Aiming to facilitate the graphical analysis of the SSSR, the mentioned three-dimensional graph is normally shown as two-dimensional projections of the original figure, and they are named nomograms, an illustrative nomogram is presented in Figure 11.

Figure 11 – Illustrative nomogram.
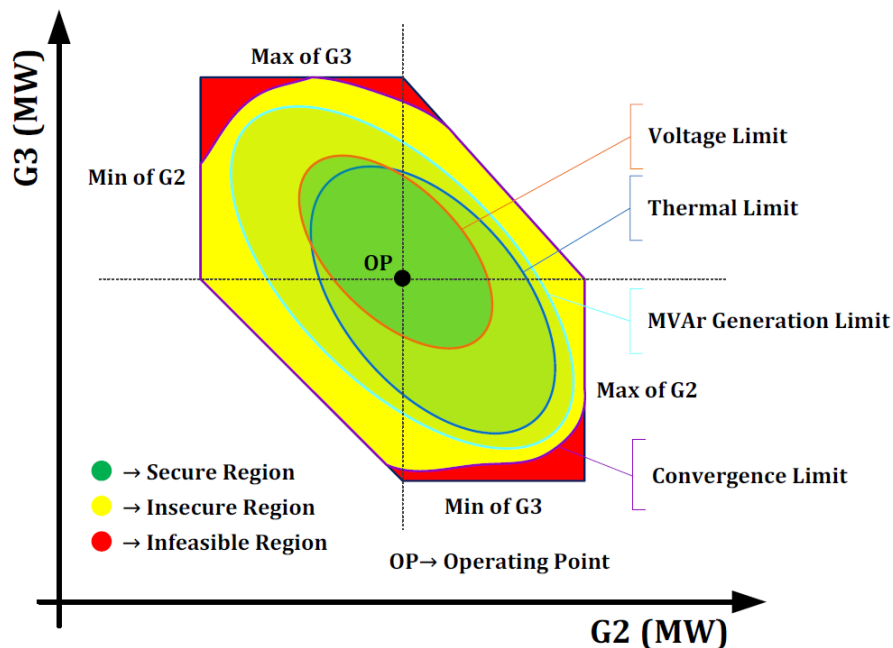
As described in [13] the SSSR possesses the following characteristics:

- Displays the security limits of a power system;

- Performs a contingency analysis of all the possible dispatch scenarios, including the original operating point;

- Allows analyzing the security condition of the current operating point;

- Monitors the conditions to attend a load, with different dispatch profiles of the three generation groups.

3.1.2 Construction Process

As it was briefly described in section 2.1.2 the SSSR construction process is comprehended of four stages, these will be addressed with more detailed in the following subsections.

3.1.2.1 *Division of the system into three generation groups*

As explained before, each axis of the SSSR represents the generation output of the generation groups. Therefore, this step is crucial for the construction of the three-dimensional graph, these groups are defined by the user according to the analysis that is going to be performed. A specific group can be composed of only one generator, by a set of generation units of the same subsystem of the same company, or a set of hydroelectric power plants of the same watershed. As described in [31], an adequate manner of determining the generation groups should follow the following suggestions:

- Join up areas of the power system in which it is wanted to monitor the interconnections and to determine the maximum and minimum power transfer between them;

- Group areas of the system conducive to receive reinforcements in the transmission network, such as new equipment of voltage control. These areas require monitoring of the nodes and components of the transmission network, aiming to determine the voltage collapse point, to prevent voltage instability, weak reactive power injection, and overloaded circuits.

A representation of the division of the power system into the generation groups is shown in Figure 12.

Figure 12 – Division of the power system
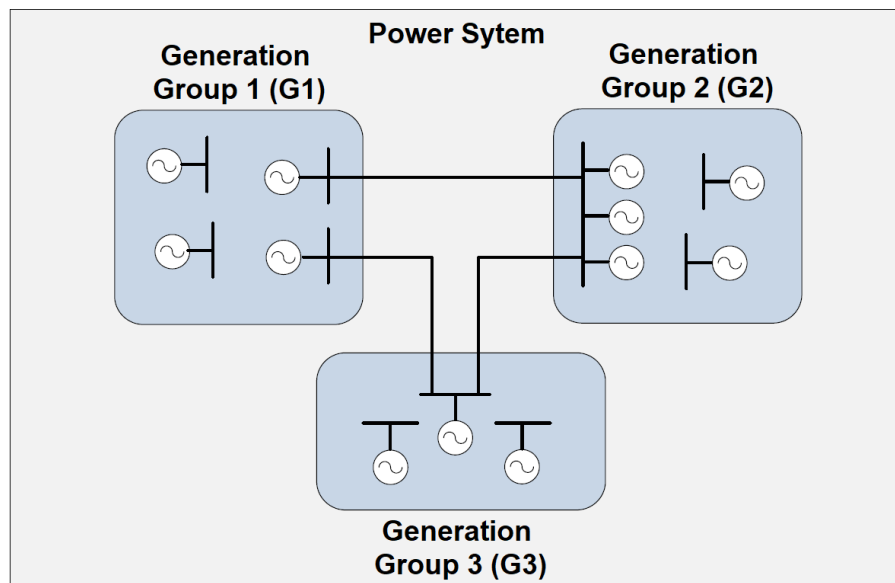
Source: [31].

It is important to emphasize that the SSSR can be an *N*-dimensional graph therefore, the system can be divided into more generation groups. Although this is not practical in terms of computational performance, since it would require an enormous

computing time besides this, the analysis would become harder since there would be several nomograms to assess hence, taking away the advantage of easy comprehension that the SSSR possesses.

In order to determine the security limits, the tool presented in [32] is used, which allows computing the maximum allowable power transfer between the three generation groups. This tool requires the division of the power system into two subregions (EXPR and IMPR) to determine the maximum power transfer between them.

In essence, this tool performs successive changes in the generation profile of the two regions mentioned before, increasing the generation in the EXPR and decreasing the generation of the IMPR at the same rate, this continues until one of the security limits is violated.

As it can be noted the methodology presented in [32] was developed for two generating regions thus, to be able to use this tool in the construction of the SSSR it has to be adapted for three generating zones. As explained in [31], the EXPR and IMPR should be formed by a maximum of two generation groups. Since the construction process of the SSSR consists of exploring different dispatch scenarios, the EXPR and IMPR will be formed by different groups along the process. In Figure 13 is presented a dispatch scenario where the generations groups G1 and G2 are part of the EXPR and the generation group G3 forms the IMPR.

Figure 13 – Exporting and importing regions of a power system

Source: [31].
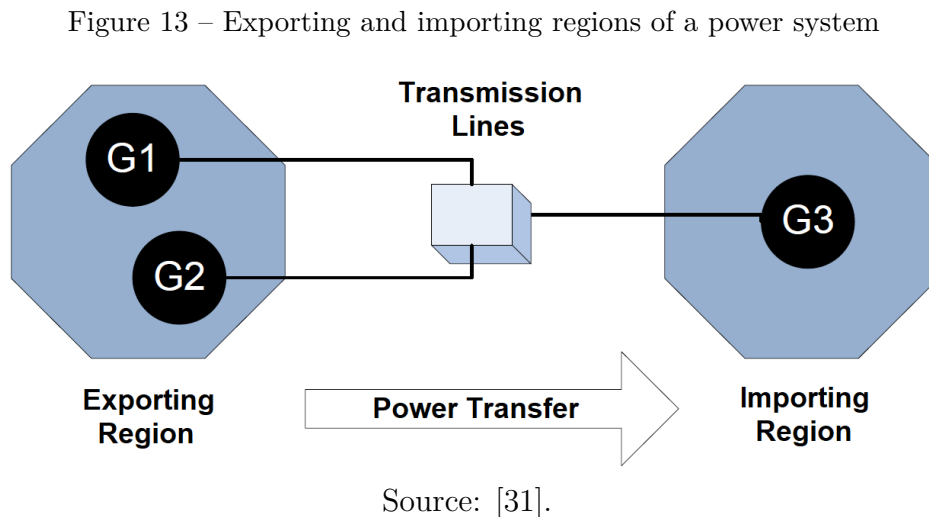
3.1.2.2 *Determination of the importing and exporting regions*

As explained before the SSSR consists of exploring dispatch scenarios around the original operating point. As the problem is treated as a three-dimensional graph there are innumerable scenarios that can be explored to attend a fixed load. The analysis of all the possible dispatch scenarios is made from a nomogram, in other words, it is a two-dimensional analysis, any of the three projections can be used to make the assessment.

The process will be demonstrated in this work using the G2xG3 nomogram, as shown in Figure 14. The group that is not part of this nomogram automatically becomes the "swing" group, and it is in charge of maintaining the power balance, therefore, it will modify its generation profile as a consequence of the modifications in the other two groups.

Figure 14 – G2xG3 nomogram analysis
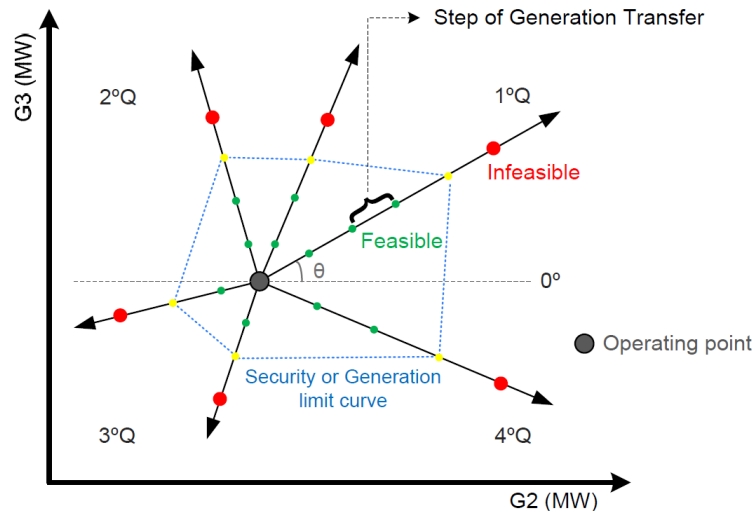
Source: [13].

In order to explore the dispatch scenarios, the nomogram shown in Figure 14 can be represented as a Cartesian plane, as shown in Figure 15, where the original operating point is the origin. To modify the generation profile of the groups a series of steps are made starting from the operating point "advancing" radially towards the opposite direction of the origin, this is performed on different angles around the original operating point, as illustrated in Figure 14. This procedure ensures that each group will increase or decrease its generation thus, forcing power transfer between them.

Figure 15 – G2xG3 nomogram as a Cartesian plane
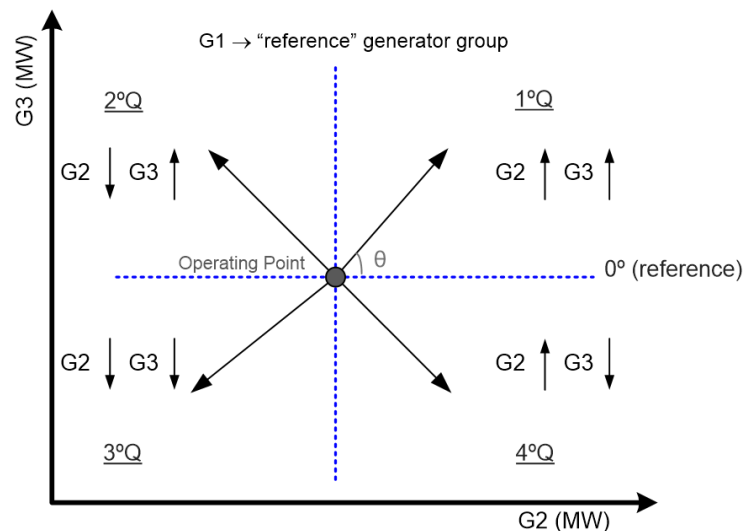
Source: [13].

It can be said that the EXPR and the IMPR are defined depending on the direction that is being analyzed on the G2xG3 plane. Figure 15 shows which groups increase and decrease their generation according to the quadrant of the analyzed direction. The angles that define the directions that are going to be explored can be obtained from 3.1 and 3.2.

$$\bar{\theta} = \theta_0 + i \cdot \alpha \tag{3.1}$$

$$\alpha = 360/N_D \tag{3.2}$$

Where:

$\bar{\theta}$ = Vector that contains the directions' angles to analyze;

θ_0 = Reference angle, standardized as 45^0;

N_D = Number of directions to analyze;

$i = 0, 1, 2, ..., N_D$;

α = Angular offset between directions.

It can be observed from the previous equations that the angular offset is homogeneous between all the directions, this way the four quadrants are explored hence, better accuracy is expected since the curves will be plotted around the operating point.

Special attention is needed for the cases where the dispatch of the three generation groups occurs in a different proportion. For example, if it is chosen a direction of the second quadrant, assuming that θ is between 90^0 and 135^0 the EXPR is formed by the group G3, and the IMPR is composed of the group G2. For these particular angles, G3 is increasing its generation at a higher range than the generation decrease of G2. Therefore, group G1, which is the "swing" group, in this specific case, has to reduce its generated power, forcing the IMPR to absorbs the power surplus of the EXPR. On the other hand, for a specific direction where θ is between 135^0 and 180^0, G3 and G2 are still forming the EXPR and IMPR respectively. However, for these angles, G3 increments its generation at a lower rate than the generation decrease of G2, thus, G1 has to increment its generated power [31]. Table 2 provides all the possible dispatch scenarios for the definition of the IMPR and EXPR, according to the quadrant and angle of the directions.

It can be seen in Table 2 that the angular analysis provides characteristics that allow the assessment of different dispatch scenarios, even with the participation of two generation groups, and three generation groups, modifying the composition of the IMPR and the EXPR according to the selected directions. The angular analysis allows to organize the different dispatch scenarios that are going to be explored, in a easy and understandable manner.

Table 2 – Definition of the IMPR and EXPR according to the quadrant and angle of the direction

Quadrant	Angle	Region	
		Exporting	Importing
1st	$0^0 < \theta < 90^0$	G2+G3	G1
2nd	$90^0 < \theta < 135^0$	G3	G1+G2
	$\theta = 135^0$	G3	G2
	$135^0 < \theta < 180^0$	G1+G3	G2
3rd	$180^0 < \theta < 270^0$	G1	G2+G3
4th	$270^0 < \theta < 315^0$	G1+G2	G3
	$\theta = 315^0$	G2	G3
	$315^0 < \theta < 360^0$	G2	G1+G3
-	$\theta = 0^0$ or 360^0	G2	G1+G3
	$\theta = 90^0$	G3	G1
	$\theta = 180^0$	G1	G2
	$\theta = 270^0$	G1	G3

Clearly, as higher the number of directions selected to analyze, higher the number of dispatch scenarios to explore, thus, the SSSR would be more accurate. Although, when a high number of directions is selected, the computational effort required to explore all these scenarios is much higher, and the computing time suffers a great impact.

3.1.2.3 *Computation of the participation factors*

Once the IMPR and the EXPR are defined, it is necessary to determine the proportion that each generation unit, and each generation group, will change their dispatch profile at each direction that is explored during the construction process of the SSSR, this is achieved by computing the participation factors.

As explained in section 2.1.2, the participation factors are divided into two types.

- Group participation factors (GPFs);

- Individual participation factors (IPFs).

As it can be seen in Table 2, there are some cases where the IMPR and the EXPR are composed by two generation groups, for these specific scenarios the GPFs are crucial, they will determine the percentage difference between two generation groups of the same region. As it was mentioned before, when the system is divided into the generation groups, these can be formed by only one unit or by a set of generators, in the last case, the IPFs are needed to determine the new generation profile of each unit when the new scenario is being explored.

- Group participation factors (GPFs):

The computing of the GPFs are obtained from the analysis of the region participation factors (RPFs), which are defined as follows:

$$\sum RPF_{EXPR} = 100\% \tag{3.3}$$

$$\sum RPF_{IMPR} = 100\% \tag{3.4}$$

The previous equations basically show that the sum of the active generated power of the groups that are part of the IMPR or the EXPR has to be equal to 100%. With the intention of calculating the percentage that each group has to increase or decrease its generation, it is needed a trigonometric analysis of one of the three nomograms, following the same thread here the G2XG3 nomogram will be used to explained (Figure 15). As explained before, the different generation profiles that are explored, depend directly on the angles (quadrants) of the direction, therefore, the GPFs will be deduced with an analysis for each quadrant.

– First quadrant:

As it can be seen in Table 2, in the first quadrant only G1 forms the EXPR, hence, its GPF is equal to 100% ($G_{G1}PF = 100\%$). To calculate the GPF of G2 and G3, from Figure 14, the following relation can be obtained:

$$G3 = G2 \cdot \tan \theta \tag{3.5}$$

In quantitative terms assuming that $G2 = 100\%$ and knowing a given value of θ it is possible to affirm that $G3 = \tan \theta\%$. To satisfy equation 3.3 performing the normalization process, the GPFs of G2 and G3 can be computed as follows:

$$G_{G3}PF = \frac{1 \cdot \tan \theta}{1 \cdot (1 + \tan \theta)} \tag{3.6}$$

$$G_{G2}PF = 1 - G_{G3}PF \tag{3.7}$$

– Second quadrant:

In the second quadrant, there are three possible scenarios, as seen in Table 2. In the first scenario where, $90^0 < \theta < 135^0$, the generation group G3 forms the EXPR, thus, $G_{G3}PF = 100\%$. And for the IMPR is necessary to make an analysis similar to the one

made for the first quadrant, since it is formed by two groups. From Figure 14 and with mathematical manipulation, (3.8) can be obtained.

$$G2 = \frac{G3}{|-\tan\theta|} \tag{3.8}$$

As mentioned before since the EXPR is only composed of G3 and $G_{G3}PF = 100\%$, therefore, (3.9) can be deduced.

$$G_{G2}PF = \frac{G_{G3}PF}{|-\tan\theta|} = \frac{1}{|-\tan\theta|} \tag{3.9}$$

The group G1 is forming the IMPR with G2, hence its GPF has to satisfy (3.4).

$$G_{G1}PF = 1 - G_{G2}PF \tag{3.10}$$

For the second scenario, where $\theta = 135^0$, the EXPR and the IMPR are composed by G3 and G2 respectively, which means that $G_{G3}PF = 100\%$ and $G_{G2}PF = 100\%$, in this specific case G3 and G2 are increasing and decreasing their internal generation at the same rate, in other words, the power transfer is only occurring between these two groups, therefore, G1 has to maintain its generation profile hence, $G_{G1}PF = 0\%$.

Finally for the third scenario when $135^0 < \theta < 180^0$, (3.9) is still a valid relation, since it is still at the second quadrant. In this case, the IMPR is formed only by G2 thus, $G_{G2}PF = 100\%$. From this premise (3.11) can be computed.

$$G_{G3}PF = G_{G2}PF \cdot |-\tan\theta| = 1 \cdot |-\tan\theta| \tag{3.11}$$

The GPF of G1 can be obtained from (3.3):

$$G_{G1}PF = 1 - G_{G3}PF \tag{3.12}$$

− Third quadrant:

For the third quadrant, a similar analysis from the firs quadrant can be made since there is only one scenario where $180^0 < \theta < 270^0$. The difference from the first quadrant is that G2 and G3 form the IMPR instead of the EXPR since they are both decreasing their generation profile. Therefore, the EXPR is only composed of G1, which means that $G_{G1}PF = 100\%$.

It is possible to affirm, from a trigonometric analysis, that the relation (3.5) is still valid for the third quadrant, since $\tan(\theta + 180) = \tan\theta$. Therefore, to calculate the GPFs

of G2 and G3 for the directions at the third quadrant, equations (3.6) and (3.7) can be used.

    — Fourth quadrant:

As is observed in Table 2, in the fourth quadrant there are three possible scenarios, and a similar analysis from the one made for the second quadrant is needed.

For the first scenario where $270^0 < \theta < 315^0$, the IMPR is only formed by G3. Therefore, $G_{G3}PF = 100\%$, and the exporting region is composed by G1 and G2, from Figure 14 it can be seen that the relation (3.8) is still valid, since $\tan(360 - \theta) = -\tan\theta$. From these analysis the GPFs of G1 and G2 can be computed with (3.9) and (3.10).

In the second scenario, when $\theta = 315^0$ the EXPR and the IMPR are formed by G2 and G3 respectively, in this case, the generation profile of G2 is increasing at the same rate of the generation decrease of G3. Therefore, $G_{G2}PF = 100\%$ and $G_{G3}PF = 100\%$. In order to keep the power balance G1 does not participate in the process thus, $G_{G1} = 0\%$.

Lastly for the third scenario with $315^0 < \theta < 360^0$, only G2 composes the EXPR, hence, $G_{G2}PF = 100\%$. The IMPR is formed by G1 and G3 and, from the trigonometric relation $\tan(360 - \theta) = -\tan\theta$, (3.11) and (3.12) are used to compute the GPFs of the mentioned groups.

    — Directions over the axes:

As seen in Table 2 when the angle of the analyzed direction is over one of the axes $(0^0, 360^0, 90^0, 360^0)$, the IMPR and the EXPR are only formed by one group, therefore, their GPFs are always equal to 100% and the remaining group does not participate in the process, thus, its GPF is equal to 0%.

    • Individual participation factors (IPFs):

The existence of more than one generator on a group brings the need of determining, at each analyzed direction, the proportion that each generator will increase or decrease its current generation in percentage terms, depending on which region (EXPR or IMPR) the group, that the generator belongs, is part of. In other words, the IPFs are calculated based on the GPFs that were explained in the previous subsection.

There are two options to calculate the IPFs:

    — Based on the maximum capability of the generation unit;

    — Based on the original dispatch (base case) of each generator.

The selection between the options available to calculate the IPFs will depend on the type of study that is desired. The following equations are used to compute the IPFs:

$$I_{GEN(i)}PF = \frac{P_{MAX(i)}}{CAP_{MAX}} \cdot G_{G(x)}PF \tag{3.13}$$

$$I_{GEN(i)}PF = \frac{P_{BASE(i)}}{DISP_{TOT}} \cdot G_{G(x)}PF \tag{3.14}$$

$$\sum_{i=1}^{N} I_{GEN(i)}PF = G_{G(x)}PF \tag{3.15}$$

Where:

$I_{GEN(i)}PF$ = IPF of generic generator i;

$P_{MAX(i)}$ = Maximum capability of generator i;

CAP_{MAX} = Maximum generation of the group that contains generator i;

$P_{BASE(i)}$ = Generation of unit i at the base case;

$DISP_{TOT}$ = Total dispatch of the group that contains generator i;

$G_{G(x)}PF$ = GPF of the group that contains generator i;

N = Number of generators in group x.

As it can be seen in (3.15), independently of the option chose to calculate the IPFs, the sum of all the IPFs of a group has to be equal to the percentage of the GPF.

3.1.2.4 *Graphic implementation*

To create the nomograms, the system has to be divided into the thee generation groups, then the number of directions that are going to be analyzed has to be chosen and also the power transfer step, it is important to emphasize that better accuracy is obtained when a high number of directions and small power transfer step are used, but the computation time suffers a large increase.

Each direction is analyzed individually, and the EXPR and IMPR have to be defined as shown in Table 2, then the GPFs and IPFs are calculated as explained previously. After calculating all the participation factors for a direction, a power step is made, and the conventional power flow is solved for the new operational point, using the conventional Newton-Raphson method. With this solution it is verified if any of the pre-established limits are violated, if one of the limits is violated a point is plotted in each nomogram. Following, a contingency analysis can be made, using a pre-established list of the most severe contingencies, aiming to verify if the system satisfies the (N-1) criterion, for each contingency a power flow is solved and the limits are verified as it was done before, when

all the contingencies are analyzed another power step is made. This process continues until one of the groups reaches its maximum or minimum generation limit and it is repeated for all the directions.

The limits used to construct the conventional SSSR are:

- Voltage on nodes;

- Thermic limit on transmission lines and transformers;

- Reactive power generation on generators;

- Active power capability on generators;

- Convergence limit.

Once the process is finished for all the directions, the connection of all the points associated with a limit violation constructs the security curve of that specific limit. In Figure 16, there is an example of a security curve of the voltage limit that was obtained from exploring 10 directions. When all the security curves are superimposed in the same plot the SSSR is formed.

Figure 16 – SSSR (10 directions) bounded by the voltage limit security curve
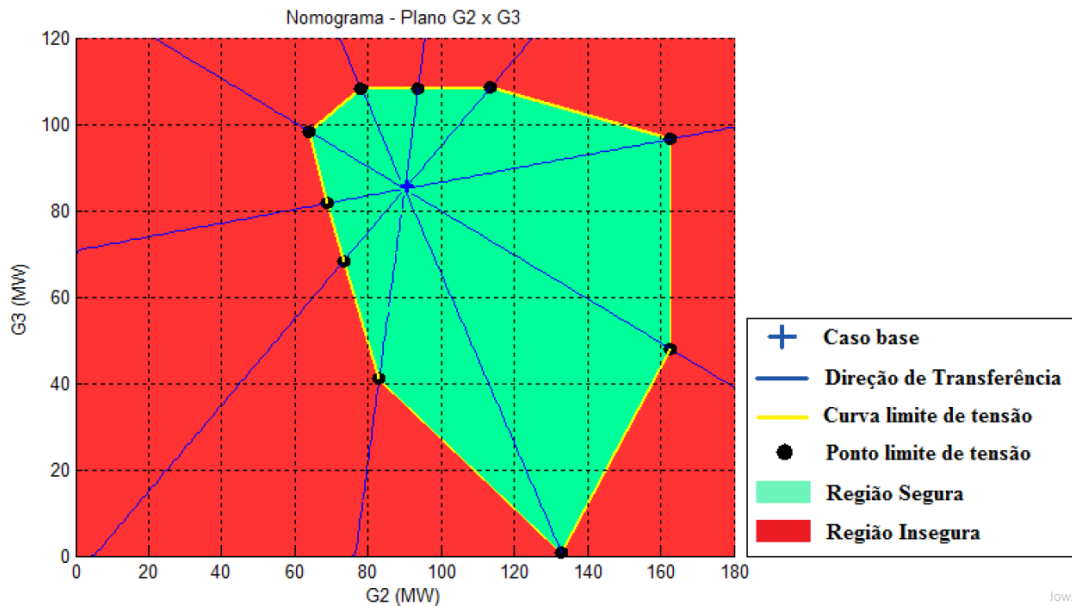
Source: [31].

3.2 VOLTAGE STABILITY INDEX REVIEW

3.2.1 **Context**

This index was proposed in [14], and it is based on the maximum power transfer theorem of the linear electric circuits, where at the MLP the Thévenin impedance matches

the load impedance. It is calculated for the PQ nodes of the analyzed system, indicating which are the most critical buses, in terms of voltage stability.

3.2.2 Definition

An electrical power system can be presented in its simplest form as a Thévenin equivalent circuit, as illustrated in Figure 17. Where $\vec{\overline{E}}_{Th}$ is the Thévenin voltage, $\overline{Z}_{Th}$ is the Thévenin impedance, $\overline{Z}_L$ is the load impedance, $\vec{\overline{V}}_L$ is the load voltage and $\vec{\overline{I}}_L$ is the load current.

Figure 17 – Thévenin equivalent circuit
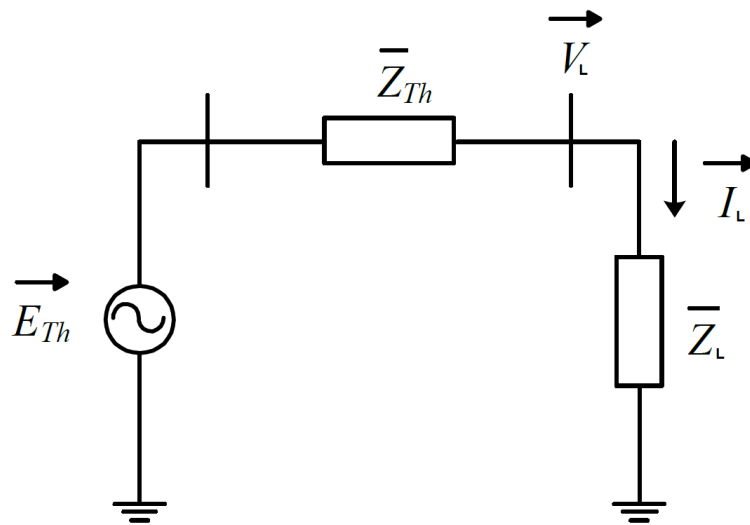
Source: [14].

From the previous circuit, equation (3.16) can be obtained.

$$\vec{\overline{I}}_L = \frac{\vec{\overline{E}}_{Th}}{\overline{Z}_{Th} + \overline{Z}_L} \tag{3.16}$$

Where:

$$\overline{Z}_{Th} = Z_{Th}\underline{/\theta}$$

$$\overline{Z}_L = Z_L\underline{/\phi}$$

The load voltage and the active power consumed by the load are given by:

$$\vec{\overline{V}}_L = \frac{\overline{Z}_L}{\overline{Z}_{Th} + \overline{Z}_L} \cdot \vec{\overline{E}}_{Th} \tag{3.17}$$

$$\vec{\overline{P}}_L = \vec{\overline{V}}_L \cdot \vec{\overline{I}}_L \cdot \cos\phi \tag{3.18}$$

From the previous expressions and adopting a purely resistive load ($\overline{Z}_L = R_L$), and a purely imaginary Thévenin impedance ($\overline{Z}_{Th} = jX_{Th} = j0.2$), if the current, voltage

and load power are normalized with the short circuit current (I_{sc}), Thévenin voltage and maximum load power (P_{max}) respectively, they can be plotted as a function of the relation X_{Th}/R_L, this is illustrated in Figure 18.

Figure 18 – Power, voltage and current as a function of the impedance

Source: [14].
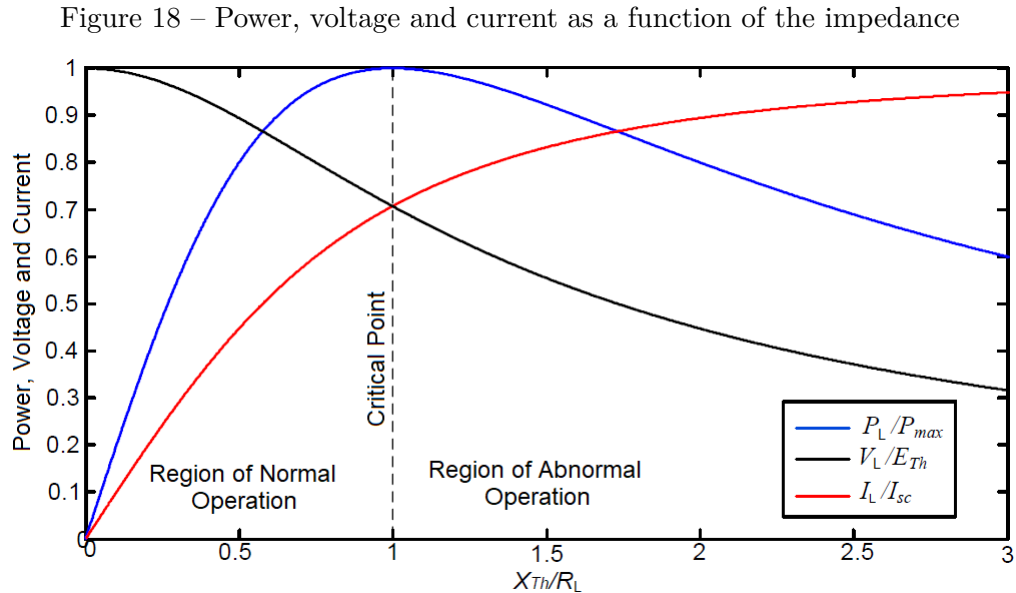
From the previous figure, it is possible to observe how at the critical point the load impedance and the Thévenin impedance have the same value. In Figure 19 this can be confirmed, since the normalized voltage (V_L/E_{Th}) is plotted as a function of the normalized load power (P_L/P_{max}) and the tip of the PV curve coincides with the values observed in Figure 18. From the previous curves it is also possible to affirm that, while the load impedance is greater than the Thévenin impedance ($Z_{Th}/Z_L < 1$), the system is operating at the normal operating region, and can be confirmed with Figure 19, since these values match with the ones on the superior half of the PV curve. On the other hand, when the load impedance is smaller than the Thévenin impedance ($Z_{Th}/Z_L > 1$), the system operates in the abnormal region, analogously the system operates on the PV curve's inferior half.

It is observed with the previous analysis that the relation between the Thévenin impedance and the load impedance can be used as a voltage stability index (VSI) [14].

$$VSI = \frac{|Z_{Th}|}{|Z_L|} \tag{3.19}$$

The VSI can be utilized following the next characteristics:

- $VSI < 1$: System operating with normal conditions;

- $VSI = 1$: System operating at the critical point;

Figure 19 – Normalized voltage as a function of the normalized power

$V_L/E_{Th} = 0{,}707$
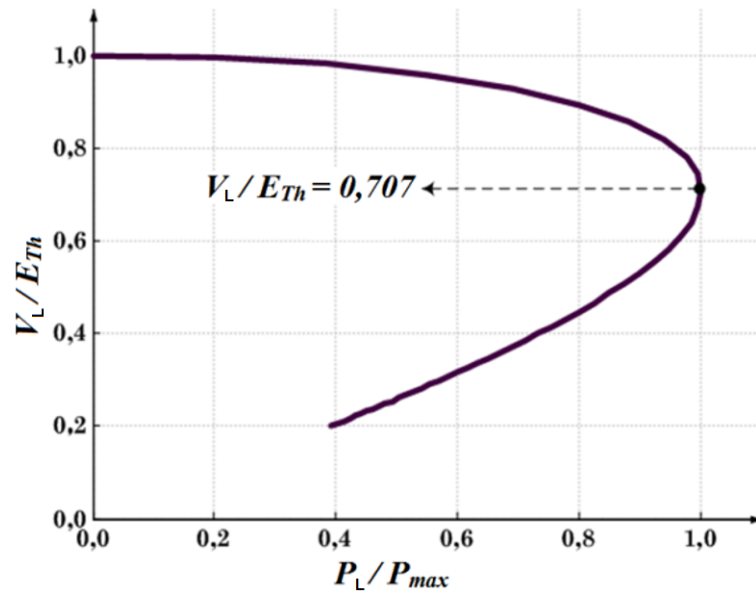
Source: [14].

- $VSI > 1$: System operating with abnormal conditions.

To compute the VSI for real power systems, it is necessary to obtain the load impedance at each PQ node, and the Thévenin impedance "seen" from each load bus. The procedures to compute these parameters are detailed in the following subsections.

3.2.3 Load impedance

Generally in power systems, the load is given in terms of the active and reactive consumed power. Nevertheless, if the VSI is used for voltage stability analysis in power systems, the load has to be represented as a constant impedance. Assuming that the load in Figure 17 is given by its consumed power ($\vec{S}_k$), its impedance can be computed as follows:

$$\overline{Z}_L = \frac{(\vec{V}_L)^2}{\vec{S}_k} \tag{3.20}$$

Where the load voltage ($\vec{V}_L$) is obtained from a power flow solution.

3.2.4 Thévenin impedance

The Thévenin impedance can be calculated from an equivalent circuit that models the entire system that is desired to be analyzed. However, the existence of PV nodes makes impossible to compute the Thévenin impedance in the conventional way. Because there is not an ideal voltage source that can reproduce the characteristics of a PV bus, that

is, maintaining the voltage and active power fixed, while leaving the phase and reactive generation to variate freely.

In order to overcome this issue, a mathematical formulation based on the electric circuit theory was proposed in [14]. Considering that the circuit shown in Figure 17 is the equivalent of a large and complex power system with PV nodes. If the conventional power flow is solved for this circuit, the Thévenin voltage "seen" from a genetic bus k with load $(\overrightarrow{S}_k)$ can be calculated with (3.21).

$$\overrightarrow{E}_{Th} = \overrightarrow{I}_L \cdot \overline{Z}_{Th} + \overrightarrow{V}_L \tag{3.21}$$

If a new operating point is considered, where the load $\overrightarrow{S}_k$ has changed to a new value $\overrightarrow{S}'_k$, maintaining a constant power factor, performing a sensitivity analysis (which will be addressed in the following subsection), a new equivalent circuit with similar characteristics to the one in Figure 17 would be obtained, where the Thévenin voltage could be computed with (3.22)

$$\overrightarrow{E}'_{Th} = \overrightarrow{I}'_L \cdot \overline{Z}'_{Th} + \overrightarrow{V}'_L \tag{3.22}$$

Considering that the change in the load profile, between the previous operating points, is infinitesimal ($\overrightarrow{S}'_k - \overrightarrow{S}_k = \Delta S_k \to 0$). From this it can be assumed that the variation in the Thévenin voltage from the first to the second operating point is negligible therefore, the Thévenin impedance can be considered constant. Subtracting (3.21) from (3.21), and isolating $\overline{Z}_{Th}$ gives the following expression:

$$\overline{Z}_{Th} = \frac{\overrightarrow{V}'_L - \overrightarrow{V}_L}{\overrightarrow{I}_L - \overrightarrow{I}'_L} \tag{3.23}$$

The Thévenin impedance expression in (3.23) is based on the mathematical artifice of linearizing the PV curve around the operating point $\overrightarrow{S}_k$.

Both the Thévenin and load impedance have to be calculated for each PQ bus, since the Thévenin equivalent circuit variates when it is "seen" from different nodes of the system. Therefore, there is a *VSI* for each PQ bus of the system.

After computing the Thévenin and load impedances, the *VSI* can be obtained easily using (3.19). To estimate the parameters of the new operating point $(\overrightarrow{S}'_k)$ without solving a power flow again, the sensitivity analysis is used, aiming to reduce the computational effort. This methodology is presented in the following subsection.

3.2.5 Sensitivity analysis

It is very common in electric power systems analysis to try to determine the system's behavior when there are changes in its different magnitudes. For example, it can be necessary verify the effects that will produce on the system the occurrence of changes in the load profiles, connected to one or more nodes.

In cases where the variations in the magnitudes can be considered sufficiently small, the new system state can be found without the necessity of solving new power flows, using the technique called sensitivity analysis, which was originally presented in [33].

The sensitivity is defined as the relation $\Delta x / \Delta y$, which is associated with small changes of some dependent variables (x) due to small changes in some independent variables (y). In power systems, two dominant types sensitivity relations are defined:

1. Electric variables sensitivity, as the voltage V_i on bus i, in relation with another electric variable, as the reactive generation Q_j on bus j;

2. System operation cost sensitivity in relation to the electric variables, as the demanded and generated active power.

It can be deduced from the deduction of the Thévenin impedance that in this work the focus will be on the first type of sensitivity.

The sensitivity analysis allows the linearization of the network's steady-state model. Thus with a converged power flow, the system's reaction after a disturb occurrence can be found simply, by directly solving the linearized model. The new state is obtained adding the previous state with the variations that were found.

An electric power system can be mathematically modeled, under steady-state conditions, as shown in (3.24).

$$\overline{g}(\overline{u}, \overline{x}, \overline{p}) = 0 \tag{3.24}$$

Where:

$\overline{g} =$ Vector that contains the classical power flow equations;

$\overline{u} =$ Vector that contains the control variables;

$\overline{x} =$ Vector containing the state variables;

$\overline{p} =$ Vector containing the active and reactive consumed power of the system.

If equation (3.24) is derived, the following expression is found:

$$\frac{\partial \overline{g}}{\partial \overline{u}} d\overline{u} + \frac{\partial \overline{g}}{\partial \overline{x}} d\overline{x} + \frac{\partial \overline{g}}{\partial \overline{p}} d\overline{p} = 0 \tag{3.25}$$

The previous equation demonstrates the relation between the system's variables and small changes in them. This can be approximated if the differentials are substituted for finite variations, as shown in (3.26).

$$\frac{\partial \overline{g}}{\partial \overline{u}} \overline{\Delta u} + \frac{\partial \overline{g}}{\partial \overline{x}} \overline{\Delta x} + \frac{\partial \overline{g}}{\partial \overline{p}} \overline{\Delta p} = 0 \tag{3.26}$$

If mathematical rigorousness is applied, (3.26) could not be written as equality, but assuming that the variations are extremely small, the associated error can be neglected.

The matrices $\partial \overline{g}/\partial \overline{u}$, $\partial \overline{g}/\partial \overline{x}$ and $\partial \overline{g}/\partial \overline{p}$, are Jacobian matrices defined in relation to the control variables, the state variables and the loads respectively. These matrices, for the sake of breverity, are denoted as $\overline{J}_u$, $\overline{J}_x$ and $\overline{J}_p$. The matrix $\overline{J}_x$ is the Jacobian matrix of the Newton-Raphson method. Therefore, 3.26 can be rewritten as follows:

$$\overline{J}_u \overline{\Delta u} + \overline{J}_x \overline{\Delta x} + \overline{J}_p \overline{\Delta p} = 0 \tag{3.27}$$

If the state variables variation $(\overline{\Delta x})$ is isolated from the previous equation, the expression that represents the variation of the state variables when there are small disturbances in the system can be found as follows:

$$\overline{\Delta x} = -(\overline{J}_x)^{-1} \cdot \overline{J}_u \cdot \overline{\Delta u} - (\overline{J}_x)^{-1} \cdot \overline{J}_p \cdot \overline{\Delta p} \tag{3.28}$$

or:

$$\overline{\Delta x} = \overline{S}_{xu} \cdot \overline{\Delta u} + \overline{S}_{xp} \cdot \overline{\Delta p} \tag{3.29}$$

Where:

$$\overline{S}_{xu} = -(\overline{J}_x)^{-1} \cdot \overline{J}_u \tag{3.30}$$

$$\overline{S}_{xp} = -(\overline{J}_x)^{-1} \cdot \overline{J}_p \tag{3.31}$$

The matrices $\overline{S}_{xu}$ and $\overline{S}_{xp}$ define state variables sensitivity in relation to the control variables and loads respectively thus, they are called the sensitivity matrices. Equation (3.29) is one of the most important equations on the sensitivity analysis, allowing the

calculation of the state variables variations when disturbances occur on the control variables and/or the system's load profiles.

As it was explained in the previous subsections, to calculate the VSI there will be only small changes in the loads hence, the first term in (3.29) will be neglected. Therefore, the new operating point will be obtained by performing a multiplication of matrices.

3.2.6 Transit Buses

Most of the electric power systems, independent of their size, possess transit buses. A transit bus is a PQ node without generation or demand and is normally used to connect a load bus to other load buses. A transit bus is not a terminal node (this is the main characteristic for its use), therefore there are at least two circuits exiting a transit bus [14].

Generally, transit buses are located in highly busy power flow paths hence, they are commonly among the most critical nodes in a power grid. This characteristic makes that monitoring transit buses becomes a crucial task in voltage stability assessment.

Aiming to compute the VSI for the transit buses, comes up the question of how to calculate this indicator because these nodes do not possess demand. This is discussed below.

Starting from a power flow solution, the active and reactive flows for the transmission lines are obtained. With the power flows determined, the transit buses are modeled as nodes with load, where the active power flows exiting the bus represent an "equivalent load". Therefore, for each transit bus, the flows of the transmission lines and transformers that are connected to the analyzed node are computed, and in case the active and reactive flow are exiting the node, they are added as load for the bus. Consequently, the active and reactive load for a transit bus is given by:

$$P_{load}^k = \sum_{m=1}^{n} P_{km} \tag{3.32}$$

$$Q_{load}^k = \sum_{m=1}^{n} Q_{km} \tag{3.33}$$

$$\overline{S}_k = P_{load}^k + jQ_{load}^k \tag{3.34}$$

Where:

$k =$ Analyzed transit bus;

$m =$ Neighboring bus connected to the transit bus;

$n =$ Number of transmission lines connected to the transit bus k with

active flow exiting the bus;

P_{km} = Active flow exiting bus k;

Q_{km} = reactive flow exiting bus k;

$\overline{S}_k$ = Apparent load on bus k.

After the "equivalent loads" are assigned to the transit nodes, the load impedance can be calculated using (3.20).

In order to calculate the Thévenin impedance, a similar process from the normal PQ nodes is performed. An infinitesimal decrease is made in the "equivalent load" of the transit bus, maintaining a constant power factor. With the new load, a sensitivity analysis is executed, to obtain a new operating point. Then the Thévenin impedance for the transit nodes can be computed using (3.23).

3.3 PROPOSED METHODOLOGY TO CONSTRUCT SSSR WITH THE VSI

As explained in section 3.1 the SSSR is a very powerful tool in power system security assessment. It has been used in several countries to analyze and prevent unsafe operation of their power systems.

It could be seen that this tool analyzes a large amount of security limits (voltage, active and reactive generation, flow on transmission lines and convergence). However, it does not provide information about the voltage instability problem. In [31] when a voltage stability analysis was desired, a different tool, like the CPF method or the QV curve was used. Therefore, aiming to increase the SSSR reliability, a new methodology is proposed, where the VSI presented in section 3.2, is added to the construction process of the mentioned tool.

The SSSR is a tool that requires a high computational effort hence, the main reason of choosing the VSI to add the voltage stability analysis feature to the SSSR is its low computational requirements, since it can take advantage of the already existing power flow solutions that are required to construct the SSSR, and performing the sensitivity analysis from a power flow solution takes a small amount of computing time, since only a matrix multiplication is needed. Different from the classical voltage stability methods (CPF, QV curves, etc.) that require a set of successive power flow solutions, to determine security margins thus, highly increasing the computing time.

Joining these tools makes the voltage stability analysis to gain an interface of easy comprehension since, instead of looking at numerical indicators, the analysis can be made from simple visual inspection, that is one of the advantages of the SSSR. Besides that, since the SSSR is constructed with a contingency analysis, the voltage instability problem will be studied taking into consideration disturbances as well.

It can be observed that the SSSR already possesses a security curve of voltage level in nodes. Voltage level was a way to analyze voltage stability in the past since the collapse point was related to a low voltage level, Therefore monitoring this parameter was sufficient to prevent voltage instability. However, in modern power systems the critical point is not always associated with a low voltage level. This is due to more complex networks, or it can be a consequence of excessive shunt compensation (capacitors), which is a piece of very common equipment used in electric grids to improve voltage levels. Although shunt capacitors improve voltage levels and power transfer capability in transmission lines, they might bring the voltage collapse point to normal operating voltage levels, which makes insufficient the analysis of this parameter for voltage stability assessment.

In order to add the VSI to the SSSR, it is proposed the insertion of three new curves to the construction process of the SSSR. Each of these curves will represent a level of voltage instability severity. As it was explained in the previous section, when $VSI < 1$ the system is working under normal conditions, thus when the VSI approaches to 1, the system is reaching the voltage collapse point. Therefore the proposed levels of voltage instability severity are:

- $0.6 < VSI < 0.7$

- $0.7 < VSI < 0.8$

- $0.8 < VSI < 1$

Figure 20 – Illustration of the voltage instability severity levels.
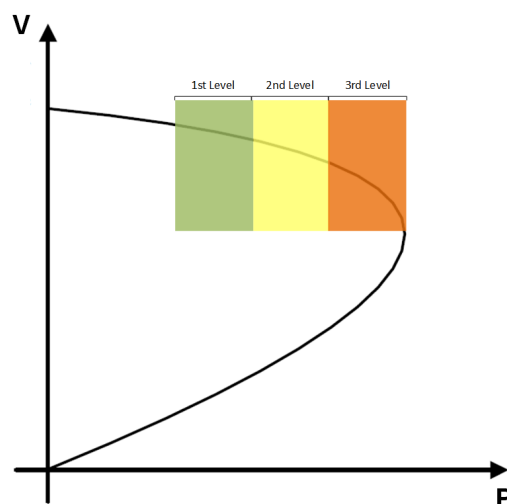
These levels were chosen based on the behavior of the VSI because it has a severe non-linearity when the system is approaching the MLP [14]. Therefore, if higher values of the VSI were chosen to determine the severity levels, the indicators shown in the

SSSR would be very close to the collapse point, thus, they would not detect the voltage instability problem satisfactorily.

The severity levels might be represented as the current position of the system with respect to the PV curve, as shown in Figure 20.

It is good to emphasize that, the mentioned figure is only an illustration of what the severity levels represent since a PV curve is obtained through the CPF, which increments the load of the system. The SSSR instead, is constructed with a fixed load profile. Although, as the SSSR represent different dispatch scenarios hence, the system is stressed in different ways. Therefore, different severity levels of voltage instability are present even with a fixed load.

As illustrated in Figure 20 beyond the critical point there is no possible solution. Therefore, if for any system it is tried to get a power flow solution with a load level beyond the critical point, the Newton-Raphson method would diverge. But as explained in [34], there are more reasons for the power flow to diverge, such as, insufficient reactive power to supply load and losses in some portion of the system, too many control adjustments in the network models, such as tap-changing or phase-shifting transformers, switchable shunt capacitors or reactors, area interchange control, and FACTS device controls.

Although voltage stability is one of the main causes of divergence of the power flow, the existence of other reasons to diverge, turn insufficient for voltage stability assessment the convergence limit tested in the conventional construction process of the SSSR. Making the proposed feature a more effective tool for detecting voltage instability.

The construction process of the SSSR will be identical, as explained in section 3.1, with the only difference that, at each direction that is being analyzed, besides evaluating if any of the limits are violated, the VSI will be calculated for each node as explained in the previous section. If at least one of the node's VSI is within one of the severity levels the corresponding operating point is plotted on the three nomograms.

Figure 21 – Heat map formed around the operating point.
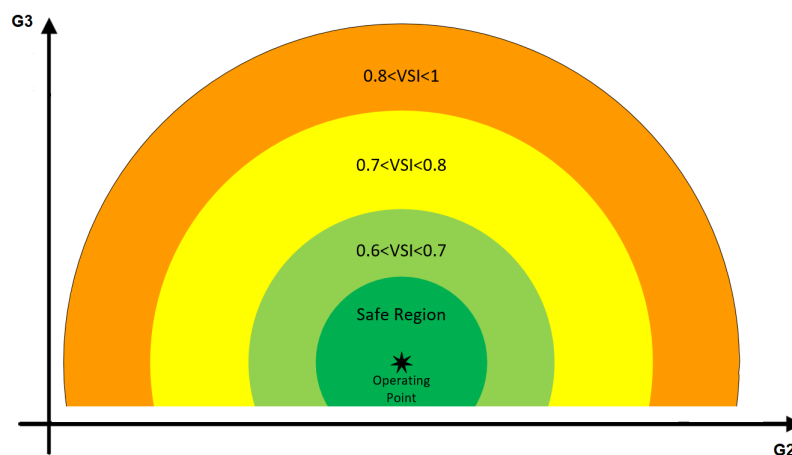
The proposed curves constructed using the VSI, allow to form subregions between them, these subregions are used to create a heat map around the operating point, as shown in Figure 21. The heat map illustrates in a simple manner which are the safest dispatch profiles to attend a load, taking into consideration the voltage stability problem.

Figure 22 shows a flow chart that summarizes the construction process of the SSSR including the voltage instability severity levels.

Figure 22 – Construction process flow chart.
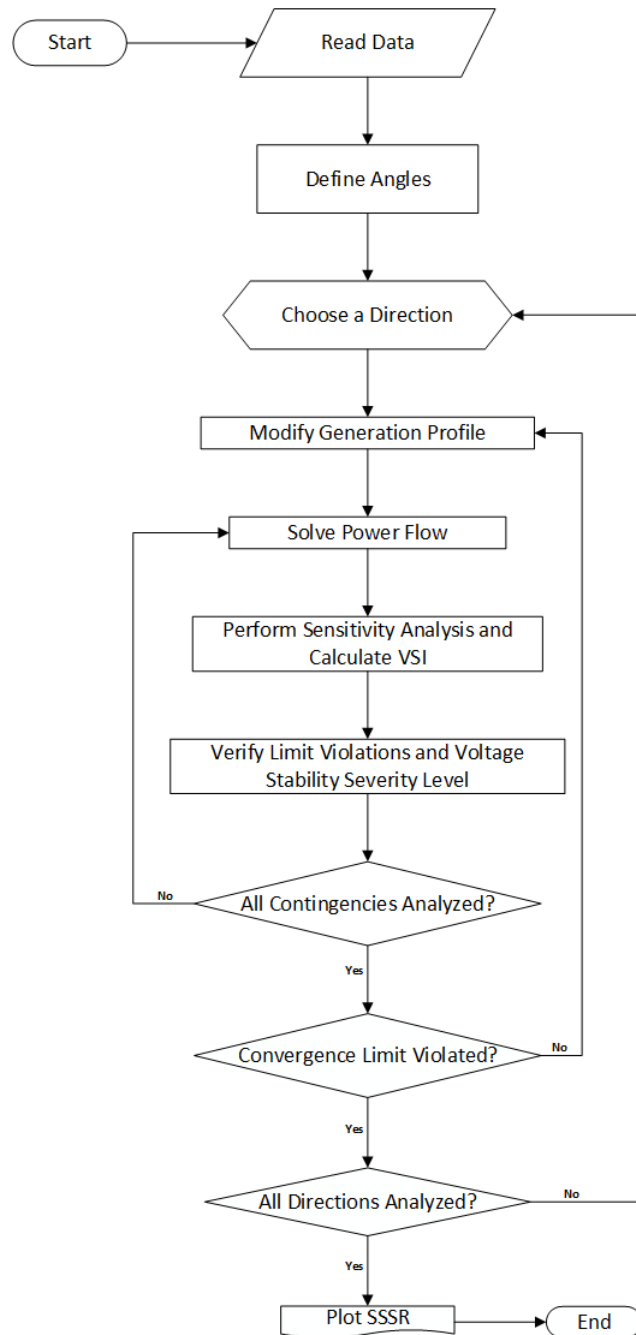
The previous algorithm was developed in the MATLAB environment to automatically obtain the SSSR.

3.4 CHAPTER SUMMARY

This chapter addressed the conventional SSSR construction process, detailing its characteristics, explaining its mathematical principles and the step by step procedure. It also presented a review of the VSI tool, detailing its mathematical formulations and advantages over the classical methods of voltage stability assessment. Finally a new methodology to construct the SSSR was proposed, which joins up the two mentioned tools. The advantages of adding a voltage stability indicator to the SSSR were discussed, as well as how they have to be interpreted in the final SSSR graphic. Finally the full algorithm was summarized in a flow chart for easy comprehension.

4 CONSTRUCTION OF STEADY-STATE SECURITY REGIONS WITH PARTICLE SWARM OPTIMIZATION

This chapter presents the second methodology proposed in this work. It consists of an alternative method to construct the SSSR based on the PSO algorithm, aiming to reduce the computational effort of this tool, and thus, turning it into a feasible method for monitoring large power systems in *real-time*.

4.1 DEFINITION OF THE VARIABLES

In order to transform the SSSR construction process into an optimization problem, the variables of the model have to be defined. The proposed methodology aims to maintain the same final result of the conventional methodology explained in section 3.1, but improving its computing time. Therefore, some of the main concepts will be the same in both methodologies.

As mentioned in the chapter, the SSSR is a three-dimensional graph whose axes represent the active generation of the three groups of generators that form the power system. It was also described how to separate the power system into the three generation groups. This step of the conventional technique is still valid for the proposed methodology, and it is a key aspect of the definition of the variables of the optimization model. Besides the group division, it was also defined that one of the generation groups is designated as the "swing" one, adjusting its generation according to the variations made in the other two sets of generators.

The variables defined for the optimization model (whose mathematical formulation will be described in the next subsection) are the two active power generations of the groups that are *not* the "swing" group. Therefore, the PSO algorithm will only handle a two-dimensional problem, and each particle's "position" will be composed of two coordinates, which are the active generation of the selected groups.

As explained before the two variables of the problem represent the generation profile of two of the generation groups. Therefore, each particle of the PSO algorithm represents a dispatch scenario of the two groups, and as it was seen in section 2.3, each particle updates its position at each iteration, thus, modifying the generation profile of the groups. Since the "swing" group is not part of the two variables, it will not have its generation profile modified by the PSO algorithm automatically. Aiming to avoid this problem, at each iteration of the PSO algorithm, if a particle has its "position" updated, the corresponding "swing" generation will be updated as follows:

$$G_s^k = G_s^0 - \Delta G_i^k - \Delta G_j^k \tag{4.1}$$

$$\Delta G_{i,j}^{k} = G_{i,j}^{k} - G_{i,j}^{0} \tag{4.2}$$

Where:

G_{s}^{k}, G_{s}^{0} = Generated power of the "swing" group at iteration k and base case, respectively;

$G_{i,j}^{k}, G_{i,j}^{0}$ = Generated power of groups i and j at iteration k and base case, respectively.

4.2 OPTIMIZATION MODEL

After defining the variables the full optimization model (objective function and constraints) is needed to solve the problem.

It is desired that the security region be as large as possible. Therefore, the distance between the original operating point and the security limits must be maximized. For the sake of clearness, G1 is taken as the "swing" group and G2 and G3 as the variables to be optimized, as illustrated in Figure 23.

Figure 23 – Objective function illustration.
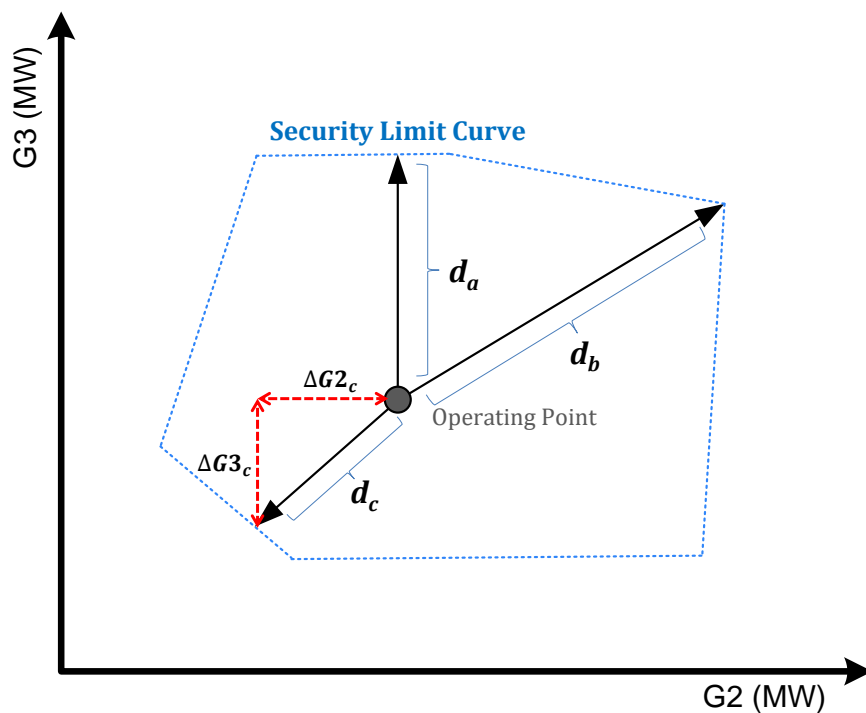
As can be seen, to define the security region, the distance from the base case must be maximized in several directions (generation scenarios). The main contribution of this methodology relies on the use of the PSO algorithm, adequately adjusted, to simultaneously maximize the generated power in these directions.

The distance between the base operating point and the security curve is given by:

$$d = \sqrt{(\Delta G_2)^2 + (\Delta G_3)^2} \qquad (4.3)$$

As explained before the distance must be maximized, although, if the objective function Z only contains this expression the particles would move uncontrollably towards the upper or lower bounds, depending on the initial position. To overcome this issue, a penalization factor is proposed to be added in the objective function, which will force $Z \to -\infty$ if a limit is violated. The penalization factor prevents the particles from moving beyond the security limits. The proposed full optimization model can be expressed as follows:

$$\text{maximize } Z = \sqrt{(\Delta G_2)^2 + (\Delta G_3)^2} - \mu \cdot L_v$$
$$\text{s.t.} \qquad (4.4)$$
$$LB_{G2,3} \leq G_{2,3} \leq UB_{G2,3}$$

Where:

$\mu =$ Penalization factor (constant with a large value);

$L_v =$ Binary constant;

$LB_{G2,3}, UB_{G2,3} =$ Upper and lower bounds of G2 and G3, respectively.

Upper and lower bounds and the population treatment will be addressed in further sections.

After each iteration of the PSO algorithm, the particles have their positions updated. Therefore, the dispatch profile of the system is modified, which is the equivalent of the power transfer steps of the conventional methodology. After this modification on the generation profile, a power flow must be solved to evaluate if a limit violation has occurred. As it can be seen in (4.4) the penalization factor μ is multiplied by a binary constant L_v. This constant is defined at each iteration of the PSO, after the power flow solution, it receives a value of 1 when a limit is violated, hence making that $Z \to -\infty$. On the other hand when none of the limits is violated the constant is set with a value of 0. This makes impossible that unsafe operating points form the SSSR since the dispatch scenarios with limits violations will never be part of the historical solutions of each particle.

The binary constant L_v as explained before is defined at each iteration of the PSO, and it can be treated by two different approaches depending on the desired SSSR. If the goal is to construct a security region without detailing which are the violated limits, L_v will receive unitary value when any of the limits are transgressed. On the other hand, if the aspiration is to create a curve for each limit violation, the optimization model (4.4) will be solved once for each one of the desired limits.

For example, if it is desired to plot the security curve of the voltage limit, the PSO algorithm is executed, and at each iteration, when the particles' position is updated and the power flow solution is obtained, only if any nodal voltage is violated the L_v is set to 1, ignoring if there is a violation of the other limits. The same procedure is applied for the rest of the desired security curves. The final SSSR is formed by all the superimposed security curves.

On the other hand, if it is desired to obtain only the safe operating region, the PSO would be executed only once, and the L_v constant would be set to 1 when any of the limits are violated. This option has the advantage of being much faster than the approach explained before, since the PSO is only executed once, this might be interesting for *on-line* monitoring applications, when it is only desired to know which are the safe dispatch scenarios to operate the system, and details about which are the transgressed limits are not of vital importance.

It is important to emphasize that for all curves, disregarding of which limit is being analyzed, the violation of active generation and convergence limits also have to be penalized by setting L_v to 1. The reason is that it is possible that one of these two limits is reached before other limits.

4.3   PSO PARAMETERS

In order to adjust the PSO algorithm for solving the problem that is being addressed in this work, some parameters need special attention. The basic concepts of the PSO algorithm have been largely discussed over the years in the literature as it was shown in section 2.3, where the most important mathematical equations of the PSO algorithm were shown. In this section, for the sake of easy reading, they are rewritten in equations (4.5) and (4.6).

For the methodology proposed in this paper, one of the simplest forms of PSO is used, that is called, according to [35], inertia weights approach (IWA), in which the particles' velocities are updated by using (4.5) and the weighting function is linearly decreased at each iteration through (4.6). Finally, the position of each particle is updated according to (4.7).

$$v_i^{k+1} = w \cdot v_i^k + c_i \cdot rand_1 \cdot (pbest_i - s_i^k) + c_2 \cdot rand_2 \cdot (gbest - s_i^k) \qquad (4.5)$$

$$w = w_{max} - \frac{w_{max} - w_{min}}{iter_{max}} \cdot iter \qquad (4.6)$$

$$s_i^{k+1} = s_i^k + v_i^{k+1} \qquad (4.7)$$

Where:

$v_i^k = $ Velocity of particle i at iteration k;

$w = $ Weighting function;

$c_j = $ Weighting coefficients (acceleration constants);

$rand_j = $ Random number between 0 and 1;

$s_i^k, s_i^{k+1} = $ Current and updated position of particle i;

$pbest_i = $ Best position in the history of particle i;

$gbest = $ Best position among of all the particles history;

$w_{max}, w_{min} = $ Initial and final inertia weight respectively;

$iter_{max}, iter = $ Maximum and current number of iterations respectively.

It is important to emphasize that, the velocity and position are composed of two components (for the x and y coordinates) since this application is being modeled as a two-dimensional problem.

4.3.1 Weighting coefficients

The first parameters that are addressed to adjust the PSO for solving the problem, are the weighting coefficients.

As it is explained in [35], generally, for solving optimization problems, both weighting coefficients (c_1 and c_2) are set as 2. With this configuration is expected that the particles behave as a part of a social group that is communicating to find the "global best" or optimal solution. In other words, the three terms of equation (4.5) are being used to update the particles' velocities, and by extension their position.

Figure 24 shows the behavior of the particles when both of the weighting coefficients are set with values higher than 0. As explained in section 2.3 this configuration is called the "Gbest" model, since all the particles follow the subject with the best position. This behavior allows finding a global optimum with high efficiency. Even if the analyzed function possesses a large number of local optimums, the PSO algorithm is capable of overcoming them and finding the optimal solution.

Several works, like the ones reviewed in section 2.3, explain that the first term in (4.5) refers to the inertia of the particle, the second term is related to the individual knowledge or cognition of each particle, and the third term is associated with the "communication" that the particles have with each other, in other words, the third term is the one that provides a social behavior to the population.

Figure 24 – Particles behavior with $c_1 > 0$ and $c_2 > 0$.
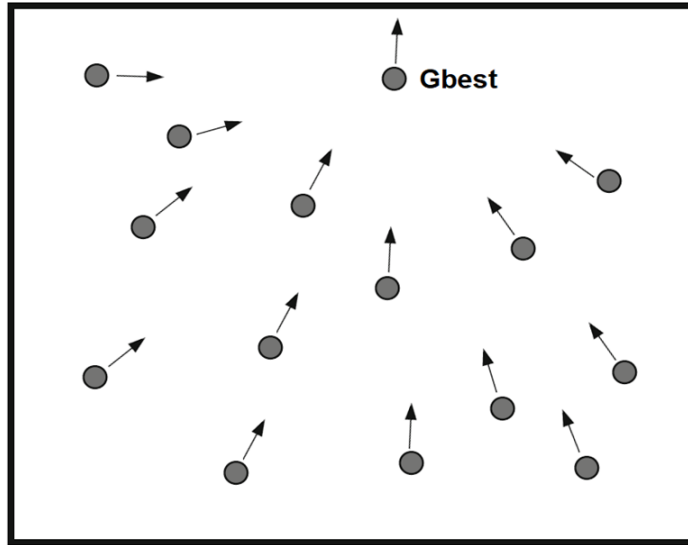
Since in this application, the objective is to construct the SSSR, which requires a set of points for being constructed, instead of an optimal point. It is proposed that the weighting coefficient c_2 is set with a value of 0, hence, neglecting the third term of equation (4.5). This allows the particles to behave as isolated individuals that update their velocities and positions taking into consideration only their own inertia and their own best position in history. In other words, they will not have the "communicating" feature of the conventional PSO, thus, not following the particle with the best global position. This behavior is illustrated in Figure 25.

Figure 25 – Particles behavior with $c_1 > 0$ and $c_2 = 0$.
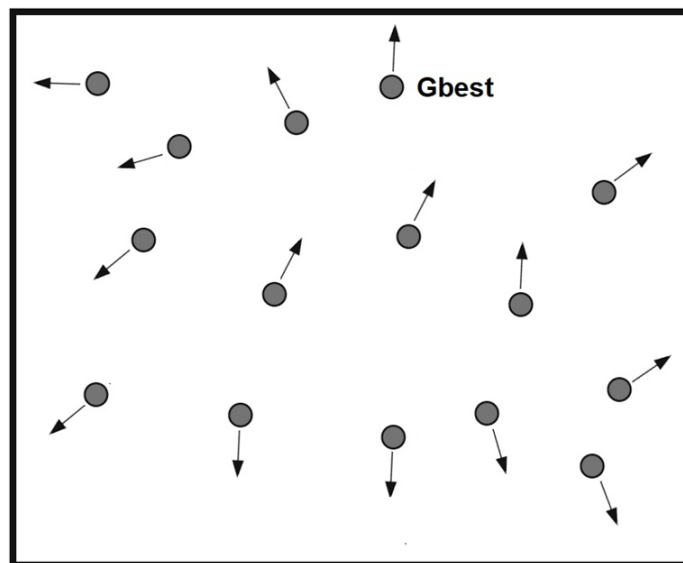
Figure 25 clearly shows the expected behavior of the particles with these adjustments. The main objective of this strategy is to construct the SSSR with a singular execution of the PSO algorithm. As explained in the previous section, the objective

function is designed for the particles to move in the opposite direction of the operating point, since the distance between them must be as big as possible. The proposed configuration allows the particles to move around the base operating point and find the security curve's edges simultaneously. It is clear that the success of this methodology has a high dependence on the randomness used in equation (4.5), and results with a low consistency might be expected. In order reduce the influence of the randomness factor of the PSO algorithm, special treatment is given to the initial population and constraints, this is addressed later in this work.

4.3.2 Weighting function

As it can be seen in equation (4.6), the weighting function decreases over the pass of the iterations. The objective of the weighting function is to add an exploration factor to the particles. Without the first factor of the mentioned equation, the particles would stop exploring possible solutions in early iterations, in other words, the particles get trapped in local optimums.

Generally, the initial and initial inertia weight is set with a higher value than the final inertia weight, this allows the particles to have a more "exploratory" behavior during the first iterations, where the particles are looking for the most feasible region of solutions, and in the final iterations, with a smaller value of inertia, the particles intensify the search on a smaller region, since it is expected that the zone with the optimal solution was found during the first iterations.

In [35] is stated that, in most of the PSO applications disregarding the type of problem, the values used as initial and final inertia weight, are 0.9 and 0.4 respectively. In this work higher values are proposed, since if small values are used, the maximum velocity (which will be explained in the next subsection) would need to be set with a high value, this will be detailed in 4.3.3.

Another reason for choosing high values for the initial and final inertia weight is the nature of the problem since the objective is not to find a singular global optimum point. Because the objective is to obtain a set of points that are as far as possible from the operating base point, it is desired for the particles to have an exploratory behavior in most of the iterations. A sensitivity analysis with different values is performed in the results chapter, which helps to conclude which are the best values for this application.

4.3.3 Maximum velocity

The maximum velocity is the last parameter of the PSO algorithm that needs to be adjusted for this application. As its name says, the maximum velocity sets a limit on the value obtained from equation (4.5). In other words, this parameter regulates the size of the steps that the particles make at each iteration.

In subsection 4.3.2 was mentioned that the use of high values of initial and final inertia weights allows setting small values of maximum velocity, this is possible because the particles have more "freedom" to move during the iterations. In this application it is very important to be able to set a small maximum velocity because it directly impacts the accuracy of the SSSR. Since if short steps are made, the probabilities of finding the edge of the security curves highly increase.

However, if small values of inertia weights are used thus, setting a large maximum velocity, it is possible that the edge of the security curve is never found. This might happen, for example, if the edge of the analyzed security curve is close to the current position of a particle, and a large step is made, the desired edge would never be reached, thus reducing the accuracy of the SSSR.

In this work, it is proposed to set the maximum velocity as a small fraction of the maximum generation limit of the groups that are the problem's variables. In this case represented by the groups G2 and G3.

$$v_{x,ymax} = G_{2,3max} \cdot (1\% - 10\%) \tag{4.8}$$

Where:

$v_{x,ymax} = x$ and y components of the velocity.

It is important to emphasize that the velocity is defined with its x and y components, as depicted in Figure 26, since, as mentioned before this application is being modeled as a two-dimensional problem. The previous equation shows that the proposed value for setting the maximum velocity is between 1% and 10% of the maximum group generation, although a sensitivity analysis will be performed in the next chapter.

Figure 26 – Velocity components.
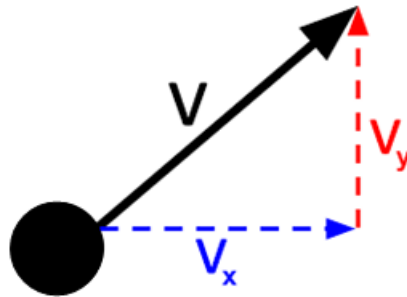
It can be noticed in equation (4.8) that, the maximum velocity is being divided into its x and y components, different from what is found in literature, where a singular maximum velocity is set for both components or for the vector sum of the components. In this work, it is proposed to set a maximum velocity for each component since there might be cases where one of the groups possesses a much lower or higher generation capacity

than the other two groups. If a single maximum velocity is set for a system with this characteristic, the result would be particles moving with excessively big or small steps on one of the axes, hence not finding the desired position.

4.4 PARTICIPATION FACTORS

Section 3.1 explained the conventional methodology for the construction process of the SSSR, which includes a detail demonstration of the participation factors (PFs). In the conventional methodology, there are needed two types of PFs, GPFs and IPFs. The need of GPFs comes from the use of power transfer between regions since the IMPR or the EXPR might be formed of two groups thus.

The mathematical formulations needed for obtaining the GPFs were demonstrated, in which a deep trigonometric analysis is required for the calculations of the mentioned PFs. Finally, a table that contained all the possible scenarios of IMPRs and EXPRs.

In the proposed methodology, since the tool of power transfer between regions is no longer used, there is no need of GPFs. Therefore, the new methodology reduces the complexity of the construction process, because the trigonometric analysis is no longer required, as well as the scenarios of Table 1.

As discussed before the particles of the PSO algorithm explore the feasible dispatch scenarios hence, at each iteration when the particles update their position a new generation profile of each group is obtained. Although, there is still the need for distributing the mentioned generation among the generators of the correspondent groups.

From the previous analysis, it is clear that the new methodology only requires IPFs in the construction process. The IPFs can be calculated in two ways, depending on the study that is performed. The two possible approaches are equal to the ones in the conventional methodology, which are:

- Based on the maximum capability of the generation unit;

- Based on the original dispatch (base case) of each generator.

Depending on the adopted approach the IPFs can be computed as follows:

$$I_{GEN(i)}PF = \frac{P_{MAX(i)}}{CAP_{MAX}} \tag{4.9}$$

$$I_{GEN(i)}PF = \frac{P_{BASE(i)}}{DISP_{TOT}} \tag{4.10}$$

Where:

$$I_{GEN(i)}PF = \text{IPF of generic generator } i;$$

$$P_{MAX(i)} = \text{Maximum capacity of generator } i;$$

$$CAP_{MAX} = \text{Maximum generation of the group that contains generator } i;$$

$$P_{BASE(i)} = \text{Generation of unit } i \text{ at the base case;}$$

$$DISP_{TOT} = \text{Total dispatch of the group that contains generator } i.$$

It can be seen that equations (4.9) and (4.10) are similar from (3.13) and (3.14), except from the term that was associated to the GPFs.

4.5 INITIAL POPULATION

Before starting the iterative process of the PSO algorithm, an initial population needs to be generated. Generally, this population is randomly generated, and it evolves through the iterations.

As explained before, since the proposed methodology is highly impacted by the randomness of the PSO algorithm, because if the initial population is randomly generated across the entire feasible space of solution, which is the total power capacity of the groups that were chosen as the problem variables, there is a high probability that some particles initiate their position with some of the limits violated. The previously described is a problem because they would start with the penalization factor active, in other words, $Z \rightarrow -\infty$, which makes it difficult for the particle to move towards a position without limit violation.

Figure 27 – Proposed initial population.
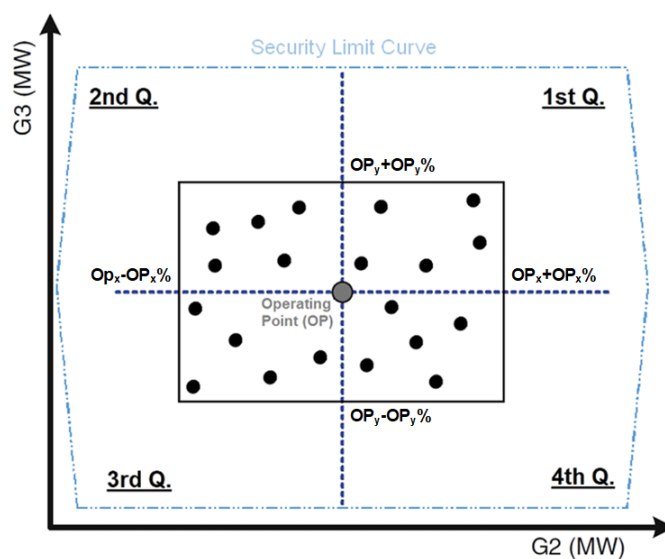
In order to overcome this problem, it is proposed for the particles to be initiated within a pre-established range, close to the base operating point. Besides bounding the initial population, it is proposed for them to be equally distributed around the base

operating point. This can be better explained if the feasible solution space is thought as a Cartesian plane, with the operating point as the origin. Therefore, if it is chosen that the population is formed of 20 particles, they would be distributed around the operating point, with 5 particles on each quadrant, this is clearly illustrated in Figure 27.

4.6 CONSTRAINTS

Clearly, the constraints of the problem that is being analyzed are the maximum and minimum active generation capacities of the groups that were chosen as the problem's variables.

Although, it is proposed to set additional constraints, aiming to improve the accuracy of the SSSR. To achieve this, it is proposed that the particles move only within the quadrant of their initial position. Since the particles are initially distributed around the base operating point, it is expected that by setting these constraints the accuracy of the SSSR is improved, because this helps the particles to be equality distributed around the operating point not only at the beginning but also when the construction process finishes.

The proposed constraints are also convenient for systems that possess a security curve extremely close to the initial operating point in any quadrant. If the proposed bounds were not used, the tendency would be the particles moving across quadrants and not shaping the security curve around the operational point. When the particles are bounded as mentioned above, it is expected that they move in the opposite direction of the base point in the four quadrants, this is illustrated in Figure 28.

Figure 28 – Expected behavior with constraints.
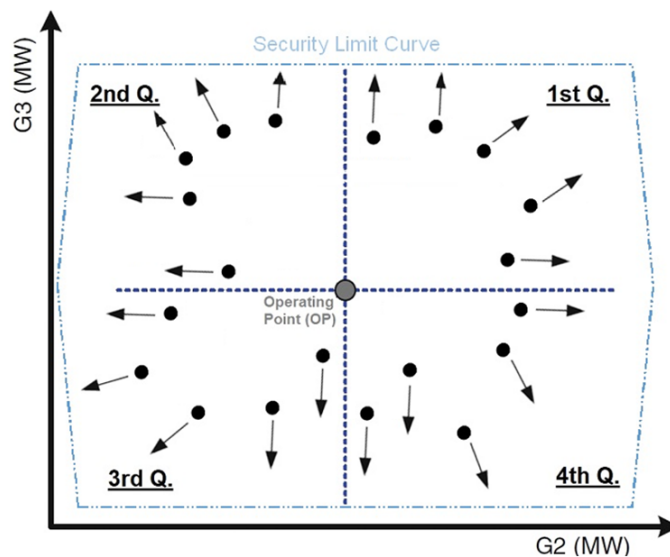
For example, if the initial position of a particle is on the first quadrant of the G2xG3 plane. The constraints of the mentioned particles would be:

$$OP_{G2} < G2 < G2_{max}$$
$$OP_{G3} < G3 < G3_{max}$$

Where:

$OP_{G2,G3}$ = Position of the base operating point in the $G2$ (x) and $G3$ (y)

coordinates;

$G2, G3_{max}$ = Maximum active generation capability of G2 and G3.

4.7   COMPUTATIONAL IMPLEMENTATION

After the iterative process of the PSO algorithm is finished, a final special treatment of the particles is needed. Firstly, since the "swing" group is not part of the problem variables and it changes its generation according to the variations on the other two groups. It is possible that the maximum or minimum active generation capacity of this group was violated because there is no constraint regarding the "swing" group during the iterative process. Therefore, when the iterative process finishes it is needed to validate, for each particle, if the associated generation of the "swing" group is within its limits. If the generation of this group is outside its permissible values, the associated particle is eliminated thus, not forming the final SSSR graph.

Figure 29 – Boundary command.
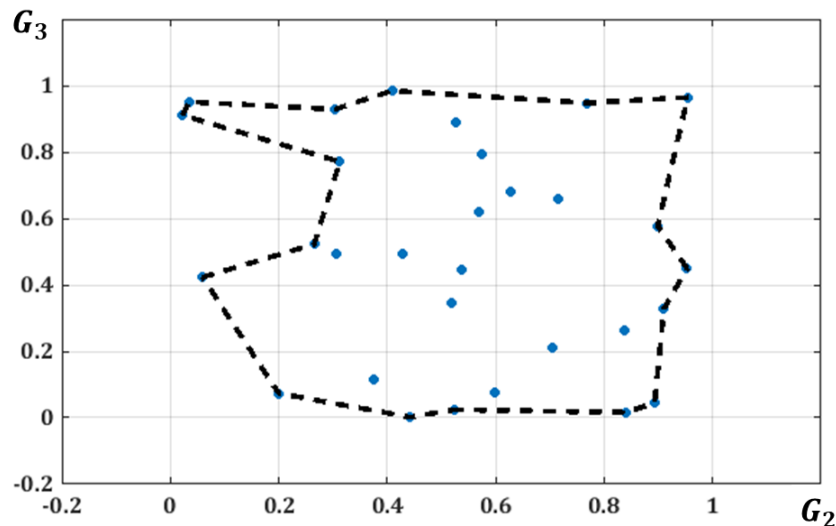
Lastly after the "swing" group validation, even with the implementation of the proposed initial population generation and constraints, there is the possibility that one or more particles do not find the edges of the security curve. Therefore, if these particles are part of the final graphic, the SSSR would be distorted. The mentioned methodology was

developed in the MATLAB environment, and to overcome the problem explained before, the command "boundary", presented in [36], was used. In essence, the command takes a set of points and returns the coordinates of the boundaries around the given set of points as illustrated in Figure 29.

The proposed methodology is summarized in the flow chart shown in Figure 30.

Figure 30 – Flow chart of the proposed methodology.
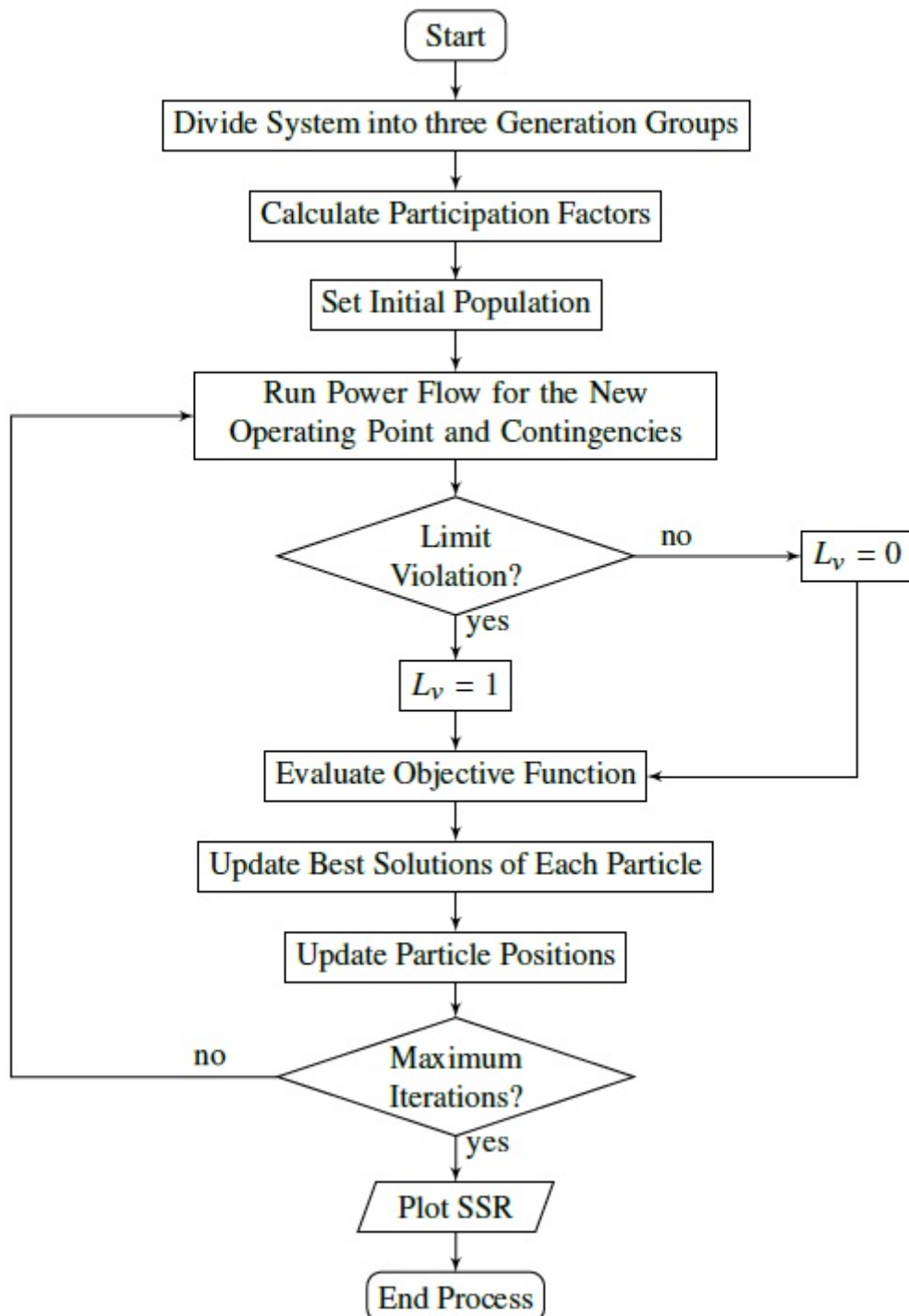
4.8 CHAPTER SUMMARY

This chapter presented an alternative methodology for the construction process of the SSSR. The mentioned methodology is based on the PSO algorithm, nevertheless, it has been adjusted for the problem that is being addressed in this work. Every step of the proposed methodology was detailed, starting from the definition of the variables, which is crucial to determine the problem dimension that the PSO will handle. The proposed optimization model was explained and mathematically demonstrated. The parameters of the PSO algorithm were explained with the purpose of being correctly adjusted for constructing the SSSR with high computational efficiency. Initial population treatment and additional constraints were proposed for the reduction of the impact of the randomness factor, which is intrinsic to the PSO. Lastly the computational algorithm was summarized in a flow chart.

5 RESULTS

This chapter aims to demonstrate both methodologies that were presented in the previous chapters. The analysis will be performed in three power systems, which are:

- 9-bus tutorial system [37];

- 39-bus New England system [38];

- 107-bus southern Brazilian equivalent system [39].

The results are divided into two sections, first the methodology involving the enhanced SSSR will be demonstrated with the systems listed before. To validate the proposed methodology, each region bounded by one of the voltage instability security levels will be compared with the loading margin of the CPF, that will be solved using the academic version of the software ANAREDE. Besides the validation of the effectiveness of the methodology, a comparison of the computational effort will be made.

The second section will demonstrate the results involving the methodology based on the PSO algorithm. The same three systems listed before are used to perform the required analysis. All the parameters that were detailed in the previous chapter will be analyzed, performing a sensitivity analysis of each one of them. The results will be qualitatively validated comparing the proposed methodology with the conventional technique, and also the computational performance of the two methods will be compared.

In order to perform fair comparisons, all the simulations were executed in the MATLAB environment, utilizing the same power flow solver. Every simulation was run in a computer with an *Intel Core i5* CPU at 2.67 GHz, 4.00 GB of RAM and *Windows 10* 64-bit operating system.

5.1 ENHANCED STEADY-STATE SECURITY REGION

5.1.1 **9-bus system**

The first system chosen to demonstrate the proposed methodology regarding the SSSR with the VSI is a tutorial 9-bus system, whose single line diagram is shown in Figure 31. All the data related to the 9-bus system can be found in Appendix A.

Figure 31 – 9-bus system single line diagram.
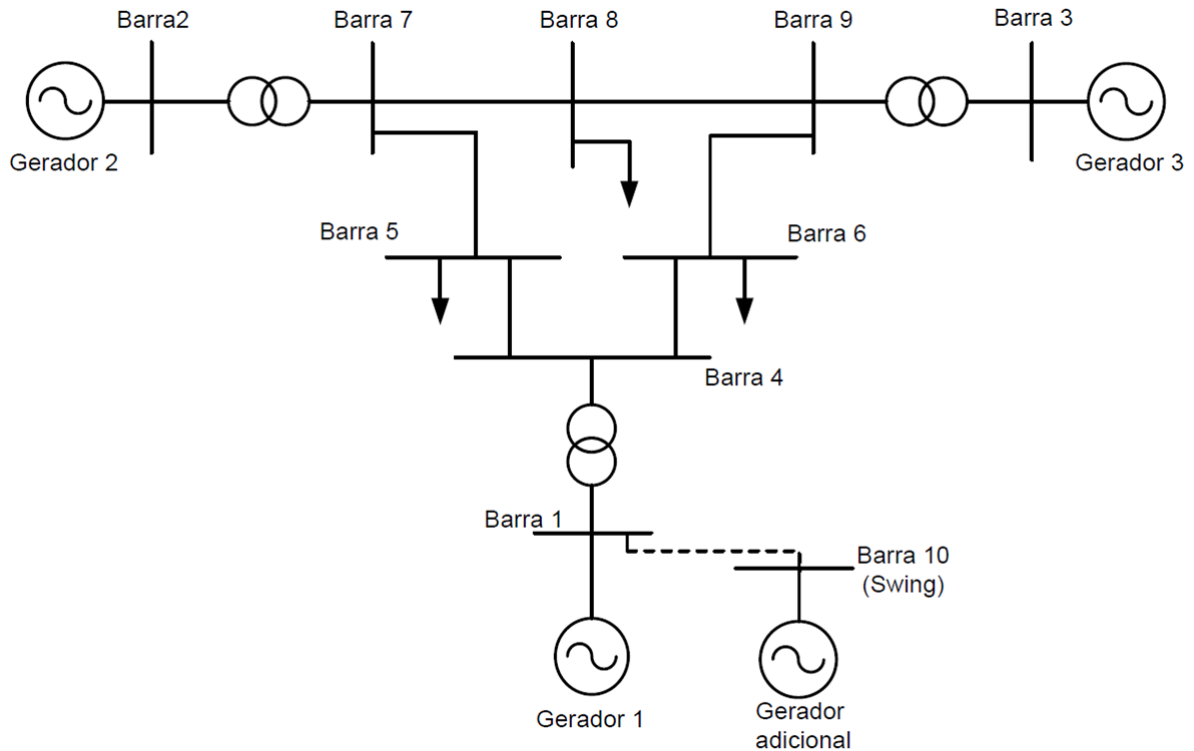
The 9-bus system possesses three PV nodes (buses 1, 2 and 3) and six PQ nodes (buses 4 to 9), additionally a fictitious "swing" bus is added, which is not part of any of the generation groups. This bus is added to supply the power losses, allowing the other generators of the system to increase or decrease their generation profile following the normal construction process of the SSSR. A detailed analysis of the impact of this additional "swing" bus is performed in [31].

Firstly a special configuration of the 9-bus system will be used to construct the SSSR. In this operating point the load of the buses is reduced with respect to the original one and excessive shunt compensation is connected to these nodes. This was performed to clearly show the regions formed on the SSSR using the VSI. Table 3 shows the load and the value of the shunt compensation used in the PQ nodes and the generation of the PV nodes of the 9-bus system.

Table 3 – 9-bus system generation, load and shunt compensation

Bus	Generation (MW)	Load		Shunt Compensation (MVAr)
		Active (MW)	Reactive (MVAr)	
1	442.8	-	-	-
2	279.7	-	-	-
3	264.2	-	-	-
5	-	428.1	171.3	230
6	-	308.3	102.8	150
8	-	342.5	119.9	120

Aiming to show the proposed methodology with detail, each step of the construction process of the SSSR will be shown. The first step, as explained in section 3.1, is to divide the system into three generation groups, since this small system only has three PV nodes the groups will be composed of one generator unit only.

The second step is to determine the EXPR and IMPR, as explained before, they depend on the direction that is being analyzed. In this case, as a tutorial, only four directions are chosen, being 45^0 the initial angle. Calculating α with equation (3.2):

$$\alpha = \frac{360^0}{4} = 90^0$$

The directions to be analyzed are given by equation (3.1):

$$\overline{\theta} = \begin{bmatrix} 45^0 + 0 \cdot 90^0 \\ 45^0 + 1 \cdot 90^0 \\ 45^0 + 2 \cdot 90^0 \\ 45^0 + 3 \cdot 90^0 \end{bmatrix} = \begin{bmatrix} 45^0 \\ 135^0 \\ 225^0 \\ 315^0 \end{bmatrix}$$

To present the rest of the calculations, the first direction is taken as example (45^0), as seen in Table 2 since 45^0 is on the first quadrant, the EXPR is composed by groups G2 and G3, hence the IMPR is formed only by G1. The GPF of G2 and G3 are given by equations (3.6) and (3.7):

$$G_{G3}PF = \frac{1 \cdot \tan 45}{1 \cdot (1 + \tan 45)} \cdot 100 = 50\%$$

$$G_{G2}PF = 100 - 50 = 50\%$$

Clearly, the GPF of G1 is equal to 100% since is the only group composing the IMPR. The IPFs are not required for the 9-bus system since all the groups contain only one generation unit, thus all the IPFs are equal to their corresponding GPFs. Assuming an operating point with a power transfer step of 2%, where the generations of G1, G2, and G3 are, 442.8 MW, 279.7 MW and 264.2 MW, respectively. A power transfer step can be made as follows:

$$G1 = 442.8 - 2 \cdot 1 = 440.8 MW$$

$$G2 = 279.7 + 2 \cdot 0.5 = 280.7 MW$$

$$G3 = 264.2 + 2 \cdot 0.5 = 265.2 MW$$

With the new operating point, a power flow should be solved to evaluate if there is any limit violation, or voltage instability severity level violation. In order to demonstrate the computations of the VSI a power flow solution is shown in Figure 32. This operating point is on the 45^0 direction, after several power transfer steps.

Figure 32 – 9-bus system power flow solution.
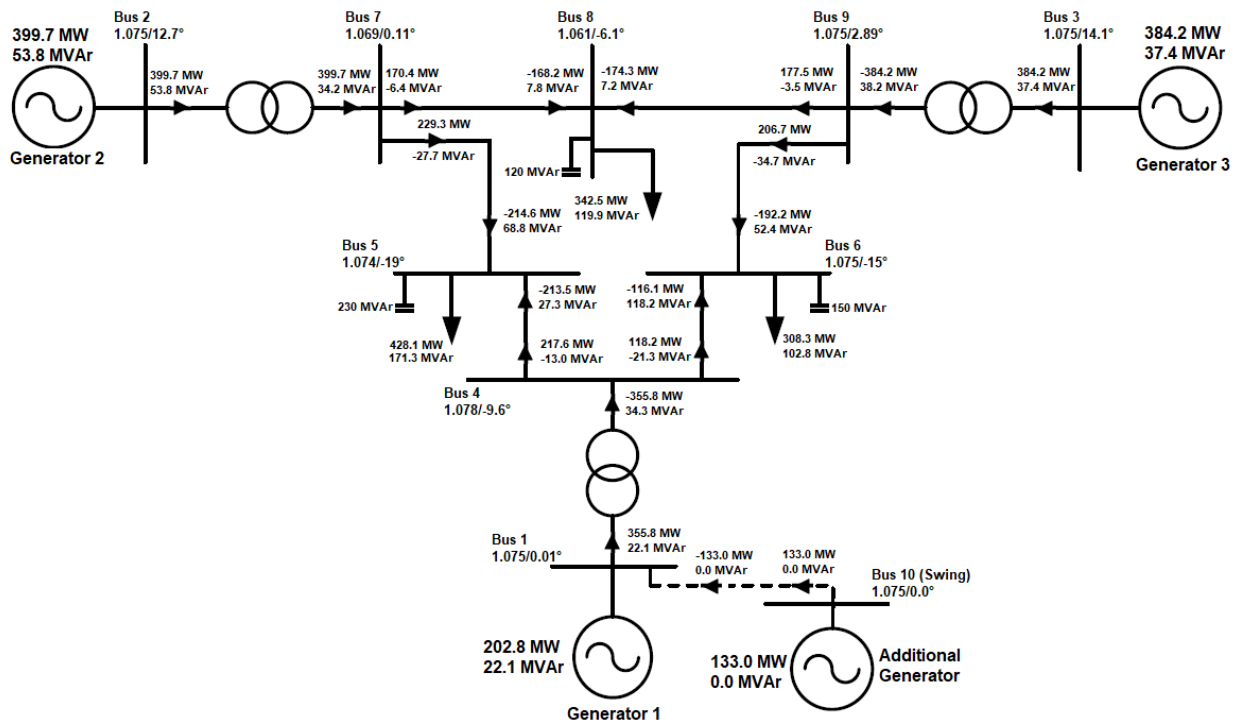
The computation of the VSI will be performed on node 7, since it is a transit bus, its load is given by the active and reactive flows of the transmission lines connected to the mentioned node, as explained in section 3.2.6, from Figure 32 and equations (3.32), (3.33) and (3.34):

$$P_7 = 399.7 MW$$

$$Q_7 = 34.2 MV Ar$$

$$S_7 = 3.997 + j0.342 p.u.$$

The angle of the power factor is given by:

$$\theta_{FP7} = \tan^{-1}\left(\frac{0.342}{3.997}\right) = 4.87^0$$

Assuming a load variation of $10^{-6}p.u.$ a sensitivity analysis can be performed with equation (3.29):

$$\overline{\Delta}_{v,\theta} = -(\overline{J}_x)^{-1} \cdot \overline{J}_p \cdot \begin{bmatrix} \vdots \\ 10^{-6} \cdot \cos 4.87 \\ \vdots \\ 10^{-6} \cdot \sin 4.87 \\ \vdots \end{bmatrix} = \begin{bmatrix} \vdots \\ 1.8 \cdot 10^{-6} \\ \vdots \\ -6.3 \cdot 10^{-6} \\ \vdots \end{bmatrix}$$

Where $\overline{J}_x$ and $\overline{J}_p$ are the Jacobian matrix of the Newton-Raphson method and the Jacobian matrix of the demanded power, respectively. The Jacobian matrix is shown in Appendix A and the Jacobian matrix of the demanded power is a diagonal matrix filled with -1. The vector of load variations is filled with 0 in all its positions except in the ones regarding the analyzed node, in this case, node 7. The new angle and voltage magnitude are given by the update:

$$V_7' = 1.0693 + 1.8 \cdot 10^{-6} = 1.0693018 \ p.u.$$

$$\theta_7' = 0.1117^0 - 6.3 \cdot 10^{-6} = 0.1116937^0$$

The current thru node 7 for both operating points are given by:

$$\overrightarrow{I}_L = \frac{3.997 - j0.342}{1.0693\underline{/-0.1117^0}} = 3.75162\underline{/-4.77885^0}$$

$$\overrightarrow{I}_L' = \frac{3.996999036 - j0.341999915}{1.0693018\underline{/-0.1116937^0}} = 3.75161\underline{/-4.77886^0}$$

With these values Z_{Th} can be computed using equation (3.23):

$$|\overline{Z}_{Th}| = \left|\frac{1.0693018\underline{/0.1116937^0} - 1.0693\underline{/0.1117^0}}{3.75162\underline{/-4.77885^0} - 3.75161\underline{/-4.77886^0}}\right| = 0.17105 p.u.$$

The load impedance can be obtained from equation (3.20):

$$\overline{Z}_L = \left| \frac{(1.0693\underline{/0.1117^0})^2}{3.997 + j0.342} \right| = 0.28502 p.u.$$

Finally the VSI of node 7 is computed from equation (3.19):

$$VSI_7 = \frac{0.17105}{0.28502} = 0.6001$$

This value of the VSI is inside the first voltage instability level proposed in section 3.3, thus this operating point is plotted into the three nomograms for the first voltage instability severity level curve. All the other limits have to be validated for each operating point. Assuming that in this tutorial only the voltage level limit, which is allowed between 0.9 and 1.1 p.u., and convergence limit are taken into consideration, it can be seen in Figure 32 that none of these limits were violated for this operating point. This tutorial was set in this manner to clearly observe how the zones created with the voltage instability levels are shaped around the base operating point, and how they illustrate the proximity to voltage collapse.

After the limit validation process mentioned before, another power transfer step is made and everything is repeated again until the convergence limit or the active power limit of one of the groups is reached. Then the next direction (angle) is analyzed following the same structure that was demonstrated before. The nomograms constructed for the 9-bus system in this particular case are shown in Figures 33, 34 and 35.

Figure 33 – 9-bus system G1xG2 plane with VSI.
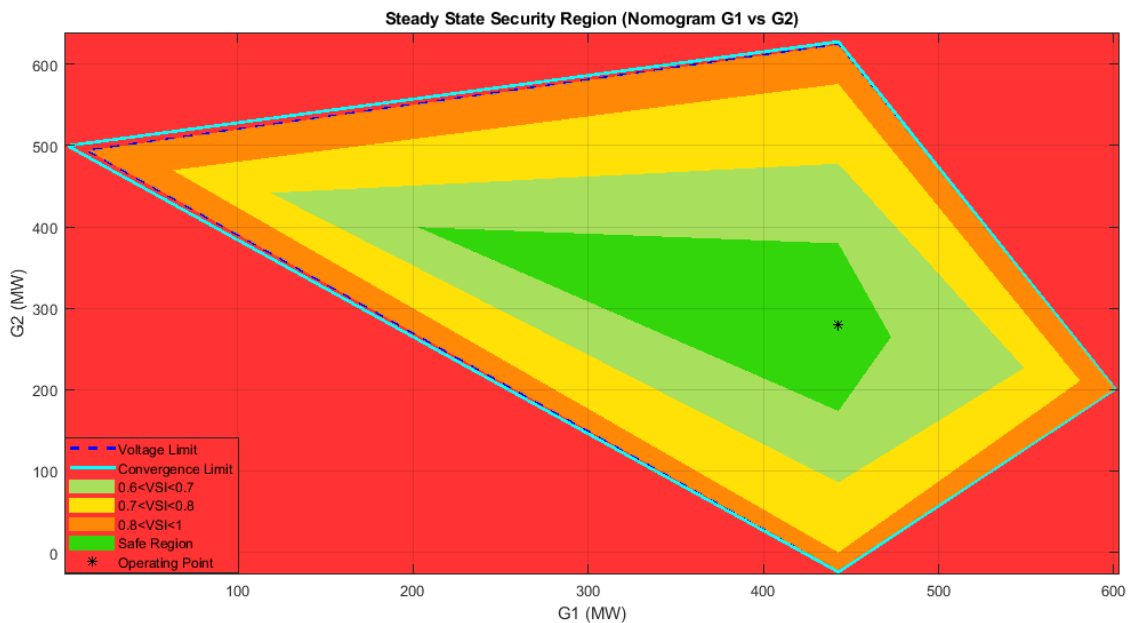
Figure 34 – 9-bus system G1xG3 plane with VSI.
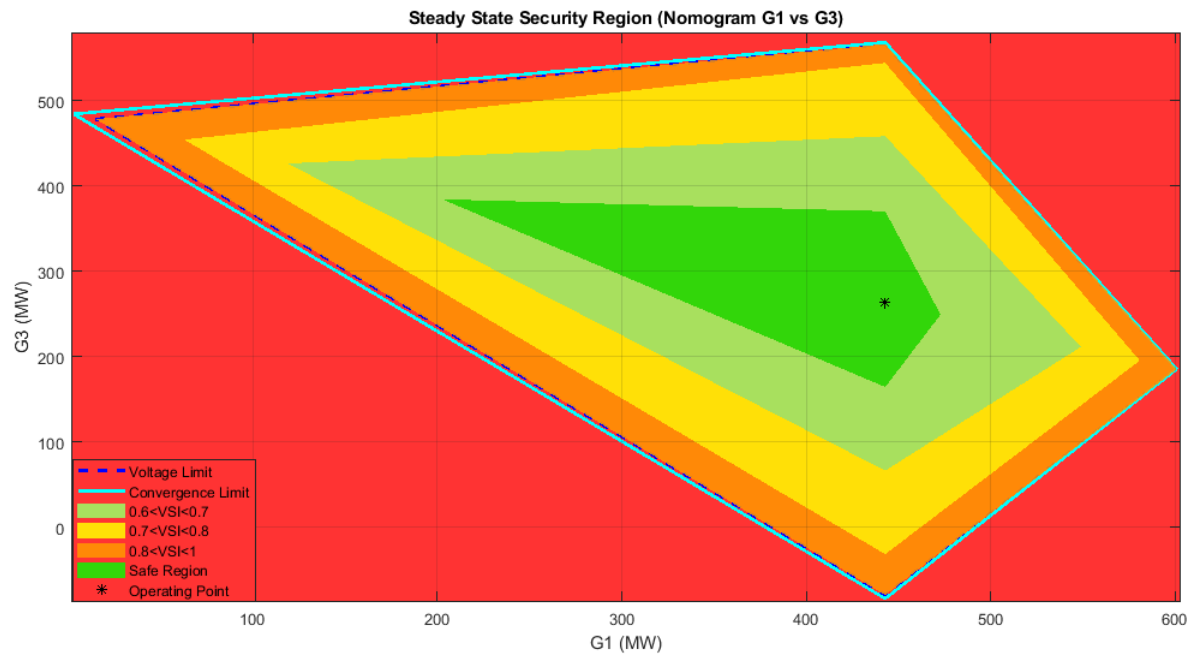
Figure 35 – 9-bus system G2xG3 plane with VSI.
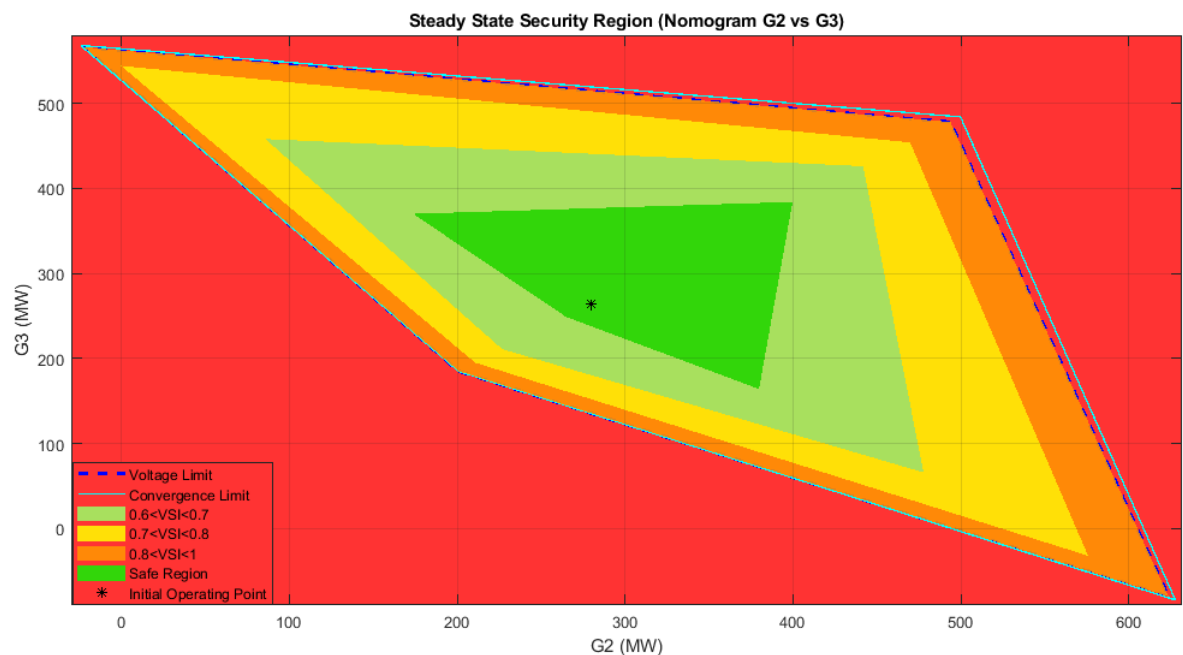
In order to compare the nomograms constructed with the proposed methodology and the ones constructed with the conventional methodology, Figure 36 shows the G2xG3 plane constructed with the conventional technique. As can be seen with the conventional methodology the SSSR does not provide any indication of voltage instability, showing possible operating conditions as safe even when they are proximate to the voltage collapse point. Although the convergence limit can be taken as an indicator of voltage instability, as explained before, not always the no convergence of the Newton-Raphson method indicates that the system is at the critical point.

Figure 36 – 9-bus system G2xG3 plane with conventional methodology.
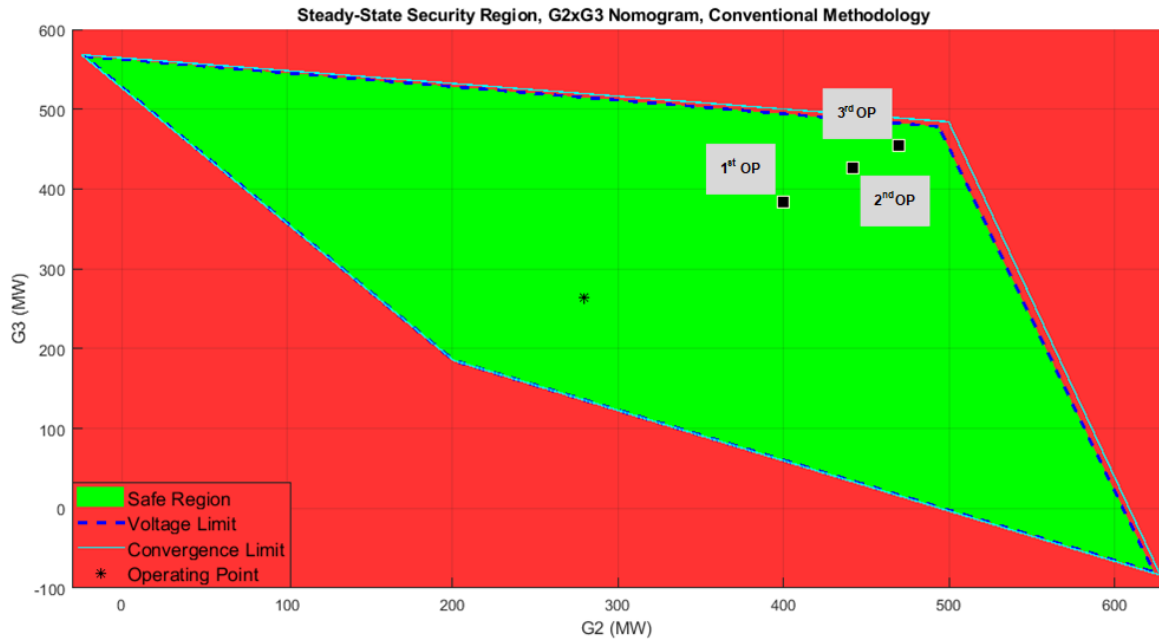
An important characteristic of a power system with voltage instability problems can be analyzed with the previous nomograms, that is, monitoring the voltage level is not sufficient for detecting voltage instability. In this case due, to excessive shunt compensation, the voltage collapse point is reached with a high voltage level. This will be clear in the validation process.

The proposed methodology is validated through the use of the CPF method. The validation process consists of running a CPF and obtain the PV curves for three operating points that were evaluated in the SSSR construction process. Each validated point is inside of different regions of the proposed voltage instability severity levels. For each obtained PV curve the loading margin will be computed, expecting that the higher the voltage instability severity level the lower is the loading margin. The simulations of the CPF are performed with the academic version of the network analysis software ANAREDE. The three operating points that are validated are marked in Figure 36, and detailed in Table 4.

Table 4 – Operating points for validation

Bus	OP 1 Generation (MW)	OP 2 Generation (MW)	OP3 Generation (MW)
1	202.9	118.8	62.85
2	399.7	441.7	469.7
3	384.2	426.2	454.2

It is important to emphasize that loads and shunt compensation are the same as the operating point for the simulations on ANAREDE, as it is done in the construction process of the SSSR. Figure 37 shows the voltage behaviour of bus 7 for the three operating points.

Figure 37 – 9-bus system, PV curve of evaluated operating points.
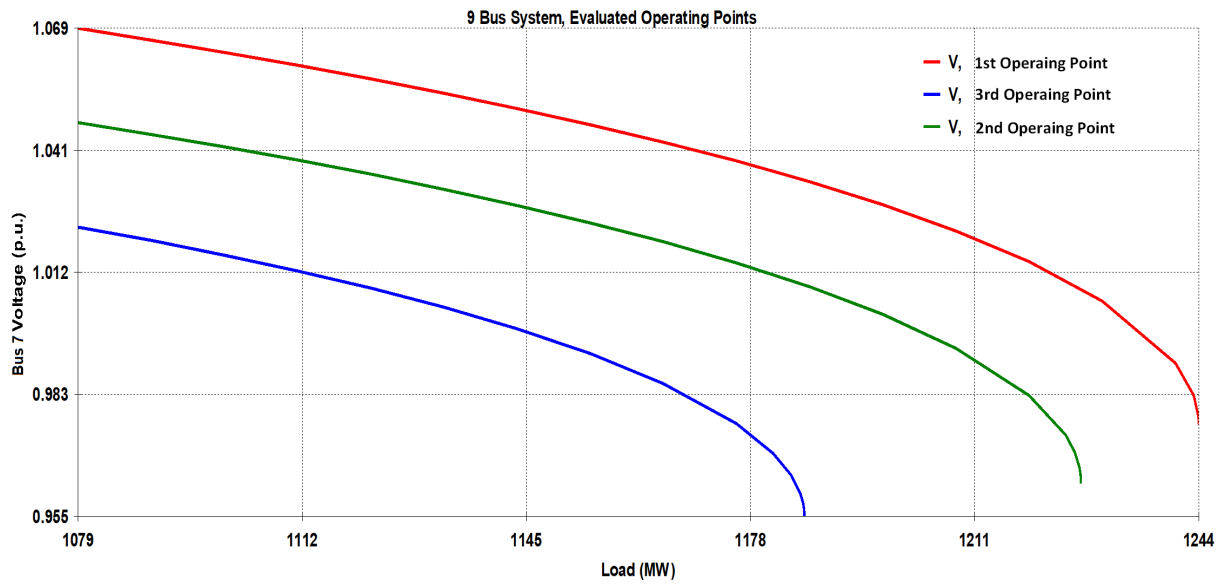
It is clear from the PV curves of the operating points that were evaluated that the voltage instability severity levels effectively detect the proximity to the voltage collapse point. Aiming to numerically demonstrate the previous statement, the loading margin of the three operating points is computed below.

The loading margin of the first operating point, which is inside the range $0.6 < VSI < 0.7$, is given by:

$$LM_1(\%) = \frac{1244 - 1079}{1079} \cdot 100\% = 15.3\%$$

The loading margin of the second operating point, which is within the second voltage instability severity level $0.7 < VSI < 0.8$, is computed as follows:

$$LM_2(\%) = \frac{1227 - 1079}{1079} \cdot 100\% = 13.7\%$$

Finally the loading margin of the third operating point, which is inside the highest severity level proposed $0.8 < VSI < 1$, is given by:

$$LM_3(\%) = \frac{1186 - 1079}{1079} \cdot 100\% = 9.9\%$$

The effectiveness of detecting voltage instability problems with the proposed SSSR is demonstrated through the PV curves and the loading margins of the three operating

points that were chosen. The next analysis will be also performed on the 9-bus system, but with a different base operating point and taking into considerations all the limits (voltage level, thermic limit on transmission lines and transformers, active and reactive generation and convergence). The generation, loads and shunt compensation at each bus for the new analysis are shown in Table 5. All the values of the limits are detailed in Appendix A.

Table 5 – 9-bus system new generation, load and shunt compensation

Bus	Generation (MW)	Load		Shunt Compensation (MVAr)
		Active (MW)	Reactive (MVAr)	
1	130.4	-	-	-
2	101.2	-	-	-
3	67.4	-	-	-
5	-	131.25	52.5	10
6	-	94.5	31.5	-
8	-	105	36.75	-

Figure 38, 39 and 40 show the nomograms obtained for the new system configuration and the following parameters were used for the construction process:

- Number of directions = 100;

- Step size = 2%;

- Contingencies = Transmission Lines 4-5, 4-6, 6-9, 7-5, 7-8 and 8-9 out of service.

Figure 38 – 9-bus system G1xG2 plane.
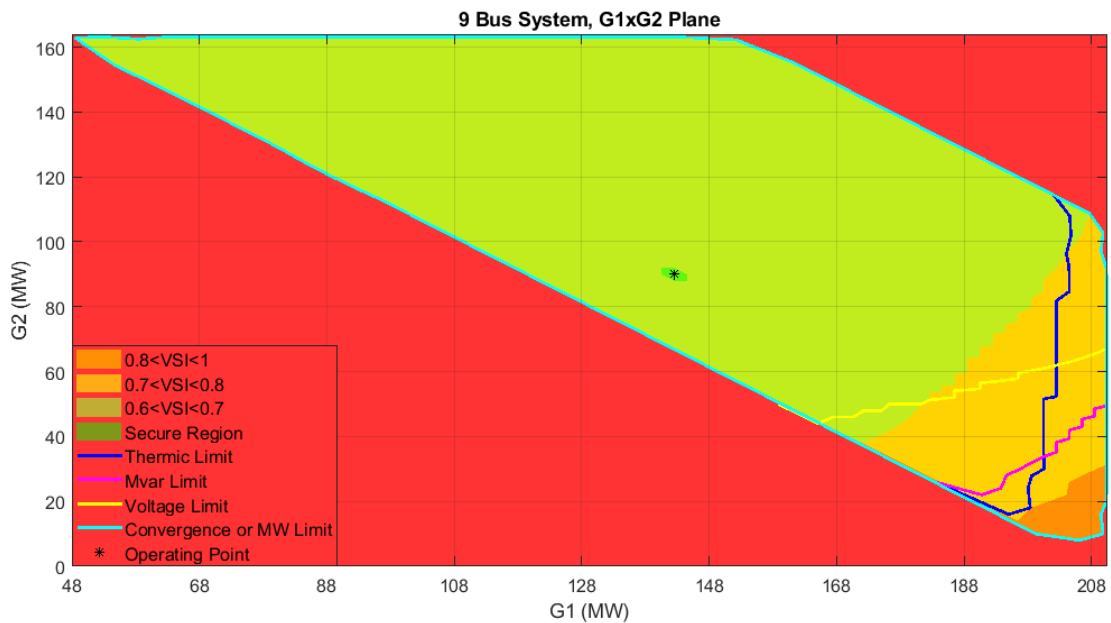
Figure 39 – 9-bus system G1xG3 plane.
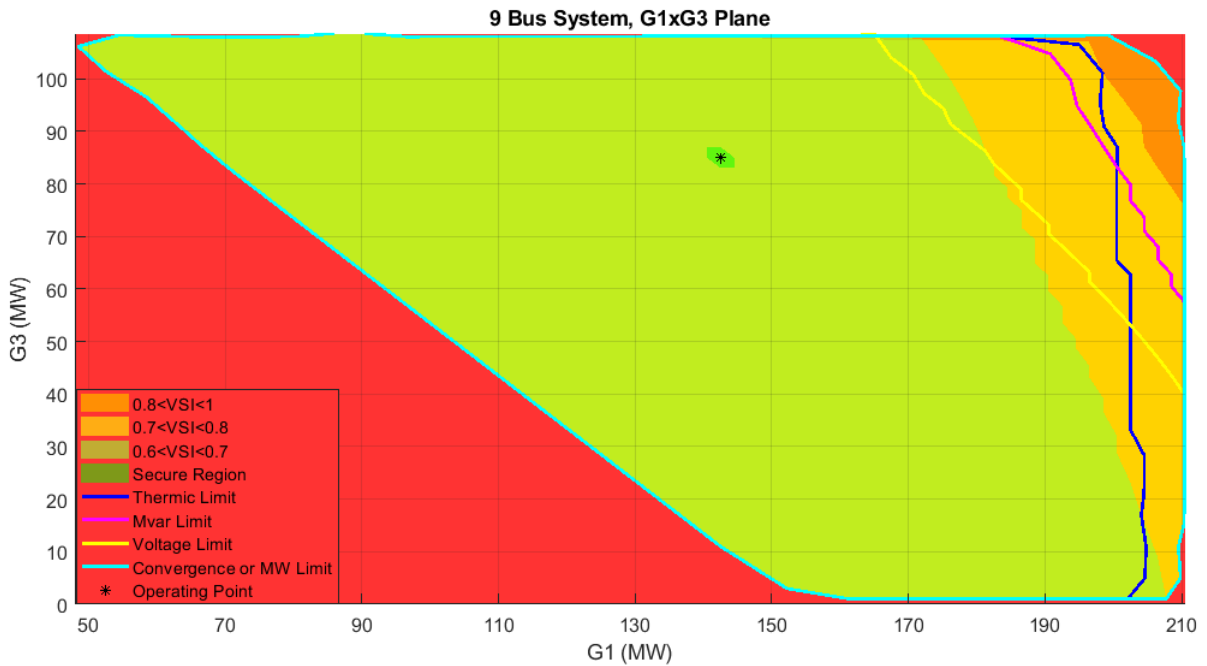
Figure 40 – 9-bus system G2xG3 plane.
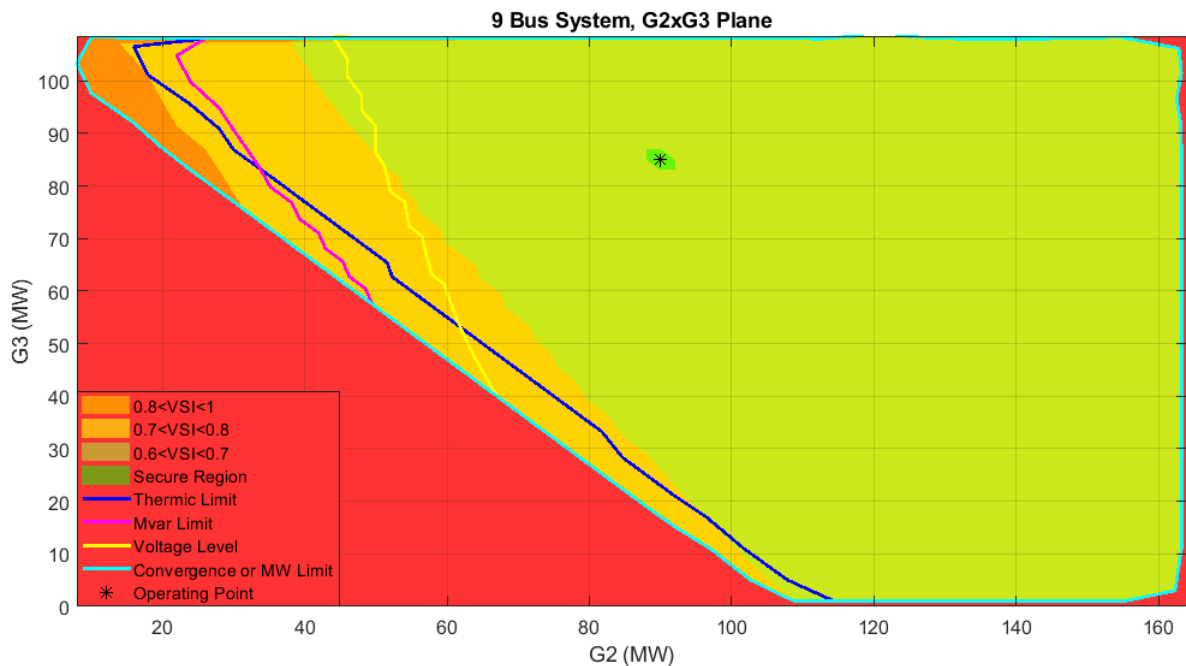
From the mentioned nomograms, it can be seen that all the limits were violated in some directions. From the final output of the computational program that was developed, it can be affirmed that all the limit violations occurred with the contingency characterized by the removal of the transmission line 4-5. Therefore, the three operating points that will be used for validation, with the help of PV curves, take into consideration the mentioned contingency. The configuration of each of the three operating points that will be evaluated with the software ANAREDE is detailed in Table 6. Figure 41 illustrates the G2xG3

nomogram constructed with the conventional methodology, and it also marks out the three operating points used for the validation to have a visual orientation of where they are located.

Figure 41 – 9-bus system G2xG3 plane with conventional methodology.
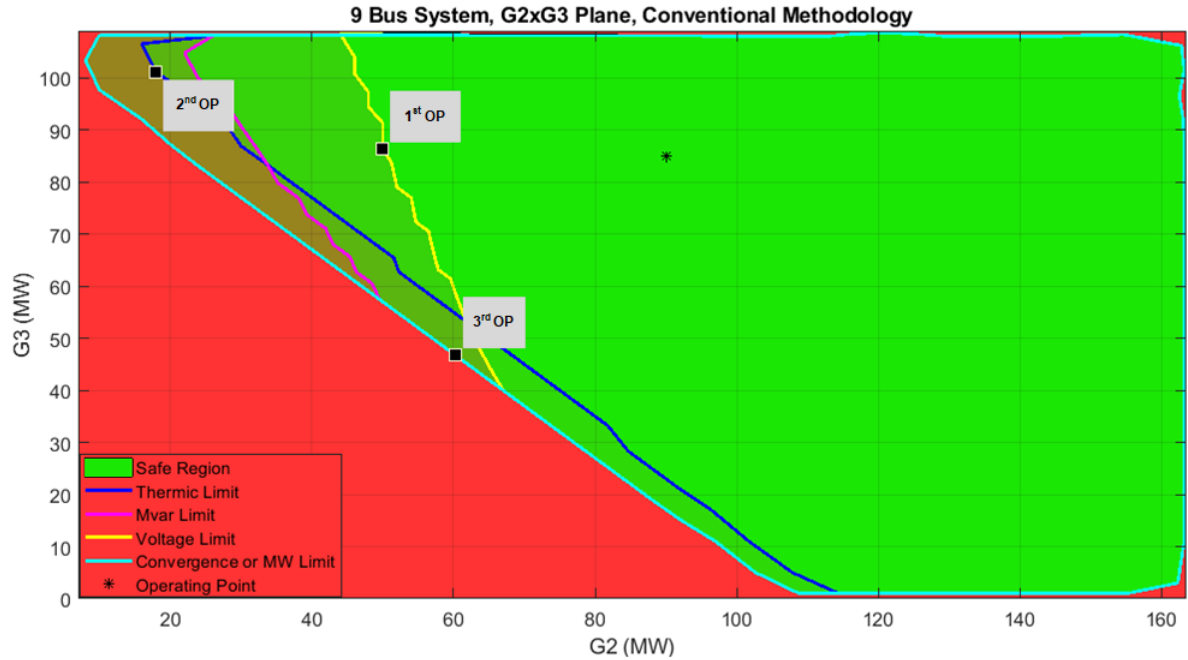
Table 6 – Operating points for validation

Bus	OP 1 Generation (MW)	OP 2 Generation (MW)	OP 3 Generation (MW)
1	181.2	198.4	210.4
2	50	18	60.3
3	86.26	101.1	46.7

The previous operating points were chosen for different reasons. The first two operating points aim to demonstrate that the proposed voltage instability levels detect efficiently the proximity to the MLP. The third operating point, as it can be seen from Figure 41, is on the edge of the SSSR, since the construction process stops if the voltage collapse point is reached or if the maximum generation of a group is reached, if the conventional methodology was used it would not be clear if the process stopped due to a voltage instability problem or simply because a group reached its maximum generation capacity, Figure 42 shows the PV curves of bus 5 for the three operating points that were chosen for the validation.

From the mentioned curves, it can be seen that the expected results were obtained. The first operating point, which is inside the second voltage instability severity level $0.7 < VSI < 0.8$, has a larger loading margin than the second operating point, which is inside the third severity level $0.8 < VSI < 1$. Finally the PV curve of the last evaluated

Figure 42 – 9-bus system, PV curve of evaluated operating points.
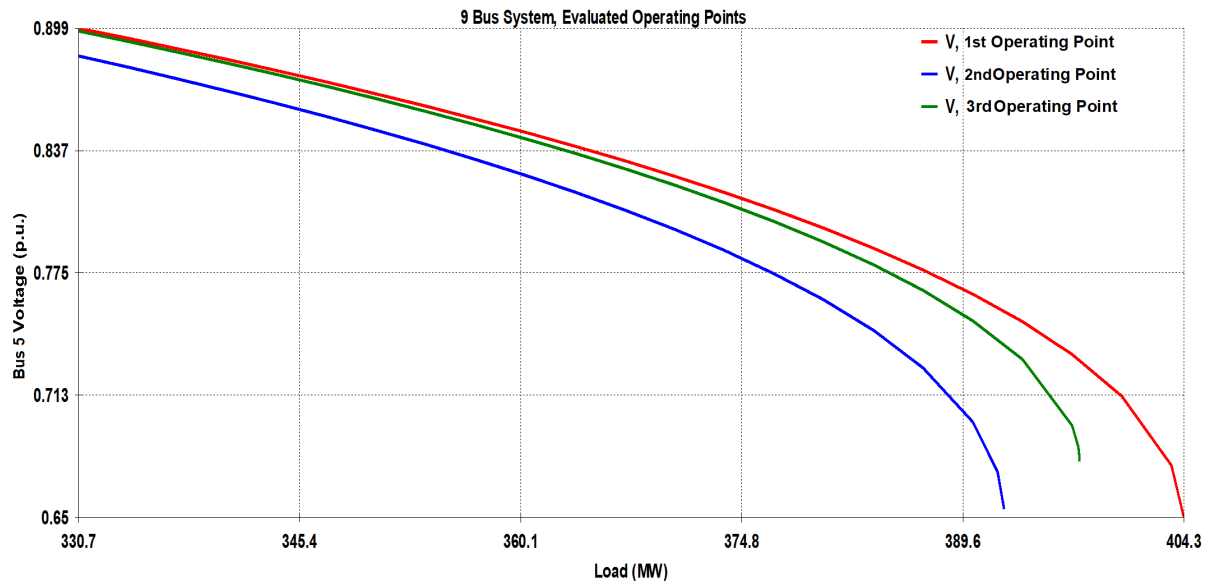
operating point demonstrated that the system is not on the voltage collapse point, hence the SSSR construction process stopped at that point because one groups reached its maximum generation capacity.

This can be proven by looking in Table 6, where the generation of bus 1 (G1) is 210.4 MW, which is the maximum capacity of the mentioned generator, as shown in Appendix A. Although this can be proven looking at the data, in *real-time* operation it would not be practical to search the correspondent points of the three nomograms to ensure that the construction process of the SSSR was stopped due to maximum generation capacity. Therefore, with the proposed subregions constructed with the VSI it becomes simpler to determine this type of situation.

The last test that will be performed on this system is about the computational effort. Where the time that requires the construction process of the SSSR with the conventional and the proposed methodology is compared. The results are shown in Table 7, which is the computing time required to construct the nomograms of Figures 38, 39, 40 and 41.

Table 7 – Computational performance

Methodology	Time (s)	Difference
Conventional	86.95	19.8%
Proposed	108.41	

The objective of the previous comparison was to demonstrate the impact that the insertion of the VSI has on the construction process of the SSSR. Table 7 clearly shows that the computing time required for the conventional and the proposed methodology are

considerably different. The mentioned difference is due to the sensitivity analysis that has to be performed for each bus at each power transfer step. The difference between the methodologies might increase for larger systems, this will be analyzed with the New England system and the southern Brazilian equivalent system.

5.1.2 New England system

The second system chosen for the analysis of the proposed methodology is the New England system, which is well known in the literature. This system has 39 nodes, among them 10 are PV buses and 29 are PQ buses. The topology of the New England system is shown in Figure 43 as well as the generation group division.

Figure 43 – New England system single line diagram and group division.

In this system, the SSSR with the proposed methodology will be constructed for a single base operating point. The transmission line data, generation data, and load data is available in Appendix B.

The SSSR is shown in the nomograms of Figures 44, 45 and 46, these were constructed with a smaller loading level than the one found in the literature. The parameters used to construct this nomograms are:

- Number of directions = 50;

- Step size = 5%;

- Contingencies = None considered.

The nomograms of the Figures below will be compared with the nomogram in Figure 47, which is the G2xG3 plane of the same system with the same loading and dispatch, but constructed with the conventional methodology. Figure 47 also shows the three operating points that will be analyzed throughout the use of the CPF and PV curves, in this case, the operating points will also be evaluated with the help of the QV curves, which are also obtained with the network analysis software ANAREDE in its academic version.

Figure 44 – New England system G1xG2 plane.
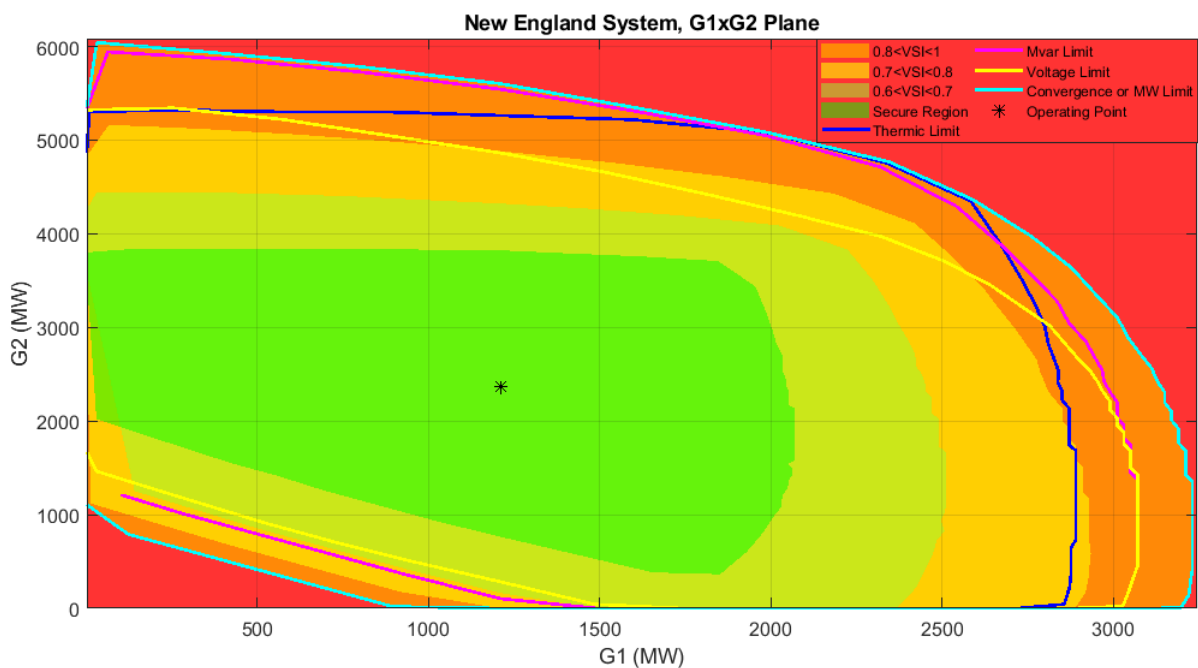
Figure 45 – New England bus system G1xG3 plane.
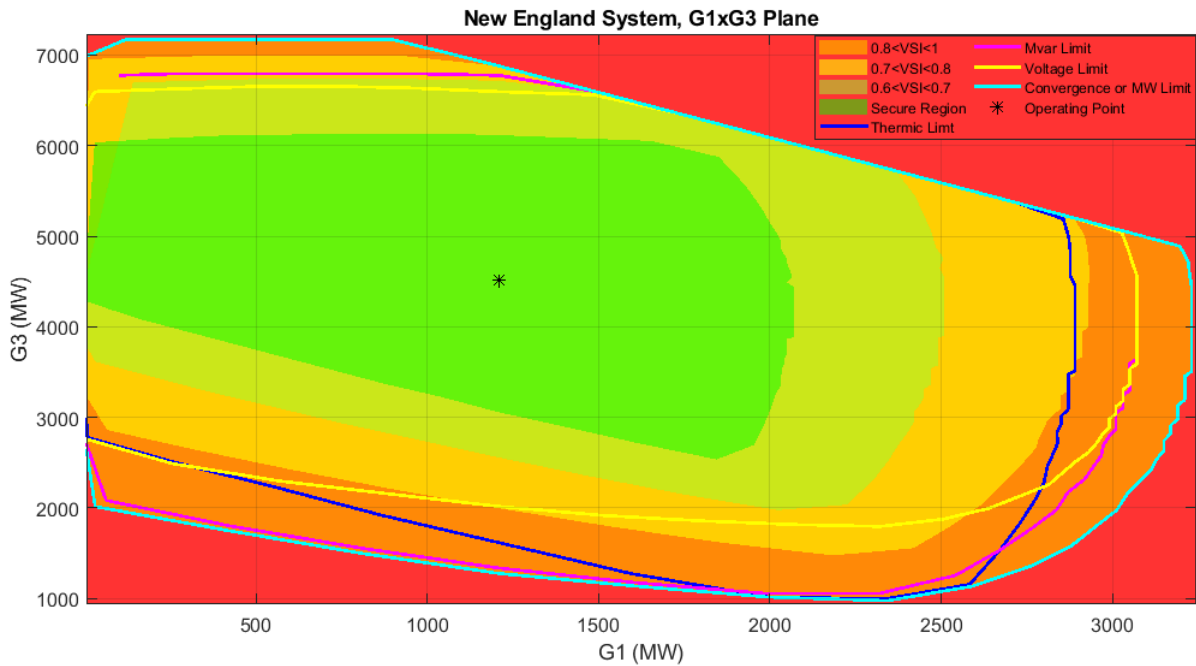
Figure 46 – New England system G2xG3 plane.
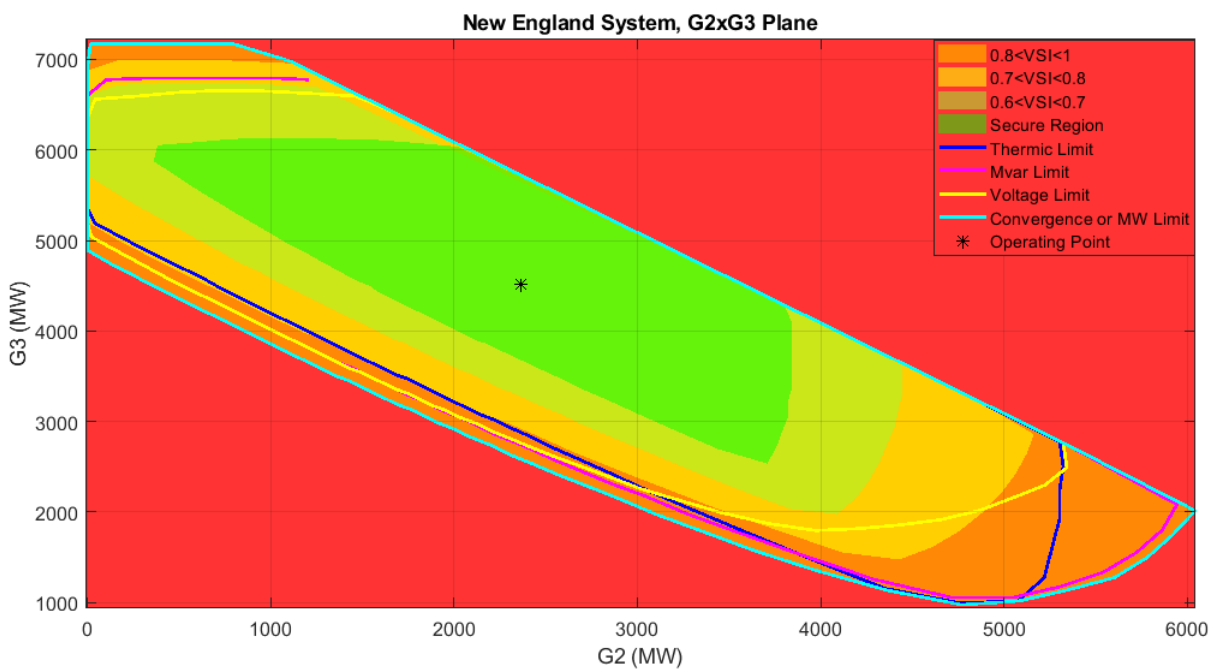
The previous nomograms show the three subregions created with the VSI and show that all the limits were violated in several directions. It can be seen that, even with this low load level, there might be voltage instability problems if the wrong dispatch profile is used. Therefore, this demonstrates the effectiveness of the proposed methodology in the voltage stability assessment. As it was done with the previous system three new operating points are chosen to validate the methodology with the classic voltage stability assessment tools, these are pointed out in Figure 47.

Figure 47 – New England system G2xG3 plane with conventional methodology.
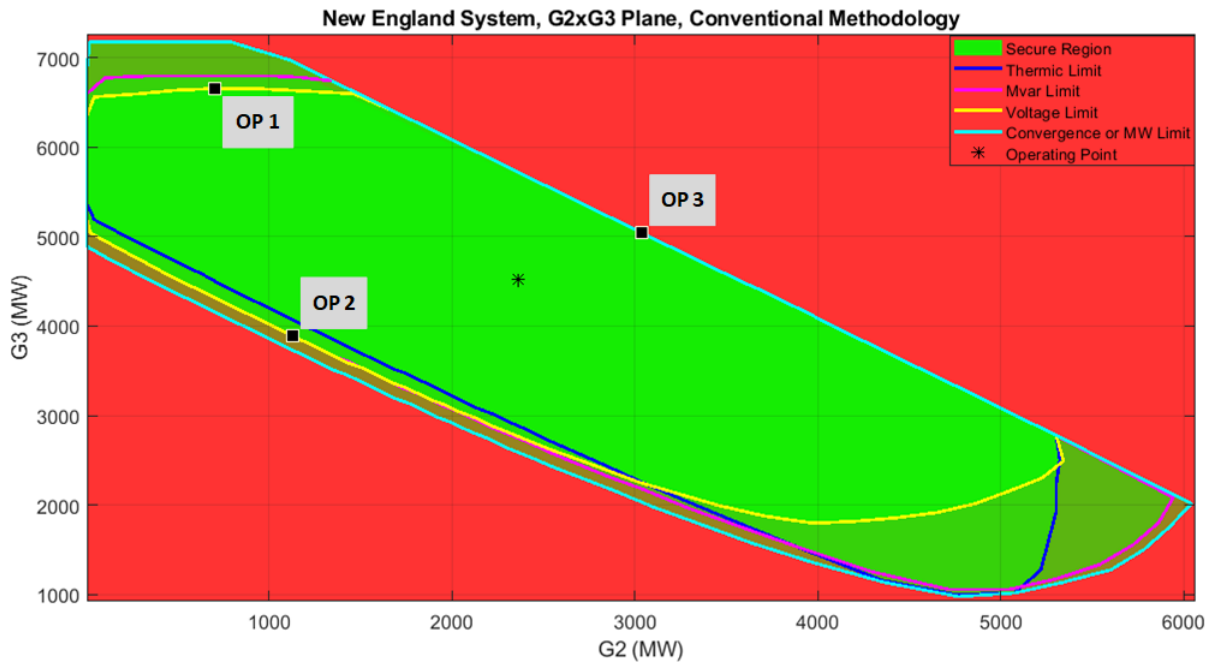
The three different dispatch configurations were chosen to demonstrate different situations that allow analyzing the accuracy of the subregions. The first operating point is inside the first severity level $0.6 < VSI < 0.7$. The second scenario is inside the third severity level $0.8 < VSI < 1$, even being "closer" than the first scenario to the base case, this aims to demonstrate that not always the dispatch configurations that are "close" to the base case are safer in terms of voltage stability. Finally, the third dispatch profile aims to show that the construction process did not stop due to the voltage instability problem since it is on the edge of the SSSR but is within the secure region. The generation of each PV bus for the three dispatch profiles is shown in Table 8.

Table 8 – Dispatch scenarios analyzed

Bus	OP 1 Generation (MW)	OP 2 Generation (MW)	OP 3 Genaration (MW)
30	368.5	215.2	279.2
31	170.6	274.3	738.3
32	193.4	311.1	837.3
33	188.1	302.5	814.1
34	151.2	243.1	654.3
35	392.1	1649.2	0.5
36	337.9	1420.8	0.5
37	795.9	464.9	603.1
38	1223.3	714.6	927.0
39	4268.3	2493.3	3234.6

The buses with the highest voltage variation of each dispatch scenario are chosen

to be displayed in the PV curves. The PV curves of the three operating points, obtain with the simulations of the CPF on the software ANAREDE, are shown in Figure 48.

Figure 48 – New England system, PV curves of evaluated operating points.
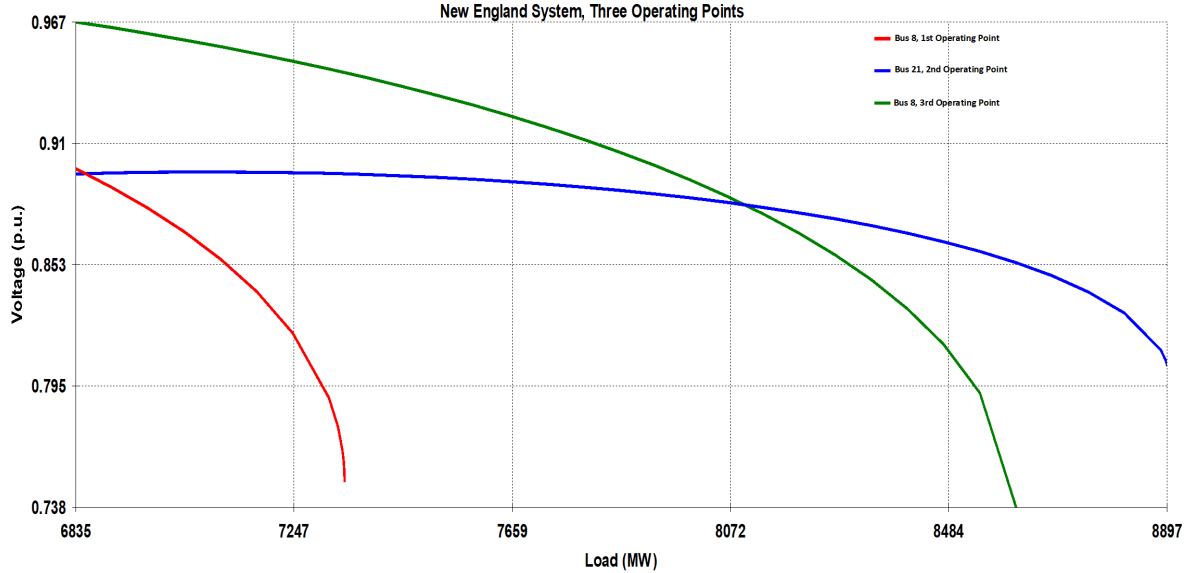
From the previous curves, it can be seen that what is expected did not happen on simulations with the CPF since it was expected that the second operating point would have the smallest loading margin, instead it is the operating point with the largest loading margin. A similar situation happened with the first operating point, it was expected to have a larger loading margin, instead it was the dispatch profile with the smallest loading margin. To perform a deep analysis of these situations, another simulation is performed on ANAREDE, obtaining the QV curves of all the buses of the New England system. Figure 49 shows the QV curves of the nodes with the smallest reactive power margin of each of the three operating points.

It can be seen from the QV curves that the expected result was obtained, that is, the second operating point with the smallest reactive power margin, followed by the third and first dispatch scenarios with nearly identical reactive power margin. Table 9 shows the loading margin and the reactive power margin of each evaluated operating point with both methodologies, the CPF and the QV curves.

Table 9 – Loading and reactive margin of evaluated operating points

Method	OP 1 Margin	OP 2 Margin	OP 3 Margin
PV Curve (%)	7.41	30.2	25.9
QV Curve (MVAr)	-608.6	-87.5	-668.3

Figure 49 – New England system, QV curves of evaluated operating points.
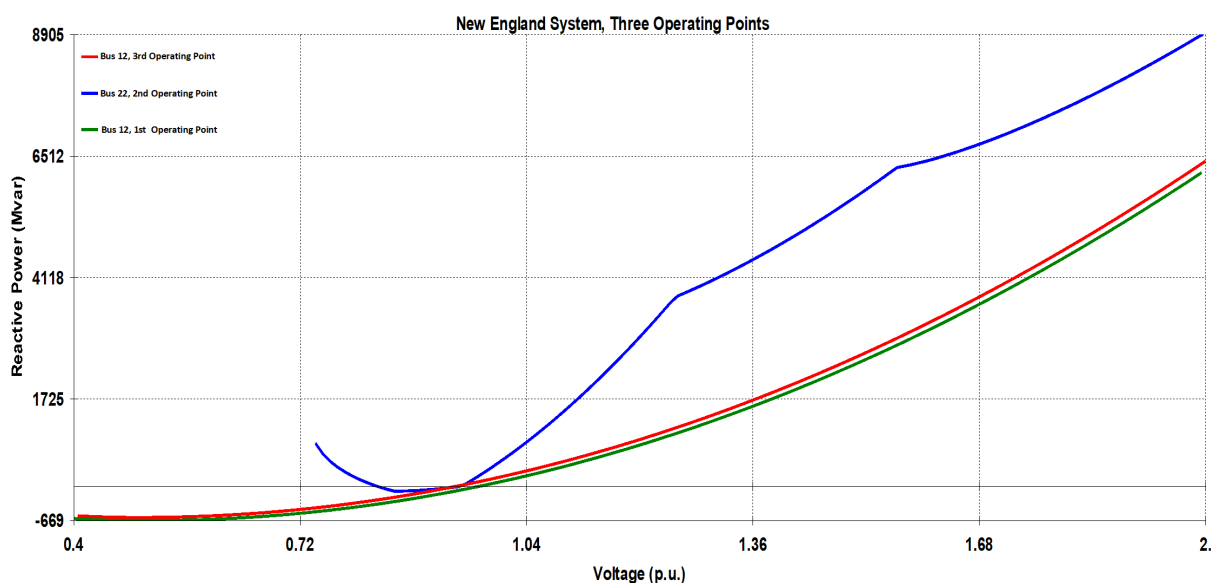
It was also shown from the previous curves and Table 9 that the third dispatch profile still has a large loading margin and a significant reactive power margin, thus the construction process did not end due to a voltage instability problem, as it was pointed out by the proposed subregions.

The difference found in both methodologies, CPF and the QV curves, can be explained due to the principle that they use to determine the loading margin and the reactive power margin respectively. Since the CPF solves successive power flows with a small increment on the load level until it reaches the voltage collapse point, it might not accurately represent the principle used in the SSSR construction process. Since the SSSR keeps a constant load level throughout the whole process. Therefore, even using the CPF with a base case as one of the operating points explored by the SSSR, it does not represent accurately the current situation, in terms of voltage stability, of different dispatch scenarios with the same load level. On the other hand, QV curves may represent the operating points explored with the SSSR more accurately with the use of the reactive power margin since it does not change the load on the system. Instead it solves a series of power flows for each bus with different reactive power injections.

The previous analysis with the classic methods of voltage stability assessment demonstrates the complex and time consuming that this analysis can be, showing the effectiveness of the SSSR constructed with the proposed voltage instability severity levels. This turns the SSSR a very practical tool that can be easily used for preventing voltage instability due to its effectiveness and for its ease manner of displaying the required information.

The last analysis will be comparing the computational performance of both, the

conventional and the proposed methodology. Table 10 shows the computing time required for both methodologies to construct the nomograms shown in Figures 44, 45, 46 and 47.

Table 10 – Computational performance

Methodology	Time (s)	Difference
Conventional	155	66.6 %
Proposed	464.8	

It can be seen from Table 10 that the proposed methodology takes a significantly larger amount of computing time than the conventional methodology, although this is expected since new information is being added to the SSSR. Even though the proposed methodology takes advantage of results already available from the conventional methodology, it still takes a considerable amount of time.

5.1.3 **107-bus southern Brazilian equivalent system**

The last system that will be used for validating the proposed methodology is an equivalent of the southern Brazilian system. This system possesses 107-buses, among them there are 25 generation nodes and 82 PQ buses, it also has 104 transmission line circuits and 67 transformers. The transmission line data, transformer data and nodes data of the base operating point are available in Appendix C, as well as the voltage limit of each node, the reactive generation limit of each PV node and the active generation capacity of each generating unit.

The system is divided into three areas, the South-east area, Mato Grosso area, and South area. These areas are used as the generation groups G1, G2, and G3, respectively for the construction process of the SSSR. The single line diagram of the 107-bus system is shown in Figure 50, as well as its division into the three mentioned areas.

In order to demonstrate the effects of the proposed methodology in the construction of the SSSR the same validations of the previous systems will be performed. Comparing the nomograms constructed with the conventional methodology and the proposed methodology, and choosing three operating points explored on the nomograms and comparing the voltage instability severity levels with the PV curves obtained through the CPF method and the QV curves, both ran in the network analysis software ANAREDE.

In the construction process the following parameters were used to obtain the SSSR:

- Number of directions = 50;

- Step size = 2%;

- Contingencies = None considered.

Figure 50 – 107-bus southern Brazilian equivalent system.

The IPFs were computed in terms of the original dispatch of each generating unit. The nomograms obtained with the proposed methodology are shown in Figures 51, 52 and 53. Figure 54 shows the G2xG3 plane obtained with the conventional methodology and also the operating points that were chosen to be analyzed with the CPF and the QV curves. The generation profile of each PV node for each operating point is shown in Table 11.

The operating points that will be analyzed with the classic methods of voltage stability assessment were chosen to demonstrate that the warnings given by the proposed voltage instability severity levels are effective for detecting proximity to voltage collapse even when the original base case is already in a dangerous situation. Also that throughout the whole feasible space of power flow solution the proposed subregions created with the VSI correspond to the correct state of the analyzed system.

In the nomograms obtained with the proposed methodology, it is possible to observe that the whole region inside the feasible power flow solution (convergence limit) is shown in orange, this indicates that the system even in the base operating point is already within the third and most dangerous voltage instability severity level. It can also be seen that the thermic limit and voltage limit are extremely near the base case. It is good to emphasize

Table 11 – Dispatch scenarios analyzed

Bus	Group	OP 1 Generation (MW)	OP 2 Generation (MW)	OP 3 Generation (MW)
12	3	305.3	283.3	341.3
16	3	814.2	755.4	910.2
20	3	915.9	849.8	1023.9
22	3	152.7	141.6	170.7
35	3	203.5	188.9	227.5
48	3	0.0	0.0	0.0
300	3	712.4	661.0	796.4
301	3	305.3	283.3	341.3
302	3	407.1	377.7	455.1
303	3	203.5	188.9	227.5
305	3	305.3	283.3	341.3
500	3	814.2	755.4	910.2
21	2	137.5	126.8	120.4
4596	2	225.9	208.3	197.8
4804	2	49.1	45.3	43.0
4523	2	49.1	45.3	43.0
800	1	1147.2	1156.2	993.2
808	1	1199.4	1208.9	1038.4
810	1	1251.6	1260	1083.6
904	1	730.2	736.0	632.2
915	1	730.2	736.0	632.2
919	1	728	728.0	632.2
925	1	991.2	999.1	858.2

that no contingencies were taken into consideration to construct these nomograms, which also indicates that the system is nearly at a total collapse point.

Figures 55 and 56 show the PV curves and QV curves that were obtained by performing simulations in ANAREDE. Each curve corresponds to a selected node of each operating point that is detailed in Table 11. Since the nomograms show that all the possible dispatch scenarios are within the highest severity level it is expected that all the evaluated operating points have a small loading margin and a small reactive power margin. The last operating point aims to demonstrate if the construction process stopped due to the convergence limit or due to a group reaching its maximum or minimum active generation capacity.

Figure 51 – 107-bus system G1xG2 plane.
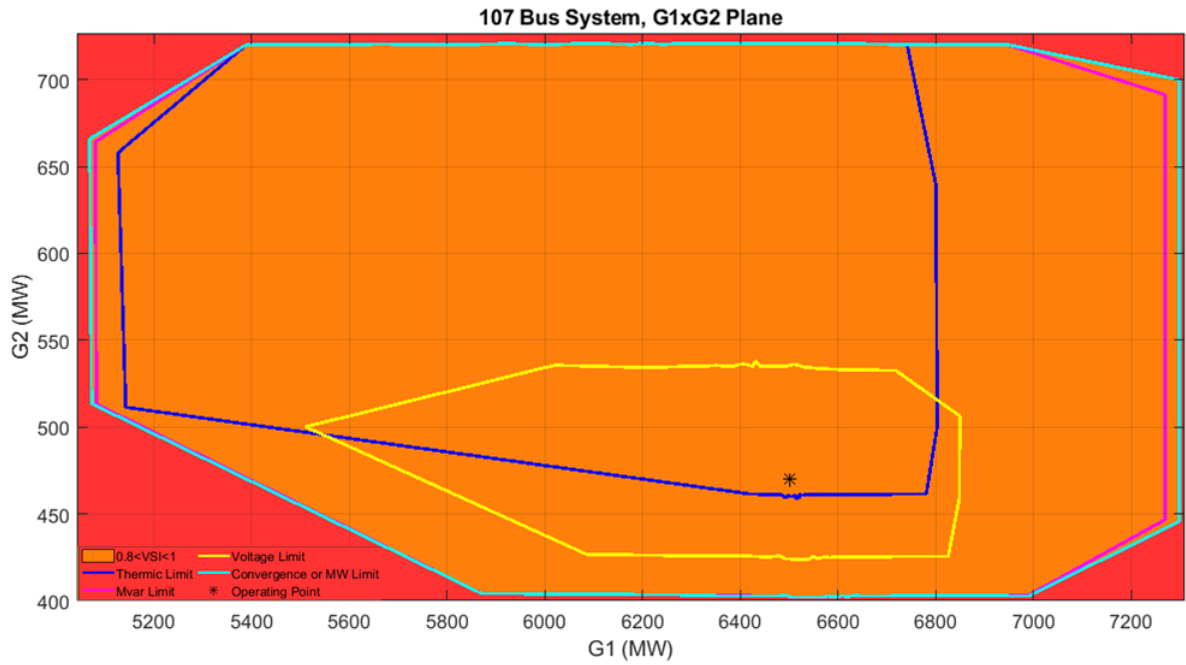
Figure 52 – 107-bus system G1xG3 plane.
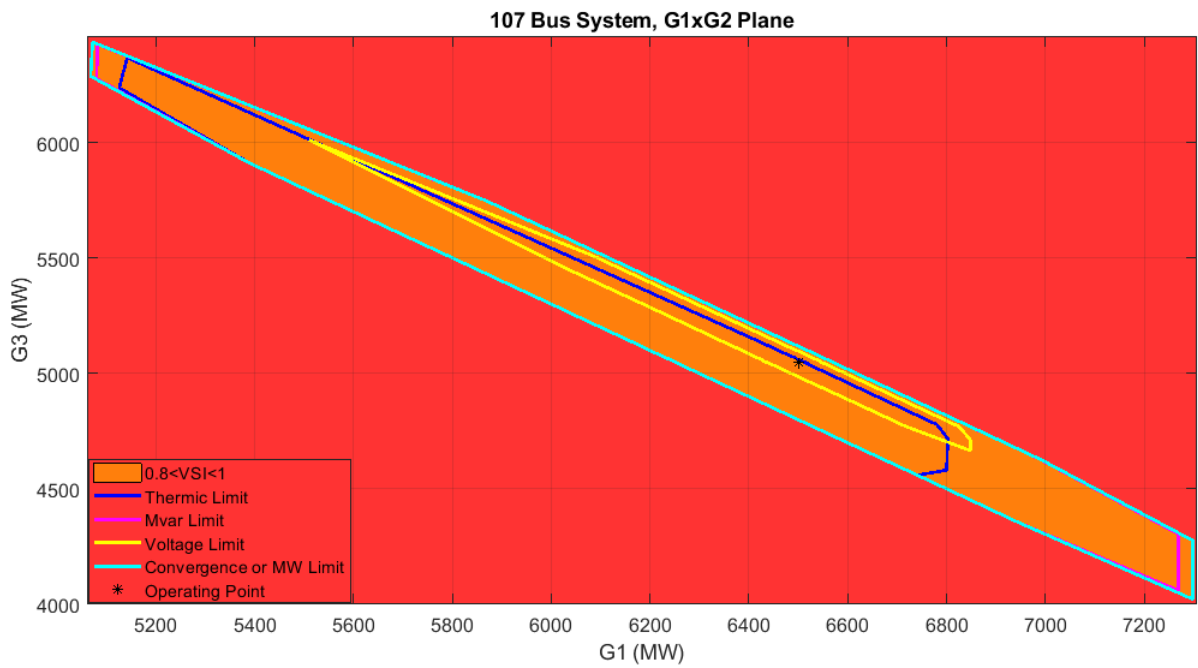
Figure 53 – 107-bus system G2xG3 plane.
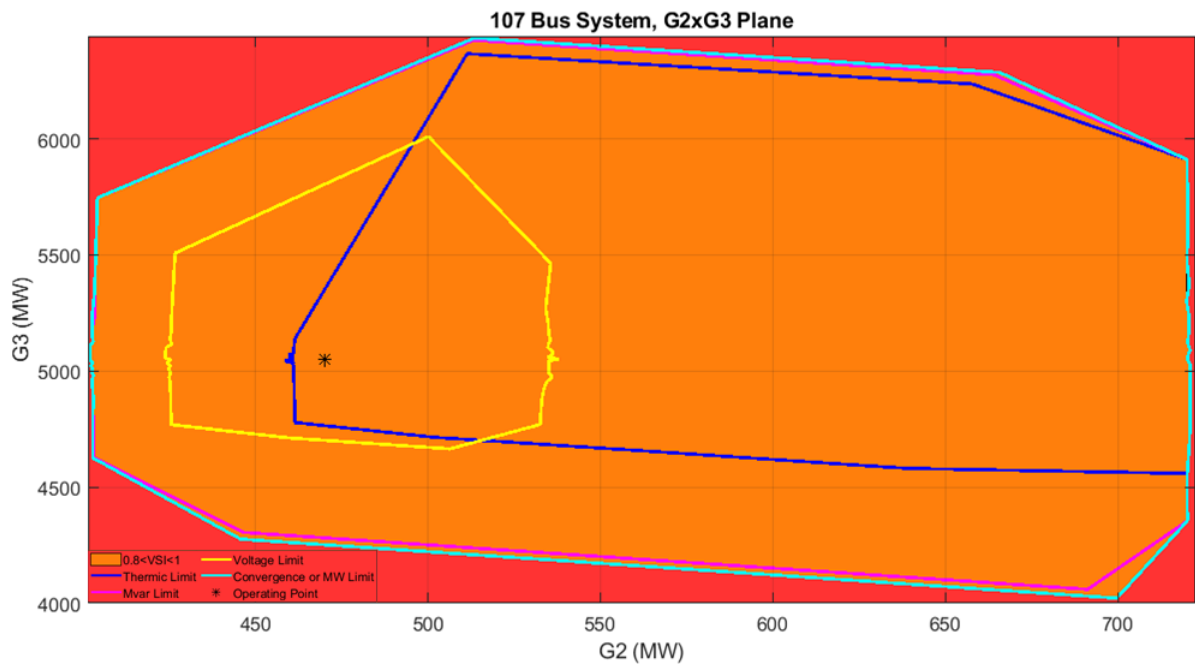
Figure 54 – 107-bus system G2xG3 plane with conventional methodology.
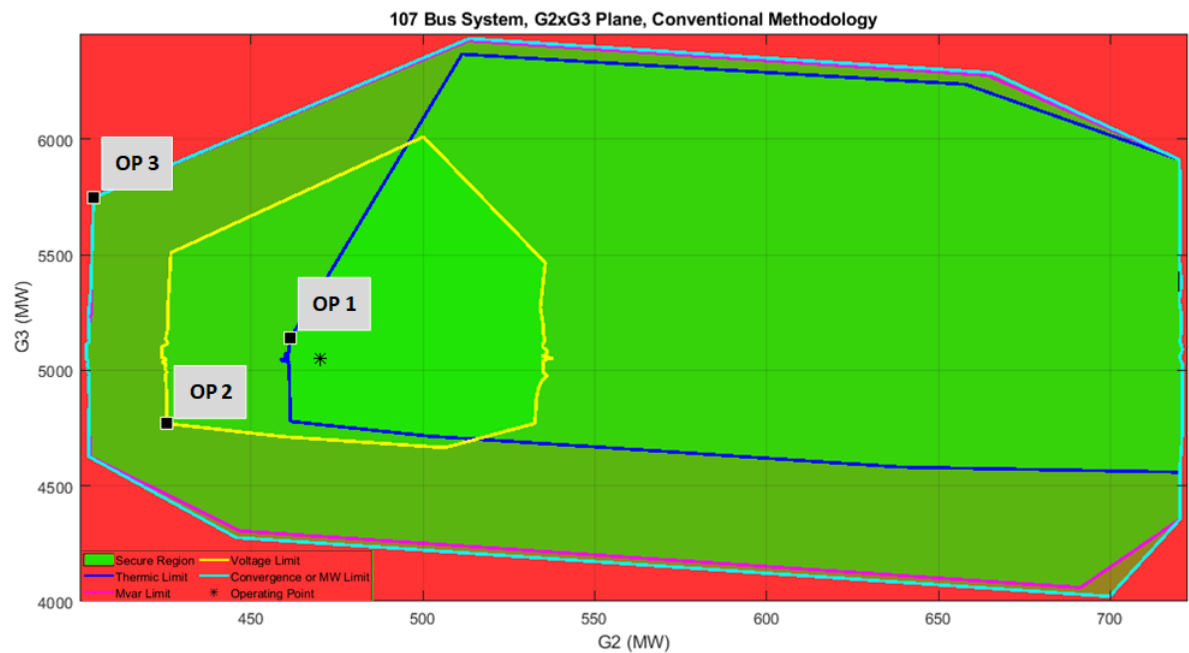
It is clear from Figure 54 that the conventional methodology does not provide any information about voltage instability, differently from the nomograms created with the proposed methodology that indicates that the whole system is near to a total blackout. The first operating point marked out in the previous figure is expected to have the largest reactive margin since it is the one with the biggest distance to the convergence limit, a smaller margin is expected for the second operating point and for the third dispatch scenario is expected a null reactive power margin and loading margin, since the system

is within the most dangerous severity level, it can be said that the construction process stopped due to the convergence limit and not because one group reached its maximum capacity.

Figure 55 – PV curves of evaluated operating points.
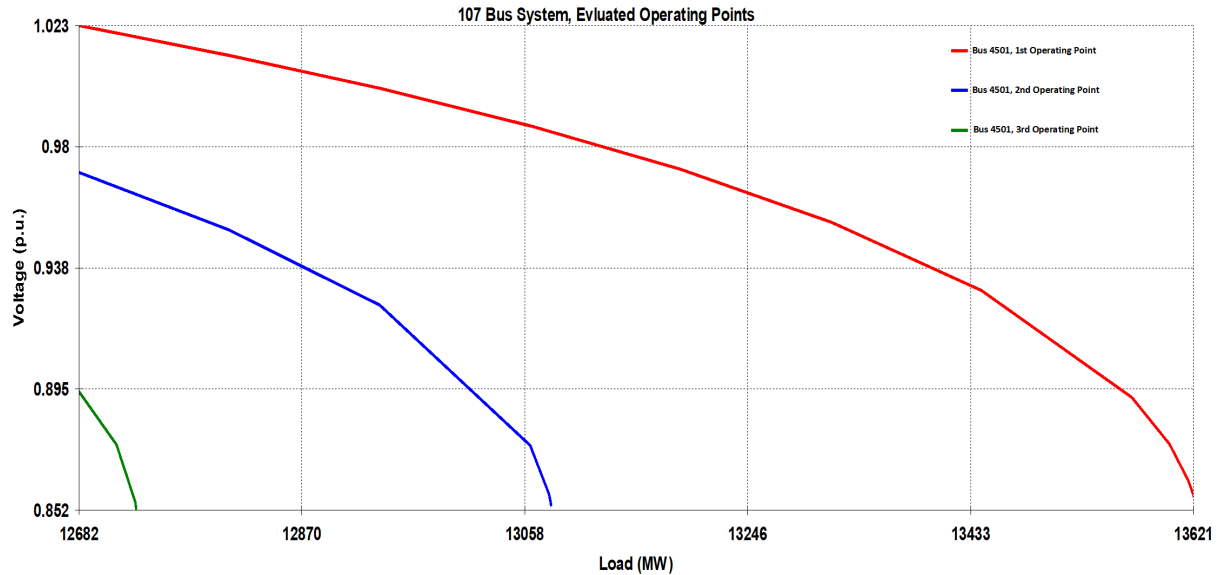
Figure 56 – QV curves of evaluated operating points.
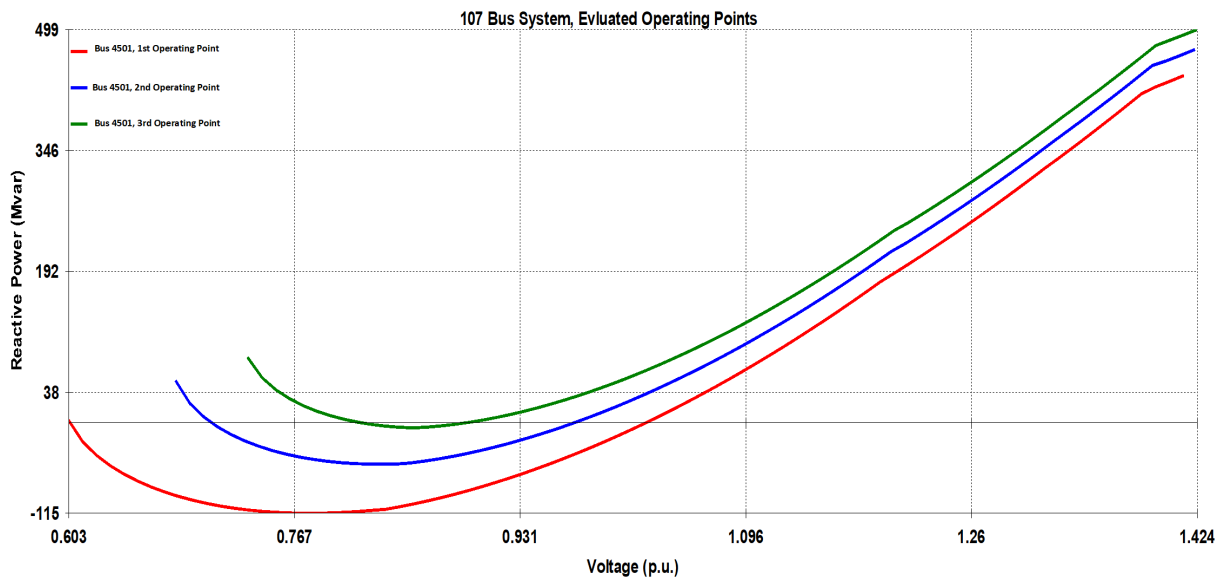
It can be seen from the PV curves and QV curves that the expected behavior of the three operating points was obtained in both methodologies. Different from the previous system where the PV curves and the QV curves did not coincide in their results. This might be due to the closeness of the operating points to the maximum allowable transfer power of the system since there is no big difference between the evaluated operating points

in terms of stressing the system in different manners. As said before the first two operating points have a larger loading margin and reactive power margin and the third operating has an extremely small loading margin and reactive margin almost null, which proofs that the construction process stopped due to a voltage stability problem. This was detected by the proposed methodology as explained before. Table 12 details the exact loading margins and reactive power margins of the operating points.

Table 12 – Loading and reactive power margin of evaluated operating points

Method	OP 1 Margin	OP 2 Margin	OP 3 Margin
PV Curve (%)	7.4	3.14	0.38
QV Curve (MVAr)	-115.3	-53.1	-6.9

The last analysis performed on this system is the computational performance, as it was shown for the previous systems, it is expected that the proposed methodology takes a larger amount of time to construct the SSSR. The computational effort required by both methodologies is compared in Table 13.

Table 13 – Computational performance

Methodology	Time (s)	Difference
Conventional	445	66.2 %
Proposed	1318	

It is clearly observed in Table 13 that the proposed methodology takes a larger amount of time, as it was seen in the previous systems. Even though the proposed methodology is more practical than the classic methods of voltage stability assessment, the computational effort required by the technique makes the proposed methodology infeasible for *on-line* environments.

Although the proposed methodology is infeasible for *real-time* monitoring, it can be very helpful for *off-line* studies, such as network expansion, generation expansion, planning of long-term operation and short-term operation, among others.

The computing time of the proposed methodology (as well as the conventional methodology) can be improved with other implementation techniques, such as parallel processing. It can also be applied with new methodologies that improve the conventional methodology's computing time. Even the conventional methodology is not feasible for *on-line* environments when a large system with a large number of contingencies is analyzed. The methodology explained in Chapter 4 aims to overcome this issue for the conventional methodology and the proposed methodology.

5.2 CONSTRUCTION OF STEADY-STATE SECURITY REGIONS BASED ON THE PSO ALGORITHM

5.2.1 **9-bus system**

As it was done for the previous methodology, the first system that will be used for the validation of the proposed methodology is the small 9-bus system, whose single line diagram was shown in Figure 31. The operating system that will be used for the simulations is shown in Table 14.

Table 14 – 9-bus system base case

Bus	Generation (MW)	Load	
		Active (MW)	Reactive (MVAr)
1	117.5	-	-
2	115	-	-
3	85	-	-
5	-	125	50
6	-	90	30
8	-	100	35

It is seen that this operating point is different from the ones used in the previous section because it does not have any shunt compensation. This was done in that manner since the objective in the previous methodology was to demonstrate cases were a system had voltage instability problems, for this methodology was used the base case found in literature, this data can be found in Appendix A.

The simulations that will be performed to demonstrate the results of the proposed methodology aim to illustrate which are the best parameters to adjust correctly the PSO algorithm for the construction of the SSSR. The first test that will be addressed is the impact of the number of particles and the number of iterations, in both the computing time and the quality of the resultant SSSR comparing with the conventional methodology.

The second test will show the different results of the SSSR for different values of the initial and final inertia weight. The third test will demonstrate the advantages of using the initial population treatment and the constraints that were explained in sections 4.5 and 4.6. Then a series of simulations will be shown to demonstrate the reproducibility of the proposed methodology since it depends on the randomness of the PSO algorithm. Finally a comparison between the conventional methodology and the proposed methodology, concerning the computational effort, will be shown. It is important to emphasize that only the conventional methodology will be reproduced with the proposed methodology in order to perform the comparisons, in other words the proposed methodology of the previous subsection will not be part of the comparisons.

5.2.1.1 *Impact of the number of particles and iterations*

As explained before the first test that is shown is the impact of the number of particles and the number of iterations in both the quality and the computational effort of the proposed methodology. Table 15 shows the computing time required by the proposed methodology to construct the SSSR of the 9-bust system with different numbers of particles and iterations. The first column in Table 15 shows the number of iterations used in the different simulations and the first row shows the number of particles, the rest of the cells display the number of seconds required by the proposed methodology.

Table 15 – Computational performance (seconds) of the proposed methodology

Ite./Part.	20	32	40	48	56
25	23.71	26.63	30.7	34.2	36.02
30	29.73	31.7	38.64	40.41	42.56
35	34.07	41.7	44.26	46.99	49.67
40	39.33	48.1	50.45	53.96	55.58
50	52.71	59.4	63.02	66.49	69.46

For the previous simulations the following parameters were used:

- Variables of the problem = G2 and G3;

- Initial and final inertial weight = 1.5 and 0.6 respectively;

- Maximum value of the velocity components = 13.1 MW, correspondent to 8% of the maximum capacity of G2;

- Contingencies = Transmission Lines 4-5, 4-6, 6-9, 7-5, 7-8 and 8-9 out of service.

In the case of the initial and final weight, high values were used since it is desired that the particles have freedom of moving through the whole process, although the impact of different values will be explored in the next subsection. Regarding the maximum velocity the same value was used for both components (x and y) since the difference of generation capacity between groups is small. The initial population treatment and the constraints proposed in sections 4.5 and 4.6 were also used for the simulations. With the initial population generated within a 20% range.

It can be observed in Table 15 that the number of iterations has a larger impact, in terms of computing time, than the number of particles. In other words, the computing time rises with a larger rate when the number of iterations grows. Since obviously the smallest number of iterations requires the smallest computing time, the quality of the SSSR of all the simulations with 25 iterations is shown in Figures 57, 58, 59, 60 and 61 to compare with the quality of the SSSR obtained with the conventional methodology.

Figure 57 – Constructed G2xG3 plane with 25 iterations and 20 particles.
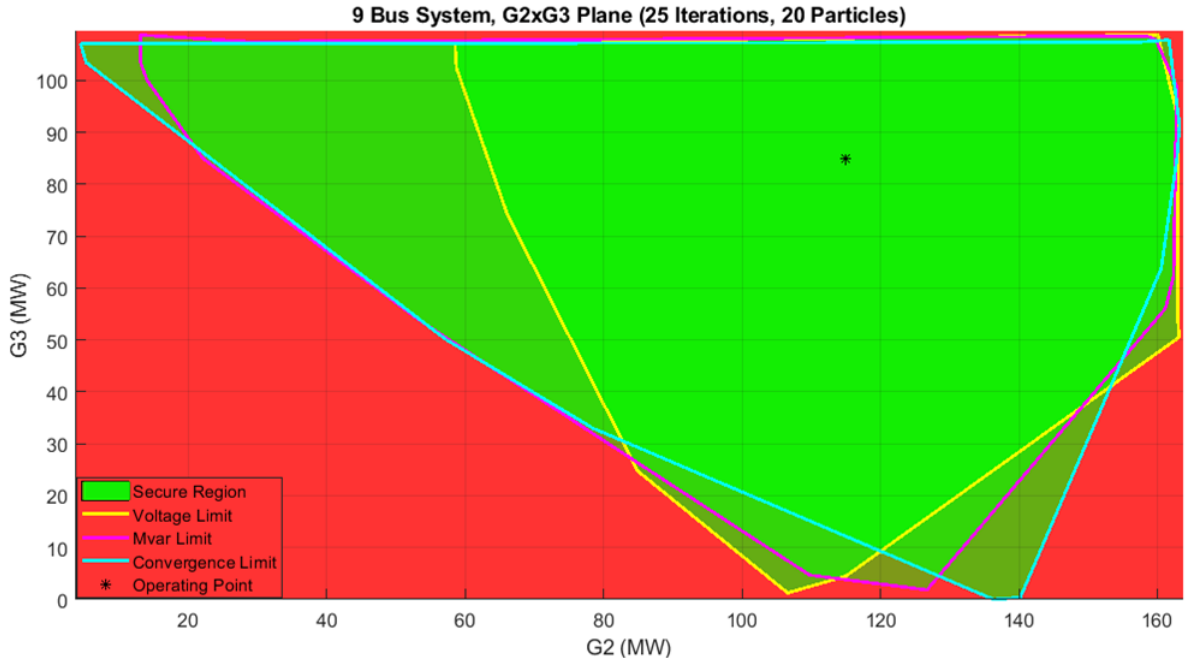
Figure 58 – Constructed G2xG3 plane with 25 iterations and 32 particles.
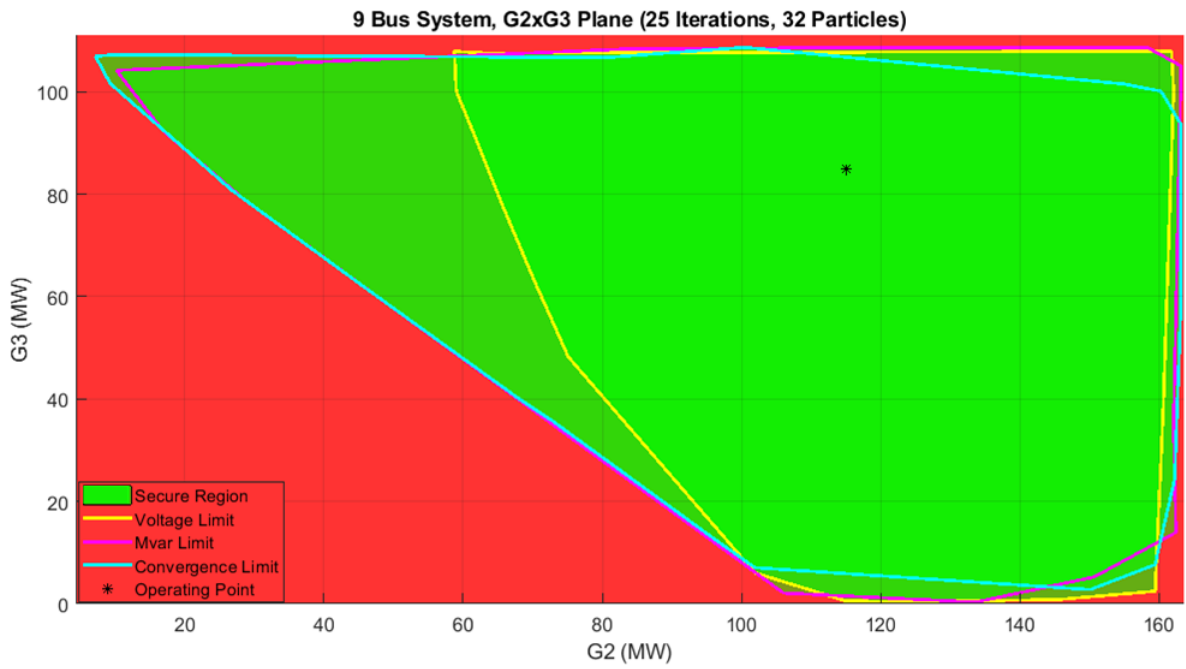
Figure 59 – Constructed G2xG3 plane with 25 iterations and 40 particles.
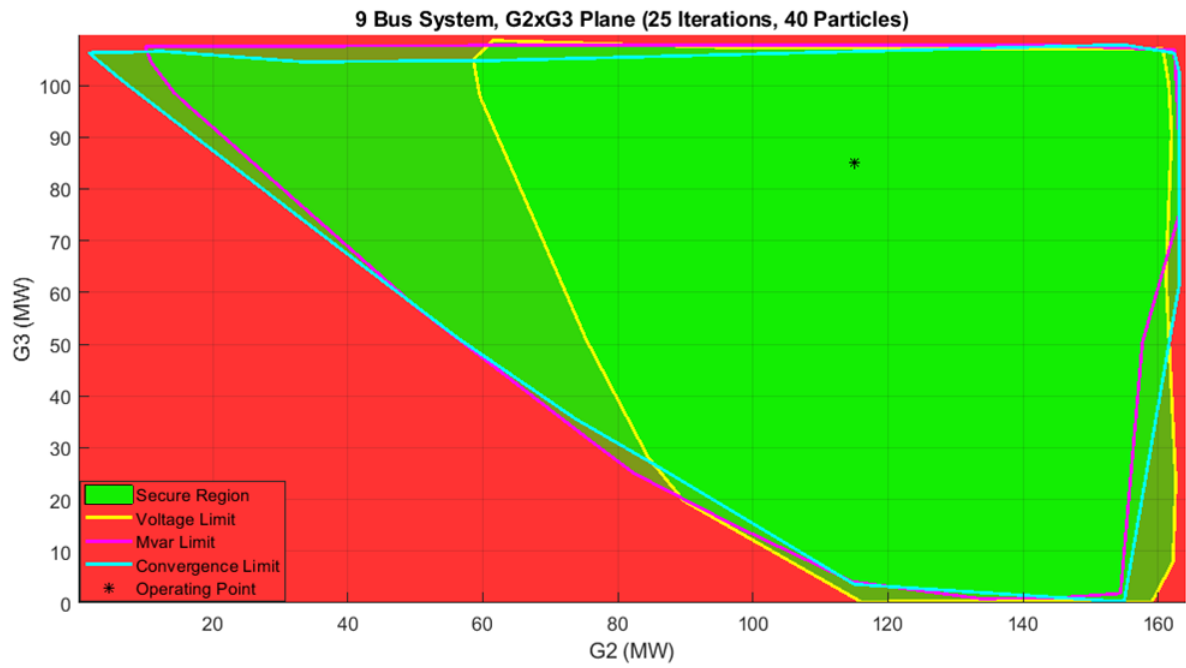
Figure 60 – Constructed G2xG3 plane with 25 iterations and 48 particles.
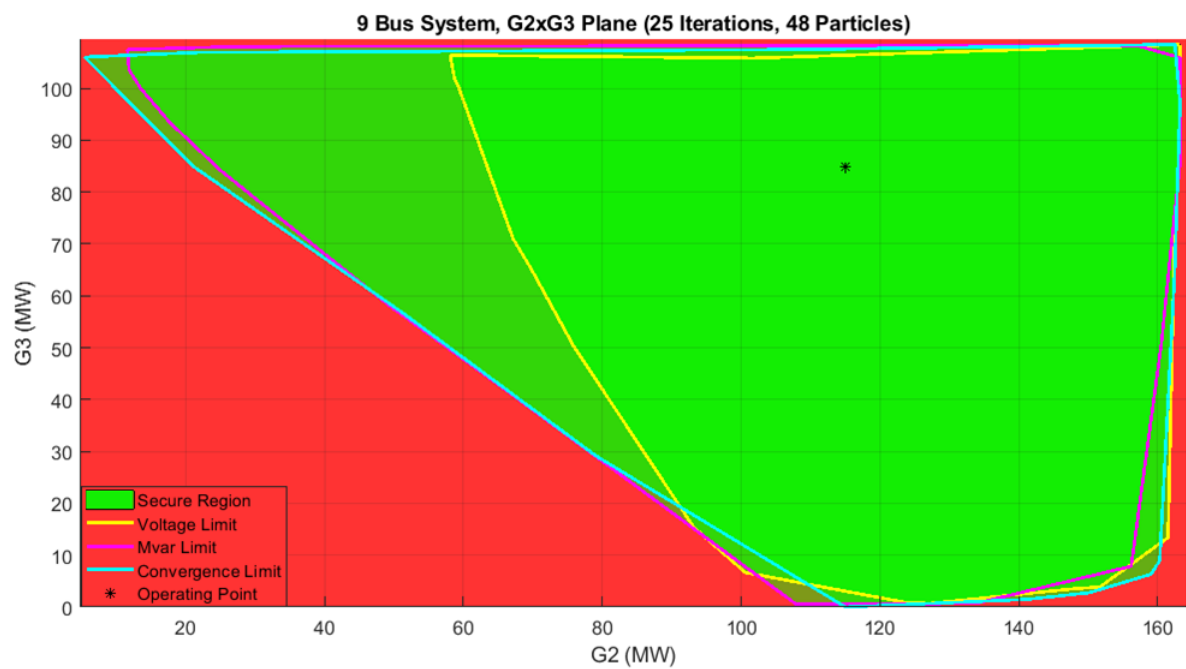
Figure 61 – Constructed G2xG3 plane with 25 iterations and 56 particles.
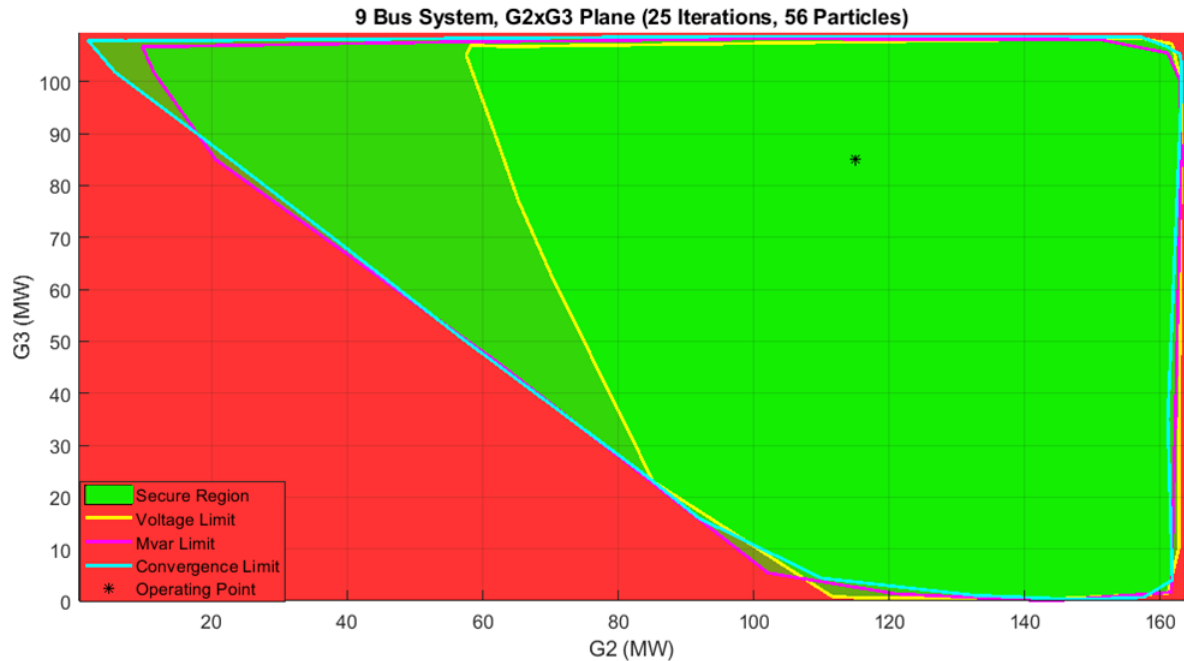
It can be seen in the previous nomograms that using less than 48 particles results in an SSSR with low quality since with few particles the methodology has a high dependence on the randomness of the PSO algorithm. From the 48 particles simulation more consistent results can be observed, but still with some distortions on the edges. Finally the simulation with 56 particles shown good results with only insignificant distortions on the lower left area of the feasible space of solution.

In order to observe the accuracy of the SSSR constructed with the proposed methodology, using 56 particles and 25 iterations, the G2xG3 plane obtained with the conventional methodology is shown in Figures 62 and 63. Aiming to perform fair comparisons with both methodologies, similar parameters were used in the proposed methodology, and also the same power flow solver. The following parameters were used for the simulations with the conventional methodology:

- Number of directions = 56;

- Power transfer step = 5% and 2%;

- Contingencies = Transmission Lines 4-5, 4-6, 6-9, 7-5, 7-8 and 8-9 out of service.

Figure 62 shows the G2xG3 nomogram constructed with a power transfer step of 5% and Figure 63 with a power transfer step of 2%. This is performed to observe the difference, in terms of quality, between them since this is a very important parameter when the computational performance of both methodologies is compared.

Figure 62 – Constructed G2xG3 plane, 5% power transfer step.
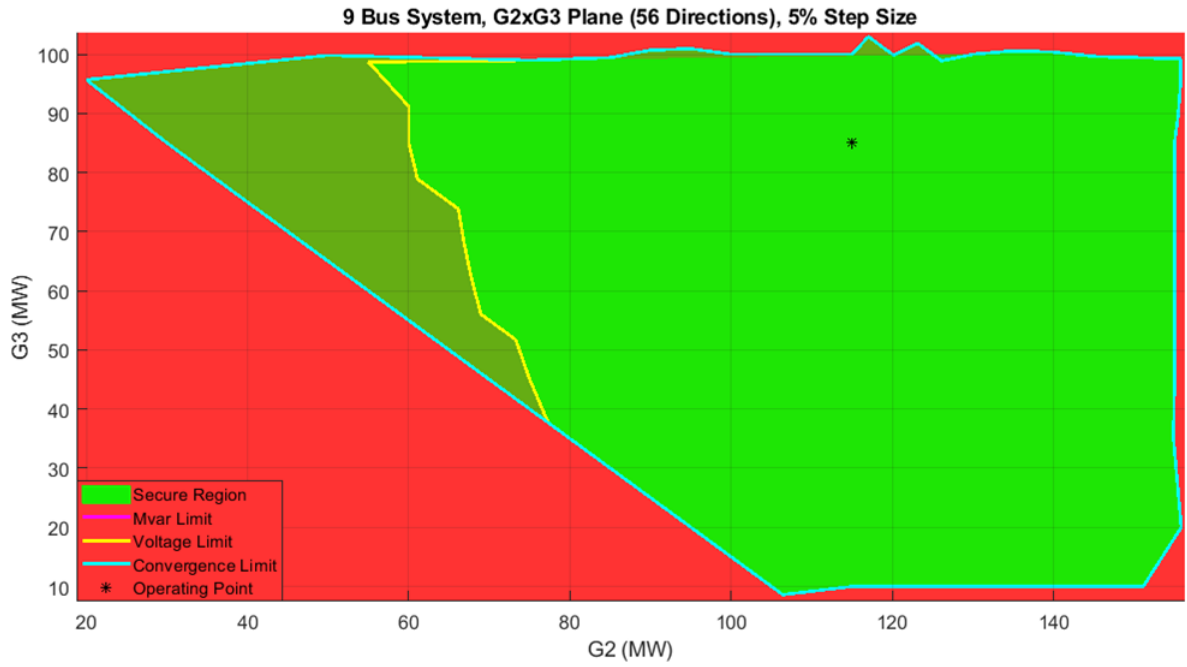
Figure 63 – Constructed G2xG3 plane, 2% power transfer step.
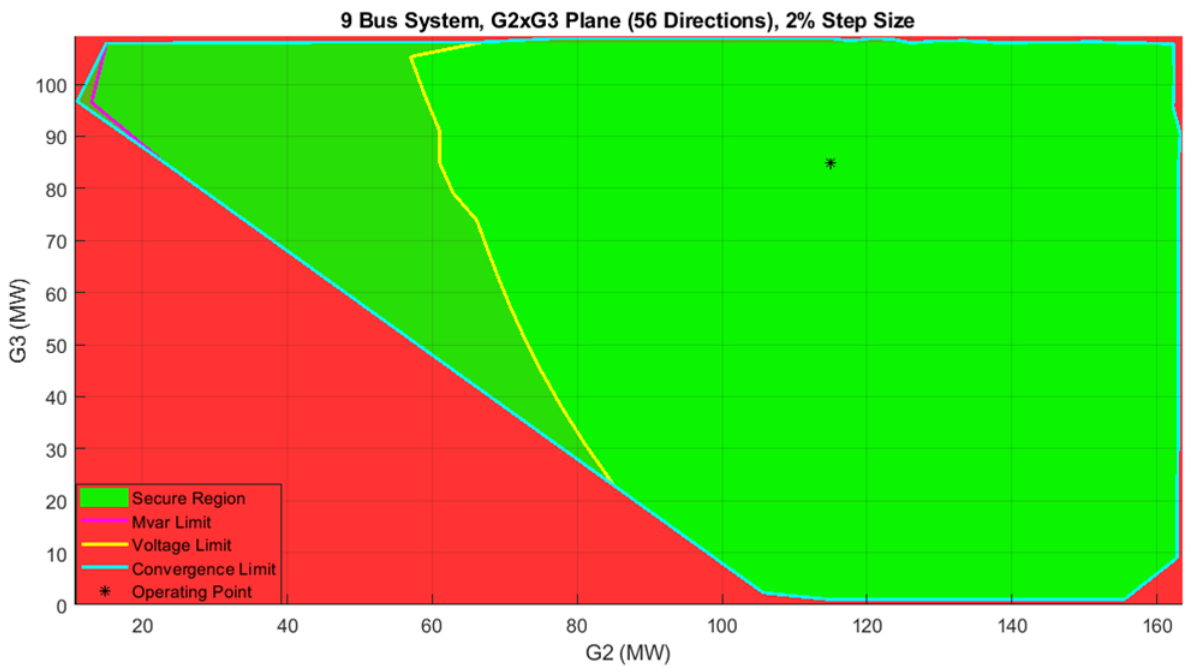
The previous figures show that the power transfer step is a crucial parameter for obtaining an SSSR with high quality in the conventional methodology, and it is clear that this greatly impacts on its computational performance, since the smaller the power transfer step the more power flows that have to be solved. For the first simulation 5% of power transfer step was chosen since it is the default value for constructing SSSR on ANAREDE but it was demonstrated that, at least for this system is not small enough to obtain an accurate result. Even with the 2% values it can be noted a little difference in the MVAr limit curve when it is compared with Figure 61, since the mentioned security curve is almost parallel to the convergence limit curve, this is due to the power transfer step size, if a smaller value is used the result would be more resemble the one obtained with the proposed methodology.

Another important fact that can be seen in Figure 63 is the impact that the number of directions has on the conventional methodology, since if a small number of directions is used the uncertainty rises, for example in the lower right corner of the SSSR of the mentioned figure it is seen that a small area is missing in comparison with Figure 61, in this case is insignificant but for other systems there might be big differences, as it will be demonstrated with another system.

Figures 64 and 65 show the G1xG2 and G1xG3 planes constructed with the proposed methodology using 25 iterations and 56 particles, with the same parameters mentioned before.

Figure 64 – Constructed G1xG2 plane with 25 iterations and 56 particles.
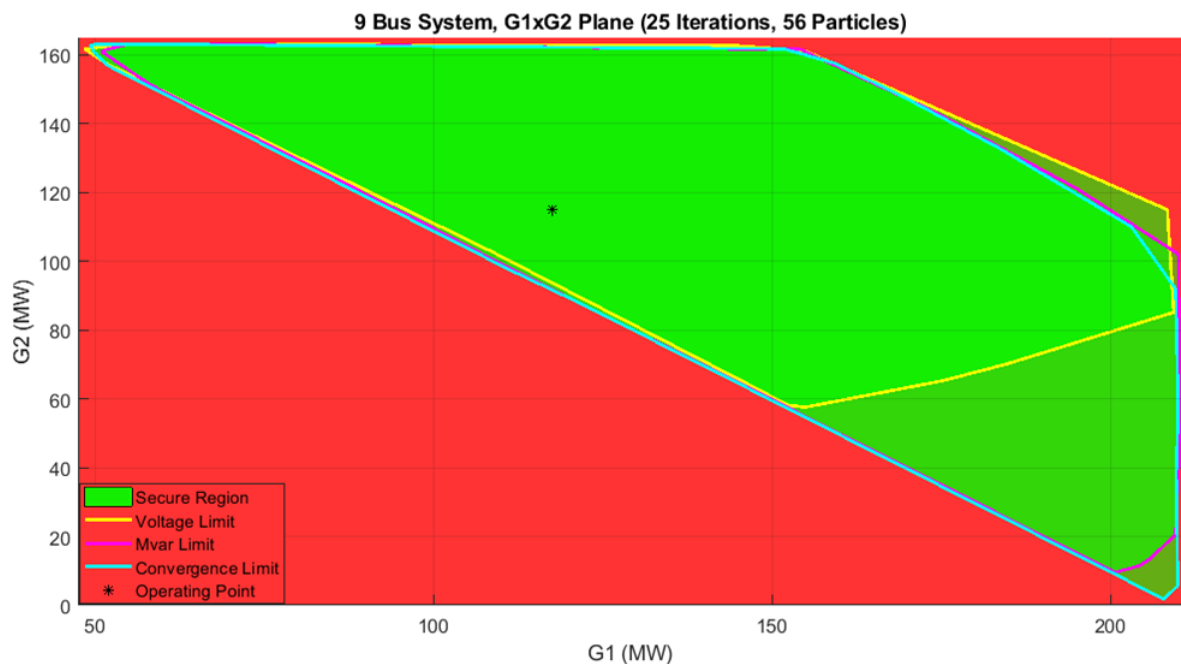
Figure 65 – Constructed G1xG3 plane with 25 iterations and 56 particles.
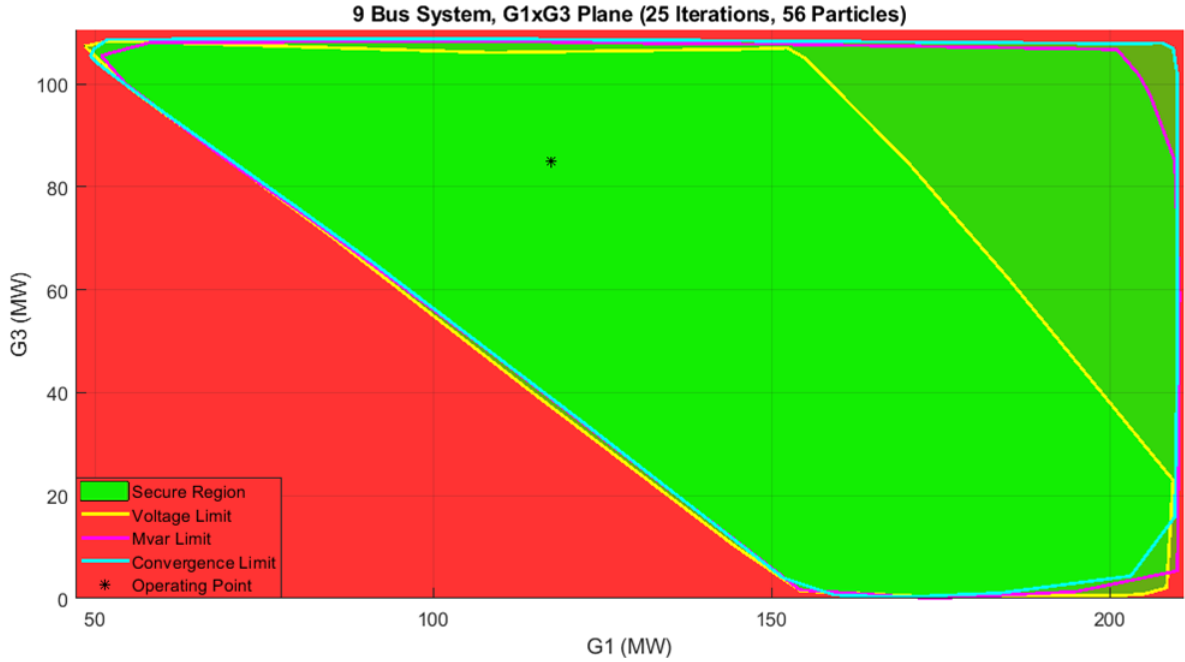
5.2.1.2 *Impact of the initial and final inertia weight*

As explained before the second test that will be performed is the impact of the initial and final inertia weight, which indirectly impacts on the selection of the maximum velocity, because if small values of inertia weight are set, the maximum velocity has to be a high number otherwise the particles have a great possibility of not reaching the edges of the security curves.

Setting small values of inertia weight, thus a high maximum velocity might be good for systems with an operating point with a large distance to the security curves since at the beginning of the iterative process of the PSO algorithm they can move with large steps approaching the security curve. Although for systems with a base case near to any security limit this can be a problem since in the first iterations the particles would try to move with large steps violating any of the pre-established limits, hence turning the objective function $Z \to -\infty$ and not being able to move during these iterations. Even though in later iterations the inertia weight is decreasing, thus the velocity decreases too, there might be not enough iterations for the particles to reach the edge of the security limit curve. This is proven in Figures 66 and 67.

Four tests will be performed to show the impact of the mentioned parameters, all of them will use an initial population of 56 particles and 25 iterations as it was done before. Although they will use different maximum velocities, firstly small values of initial and final inertia weight are used: 0.9 and 0.4 respectively, with maximum velocities of 13.1 MW and 48.96 MW that correspond to 30% and 8% of the maximum capacity of G2.

Figure 66 – Constructed G2xG3 plane, inertias: 0.9 and 0.4, max. vel: 13.1 MW.
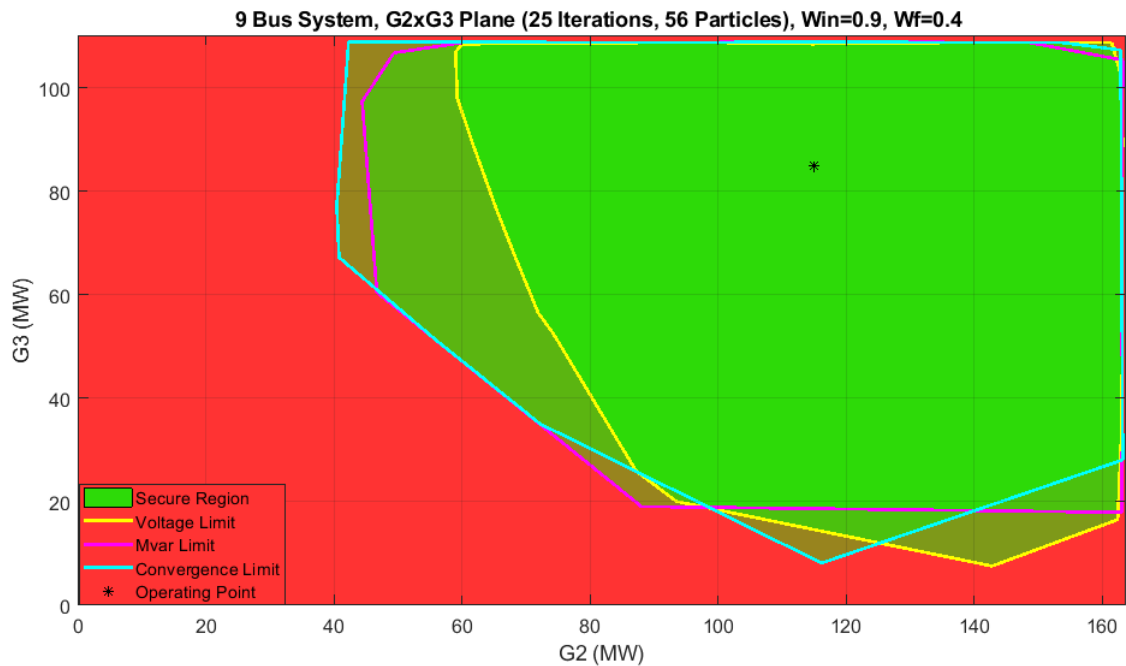
Figure 67 – Constructed G2xG3 plane, inertias: 0.9 and 0.4, max. vel: 48.96 MW.
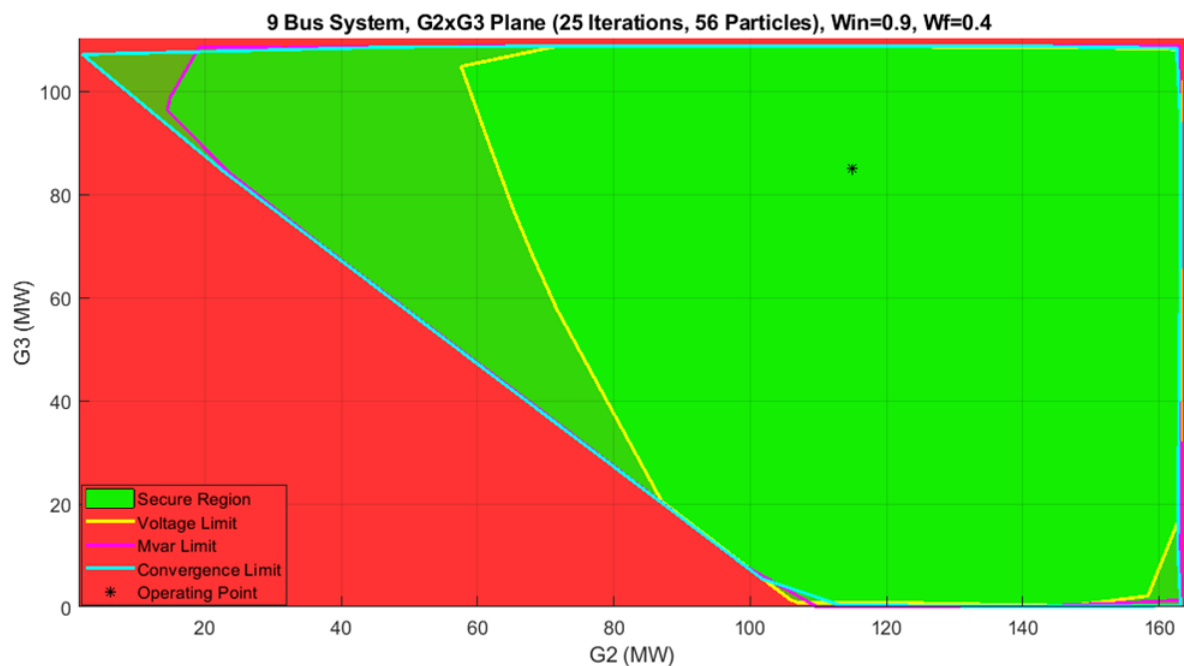
It can be easily observed on the previous nomograms that when a small maximum velocity is set with small values of initial and final inertia weights the results do not have the desired precision. It could also be seen that when a high maximum velocity is set the results are very accurate, but this system presents the characteristic that was explained before (security curve far from the base case) this adjustment might not work for other systems.

Figures 68 and 69 present the nomograms constructed with the same parameters

used before except for the initial and final inertia weight that are set as 2 and 0.6 respectively.

Figure 68 – Constructed G2xG3 plane, inertias: 2 and 0.6, max. vel: 13.1 MW.
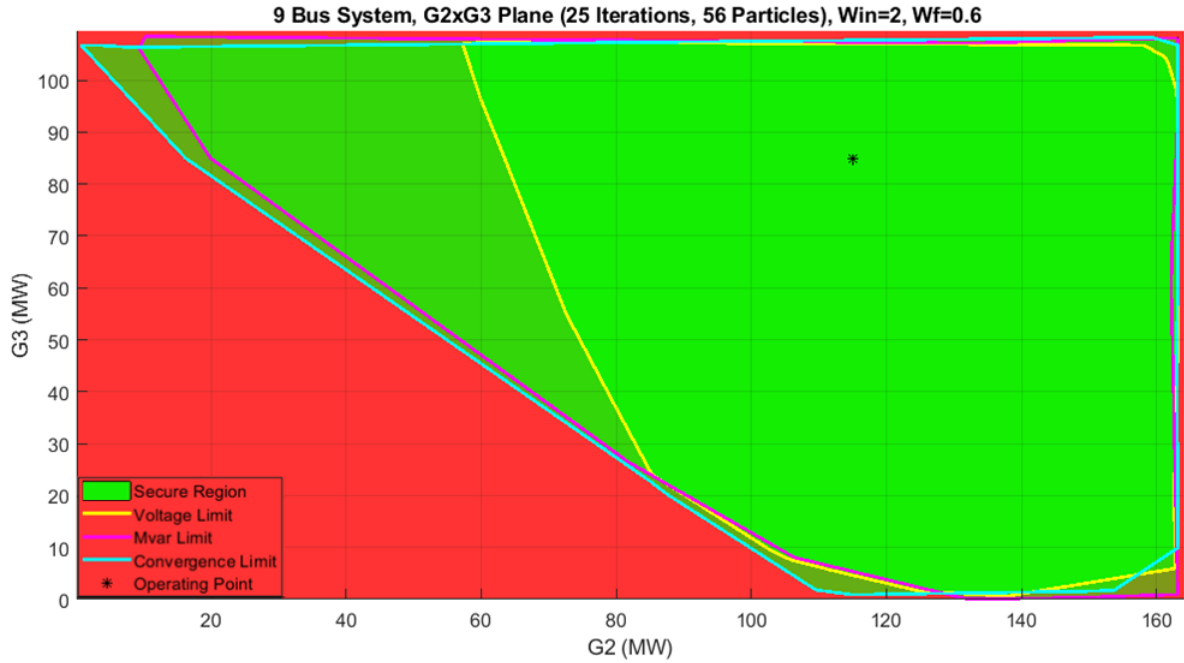
Figure 69 – Constructed G2xG3 plane, inertias: 2 and 0.6, max. vel: 48.96 MW.
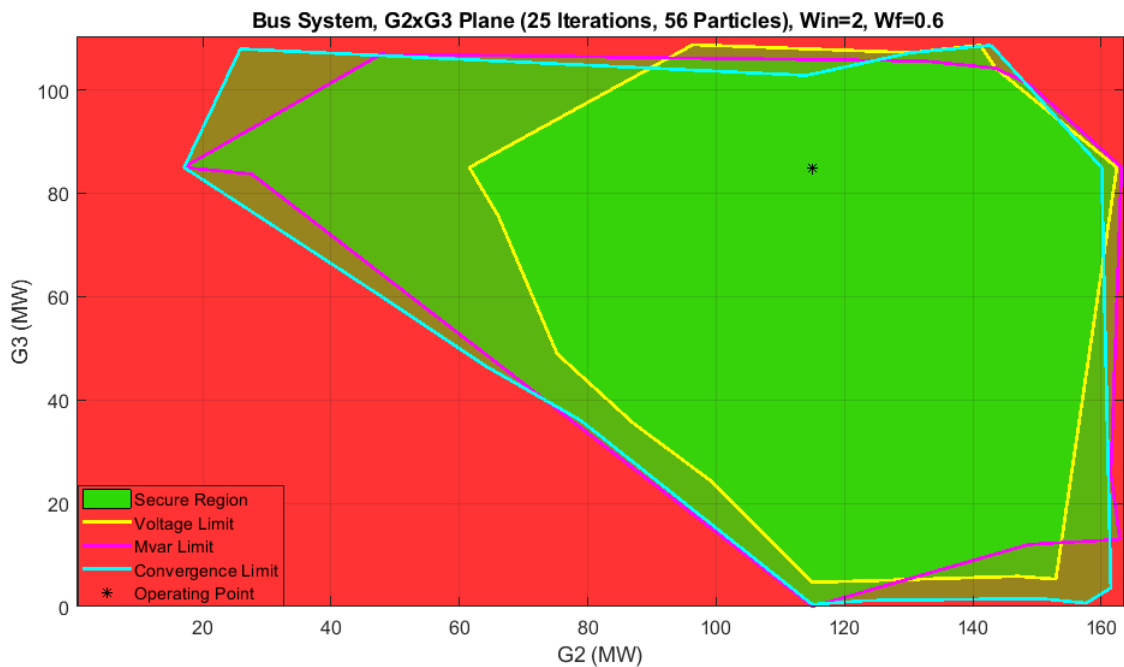
From the previous nomograms it is possible to see that the opposite result from the first test is obtained, that is, with high values of inertia weight and a small maximum velocity the result has good accuracy since the particles move in short steps during the whole construction process. And with high values of inertia and a large maximum velocity the results do not have the desired precision since the particles move with large steps

during the whole iterative process and have trouble to stay on the edges of the security curve. Even though the nomogram in Figure 68 shows an acceptable accuracy, the results obtained in Figure 61 were slightly better, therefore, the initial and final inertia used for obtaining this nomogram will be used in the rest of the simulations (1.5 and 0.6).

5.2.1.3 *Effectiveness of initial population treatment and constraints*

As mentioned before, all the previous simulations were using the initial population treatment explained in section 4.5, which consists of generating the initial population within a range around the base case, in this case was used a 20% range, and distributing the population equally on the four quadrants. Also the proposed constraints explained in section 4.6 were used, which allow the particles to move only within their initial quadrant. Figure 70 shows the G2xG3 nomogram constructed with the same parameters of Figure 61 but without using the mentioned constraints and initial population treatment.

Figure 70 – Constructed G2xG3 plane, without proposed initial pop. treatment and constraints.
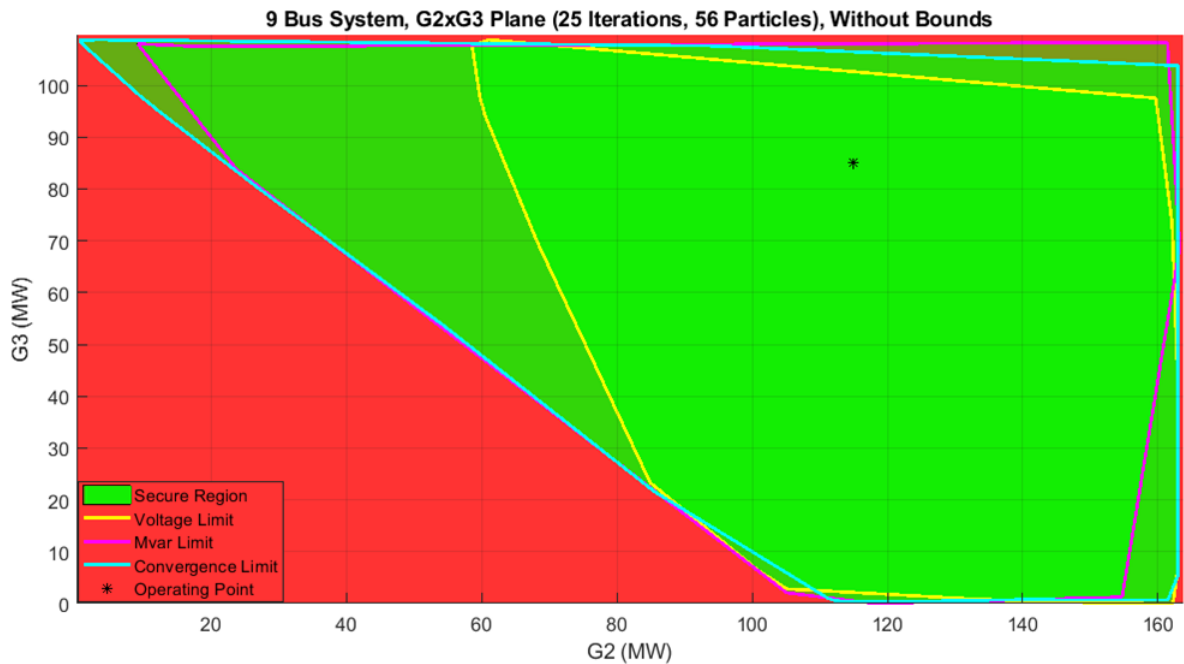
From the previous figure, it is possible to observe that the quality of the SSSR is clearly lower than the one constructed in Figure 61 where the initial population treatment and proposed constraints were used.

It was explained in Chapter 4 that for each security curve (voltage limit, MVAr limit, convergence limit or thermic limit) the proposed optimization model has to be solved. In Figure 71 it is shown the final position of the particles for the convergence limit curve.

Besides the quality difference between using the proposed initial population treatment and constraint, there is a difference in the computational performance, since for this simulation the required time was 38.6 seconds which is 2.58 seconds higher than the

Figure 71 – Final Particles position of convergence limit curve.
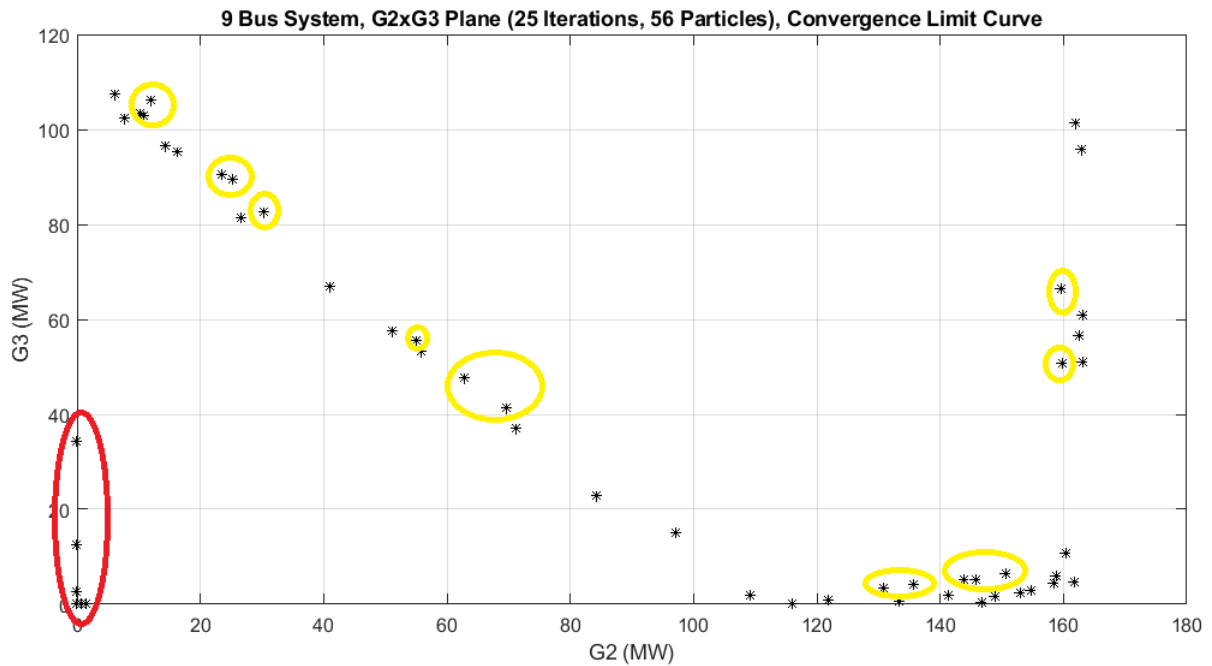
computing time required to obtain Figure 61. The difference is due to the particles that are inside the red oval, these particles were initiated outside the feasible area and could never find the edge of the security limit, because since the beginning of the process the objective function $Z \to -\infty$. When particles are outside the feasible space of solution the power flow that is being solved for the associated dispatch scenario is not convergent, therefore, it takes more iterations (of the Newton-Raphson method) to stop the process thus, increasing the computing time. Therefore, the computing time difference will vary depending on the initial population, since if more particles are outside the feasible space of solution the more computational effort the process will require.

Another aspect that can be observed in the previous image is that the treatment that is made with the command "*boundary*" to the final position of the particles, is very effective for avoiding distortions when particles do not reach the edges of the security curves, in the previous image this situation is seeing on the particles inside the yellow circles. Also, the treatment made with the particles that violate a limit, in this case the convergence limit, are eliminated and do not distort the final SSSR, this also ensures that no unsafe dispatch scenarios will be displayed on the constructed nomograms.

5.2.1.4 *Reproducibility of the proposed methodology*

In this subsection, a reproducibility analysis will be performed to demonstrate that the randomness used in the PSO algorithm does not have a high impact on the reproducibility of the SSSR. In order to demonstrate this, the voltage limit security curve

will be plotted 10 times superimposed on the same figure. Only the voltage limit curve will be plotted for the sake of clearness since if all the security curves were superimposed it would result in a confusing figure. For the 10 simulations a new initial population was generated each time, with the proposed treatment and constraints. Figure 72 shows the simulations on the superimposed graph.

Figure 72 – 9-bus system, G2xG3 plane, 10 run test.
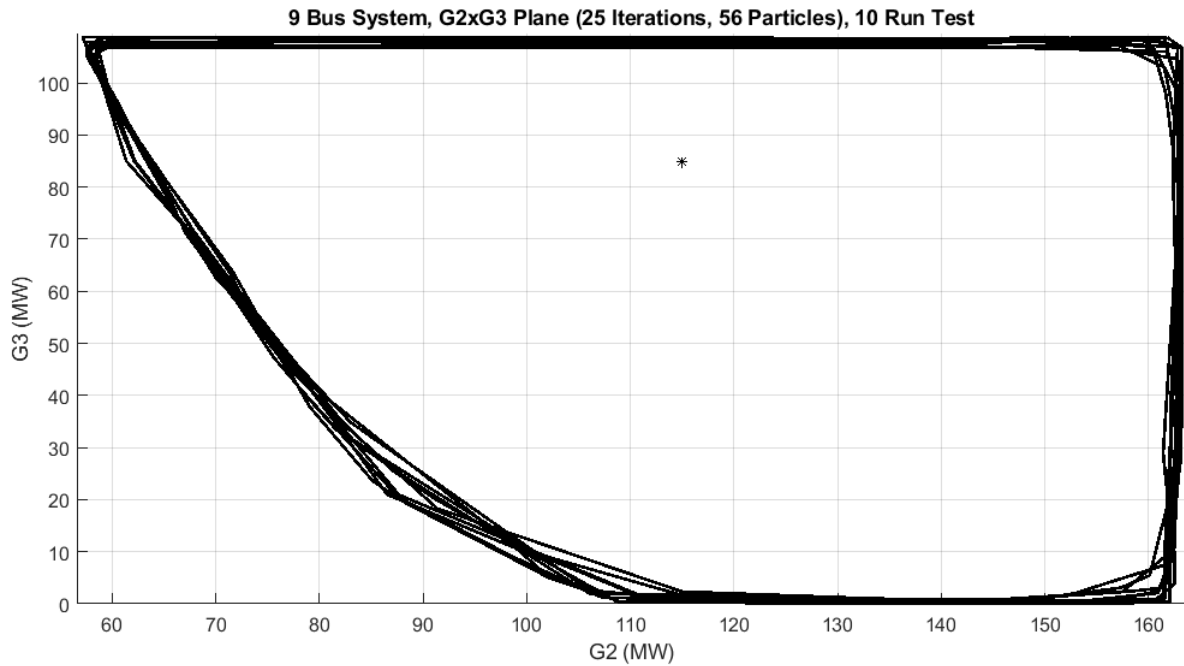
The previous nomogram shows that all the simulations resulted in nearly identical curves with only slight differences on the edges of the graph, this clearly demonstrates that the proposed methodology is an effective technique for the construction of the SSSR.

Aiming to have a numerical measurement of the reproducibility of the proposed methodology Table 16 shows the area inside each of the curves of the proposed methodology, that illustrated in Figure 72. The area is divided by 10^3 thus, converting it into *p.u.*

Table 16 – Reproducibility evaluation

Run	1st	2nd	3rd	4th	5th	6th	7th	8th	9th	10th
Area (p.u)	9.27	9.16	9.23	9.14	9.17	9.28	9.16	9.11	9.16	9.27

The previous table confirms what was seen in Figure 72, this is that the difference between each simulation is small, the biggest difference is of 0.17 *p.u.*

5.2.1.5 *Computational performance*

In this subsection, the most important analysis will be performed since the aim of this methodology is to improve the computing time required to construct the SSSR by the conventional methodology. The comparison between methodologies will be made on

the time required for the construction of the nomograms presented in Figures 61 and 63, which were constructed with similar parameters and with the same power flow solver to perform a fair comparison.

Table 17 shows the computing time required by the construction process of both methodologies, the column name "gain" refers to the computing time gain, in percentage terms, of the proposed methodology over the conventional technique.

Table 17 – Comparison between the proposed and conventional methodology

Methodology	Number of Particles/Directions	Time (s)	Gain
Proposed	56	36.02	-
Conventional	56	45.41	20.68%

The previous table shows that the proposed methodology presents a significant gain, in terms of computing time, with relation to the conventional methodology, which achieves the main objective of the proposed methodology. It will be demonstrated with the rest of the systems that this difference is larger when bigger systems are analyzed, due to the generation capacity of the groups or the accuracy of the SSSR with respect to the number of directions, these characteristics will be shown in the following sections.

5.2.2 New England system

The second system that will be used for validation of the proposed methodology is the New England system, the single line diagram of this system was shown in Figure 43. This system was chosen to demonstrate that the methodology works for a larger size system and, as it was seen in the previous section that its SSSR has a particular shape, this is another fact that will be proven with this system, that the proposed methodology is effective when the shape of the SSSR is not square like.

The base case (generation profile and load) are the same that was used for the construction of the SSSR of the previous methodology, although there is a slight difference in the generation capacity of the PV nodes, this was done to observe different situations on the same system. The capacities of the PV nodes can be found in Appendix B.

5.2.2.1 *Quality comparison*

The parameters used for the construction of the SSSR with the proposed methodology are detailed as follows:

- Variables of the problem = G2 and G3;

- Number of particles = 56;

- Number of iterations = 25;

- Initial and final inertial weight = 1.5 and 0.6 respectively;

- Maximum value of the velocity components = 325 MW, correspondent to 5% of the maximum capacity of G3;

- Contingencies = Transmission Lines 26-27, 26-29 out of service.

The tests with the 9-bus system in the previous subsection showed that the best performance, in terms of quality and computational effort, was obtained with 56 particles and 25 iterations, thus, this combination is also used for the tests in this system. It was also explained that the initial and final inertia weights with values of 1.5 and 0.6 respectively offer good quality and the best precision since a small maximum velocity can be set. Additionally, the initial population was generated within a range of 20% around the base case and the proposed constraints were used.

Lastly, it can be seen from the used parameters that a single value is used for both components of the velocity since for this system the generation capacity is similar in the three generation groups. Figures 73, 74 and 75 show the nomograms created with the proposed methodology for the New England system.

Figure 73 – Constructed G1xG2 plane with 25 iterations and 56 particles.
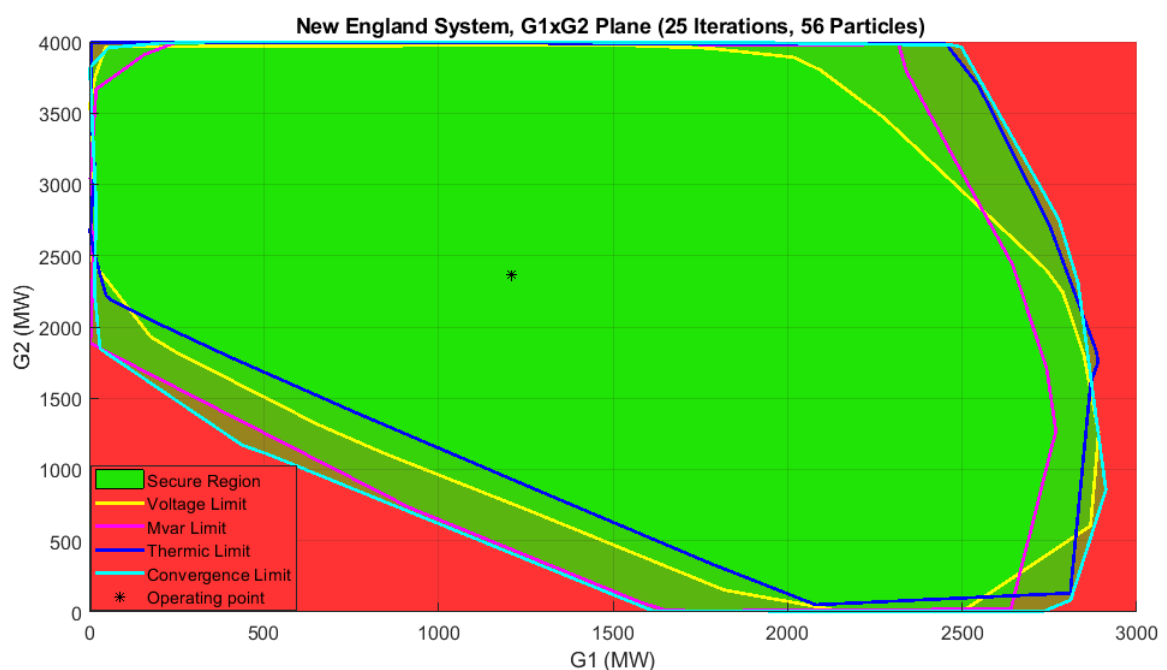
Figure 74 – Constructed G1xG3 plane with 25 iterations and 56 particles.
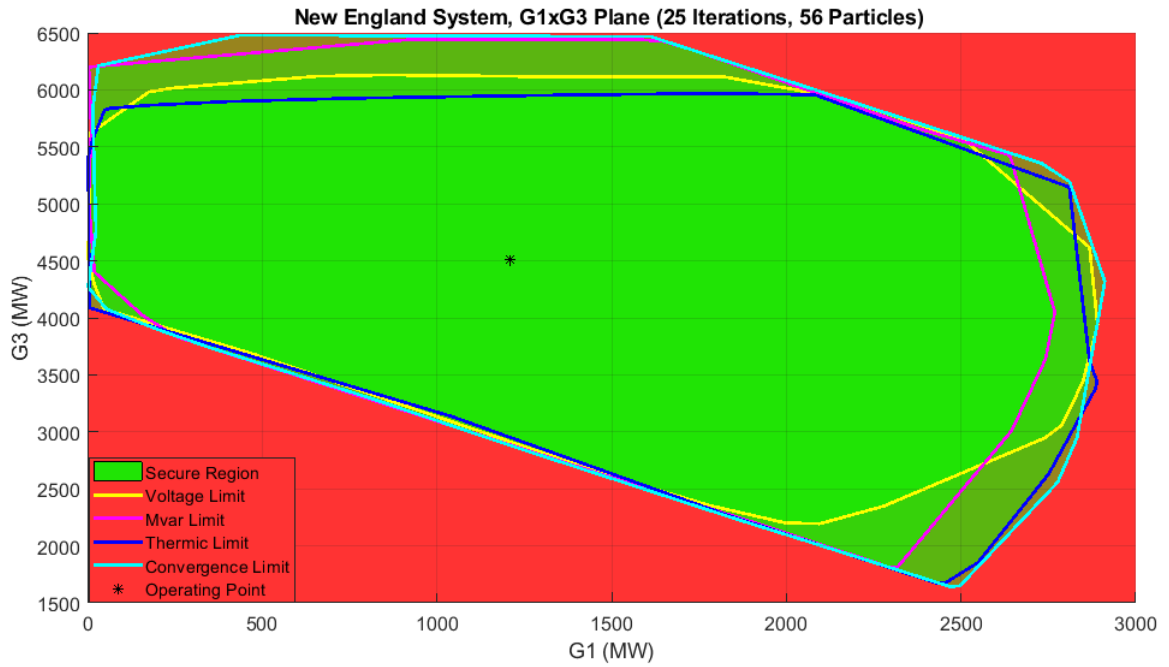
Figure 75 – Constructed G2xG3 plane with 25 iterations and 56 particles.
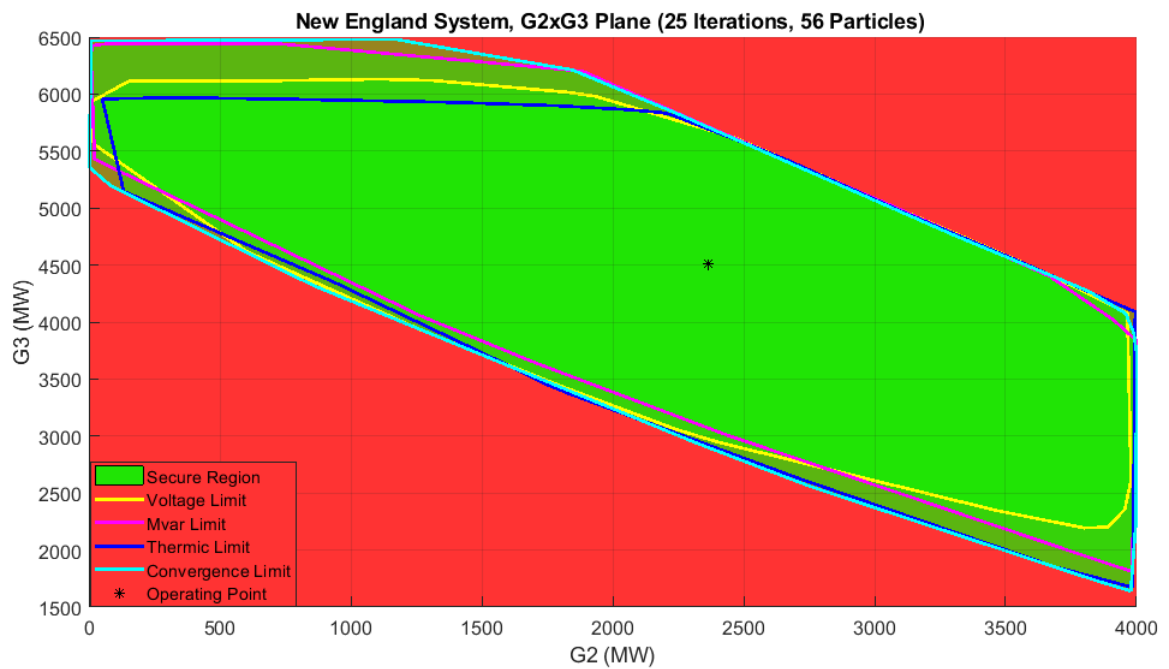
It can be seen from the previous nomograms that there are only small errors in some edges of the SSSR, where the thermic limit curve and the voltage limit curve are beyond the convergence limit curve, although this only happens on operating points that are with a considerable distance from the base case. These little errors occur due to the randomness of the PSO algorithm, although with the proposed initial population treatment and the proposed constraints the impact of the randomness is highly reduced as it was shown with the 9-bus system.

In order to compare the quality and performance of the proposed methodology and the conventional methodology, similar parameters were used, the parameters used for the construction of the SSSR with the conventional technique are listed below:

- Number of directions = 56;

- Power transfer step = 5%;

- Contingencies = Transmission Lines 26-27, 26-29 out of service.

As it was explained before the same power flow solver is used in both methodologies, in this case a 5% step size is used with the conventional methodology, which is the default value of the software ANAREDE. Figures 76, 77 and 78 show the SSSR constructed with the conventional method.

Figure 76 – Constructed G1xG2 plane, 5% power transfer step size.
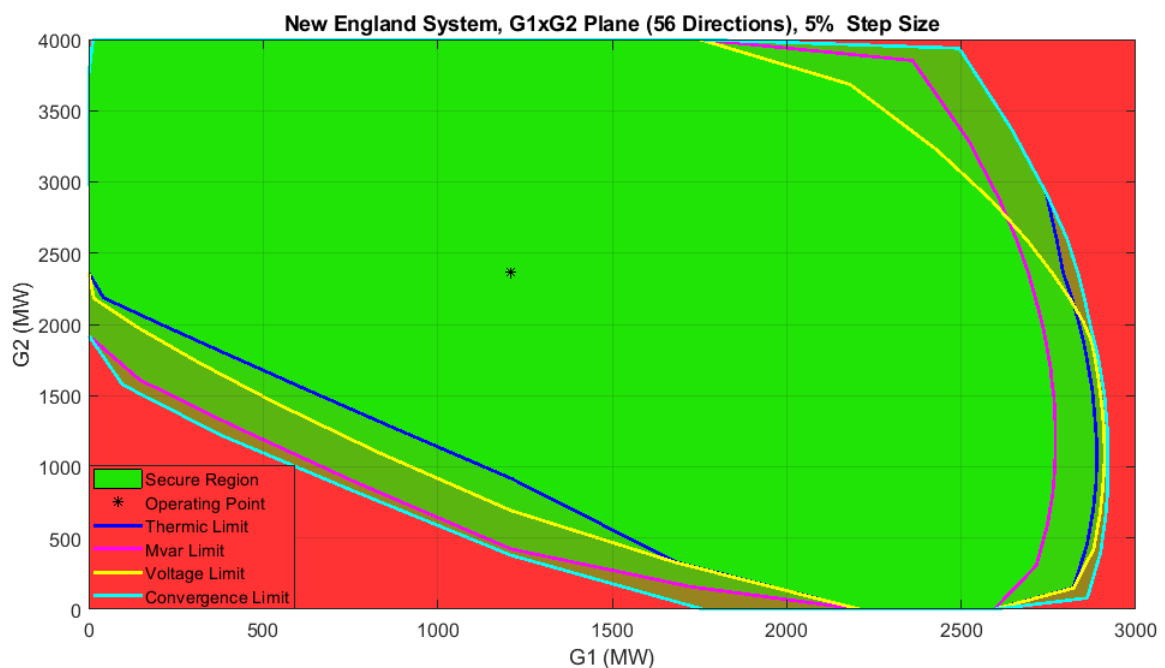
Figure 77 – Constructed G1xG3 plane, 5% power transfer step size.
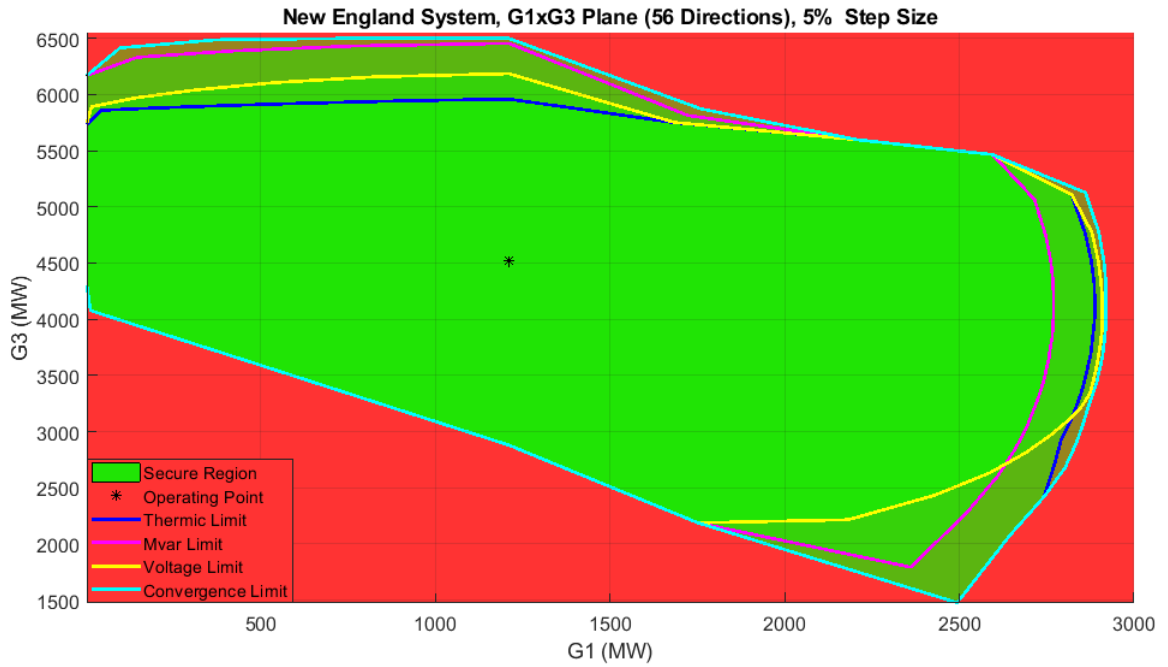
Figure 78 – Constructed G2xG3 plane, 5% power transfer step size.
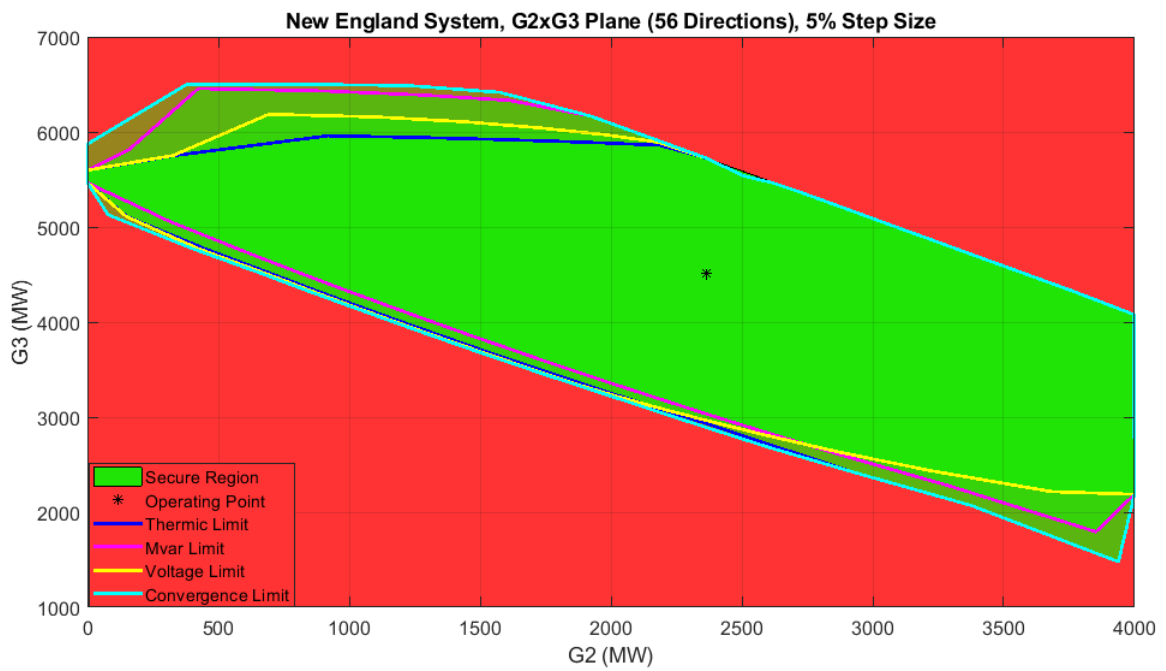
It can be seen from the previous figures, in comparison with the nomograms constructed with the proposed methodology, that both methodologies obtain nearly identical results with only slight differences in the operating points that are from a long distance to the base case. The mentioned small difference would not have a negative impact if the tool is being used for *on-line* operation since it is not possible to make a drastic change in the dispatch profile of a real system in a short period of time.

For *real-time* monitoring of a power system the SSSR would need to be constructed with a periodicity of a pre-established time, like 10 or 15 minutes, where the operating points near to the base case would be guaranteed to have trustworthy precision. The small distortions on the edges of the curves are highly compensated with the computational performance of the proposed methodology as it was demonstrated for the 9-bus system and will be shown later for the New England system.

5.2.2.2 *Effectiveness of the initial population treatment and proposed constraints*

This subsection will show the effects of the initial population treatment and the proposed constraints, both in the quality of the SSSR and the computational performance of using the mentioned characteristics.

In order to perform the mentioned comparison, the SSSR of the New England system was constructed with the same parameters mentioned before for the proposed methodology, except that the initial population is randomly generated thru the whole feasible solution space, which are all the possible dispatch scenarios between the maximum and minimum capacities of the generation groups. Additionally the particles have no restriction to move across quadrants in other words, the only constraints of the problem are the maximum and minimum group generation capacities. Figures 79, 80 and 81 show the SSSR constructed with the characteristics mentioned before.

It can be seen in the mentioned figures that not using the proposed initial population and constraints directly affects the quality of the SSSR, not only on the operating points that are far from the base case but also on the secure region. The largest impact can be observed on the thermic limit curve, which largely reduces the secure region of the SSSR on the 3 nomograms. This would be problematic in operation since dispatch profiles that are safe to operate are being shown as unsafe, which would reduce the reliability of the proposed methodology.

All the previously explained proofs that the proposed characteristics provide reliability to the tool for *on-line* operation. Besides the quality of the SSSR, there is also another important aspect that is affected by the initial populations and constraints. As it was explained for the 9-bus system the computational performance is also affected by the mentioned characteristics, Table 18 shows a comparison between the usage or not usage of proposed treatment.

Figure 79 – Constructed G1xG2 plane, without proposed initial pop. treatment and constraints.
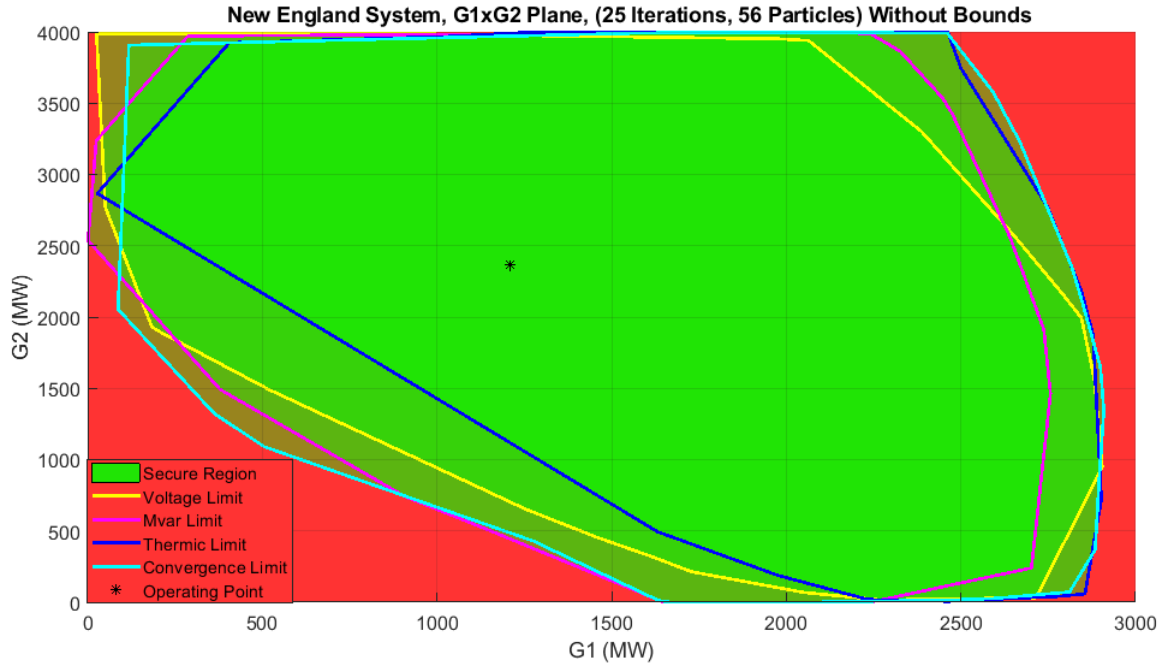
Figure 80 – Constructed G1xG3 plane, without proposed initial pop. treatment and constraints.
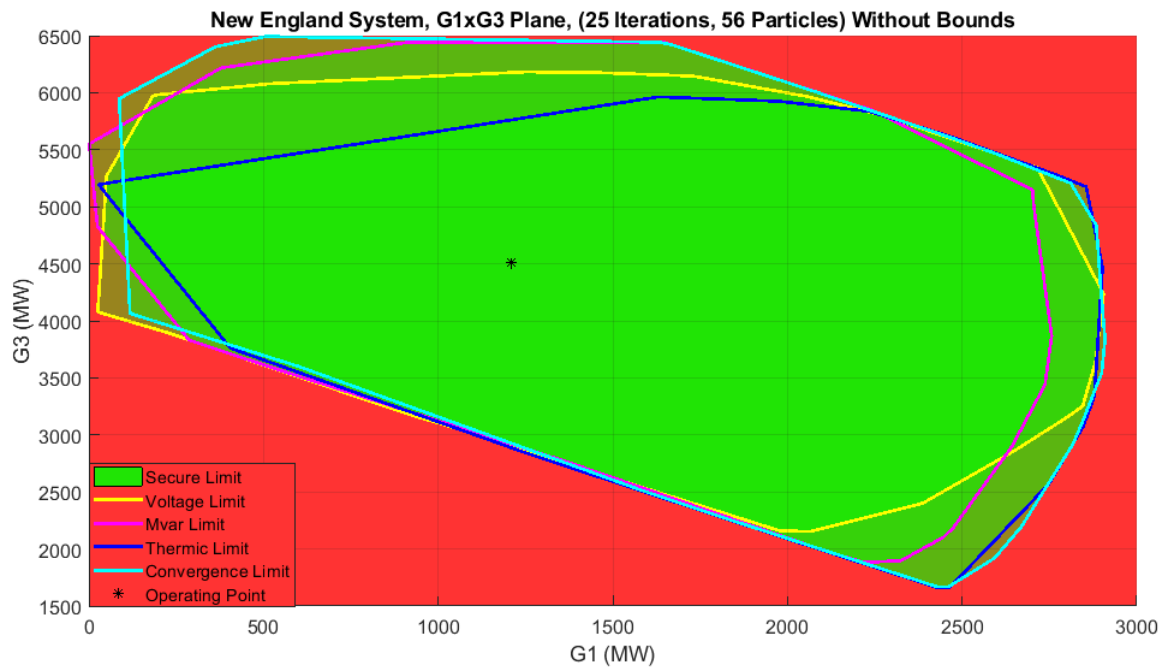
Figure 81 – Constructed G2xG3 plane, without proposed initial pop. treatment and constraints.
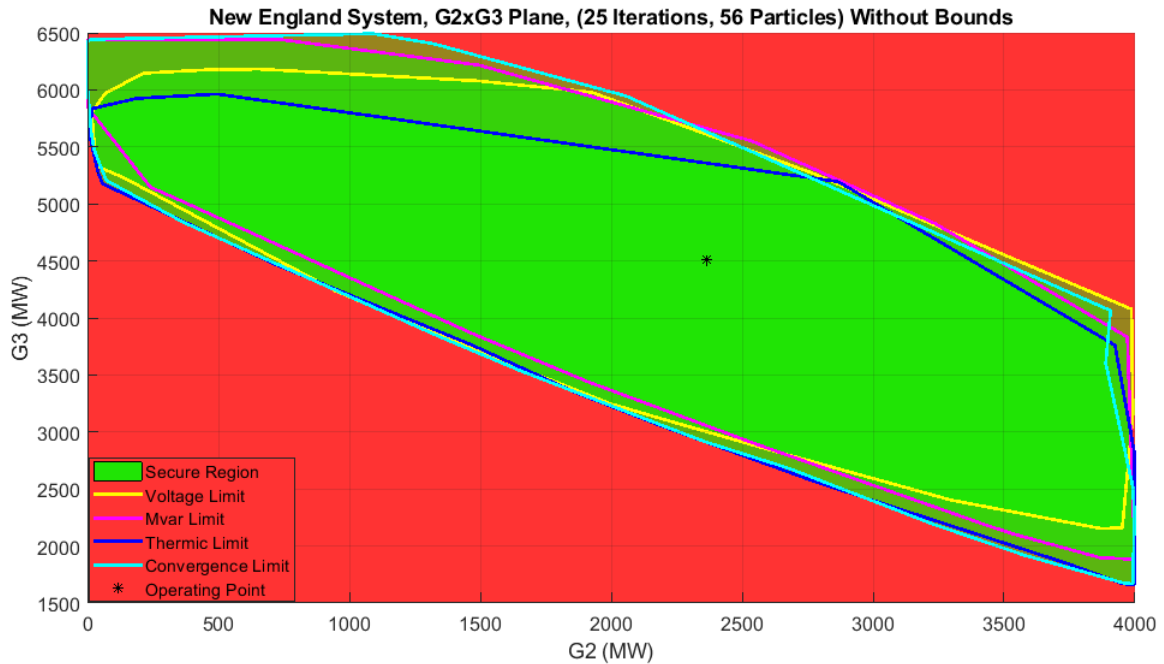
Table 18 – Computational performance comparison

Characteristics	Numb. of Part.	Numb. of Ite.	Time (s)	Difference
Proposed	56	25	111.16	33.5 %
Without Prop. Treat.	56	25	167.22	

Table 18 demonstrates that besides the quality differences between the proposed methodology with the mentioned characteristics, there is a large difference in terms of computing time, due to what was mentioned in the previous section, that particles are generated outside the convergence limit curve, therefore, the dispatch profile associated to these particles require a higher computational effort since the power flows reach their maximum allowable iterations.

For the 9-bus system, the difference was insignificant but, as shown for the New England system, the computational effort can be largely improved by using the proposed initial population treatment and constraints.

5.2.2.3 *Reproducibility of the proposed methodology*

This subsection shows a test similar to the one made for the 9-bus system, a security curve will be constructed 10 times with the conventional methodology, with a different initial population each time, the final graphs are displayed superimposed on the same figure, aiming to demonstrate that there are no significant differences at each execution of the proposed algorithm even with systems like the New England, whose SSSR has a peculiar shape.

In this case the secure region of Figure 75 will be constructed, in other words, the proposed optimization model is solved only once but, the binary constant L_v from equation 4.4 is set as 1 when any of the limits are violated. Figure 82 shows the superimposed curves of the 10 runs performed.

Figure 82 – New England system, G2xG3 plane, 10 run test.
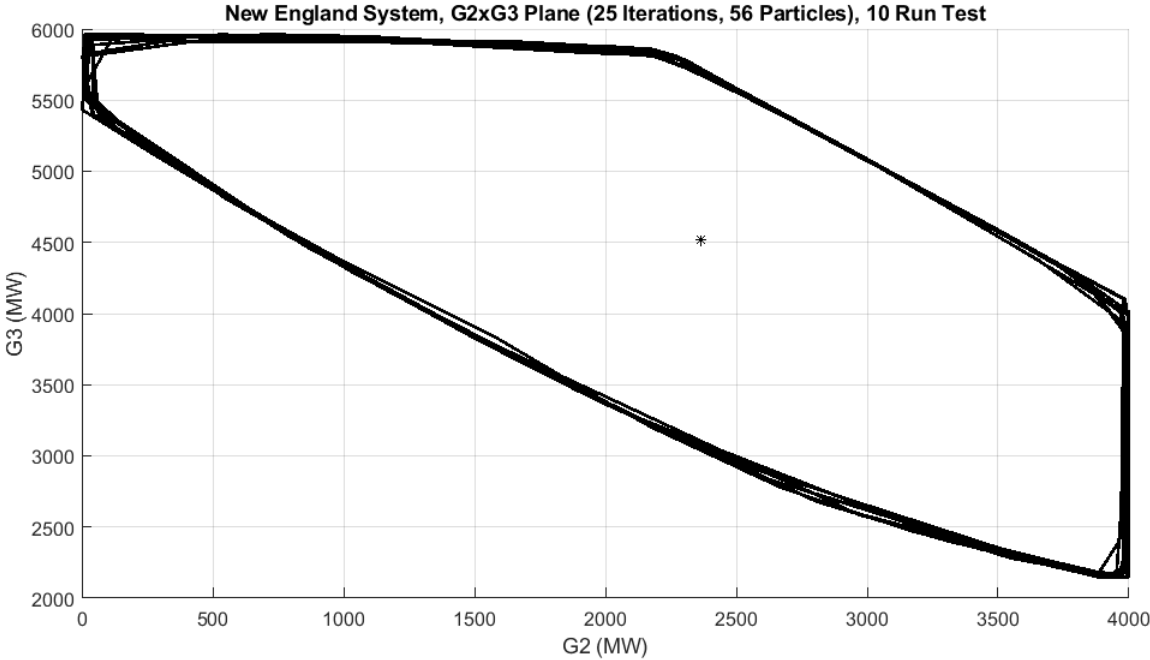
Figure 82 shows that for the 10 runs the final region was nearly identical, demonstrating that the proposed methodology is reliable, even for oddly shaped regions. Another aspect that can be analyzed with this manner of constructing the nomograms is the computing performance, since this could be an interesting way of *on-line* monitoring of a power system.

As mentioned before the optimization model is solved only once for the construction of the previously shown nomogram, which vastly reduces the computing time. As explained before the curve that was constructed is the secure region of Figure 75, which is the region where the system can operate without any limit violation. The disadvantage of creating the SSSR in this manner is that there is no information on which is the limit that is being violated, although for *real-time* operation, where is only needed to be in a safe operating point, it could be an interesting way of constructing the SSSR. Table 19 shows a comparison between constructing only the secure region and constructing each security curve.

As can be observed in Table 19 the computing time difference is enormous, therefore, in cases where the system is very large or if a vast number of contingencies need to be tested, this option could be interesting for *on-line* applications.

Table 19 – Computational performance comparison

Characteristics	Number of Particles	Number of Iterations	Number of Security Curves	Time (s)	Difference
Proposed	56	25	4	111.16	75.8%
Reduced	56	25	1	26.88	

5.2.2.4 *Computational performance*

The last analysis performed with the New England system is the comparison of the computational performance between the conventional and proposed methodologies. The comparison is performed from the computing time that both methodologies take to construct the nomograms shown in the subsection that compared the quality of the SSSR of both methodologies. It is important to emphasize that both methodologies were adjusted with similar parameters and the same power flow solver was used in both of them. Table 20 shows the mentioned comparison.

Table 20 – Comparison between the proposed and conventional methodology

Methodology	Number of Particles/Directions	Time (s)	Gain
Proposed	56	111.16	-
Conventional	56	246	54.8 %

It is clear from Table 20 that the proposed methodology has a better performance than the conventional methodology, also if it is taken into consideration the comparison that was made for the 9-bus system, it can be seen that for the New England system the computational performance difference is higher, this is due to the size of the system, since all the generation groups have a large generation capacity, which translates in a vast amount of power transfer steps that the conventional methodology has to complete.

On the other hand, the proposed methodology only needs to set a maximum velocity as a fraction of the generation capacity of the groups that are the variables of the system, this makes a genetic adjustments for all the systems independently of their size, and the computational performance difference depends only on the time that the power flow requires to be solved and the number of contingencies that are performed.

As can be deducted from the two systems that were analyzed, the computational performance of the proposed methodology is superior compared with the conventional methodology, and the difference can be variable depending on the number of steps that the proposed technique requires in the construction process. Therefore, it could be thought that the proposed methodology has a better performance, in terms of computing time, than the conventional methodology when the system presents low loading levels since under this conditions the system presents a base case far from the security limits, thus it would require more power transfer steps of the conventional methodology. This will be

analyzed with the next system that is used for the validation of the proposed methodology, which is the southern Brazilian equivalent system, which as it was demonstrated in the previous section is close to the maximum allowable power.

5.2.3 **107-bus southern Brazilian equivalent system**

The last system that is used to show the performance of the proposed methodology is the 107-bus southern Brazilian equivalent system, whose single line diagram was shown in Figure 50. This system was chosen to demonstrate the performance of the proposed methodology in large systems with a high loading level since as demonstrated with the SSSR constructed with the VSI zones, the 107-bus system is close to the voltage collapse point.

The base case (generation profile and load) and all the limits are the same used to show the results of the SSSR constructed with the VSI regions. Also, the same groups are used, the maximum generation capacity of each group is shown in Table 21.

Table 21 – Maximum generation capacity of generation groups

Area	Group	Maximum Generation Capacity (MW)
South East	1	10167.2
Mato Grosso	2	721
South	3	8862

As can be observed in the previous table this system possesses a large difference between the generation capacities of the groups, therefore, a maximum velocity for each component (x and y) is needed. This system will also serve to show the impact of the maximum velocity since the previous systems had similar generation capacities between their groups and a single maximum velocity was set.

5.2.3.1 *Quality comparison*

In order to compare the quality of the SSSR constructed with the proposed and conventional methodology, Figures 83, 84, 85 and 86 show the G2xG3 plane constructed with the conventional methodology with different number of directions.

The parameters used to construct the mentioned figures are detailed below:

- Number of directions = 56, 100, 150 and 250;

- Power transfer step = 5%;

- Contingencies = None considered.

Figure 83 – 107-bus system, G2xG3 plane, 56 directions.
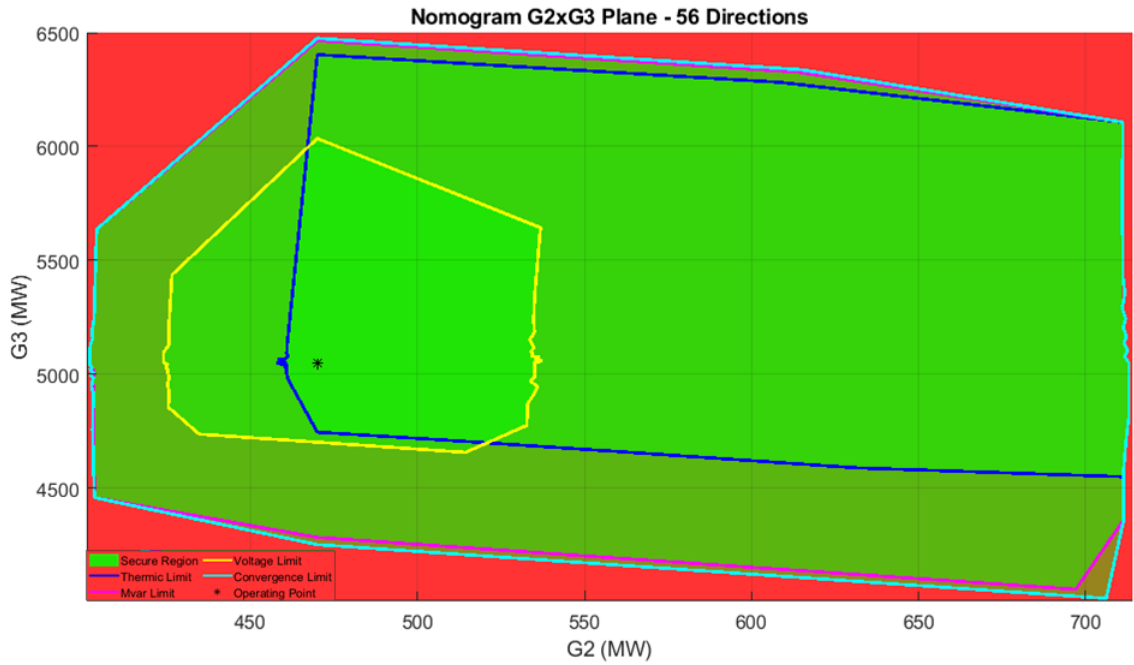
Figure 84 – 107-bus system, G2xG3 plane, 100 directions.
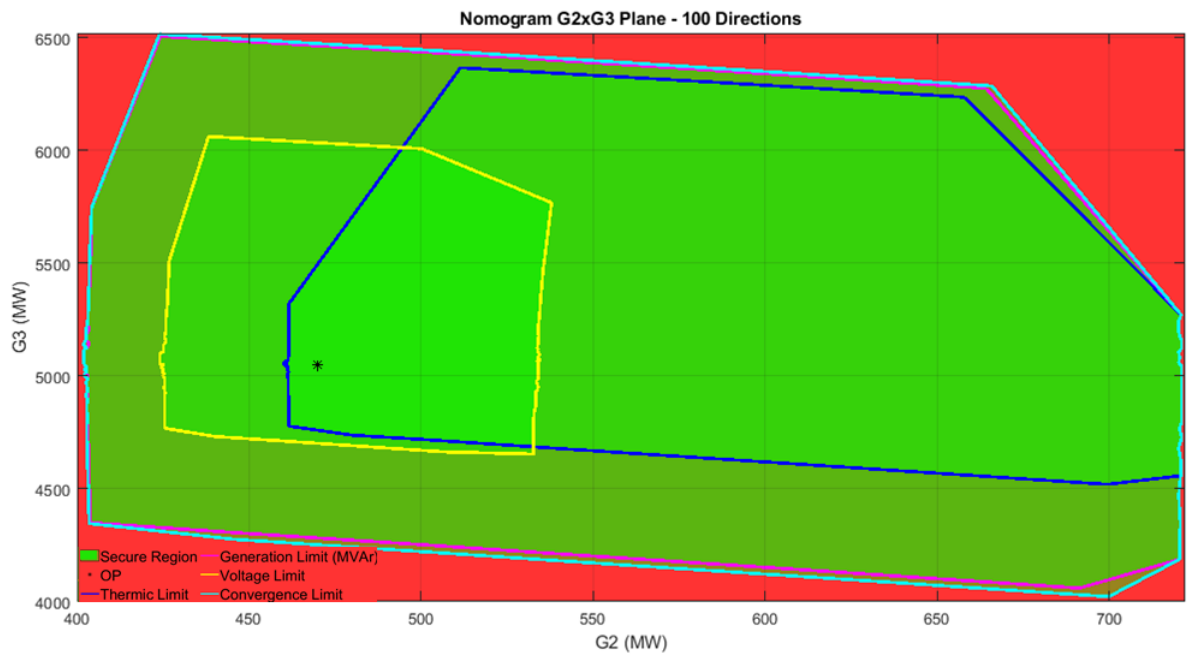
Figure 85 – 107-bus system, G2xG3 plane, 150 directions.
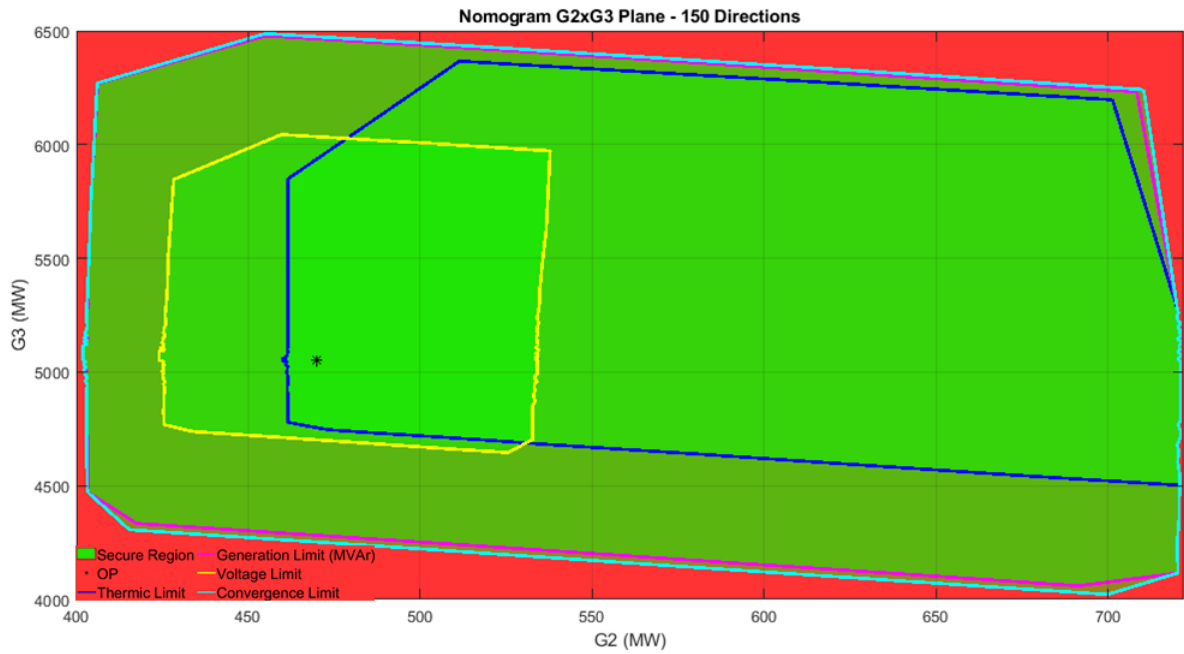
Figure 86 – 107-bus system, G2xG3 plane, 250 directions.
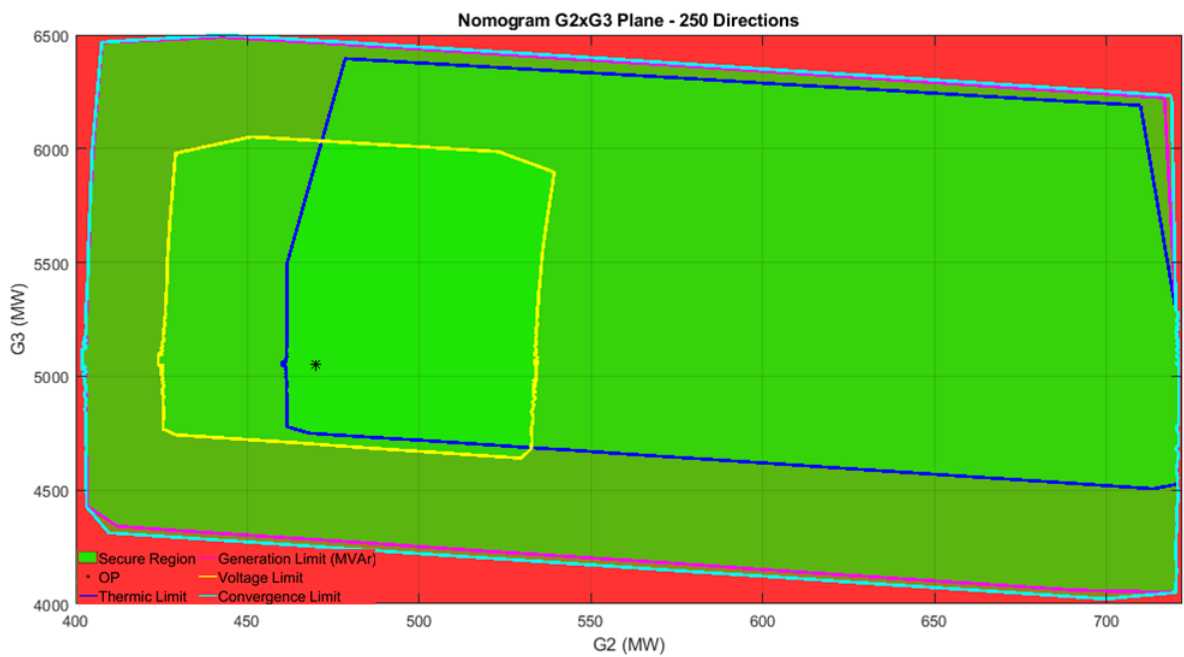
The previous nomograms show the impact that the number of directions has in the quality of the SSSR constructed with the proposed methodology, with a small number of directions the constructed SSSR cuts the secure region, displaying a safe region smaller than the correct one, since this system is close to the collapse point, this could be critical in *real-time* operation, because a decision which is not the best one could be taken following the SSSR.

The parameters used to construct the SSSR with the proposed methodology are shown below:

- Number of particles = 56;

- Number of iterations = 25;

- Initial and final inertial weight = 1.5 and 0.6 respectively;

- Maximum value of the velocity components = 72.1 MW and 443.1 MW, correspondent to 10% and 5% of the maximum capacity of G2 and G3, respectively;

- Contingencies = None considered.

The parameters are the same used with the two previous systems, except for the maximum velocity which depends on the generation capacity of the groups. The initial population was randomly generated within a range of 20% around the base case. Figures 87, 88 and 89 illustrate the nomograms constructed with the proposed methodology.

Figure 87 – 107-bus system, G1xG2 plane with 25 iterations and 56 particles.
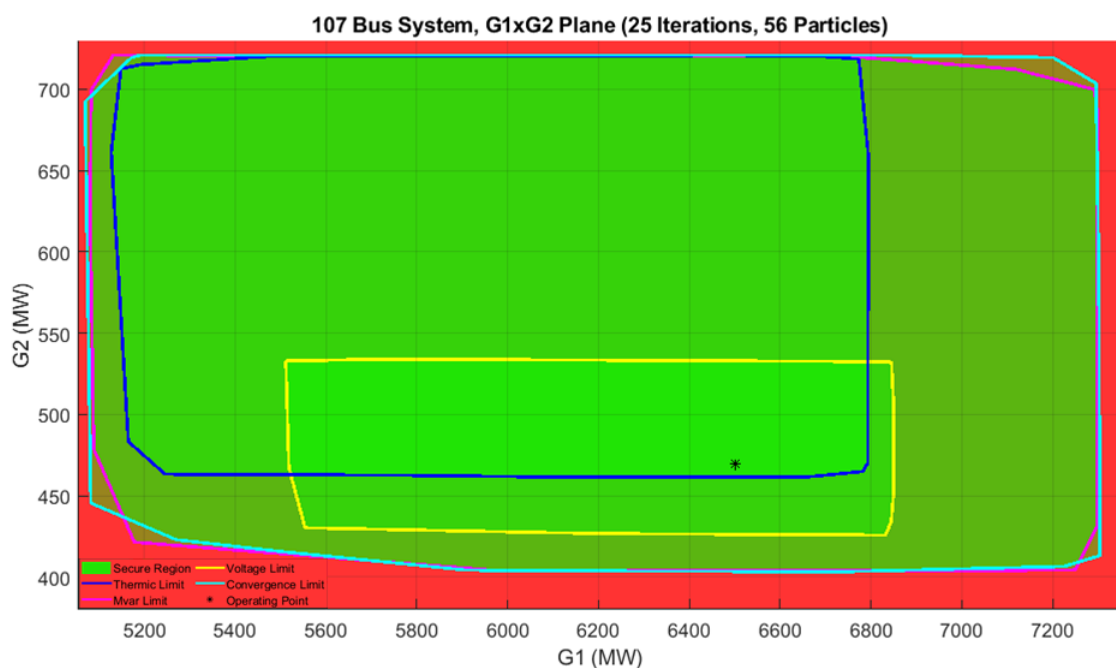
Figure 88 – 107-bus system, G1xG3 plane with 25 iterations and 56 particles.
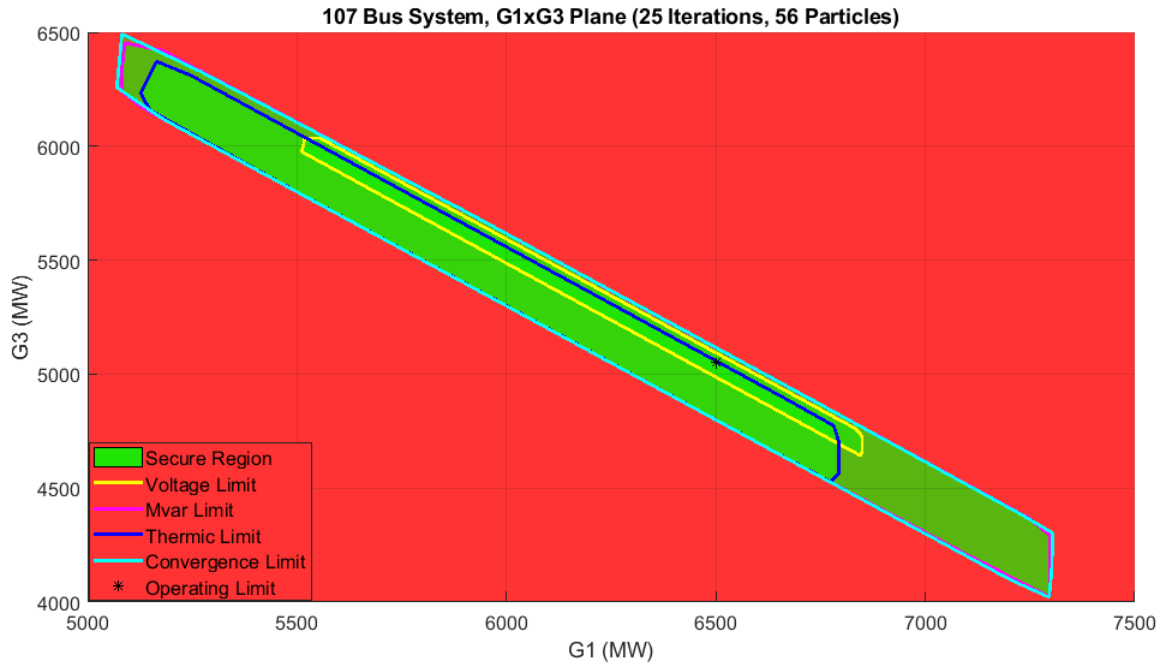
Figure 89 – 107-bus system, G2xG3 plane with 25 iterations and 56 particles.
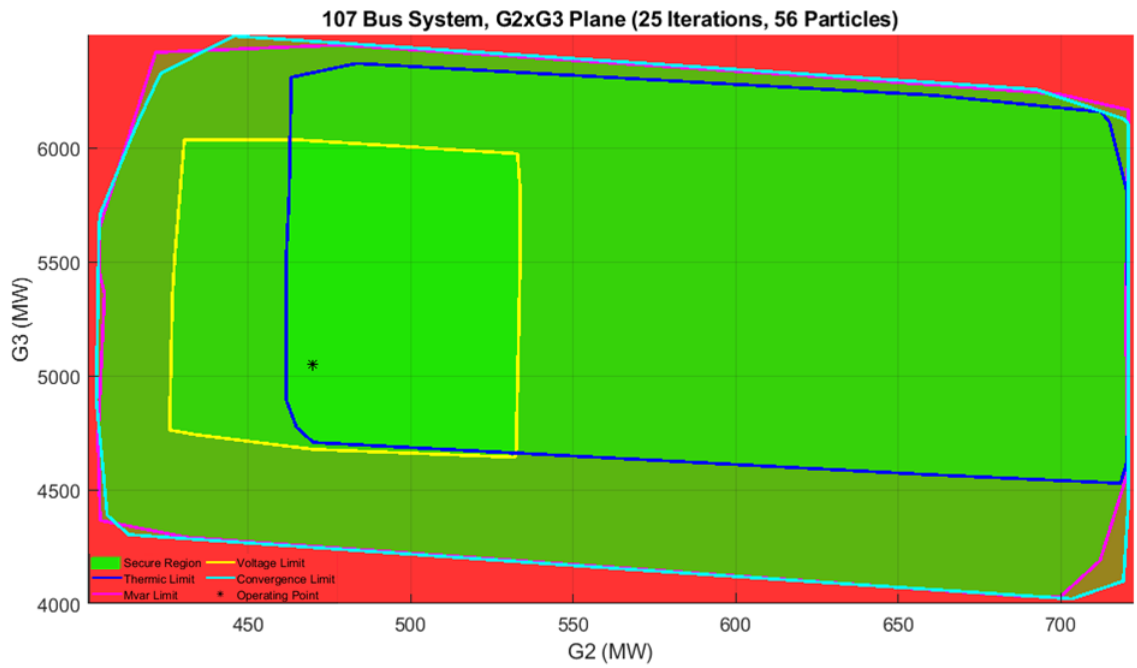
The previous nomograms show that the proposed methodology constructs with accuracy the SSSR only with 56 particles, the result that was obtained is comparable to the one constructed with 250 directions with the conventional methodology, this has an enormous impact on the computational performance, which will be analyzed later. The conventional methodology has problems to obtain an accurate result since between the directions that are chosen around the operating point there are uncertainties that can only be explored choosing a large number of directions impacting negatively in the computational performance.

On the other hand, the proposed methodology does not have the mentioned problem, since the particles move through the whole feasible space of solution, exploring the possible dispatch scenarios without being restricted to a pre-established direction. The proposed methodology proofs to be effective for all the systems that were tested using the same parameters in all the cases, with the exception of the maximum velocity that depends on the capacity of the generation groups.

The results obtained with the proposed methodology show again that, there are small distortions on the edges of the SSSR, this was also present on the results obtained for the previous systems. It is important to emphasize that this problem only occurs with operating points that are far from the base case in all the analyzed cases, which would not be a problem if the tool is used for *on-line* monitoring, since the main interest are always the nearest (to the base case) dispatch scenarios to make any decisions in the operation of the system.

5.2.3.2 *Impact of maximum velocity*

As it was shown in Table 21 the southern Brazilian equivalent has large differences between the capacity of its generation groups, more precisely G2 presents an enormous difference with respect to the other two groups. The nomograms that were shown in Figures 87, 88 and 89 were constructed with different limits for each velocity components, as it was explained in section 4.3.3. It is clear that accurate results were obtained utilizing the proposed manner of treating the maximum velocity.

The objective of this subsection is to analyze the impact of using a single limit for both of the velocity components. It was explained that the maximum velocity is set according to the size of the system, therefore there will be performed two tests to show the impact of the mentioned parameter. Both simulations are executed using the same parameters that were detailed for the previous simulations, except for the maximum velocity. Figure 90 shows the G2xG3 nomogram constructed with a single maximum velocity of 72.1 MW that is equivalent to 10% of the maximum capacity of G2. Finally, Figure 91 illustrates the G2xG3 nomogram created with a maximum limit of the velocity components of 443.1 MW, correspondent to 5% of the capacity of G3.

Figure 90 – 107-bus system, G2xG3 plane, maximum velocity: 72.1 MW.
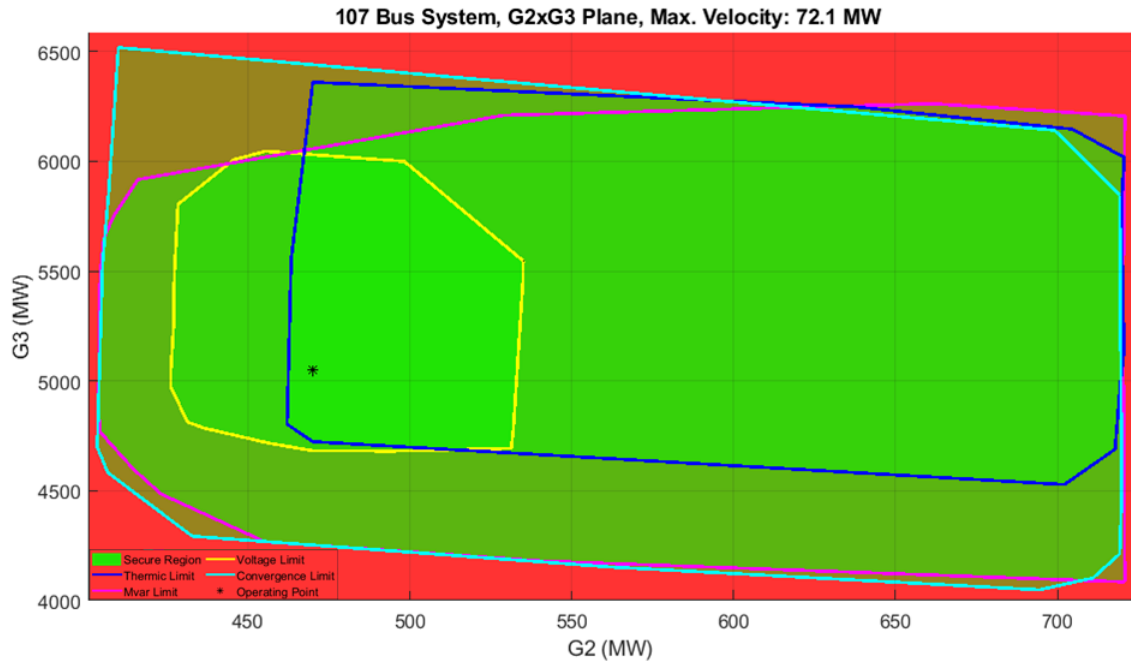
Figure 91 – 107-bus system, G2xG3 plane, maximum velocity: 443.1 MW.
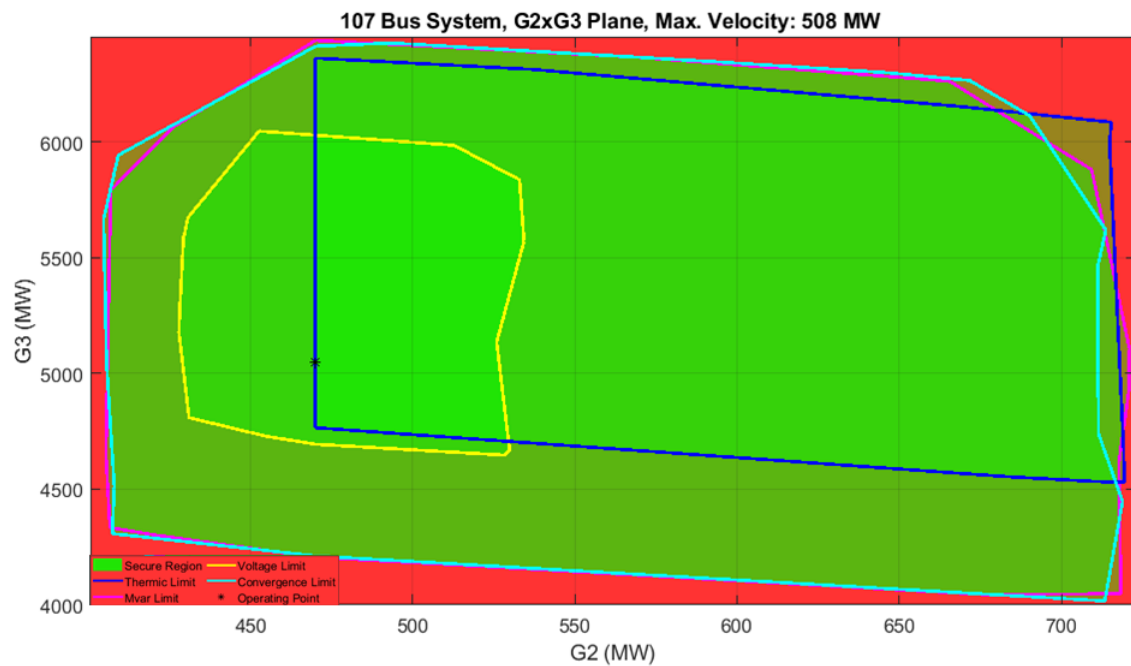
It is clearly observed in the previous figures that the accuracy suffers a large reduction when a single maximum velocity is set for both components. From Figure 90, where the maximum velocity is small, it can be seen that there are some security curves that do not reach the desired position in the "y" axis, since the space that has to be covered in this dimension is very large, in other words, because the maximum capacity of G3 is very large, the steps made by the particles are too small in some security curves, and they do not form the SSSR in the correct way.

On the other hand, with Figure 91, where the maximum velocity is large, it can be seen that the accuracy of the security curves that are near to the operating point is poor. For example, the thermic limit curve is over the base case, this problem occurs because the steps are excessively big on the "x" axis, since the maximum generation of G2 is much smaller, hence, the particles could not find the desired position.

5.2.3.3 *Effectiveness of the initial population treatment and proposed constraints*

This section aims to demonstrate the effectiveness of the proposed initial population treatment and constraints. Special attention is put in the constraints since this system has the security curves extremely close to the base case. Figure 92 shows the G2xG3 plane obtained with the same parameters that were detailed for the previous simulations, with the difference that the proposed constraints are not used, thus, the maximum and minimum generation capacity of the groups are the only constraints of the problem.

Figure 92 – Constructed G2xG3 plane, without proposed constraints.
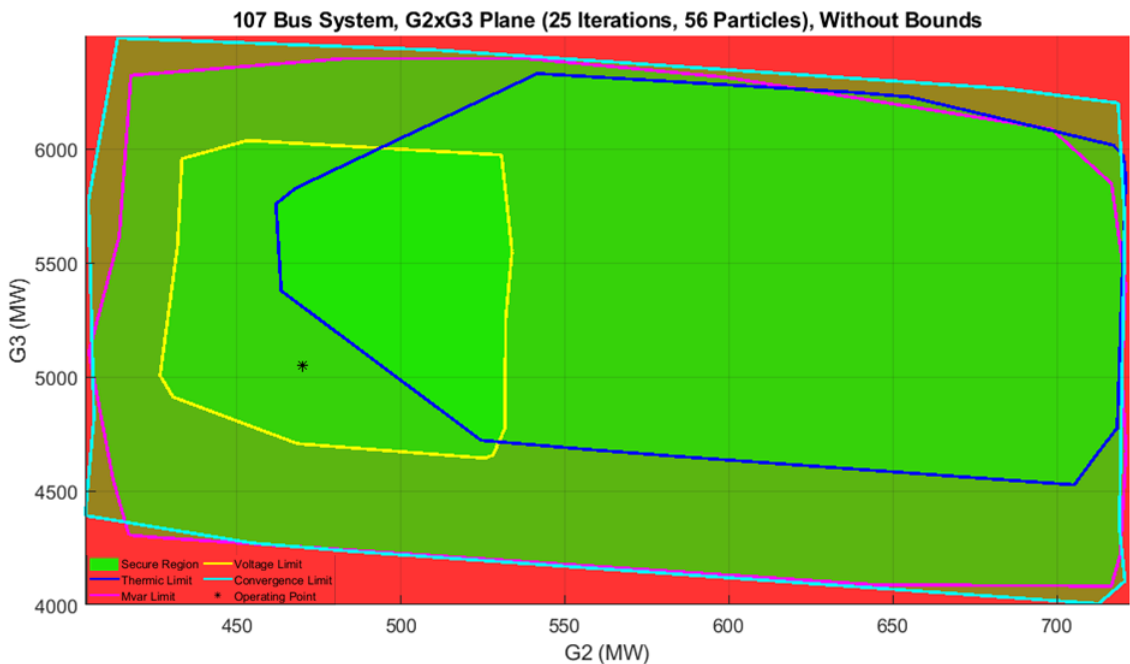
It is important to emphasize that the initial population was used as it is proposed, in other words it was generated within a range of 20% around the base case and equally distributed on the four quadrants, this was done in this way since for this system if the initial population was randomly generated throughout the whole feasible space of solution, the result would not even be alike to the SSSR, due to the closeness of the security curves to the operating point.

From Figure 92 the effects of the proposed constraints are clearly seen, especially with the thermic limit security curve, since the mentioned curve is extremely close to the operating point, the tendency of the particles is to move to the right of the base case. Therefore, it is not possible to create the security curve around the operating point without the proposed constraints, that allow the particles to move only within their initial quadrant.

5.2.3.4 *Computational performance*

As it was done for the previous systems, a comparison between the computational performance of the proposed and conventional methodologies is shown in this subsection. The comparison is made taking into consideration the computing time required for both methodologies to construct the nomograms shown in Figures 83, 84, 85, 86 and 89. Table 22 shows the computational performance of both methodologies.

Table 22 – Comparison between the proposed and conventional methodology

Methodology	Number of Particles/Directions	Time (s)	Gain
Proposed	56	204.04	-
Conventional	56	241.3	15.4 %
	100	440.13	53.6 %
	150	678.15	69.9 %
	250	1099.25	84.4 %

As was seen before the number of directions has a huge impact on the quality of the SSSR with the conventional methodology, and the proposed technique can maintain a constant precision with a small number of particles for all the analyzed systems. The computing time required by the conventional methodology also suffers an enormous impact as it can be seen in Table 22. The accuracy of the proposed technique is comparable to the one constructed using 250 directions with the conventional methodology, when this number of directions is used, the gain in terms of computational performance, obtained with the proposed technique is significant.

Table 22 demonstrates that even with a small number of directions the performance of the proposed methodology is considerably better than the conventional technique, demonstrating the advantages of the construction process utilizing the PSO algorithm, in terms of quality and computational performance.

5.3   CHAPTER SUMMARY

This chapter presented the results that demonstrated the methodologies proposed in Chapters 3 and 4. Both methodologies were analyzed with 3 systems, a small size 9-bus system, the well known New England system, and the larger southern Brazilian equivalent system.

Firstly, the methodology that added voltage instability indicators to the conventional construction process was demonstrated. The results were validated through the use of the classical methods of voltage stability assessment, which are the CPF and the QV curves. The constructed nomograms were compared with the conventional methodology in order to clearly observe the advantages of the proposed methodology. The computational performance was also compared between the methodologies.

Finally, the results of the construction process based on the PSO algorithm were shown for the mentioned systems. The small 9-bus system was used to demonstrate the impact of the number of particles and iterations on the results, regarding quality and computational performance. All the parameters used in the PSO algorithm and their impact on the quality and computing time required by the proposed methodology were analyzed. Since the PSO algorithm uses randomness in its process, the reproducibility of the proposed technique was tested to validate the robustness of the proposed tool. Lastly, the computational performance of the proposed and conventional techniques was analyzed for all the systems.

6 CONCLUSIONS AND FUTURE WORKS PROPOSAL

6.1 CONCLUSIONS

This work presented two methodologies related to the construction process of the Steady-State Security Regions, which is a tool that has gained importance around the world for the power system security assessment. The SSSR is a robust tool that allows evaluating the security of electric networks in an efficient way. However, the conventional SSSR does not include any indicator of the voltage stability condition of the analyzed system.

In that context, the first methodology that was proposed in this work is based on adding a voltage stability indicator to the conventional technique that is used to construct the SSSR. The proposed technique adds the mentioned indicators based on the VSI, which is an index that identifies the proximity to a voltage instability condition. This is done through the characteristic of the power systems that are near to the voltage collapse point, that is, when the Thévenin impedance matches the load impedance.

The proposed methodology consists of creating three subregions that resemble a heat map. This methodology takes advantage of one of the characteristics that the SSSR possesses, which displays the available data in nomograms that allow the analysis of a power system by a simple visual inspection. The proposed technique provides the SSSR a practical way of showing the voltage stability condition of the current operating point and all the possible dispatch scenarios (taking into consideration possible contingencies) within the feasible solution region.

The results of the first methodology were validated through the use of the classical methods of voltage stability assessment, which are the continuation power flow, through the PV curves, and the QV curves. These methods were used through the academic version of the software ANAREDE. It is possible to confirm that using the SSSR with the proposed indicators is a more practical manner of analyzing the voltage stability problem for several dispatch scenarios than the classical methods.

Although the voltage stability index utilizes direct and simple mathematical approaches, such as the sensitivity analysis, when it is combined with the SSSR conventional construction process, the computational performance required by the proposed approach is significantly larger than the conventional technique. Such behavior is mainly due to the enormous amount of dispatch scenarios that are analyzed and for each one of them the VSI has to be calculated for every bus. Although this was expected since more information is being added to the conventional SSSR.

The second proposed methodology presents an alternative way of constructing the SSSR, aiming to significantly reduce the computational effort of the conventional technique

in order to turn the mentioned tool into a feasible manner of monitor power systems in *real-time* operation.

The proposed technique is based on the PSO algorithm, which is a heuristic optimization methodology that requires a low computational effort. The conventional PSO algorithm was modified and adjusted for this application. The modified PSO approach consists of eliminating the social behavior of the particles and letting them take into consideration only their own inertia and experience to update their position. This modification is necessary since, to construct the SSSR, a set of points around the base case is required, instead of a single global optimum point.

An objective function was proposed to build the desired security curve with the optimization algorithm. This function maximizes the distance between the operating point and the edge of the limit that is being analyzed. The proposed objective function contains a penalization factor that prevents the particles from moving beyond the limit of the parameter that is being analyzed. The penalization factor is activated with the evaluation of a power flow solution that is obtained at each iteration of the PSO algorithm.

The proposed PSO settings change the behavior of the particles, turning the proposed methodology vulnerable to the randomness that is used in the PSO algorithm to update their position. Therefore, a series of adjustment to the PSO parameters were performed. These adjustments include the generation of the initial population, constraints that allowed the particles to move only within their initial quadrant, separation of the maximum velocity on its components (x and y), and utilization of high values of initial and final inertia weight. These adjustments aimed to reduce the effects of randomness on the proposed methodology.

Each of the PSO parameters was tested through the analysis performed on the three test systems. With these analyses, a generic adjustment that proofed to work correctly for all the analyzed systems was determined. These adjustments are 56 particles, 25 iterations, generation of the initial population within a range of 20% around the operating point, the maximum velocity of 1%-10% of the generation capacity of the groups, and initial and final inertia weight of 1.5 and 0.6 respectively, these adjustments are expected to be valid for any power system but further tests would be needed to validate this.

With the previous configuration, a series of tests were performed. The results demonstrated that the use of these parameters is crucial to obtain satisfying results in terms of quality and computational performance. The reproducibility of the mentioned configuration was also tested through the execution of a set of simulations. These simulations were superimposed on the same figure, and the results showed that all the parameter adjustments reduced the impact of the randomness of the PSO algorithm to little distortions on the edges of the security curves when the mentioned edges are far from the base case.

The results were compared with the conventional methodology in terms of computational performance and quality of the SSSR. It can be noted that the proposed technique achieves improvements of computational performance. The difference between the proposed and conventional methodologies vary depending on the system. However, the gain in terms of computing time was significant for all the analyzed systems.

It can be affirmed that the difference between the methodologies is larger when the system has a large generation capacity. In this case the conventional methodology has to perform a large number of power transfer steps. The number of steps performed by the proposed methodology is not affected by the system size since the maximum velocity is set according to the capacity of the selected groups.

The simulations executed with the conventional and proposed methodologies were performed setting similar parameters, aiming to obtain fair comparisons. Although it was demonstrated with the southern Brazilian system that the conventional methodology might require a large number of directions to obtain an accurate result, this has an enormous impact on its computational performance. On the other hand, the conventional methodology proofed to have constant results with the same number of particles for all the analyzed systems, since the particles are allowed to move across the whole feasible space of solution instead of moving with pre-established directions like it is done in the conventional methodology.

It was explained that the optimization model has to be solved once for each security curve (voltage, thermic, MVAr and convergence limits) that is desired on the SSSR. Although an alternative way of constructing the SSSR was shown with the New England system, which consists on solving the optimization model only once, penalizing any limit violation, in order to obtain only the safe region of the SSSR, this reduces significantly the computational effort with the disadvantage of not being able identify which are the violated limits. This could be an interesting application for *on-line* monitoring when the analyzed system is extremely large and a reduction on the computational effort is required.

The proposed methodology already presents a vast improvement when compared with the conventional technique, in terms of computational performance. Although, it still has great potential of being improved with the implementation of parallel processing on multi-core CPUs or computer clusters. With these improvements the proposed methodology could be used for large-scale systems in *real-time* operation and the construction of dynamic security regions, which require a larger computing time.

6.2 FUTURE WORKS PROPOSAL

The future scope of this work is listed below:

- Implementation of parallel processing on multi-core CPUs or computer clusters;

- Research a method of representing the scenario when the base case is already with a limit violation.

- Addition of voltage stability indicators to the proposed methodology based on the PSO algorithm;

- Implementation of dynamic constraints to the PSO algorithm for improvement of quality and computational performance;

- Research of other heuristic methods that might improve the PSO algorithm performance for the construction of SSSRs;

- Implementation of the proposed methodology on dynamic security regions.

REFERENCES

[1] Carson W Taylor Neal J Balu and Dominic Maratukulam. *Power system voltage stability.* McGraw-Hill, 1994.

[2] Prabha Kundur, Neal J Balu, and Mark G Lauby. *Power system stability and control*, volume 7. McGraw-hill New York, 1994.

[3] ANDEE ANEEL. Atlas de energia elétrica do brasil. *Agência Nacional de Energia, Brasília*, 2008.

[4] Claudio A Canizares et al. Voltage stability assessment: concepts, practices and tools. *IEEE/PES power system stability subcommittee special publication*, (SP101PSS), 2002.

[5] Pouyan Pourbeik, Prabha S Kundur, and Carson W Taylor. The anatomy of a power grid blackout-root causes and dynamics of recent major blackouts. *IEEE Power and Energy Magazine*, 4(5):22–29, 2006.

[6] Lei Wang and Kip Morison. Implementation of online security assessment. *IEEE Power and Energy Magazine*, 4(5):46–59, 2006.

[7] Prabha Kundur, John Paserba, Venkat Ajjarapu, Göran Andersson, Anjan Bose, Claudio Canizares, Nikos Hatziargyriou, David Hill, Alex Stankovic, Carson Taylor, et al. Definition and classification of power system stability. *IEEE transactions on Power Systems*, 19(2):1387–1401, 2004.

[8] Kip Morison, Lei Wang, and Prabha Kundur. Power system security assessment. *IEEE power and energy magazine*, 2(5):30–39, 2004.

[9] Savu Crivat Savulescu. *Real-time stability assessment in modern power system control centers*, volume 42. John Wiley & Sons, 2009.

[10] Jorge Jardim, Carlos Neto, and Marcelos Groetaers Dos Santos. Brazilian system operator online security assessment system. In *2006 IEEE PES Power Systems Conference and Exposition*, pages 7–12. IEEE, 2006.

[11] CA Silva Neto, Marco A Quadros, Marcelos Groetaers Santos, and Jorge Jardim. Brazilian system operator online security assessment system. In *IEEE PES General Meeting*, pages 1–7. IEEE, 2010.

[12] L Franchi, A Gambelunghe, R Salvati, and M Sforna. Online dynamic security assessment at the italian independent system operator. In *2003 IEEE Bologna Power Tech Conference Proceedings,*, volume 3, pages 8–pp. IEEE, 2003.

[13] Felipe CB Almeida, João A Passos Filho, José LR Pereira, Ricardo M Henriques, and André LM Marcato. Assessment of load modeling in power system security analysis based on static security regions. *Journal of Control, Automation and Electrical Systems*, 24(1-2):148–161, 2013.

[14] Jhonatan Nascimento Costa, E. C. Brandao, and João Alberto Passos Filho. Desenvolvimento de um Índice para avaliação de segurança de tensão de sistemas elétricos de potência baseado em equivalentes de thevenin. In *Simpósio Brasileiro de Sistemas Elétricos*. Foz do Iguaçu. Anais do SBSE, 2014.

[15] Simone Bezerra Chaves. Análise estática e dinâmica de sistemas de potência via aplicativo computacional integrado: Organon. Master's thesis, Universidade Federal Fluminense, 2008.

[16] Ricardo Padilha Pareto. Construção da região de segurança estática de sistemas elétricos de potência utilizando direções de transferência de geração ramificadas. Master's thesis, Universidade Federal do Rio de Janeiro, 2016.

[17] Thiago Jose Masseran Antunes Parreiras, Sergio Gomes Junior, and Glauco Nery Taranto. Damping nomogram method for small-signal security assessment of power systems. *IEEE Latin America Transactions*, 15(5):877–883, 2017.

[18] F Wu and Sadatoshi Kumagai. Steady-state security regions of power systems. *IEEE Transactions on Circuits and Systems*, 29(11):703–711, 1982.

[19] Sijie J Chen, Qixin X Chen, Qing Xia, and Chongqing Q Kang. Steady-state security assessment method based on distance to security region boundaries. *IET Generation, Transmission & Distribution*, 7(3):288–297, 2013.

[20] Wei Wei, Hongjie Jia, Pei Zhang, Chengshan Wang, Jianzhong Wu, and Stephen T Lee. Development of power system voltage stability region (psvsr) for static voltage security assessment. In *2006 International Conference on Power System Technology*, pages 1–6. IEEE, 2006.

[21] Sandro Corsi and Glauco N Taranto. A real-time voltage instability identification algorithm based on local phasor measurements. *IEEE transactions on power systems*, 23(3):1271–1279, 2008.

[22] HK Nam, CG Song, DJ Kim, YH Moon, and KY Lee. A new efficient unified strategy to compute voltage collapse point and voltage stability enhancement by generation shift. In *IEEE Power Engineering Society. 1999 Winter Meeting (Cat. No. 99CH36233)*, volume 1, pages 640–645. IEEE, 1999.

[23] P Kessel and H Glavitsch. Estimating the voltage stability of a power system. *IEEE Transactions on power delivery*, 1(3):346–354, 1986.

[24] A Tiranuchit and RJ Thomas. A posturing strategy against voltage instabilities in electric power systems. *IEEE Transactions on Power Systems*, 3(1):87–93, 1988.

[25] MH Haque. A fast method for determining the voltage stability limit of a power system. *Electric power systems research*, 32(1):35–43, 1995.

[26] LA Ll Zarate and CA Castro. Fast method for computing power system security margins to voltage collapse. *IEE Proceedings-Generation, Transmission and Distribution*, 151(1):19–26, 2004.

[27] J. Kennedy and R. Eberhart. Particle swarm optimization. In *Proceedings of ICNN'95 - International Conference on Neural Networks*, volume 4, pages 1942–1948 vol.4, Nov 1995.

[28] James Kennedy. The particle swarm: social adaptation of knowledge. In *Proceedings of 1997 IEEE International Conference on Evolutionary Computation (ICEC'97)*, pages 303–308. IEEE, 1997.

[29] Yuhui Shi and Russell Eberhart. A modified particle swarm optimizer. In *1998 IEEE international conference on evolutionary computation proceedings. IEEE world congress on computational intelligence (Cat. No. 98TH8360)*, pages 69–73. IEEE, 1998.

[30] Yamille Del Valle, Ganesh Kumar Venayagamoorthy, Salman Mohagheghi, Jean-Carlos Hernandez, and Ronald G Harley. Particle swarm optimization: basic concepts, variants and applications in power systems. *IEEE Transactions on evolutionary computation*, 12(2):171–195, 2008.

[31] Felipe de Castro Brum Almeida. Avaliação do desempenho dos dispositivos de controle e modelagem de carga a partir de regiões de segurança estática. Master's thesis, Universidade Federal de Juiz de Fora, 2011.

[32] Lucas Bittar Barbosa. Desenvolvimento de uma ferramenta automática para a determinação da máxima transferência de potência entre áreas/regiões em regime permanente. *Universidade Federal Fluminese, Niterói, RJ*, 2009.

[33] John Peschon, Dean S Piercy, William F Tinney, and Odd J Tveit. Sensitivity in power systems. *IEEE Transactions on Power Apparatus and Systems*, (8):1687–1696, 1968.

[34] Feng Dong, Ted Kostyniak, and Baldwin Lam. Dealing with power flow solution difficulties. *Siemens, PTI eNeswletters, USA*, 2012.

[35] Kwang Y Lee and Mohamed A El-Sharkawi. *Modern heuristic optimization techniques: theory and applications to power systems*, volume 39. John Wiley & Sons, 2008.

[36] MathWorks. Boundary, 2014.

[37] Paul M Anderson and Aziz A Fouad. *Power system control and stability*. John Wiley & Sons, 2008.

[38] T Athay, R Podmore, and S Virmani. A practical method for the direct analysis of transient stability. *IEEE Transactions on Power Apparatus and Systems*, (2):573–584, 1979.

[39] WF Alves. Proposition of test-systems to power systems analysis. *Niteroi, RJ*, 2007.

APPENDIX A – Data of the 9-bus System

Appendix A presents the data that was used for all the simulations performed in the results Chapter, regarding the 9-bus system.

A.1 Data I

This section presents the data used to obtain the nomograms showed in Figures 33, 34 and 35.

A.1.1 **Node data**

Node data of the base case utilized for the construction of the mentioned nomograms.

Table 23 – Node data of the 9-bus system

Bus	Type	V (p.u.)	P_G (MW)	P_L (MW)	Q_L (MVAr)	Shunt (MVAr)
1	PV	1.075	442.8	0	0	0
2	PV	1.075	279.7	0	0	0
3	PV	1.075	264.2	0	0	0
4	PQ	1	0	0	0	0
5	PQ	1	0	428.13	171.25	230
6	PQ	1	0	308.25	102.75	150
7	PQ	1	0	0	0	0
8	PQ	1	0	342.51	119.87	120
9	PQ	1	0	0	0	0
10	Swing	1.075	0	0	0	0

The maximum and minimum voltage allowed for all the buses on the 9-bus system is presented in Table 24. The same values were used for all the simulations performed with this system.

Table 24 – Voltage limits on the 9-bus system

Voltage Limit	
Minimum	**Maximum**
0.9 p.u.	1.1 p.u.

The limits of the active and reactive generation of the PV buses and the Swing bus used for the construction of the mentioned nomograms are presented in Table 25.

Table 25 – Generation data of the 9-bus system

Bus	P_{min} (MW)	P_{max} (MW)	Q_{min} (MVAr)	Q_{max} (MVAr)
1	-300	1000	-9999	9999
2	-300	1000	-9999	9999
3	-300	1000	-9999	9999
10	-9999	9999	-9999	9999

Negative values were used in the minimum capacity of the PV buses in order to clearly observe the 3 subregions around the operating point.

A.1.2 Transmission line and transformer data

The parameters of the transmission lines are detailed in Table 26, emphasizing that the thermic limit was not taking into consideration for the mentioned nomograms, but the values shown in Tables 26 and 27 are used for the rest of the simulations.

Table 26 – Transmission line data of the 9-bus system

From Bus	To Bus	R (%)	X (%)	B (MVAr)	Thermic Limit (MVA)
4	5	1	8.5	17.6	300
4	6	1.7	9.2	15.8	300
6	9	3.9	17	35.8	200
7	5	3.2	16.1	30.6	200
7	8	0.85	7.2	14.9	300
8	9	1.19	10.08	20.9	300
10	1	0	0.01	0	9999

The parameters of the transformers data are shown in Table 27 below.

Table 27 – Transformer data of the 9-bus system

From Bus	To Bus	R (%)	X (%)	Tap	Thermic Limit (MVA)
1	4	0	5.76	1	247
2	7	0	6.25	1	192
3	9	0	5.86	1	128

The tutorial of the methodology that adds the VSI regions to the SSSR showed a sensitivity analysis where the Jacobian matrix is not explicitly shown, Table 28 shows the numeric values of the Jacobian matrix used in the mentioned tutorial.

Table 28 – Jacobian matrix

11576.09	0.00	0.00	-19.84	0.00	0.00	0.00	0.00	0.00	-11556.25	1.89	0.00	0.00	3.11	0.00	0.00	3.74	0.00	0.00	-1.24		
0.00	17.95	0.00	0.00	0.00	0.00	-17.95	0.00	0.00	0.00	0.00	3.72	0.00	0.00	0.00	0.00	0.00	0.00	0.00	0.00		
0.00	0.00	19.35	0.00	0.00	0.00	0.00	0.00	-19.35	0.00	0.00	0.00	3.57	0.00	0.00	-1.00	0.00	0.00	3.57	0.00		
-19.84	0.00	0.00	45.71	-13.52	-12.34	0.00	0.00	0.00	0.00	-3.12	0.00	0.00	3.57	0.55	0.00	0.00	0.00	0.00	0.00		
0.00	0.00	0.00	-13.02	19.07	0.00	-6.05	0.00	0.00	0.00	0.00	0.00	0.00	-3.44	-1.24	0.60	-3.29	0.00	0.00	0.00		
0.00	0.00	0.00	-11.91	0.00	17.60	0.00	0.00	-5.69	0.00	0.00	-3.72	0.00	-3.16	0.00	0.00	0.00	0.00	-3.17	0.00		
0.00	-17.95	0.00	0.00	-6.94	0.00	40.53	-15.64	0.00	0.00	0.00	0.00	0.00	0.00	0.87	0.00	3.00	-0.14	0.00	0.00		
0.00	0.00	0.00	0.00	0.00	0.00	-15.25	26.06	-10.82	0.00	0.00	0.00	0.00	0.00	0.00	0.54	-3.27	-0.29	-2.83	0.00		
0.00	0.00	-19.35	0.00	0.00	-6.60	0.00	-11.23	37.18	0.00	1.24	0.00	-3.57	0.00	0.00	0.00	0.00	0.41	2.62	0.00		
0.00	0.00	0.00	0.00	0.00	0.00	0.00	0.00	0.00	1E+10	1E+10	0.00	0.00	0.00	0.00	0.00	0.00	0.00	0.00	1.24		
-11556.25	0.00	0.00	0.00	0.00	0.00	0.00	0.00	0.00	1.33	0.00	1E+10	0.00	0.00	0.00	0.00	0.00	0.00	0.00	-10750		
2.03	0.00	0.00	-3.36	0.00	0.00	-4.00	0.00	-3.84	0.00	0.00	0.00	1E+10	-18.40	0.00	0.00	-16.79	0.00	-17.99	0.00		
0.00	4.00	0.00	0.00	0.00	0.00	0.00	0.00	0.00	0.00	-18.46	0.00	0.00	0.00	-12.59	-11.48	0.00	0.00	0.00	0.00		
0.00	0.00	3.84	0.00	0.00	0.00	0.00	0.00	0.00	0.00	0.00	0.00	0.00	0.00	14.56	0.00	0.00	0.00	0.00	0.00		
3.36	0.00	0.00	-3.85	-0.59	1.08	3.52	0.00	3.40	0.00	0.00	0.00	0.00	42.39	0.00	14.46	-5.66	0.00	-5.29	0.00		
0.00	0.00	0.00	3.71	-7.23	0.00	0.00	0.00	0.00	0.00	0.00	-16.70	0.00	-12.07	-6.46	0.00	37.90	-14.75	0.00	0.00		
0.00	0.00	0.00	3.40	0.00	-6.81	-3.21	0.15	3.04	0.00	0.00	0.00	0.00	-11.05	0.00	0.00	-14.26	22.31	-10.06	0.00		
0.00	0.00	0.00	0.00	-0.94	0.00	3.50	-6.54	-2.82	0.00	0.00	0.00	0.00	0.00	0.00	0.00	0.00	-10.59	34.57	0.00		
0.00	4.00	0.00	0.00	0.00	0.00	0.00	-0.44	0.00	0.00	0.00	0.00	0.00	0.00	0.00	-6.14	0.00	0.00	0.00	0.00		
0.00	0.00	0.00	0.00	0.00	-0.58	0.00	0.00	0.00	0.00	0.00	0.00	-18.00	0.00	0.00	0.00	0.00	0.00	0.00	0.00		
0.00	0.00	3.84	0.00	0.00	0.00	0.00	0.00	0.00	0.00	0.00	0.00	0.00	0.00	0.00	0.00	0.00	0.00	0.00	0.00		
-1.33	0.00	0.00	0.00	0.00	0.00	0.00	0.00	0.00	1.33	-10750.00	0.00	0.00	0.00	0.00	0.00	0.00	0.00	0.00	1E+10		

A.2 Data II

This section shows the data utilized to obtain the nomograms shown in Figures 38, 39 and 40.

A.2.1 **Node data**

The node data used in the execution of the proposed methodology, where the mentioned nomograms were obtained, is shown in Table 29.

Table 29 – Node data of the 9-bus system

Bus	Type	V (p.u.)	P_G (MW)	P_L (MW)	Q_L (MW)	Shunt (MVAr)
1	PV	1.075	130.4	0	0	0
2	PV	1.075	101.2	0	0	0
3	PV	1.075	67.4	0	0	0
4	PQ	1	0	0	0	0
5	PQ	1	0	131.25	52.5	10
6	PQ	1	0	94.5	31.5	0
7	PQ	1	0	0	0	0
8	PQ	1	0	105	36.75	0
9	PQ	1	0	0	0	0
10	Swing	1.075	0	0	0	0

The generation data utilized in this simulation is available in Table 30. This generation data was also used in the simulations associated with the proposed methodology which was based on the PSO algorithm.

Table 30 – Generation data of the 9-bus system

Bus	Pmin	Pmax	Qmin	Qmax
1	0	210.4	-130	130.4
2	0	163.2	-101	101.2
3	0	108.8	-67.4	67.4
10	0	9999	-9999	9999

A.3 Data III

This section shows the node data that was used in all the simulations that were executed with the 9-bus system, associated with the methodology based on the PSO algorithm.

A.3.1 **Node data**

Table 31 – Node data of the 9-bus system

Bus	Type	V (p.u.)	P_G (MW)	P_L (MW)	Q_L (MVAr)	Shunt (MVAr)
1	PV	1.075	117.5	0	0	0
2	PV	1.075	115	0	0	0
3	PV	1.075	85	0	0	0
4	PQ	1	0	0	0	0
5	PQ	1	0	125	50	0
6	PQ	1	0	90	30	0
7	PQ	1	0	0	0	0
8	PQ	1	0	100	35	0
9	PQ	1	0	0	0	0
10	Swing	1.075	0	0	0	0

APPENDIX B – Data of the New England System

This appendix presents the data that was used for all the simulations performed in the results Chapter, regarding the New England system.

B.1   Data I

This section presents the data used to obtain the nomograms showed in Figures 44, 45 and 46.

B.1.1   **Node data**

The node data available in Table 32 was used in the simulations of the mentioned nomograms and for all the simulations associated with the results obtained with the methodology based on the PSO algorithm.

Table 32 – Node data of the New England system

Bus	Type	V (p.u.)	P_G (MW)	P_L (MW)	Q_L (MVAr)	Shunt (MVAr)
1	PQ	1	0	0.0	0.0	0
2	PQ	1	0	0.0	0.0	0
3	PQ	1	0	357.9	2.7	0
4	PQ	1	0	555.8	204.5	0
5	PQ	1	0	0.0	0.0	0
6	PQ	1	0	0.0	0.0	0
7	PQ	1	0	259.8	93.4	0
8	PQ	1	0	580.2	195.6	0
9	PQ	1	0	0.0	0.0	0
10	PQ	1	0	0.0	0.0	0
11	PQ	1	0	0.0	0.0	0
12	PQ	1	0	9.4	97.8	0
13	PQ	1	0	0.0	0.0	0
14	PQ	1	0	0.0	0.0	0
15	PQ	1	0	355.7	170.1	0
16	PQ	1	0	366.1	35.9	0
17	PQ	1	0	0.0	0.0	0
18	PQ	1	0	175.6	33.3	0
19	PQ	1	0	0.0	0.0	0
20	PQ	1	0	755.8	114.5	0
21	PQ	1	0	304.6	127.8	0

22	PQ	1	0	0.0	0.0	0
23	PQ	1	0	275.1	94.1	0
24	PQ	1	0	343.0	-102.6	0
25	PQ	1	0	249.0	54.1	0
26	PQ	1	0	154.5	18.9	0
27	PQ	1	0	312.3	83.9	0
28	PQ	1	0	229.0	30.7	0
29	PQ	1	0	315.2	29.9	0
30	PV	1.048	250	0.0	0.0	0
31	PV	0.982	573.2	10.2	5.1	0
32	PV	0.983	650	0.0	0.0	0
33	PV	0.997	632	0.0	0.0	0
34	PV	1.012	508	0.0	0.0	0
35	PV	1.049	650	0.0	0.0	0
36	PV	1.064	560	0.0	0.0	0
37	PV	1.028	540	0.0	0.0	0
38	PV	1.027	830	0.0	0.0	0
39	PV	1.03	2896	1226.9	277.9	0
40	Swing	1.03	0	0.0	0.0	0

The maximum and minimum voltage allowed for all the buses on the New England system is presented in Table 33. The same values were used for all the simulations performed with this system.

Table 33 – Voltage limits on the 9-bus system

Voltage Limit	
Minimum	**Maximum**
0.9 p.u.	1.1 p.u.

The limits of the active and reactive generation of the PV buses and the Swing bus used for the construction of the mentioned nomograms are presented in Table 34.

Table 34 – Generation data of the New England system

Bus	P_{min} (MW)	P_{max} (MW)	Q_{min} (MVAr)	Q_{max} (MVAr)
30	0	412.5	-1100	1100
31	0	1625	-1100	1100
32	0	1625	-1100	1100
33	0	1625	-1100	1100
34	0	1625	-1100	1100
35	0	2000	-1100	1100
36	0	2000	-1100	1100
37	0	900	-1100	1100
38	0	1380	-1100	1100
39	0	4807.5	-1100	1100
40	-9999	9999	-9999	9999

B.1.2 Transmission line and transformer data

The parameters of the transmission lines are shown in Table 35, these parameters are the same for all the simulations performed for both methodologies proposed in this work.

Table 35 – Transmission line data of the New England system

From Bus	To Bus	R (%)	X (%)	B (MVAr)	Thermic Limit (MVA)
1	2	0.35	4.11	69.87	1800
1	39	0.1	2.5	75	1800
2	3	0.13	1.51	25.72	1800
2	25	0.7	0.86	14.6	1800
3	4	0.13	2.13	22.14	1800
3	18	0.11	1.33	21.38	1800
4	5	0.08	1.28	13.42	1800
4	14	0.08	1.29	13.82	1800
5	6	0.02	0.26	4.34	1800
5	8	0.08	1.12	14.76	1800
6	7	0.06	0.92	11.3	1800
6	11	0.07	0.82	13.89	1800
7	8	0.04	0.46	7.8	1800
8	9	0.23	3.63	38.04	1800
9	39	0.1	2.5	120	1800

10	11	0.04	0.43	7.29	1800
10	13	0.04	0.43	7.29	1800
13	14	0.09	1.01	17.23	1800
14	15	0.18	2.17	36.6	1800
15	16	0.09	0.94	17.1	1800
16	17	0.07	0.89	13.42	1800
16	19	0.16	1.95	30.4	1800
16	21	0.08	1.35	25.48	1800
16	24	0.03	0.59	6.8	1800
17	18	0.07	0.82	13.19	1800
17	27	0.13	1.73	32.16	1800
21	22	0.08	1.4	25.65	1800
22	23	0.06	0.96	18.46	1800
23	24	0.22	3.5	36.1	1800
23	36	0.05	2.72	0	1800
25	26	0.32	3.23	51.3	1800
26	27	0.14	1.47	23.96	1800
26	28	0.43	4.74	78.02	1800
26	29	0.57	6.25	102.9	1800
28	29	0.14	1.51	24.9	1800
40	39	0	0.01	0	9999

Table 36 shows the parameters of the transformers of the New England system, which are the same for all the simulations.

Table 36 – Transformers data of the New England system

From Bus	To Bus	R (%)	X (%)	Tap	Thermic Limit (MVA)
2	30	0	1.81	1.025	1800
6	31	0	2.5	1.07	1800
10	32	0	2	1.07	1800
12	11	0.16	4.35	1.006	1800
12	13	0.16	4.35	1.006	1800
19	20	0.07	1.38	1.06	1800
19	33	0.07	1.42	1.07	1800
20	34	0.09	1.8	1.009	1800
22	35	0	1.43	1.025	1800
25	37	0.06	2.32	1.025	1800
29	38	0.08	1.56	1.025	1800

B.2 Data II

This section presents the generation data that was used in all the simulations that were performed with the methodology based on the PSO algorithm, the generation data was the only change between the simulations performed with both of the proposed methodologies of this work.

B.2.1 **Generation data**

The generation data is shown in Table 37.

Table 37 – Generation data of the New England system

Bus	P_{min} (MW)	P_{max} (MW)	Q_{min} (MVAr)	Q_{max} (MVAr)
30	0	1000	-900	900
31	0	1000	-900	900
32	0	1000	-900	900
33	0	1000	-900	900
34	0	1000	-900	900
35	0	1500	-900	900
36	0	1500	-900	900
37	0	1000	-900	900
38	0	1000	-900	900
39	0	3500	-900	900
40	-9999	9999	-9999	9999

APPENDIX C – Data of the southern Brazilian equivalent system

This appendix presents the data that was used for all the simulations performed in the results Chapter, regarding the southern Brazilian equivalent system.

C.1 Data I

The results presented in this section are valid for all the simulations performed with the southern Brazilian equivalent system for both methodologies that were proposed in this work.

C.1.1 **Node data**

Table 38 shows the data of the nodes of the southern Brazilian equivalent system.

Table 38 – Node data of the southern Brazilian equivalent system

Bus	Type	V (p.u.)	P_G (MW)	P_L (MW)	Q_L (MVAr)	Shunt (MVAr)	Voltage Limit Group
12	PV	1	300	0	0	0	D
16	PV	1	800	0	0	0	D
18	Swing	1.02	0	0	0	0	D
20	PV	1.01	900	0	0	0	D
21	PV	1	140	0	0	0	D
22	PV	1	150	0	0	0	D
35	PV	1	200	0	0	0	D
48	PV	1	0	0	0	0	D
86	PQ	1.033	0	66	1.2	0	C
100	PQ	1.056	0	0	0	0	A
101	PQ	1.069	0	0	0	-200	A
102	PQ	1.059	0	0	0	-100	A
103	PQ	1.072	0	0	0	0	A
104	PQ	1.061	0	910	235	0	A
106	PQ	1.05	0	0	0	-100	A
120	PQ	1.041	0	180	90	0	C
122	PQ	1.067	0	200	38	0	A
123	PQ	1.035	0	450	175	0	C
126	PQ	1.037	0	290	95	0	C
131	PQ	1.027	0	0	0	0	C
134	PQ	1.027	0	0	0	0	C

136	PQ	1.028	0	54	23	0	C
138	PQ	1.036	0	72	34	0	C
140	PQ	1.023	0	700	250	0	C
210	PQ	1.048	0	0	0	0	A
213	PQ	1.05	0	93	39	0	C
216	PQ	1.049	0	53	25	0	C
217	PQ	1.05	0	364	58	0	C
218	PQ	1.025	0	600	200	0	C
219	PQ	1.028	0	0	0	0	C
220	PQ	1.052	0	0	0	0	C
225	PQ	1	0	0	0	0	C
228	PQ	1.016	0	86	34	0	C
231	PQ	1.01	0	89.7	31.9	0	C
233	PQ	1.039	0	0	0	0	A
234	PQ	1.027	0	1000	350	0	C
300	PV	1.02	700	0	0	0	D
301	PV	1.01	300	0	0	0	D
302	PV	1.02	400	0	0	0	D
303	PV	1.02	200	0	0	0	D
305	PV	1	300	0	0	0	D
320	PQ	1.049	0	0	0	0	A
325	PQ	1.046	0	0	0	0	A
326	PQ	1.033	0	274	104	0	C
360	PQ	1.046	0	0	0	0	A
370	PQ	1.049	0	0	0	0	A
396	PQ	1.041	0	0	0	0	C
500	PV	1.02	800	0	0	0	D
535	PQ	1.035	0	0	0	0	A
536	PQ	1.023	0	700	150	0	B
800	PV	1.02	1100	0	0	0	D
808	PV	1.02	1150	0	0	0	D
810	PV	1.02	1200	0	0	0	D
814	PQ	1	0	735.4	191	0	C
824	PQ	1.038	0	0	0	0	A
834	PQ	0.991	0	13.4	4.2	0	C
839	PQ	0.999	0	0	0	0	C
840	PQ	0.986	0	159	36	0	D

848	PQ	0.999	0	94	18	0	D
856	PQ	1.035	0	0	0	0	A
895	PQ	1.044	0	0	0	0	A
896	PQ	1.028	0	0	0	0	A
897	PQ	1.039	0	0	0	0	A
898	PQ	1.012	0	0	0	0	C
904	PV	1.02	700	0	0	0	D
915	PV	1.02	700	0	0	0	D
919	PV	1	700	0	0	0	D
925	PV	1.02	950	0	0	0	D
933	PQ	1.038	0	0	0	0	A
934	PQ	1	0	237	59	0	C
938	PQ	1.043	0	0	0	0	A
939	PQ	1	0	1149	53.06	0	C
955	PQ	1.058	0	0	0	0	A
959	PQ	1.033	0	0	0	100	A
960	PQ	1	0	844.7	469.1	0	C
964	PQ	1.037	0	0	0	0	A
965	PQ	1	0	755.6	56.24	0	C
976	PQ	1.012	0	0	0	0	A
995	PQ	1.05	0	0	0	0	A
1015	PQ	0.998	0	70	2	0	C
1030	PQ	1.052	0	0	0	0	A
1047	PQ	1.017	0	0	0	0	C
1060	PQ	1.043	0	0	0	0	A
1210	PQ	1	0	1228	425	0	C
1503	PQ	1.061	0	0	0	0	A
1504	PQ	1.026	0	145	63	0	D
2458	PQ	1	0	403	126	0	C
4501	PQ	1.026	0	31.4	7.1	-45	C
4521	PQ	1.034	0	0	0	0	C
4522	PQ	1.032	0	0	0	-20	C
4523	PV	1.01	50	0	0	0	D
4530	PV	1.02	0	0	0	0	D
4532	PQ	1.041	0	0	0	0	C
4533	PQ	1.014	0	75.4	16.1	0	D
4542	PQ	1.025	0	0	0	0	C

4552	PQ	1.007	0	12.6	1.2	-20	C
4562	PQ	1.012	0	23.8	7.4	0	C
4572	PQ	1.009	0	18	6.4	0	C
4582	PQ	1.018	0	65.5	16.7	30	C
4592	PQ	1.018	0	0	0	0	C
4596	PV	1	230	0	0	0	D
4623	PQ	1.018	0	128.2	40.76	0	D
4703	PQ	1.003	0	182.1	29.75	0	D
4804	PV	1	50	0	0	0	D
4805	PQ	1.025	0	0	0	0	D
4807	PQ	1.025	0	128.9	36.3	0	D
4862	PQ	1.046	0	0	0	-30	C

The voltage limits of each group are shown in Table 39.

Table 39 – Voltage limits on the southern Brazilian equivalent system

Group	Voltage Limit	
	Minimum (p.u.)	Maximum (p.u)
A	0.95	1.1
B	0.95	1.08
C	0.95	1.07
D	0.95	1.05

The generation data is available in Table 40.

Table 40 – Generation data of the southern Brazilian equivalent system

Bus	P_{min} (MW)	P_{max} (MW)	Q_{min} (MVAr)	Q_{max} (MVAr)
12	0	1104	-540	420
16	0	1312	-720	480
18	0	2280	-9999	9999
20	0	1488	-640	640
21	0	216	-80	84
22	0	324	-120	126
35	0	381	-180	180
48	0	0	-1080	1200
300	0	1192	-440	392
301	0	400	-140	140
302	0	510	-150	150

303	0	1680	-600	600
305	0	380	-120	120
500	0	1396.2	-540	540
800	0	1674	-800	800
808	0	1240	-600	600
810	0	1260	-400	532
904	0	1450	-475	475
915	0	1140	-516	465
919	0	728	-148	220
925	0	1420	-440	420
4523	0	60.8	-42	30
4530	0	0	-54.5	63.96
4596	0	320	-160	160
4804	0	124.2	-86	59

C.1.2 Transmission line and transformer data

The parameters of the transmission lines are shown in Table 41, as explained before these parameters are the same for all the simulations performed for both methodologies proposed in this work.

Table 41 – Transmission line data of the southern Brazilian equivalent system

From Bus	To Bus	R (%)	X (%)	B (MVAr)	Thermic Limit (MVA)
100	101	0.172	2.72	231.4	1665
100	101	0.171	2.7	230.2	1665
100	210	0.209	2.935	254.6	1732
100	535	0.153	2.4	203.8	1665
101	102	0.156	2.46	208.5	1665
101	103	0.152	2.39	202.6	1665
102	1503	0.11	1.91	161.85	1665
104	103	0.196	3.1	264.9	1665
104	1503	0.05	0.82	69.36	1665
106	104	0.152	2.39	202.7	1665
106	104	0.152	2.39	203.1	1665
122	103	0.105	1.619	136.35	1665
123	120	0.359	3.945	66.68	598

126	86	0.109	1.826	51.18	1532
126	86	0.109	1.824	51.18	1532
126	120	0.6	5.95	92.8	598
126	120	0.606	6.02	93.8	598
134	131	0.092	1.01	16.9	717
134	396	0.32	3.509	59.24	699
136	120	0.436	4.3	66.6	598
136	120	0.436	4.3	66.6	598
136	131	0.348	3.42	52.8	717
136	134	0.375	4.13	69.9	598
136	138	0.649	6.46	100.8	728
136	138	0.558	6.19	105.7	766
140	138	0.652	6.5	101.4	728
140	138	0.558	6.19	105.7	766
210	370	0.147	2.32	196.6	1665
213	216	0.219	2.42	40.7	598
216	396	0.129	1.414	23.77	699
217	216	0.565	6.248	106.73	717
217	218	0.507	5.61	95.6	766
217	218	0.507	5.61	95.6	766
218	234	0.43	4.799	82.2	639
218	234	0.43	4.799	82.2	639
219	234	0.035	0.433	7.34	639
219	234	0.035	0.433	7.34	639
220	217	0.226	2.396	43.235	766
220	219	0.726	7.704	138.01	766
225	231	4.1	19.76	36.08	197
225	231	1.27	13.62	49.47	197
231	4501	4.51	21.69	40.25	197
231	4501	1.49	16.09	55.4	197
233	210	0.28	3.99	355.36	2598
233	320	0.27	3.87	344.03	2598
320	210	0.125	1.937	149.96	1948
320	360	0.082	1.256	98.99	2078
325	360	0.1	1.519	119.67	2251
325	370	0.28	4.84	419.5	2205
326	134	0.07	0.76	12.287	860

326	396	0.24	2.74	45.47	623
370	535	0.0931	1.3758	112.3	2205
824	933	0.01	0.124	15.204	2182
824	933	0.01	0.126	15.428	2182
834	934	2.444	12.652	21.706	359
839	898	1.13	6.99	12.617	189
839	1047	1.22	7.69	13.81	189
839	2458	0.22	1.09	1.8601	319
839	2458	0.17	1.03	2.0537	356
856	933	0.052	0.654	80.493	2273
856	1060	0.056	0.697	85.746	2182
895	122	0.308	3.958	444.84	1299
895	122	0.308	3.958	444.84	1299
896	897	0.05	0.73	78.06	1637
898	1047	0.15	0.89	1.6317	324
933	895	0.2	2.55	312.72	2110
933	955	0.162	2.048	250.17	2110
933	959	0.2	2.69	336.4	2182
934	1047	3.045	15.738	27.123	319
934	1047	3.041	15.718	27.089	319
938	955	0.2556	2.9224	360.4	2037
938	959	0.127	1.603	195.89	1266
939	1015	1.271	6.562	11.305	306
939	1015	1.283	6.564	11.522	306
955	964	0.1877	2.3467	287.24	1688
959	895	0.05	0.44	47.58	2110
960	834	2.21	11.475	19.687	319
960	1015	1.892	9.776	16.845	319
960	1015	1.895	9.704	17.029	319
964	976	0.0733	0.9164	112.17	1688
976	995	0.282	3.852	493.7	1688
995	964	0.1643	3.0339	354.88	2182
995	1030	0.073	0.92	112.26	2182
995	1060	0.172	2.17	265.16	2110
1030	955	0.047	0.59	71.818	2182
1060	897	0.076	1.171	124.58	2370
4501	4522	3.76	20.68	35.66	287

4501	4522	1.64	12.46	61.5	239
4522	4521	1.53	7.6	14.25	200
4522	4532	3.25	17.92	32.75	287
4522	4532	3.25	17.92	32.75	287
4532	4542	1.62	9.68	19.15	150
4542	4552	1.83	10.93	18.6	150
4552	4572	1.4	8.38	17	150
4562	4572	0.94	5.59	10.644	150
4562	4582	1.24	7.38	13.28	150
4592	4542	1	6.17	12.6	239
4623	4533	17.06	45.5	11.39	100
4703	4533	0.9	2.31	0.58	100
4703	4533	0.9	2.31	0.58	100
4805	4807	3.089	8.134	2.085	86
4805	4807	3.089	8.134	2.085	86
4862	4532	2.57	23.68	97.42	556
4862	4532	2.57	23.68	97.42	556

The data of the transformers is shown in Table 42.

Table 42 – Transformers data of the southern Brazilian equivalent system

From Bus	To Bus	R (%)	X (%)	Tap	Thermic Limit (MVA)
86	48	0	0.71475	1	1050
86	122	0	1.913	1	750
86	122	0	1.913	1	750
100	20	0	1.264	1	1520
100	213	0	2.357	1	560
102	120	0	2.403	1	560
103	123	0	2.419	1	560
106	140	0	2.923	1	560
106	140	0	2.668	1	560
131	22	0	8.8333	1	378
134	12	0	1.335	0.999	1136
136	16	0	1.536	1	1280
210	18	0	0.66667	1	2400
210	217	0	1.72	1	560

210	217	0	1.72	1	560
220	35	0	4.4965	1.025	417
225	217	0	2.721	0.955	225
225	217	0	2.938	0.955	560
228	219	0	3.595	1	225
234	233	0	1.113	1	1050
234	233	0	1	1	1050
320	300	0	1.3567	1	1200
325	301	0	2.6325	1	500
325	326	0	2.16	1	400
325	326	0	2.16	1	400
360	302	0	1.9367	1	537
370	303	0	1.0575	1	1740
396	305	0	2.2	1.025	450
535	500	0	1.025	1	1500
536	535	0	1.533	1	700
536	535	0	1.42	1	750
814	895	0.032	1.146	0.9652	600
814	895	0.03	1.1651	0.9652	600
824	800	0	1.68	1.024	1676
839	840	0	6.64	1	150
839	840	0	6.29	1	150
856	810	0	1.05	1	1260
897	808	0	1.02	1.024	1344
898	848	0	6.36	1	150
934	933	0.031	1.207	0.9747	672
939	938	0.031	1.15	0.9586	672
939	938	0.032	1.163	0.9586	672
939	938	0	1.277	0.9586	672
960	959	0.032	1.163	0.9917	672
960	959	0.031	1.166	0.9917	672
965	964	0.02	1.211	0.9717	672
965	964	0.02	1.233	0.9717	672
995	904	0	1.1538	1	1625
1030	915	0	2.0655	1	1254
1047	919	0	1.7022	1.025	788
1060	925	0	1.515	1.024	1402

1210	976	0.03	1.219	1.01	672
1210	976	0.039	1.138	1.01	672
1210	976	0.036	1.217	1.01	672
1503	1504	0	5.2	1	300
2458	896	0	1.27	0.9938	600
4521	4523	0	20.71	1	9999
4522	4623	0	7.95	1	100
4522	4623	0	7.95	1	100
4532	4530	0	14.3	1	9999
4532	4533	0	8.6	1	100
4532	4533	0	8.6	1	100
4532	4533	0	8.6	1	100
4533	4596	0	3.7635	1	9999
4592	21	0	6.4	1	9999
4805	4804	0	13.333	1	138
4862	4807	0	4.05	1	300